UNIVERSITY OF CATANIA

International PhD in Chemical Sciences

XXVI Cycle

VALENTINA OLIVERI

New Glycoconjugates for the Treatment of Diseases related to Metal Dyshomeostasis

PhD Thesis

Tutor: Prof. Graziella Vecchio

Coordinator: Prof. Roberto Purrello

2010-2013

ABSTRACT

Metal dyshomeostasis has been involved in the etiology of a great number of pathologies such as Wilson's, Alzheimer's, Parkinson's and Niemann-Pick diseases, Friedreich's ataxia, transfusion-related iron overload diseases and cancer. Neurodegenerative diseases and cancer have long been viewed as among the most enigmatic and problematic issues in biomedicine and their multiple facets have been well-documented. The precise mechanisms responsible for triggering these disorders remain unclear; however, they share multifactorial pathogenic mechanisms related to metal dyshomeostasis and, as a consequence, oxidative stress. Considering the multifactorial nature of these diseases, it is becoming more and more evident that the next generation of therapies must have multiple functions to combat the multiple mechanisms of disease progression and metal ions represent a promising therapeutic target as they could be a starting point to hit multiple targets. On the other hand, especially in the treatment of cancer, drugs may be directed to the site of action in order to reduce their side effects on healthy tissues and enhance their uptake by targeted cells.

This PhD thesis centers on the synthesis and evaluation of multifunctional molecules to interfere with different key target points of neurodegeneration and cancer.

8-hydroxyquinoline, a metal chelator, has been chosen as a basic molecular scaffold to build selective prodrugs and multifunctional metal-binding compounds on the basis of the rekindled interest in this compound and its derivatives for the treatment of Alzheimer's disease and cancer.

The synthesis, characterization and biological evaluation of new covalent glycoconjugates with 8-hydroxyquinolines are reported here. Glycosylation has been a successful strategy for improving several features of these systems. Apart from the increase in solubility, sugar moiety confers selectivity and multifunctionality.

In this thesis, glucosylated and galactosylated prodrugs of hydroxyquinolines were designed and synthetized in order to exploit unique and frequent features of cancer cells such as the high expression of certain proteins (e.g. β-glucosidases and glucose transporters) and the high levels of Cu^{2+}. The main advantages of these glycosylated compounds are targeting and prevention of side effects due to systemic chelation. The chelating function of these compounds is masked and they must be subject to hydrolysis through specific β-glucosidases

or β-galactosidases to liberate the active aglycone in targeted cells. The obtained results suggest that glucose- and galactose-bearing 8-hydroxyquinoline prodrugs could be suitable for prodrug monotherapy and antibody-directed enzyme prodrug therapy, respectively.

Chelating 8-hydroxyquinoline conjugates with monosaccharides and disaccharides have also been synthetized in order to compare their properties to those of the glycosylated prodrugs. Unlike these latter compounds, they are able to complex Cu^{2+} and Zn^{2+} ions with high stability constants, essentially leading to the formation of ML species. These systems are promising compounds for the treatment of diseases related to metal dyshomeostasis.

Finally, the synthetized cyclodextrin conjugates are promising multifunctional molecules that combine antioxidant, SOD-like activity, chelating, antiaggregant and inclusion abilities into one compound as demonstrated in this thesis. Cyclodextrin-hydroxyquinoline conjugates have significant antioxidant capacity and the possibility to form inclusion complexes with coformulating drugs and/or endogenous compounds such as cholesterol. The compounds can complex Cu^{2+} and Zn^{2+} ions with high conditional stability constants. Moreover, these derivatives are also able to strongly inhibit metal-induced protein aggregation and the formation of amyloid fibrils. The antiproliferative studies, carried out for this class of compounds, bode well for administering relatively high concentrations of these derivatives, for use as antioxidant and antiaggregant drugs, if necessary, without damage to healthy tissues. Overall, these conjugates compounds have great potential as therapeutic agents in the treatment of neurodegenerative diseases related to oxidative stress and metal dyshomeostasis, such as Alzheimer's and especially Niemann-Pick C diseases.

Contents

1. INTRODUCTION

The application of inorganic chemistry in medicine is becoming more and more prominent since metals play a pivotal role in many life-related processes.

Sodium, potassium, magnesium and calcium are essential for nerve conduction, muscle contraction, stabilization of nucleic acids and a plethora of other biological systems and thus they are the dominant metal ions in a living organism. Nevertheless, the metal ions incorporated into proteins are often not these abundant metal ions but are trace elements such as iron, copper, manganese, zinc, cobalt and nickel. Proteins that bind transition metals are usually catalytic enzymes with the transition metal ion being essential for their activity. Under physiological conditions, most transition metals can exist in multiple valence states and thus can readily participate in single electron transfer reactions, making them attractive for inclusion in biological systems. Metal ions are also found as components of prosthetic groups, cofactors and complexes prior to insertion into proteins.

Homeostasis of metal ions is a complex process, maintained through tightly regulated mechanisms of uptake, storage and secretion. Several metal ion transporters participate in the conservation of the required levels of the various metal ions in the cellular compartments.

Altered metal homeostasis can lead to the metal binding to protein or replacement of other metals from their natural binding sites. Several results have provided evidence that toxic metals can interact with DNA and proteins causing oxidative deterioration of biological macromolecules. Thus the metal dyshomeostasis has been involved in the etiology of a great number of pathologies such as Wilson's (WD),[1] Alzheimer's (AD),[2,3] Parkinson's (PD)[4] and Niemann-Pick[5] diseases (NPC), Friedreich's ataxia,[6] transfusion-related iron overload diseases[7] and cancer.[8]

Furthermore, in some of these cases metals are implicated in redox reactions leading to production of ROS (Reactive oxygen Species) and thus oxidative stress.[9]

The different metal ions may be grouped into redox-active ions such as Fe^{2+}, Cu^{2+}, Co^{2+} and to a lesser extent Mn^{2+}; and non-redox-active ions such as Ca^{2+} and Zn^{2+}. Copper, zinc and iron have been chosen as the focus of this introduction as they are biologically relevant particularly with respect to human health.

1.1 Copper

Copper is an essential trace element for living organisms, taking part in several processes of metabolism, including mitochondrial oxidative phosphorylation, iron metabolism, free radical detoxification, neurotransmitter synthesis and denaturation, connective tissue synthesis and pigment formation.[10] Copper is a transition metal characterized by a low redox potential between Cu^{2+} and Cu^{+} 0.158 V in water that explains its capacity to exchange electrons with other systems. The biological utility of copper mainly derives from this ability to cycle between its oxidized and reduced forms. A healthy human adult (70 Kg) contains about 110 mg of copper that is involved as cofactor of different redox enzymes. The best known among these are reported in Table 1.[11] In addition to its enzymatic roles, copper plays non-enzymatic functions in angiogenesis,[12] nerve myelination, activity of endorphin and brain development.[13] Copper is essential for reproduction, regulation of gene expression and for normal growth and development.

Table 1. Some Cu-dependent enzymes in mammals.

Enzyme	Function
Superoxide dismutase	Free radical detoxification
Cytochrome c oxidase	Dioxygen reduction into water
Ceruloplasmin	Ferroxidase
Dopamine β-hydroxylase	Oxygenase, converts dopa into norepinephrine
Tyrosinase	Monophenol oxidase, melanin synthesis
Lysyl oxidase	Cross-linking of collagen and elastin
Metallothionein	Storage of excess Copper
Amyloid Precursor Protein	Normal function unknown
Angiogenin	Induction of blood vessel formation
Hephaestin	Ferroxidase

Despite its physiological role, copper can be toxic. Copper can catalyze the formation of ROS *via* a Fenton-like reaction. Cu^{2+}, in the presence of superoxide anion radical or biological reductants such as ascorbic acid or gluthatione, can be reduced to Cu^{+}. This latter is able to

catalyze the formation of reactive hydroxyl radicals through the decomposition of hydrogen peroxide *via* the Fenton reaction:

$Cu^{+} + H_2O_2 \rightarrow Cu^{2+} + {}^{\bullet}OH + OH^{-}$ (Fenton reaction).

The hydroxyl radical is extremely reactive and can further react with practically any biological molecules in the near vicinity. ${}^{\bullet}OH$ can abstract hydrogen atom leaving behind a carbon-centered radical (e.g. a lipid radical from unsaturated fatty acids). Copper is also capable of causing DNA strand breaks and oxidation of bases *via* ROS.In addition, copper can possibly displace other essential metals in proteins.

For these reasons, copper homeostasis is tightly controlled in all organisms.

Copper uptake into cells is thought to be mediated by the plasma membrane protein CTR1 (as for high affinity copper uptake) with some involvement of the divalent metal transporter and potentially other unidentified uptake systems (Figure 1). Essentially, no free copper is available in eukaryotic cells since the ion is always complexed with other molecules. Small molecules such as glutathione (GSH) and metallothioneins bind copper for storage and/or detoxification and may provide an exchangeable pool of copper.[14] Futhermore, proteins called metallochaperones[15] also bind copper and target it to specific sites inside the cell. Copper chaperone for superoxide dismutase (CCS) delivers copper to Cu/Zn-SOD in cytosol and mitochondria, cytochrome c oxidase copper chaperone (COX17) mediates copper transfer within the mitochondrial intermembrane space for metallation and assembly of cytochrome c oxidase, and HAH1 transfers copper to the copper-ATPases, ATP7A and ATP7B for delivery to the secretory pathway and for efflux of excess copper from the cell (Figure 1).

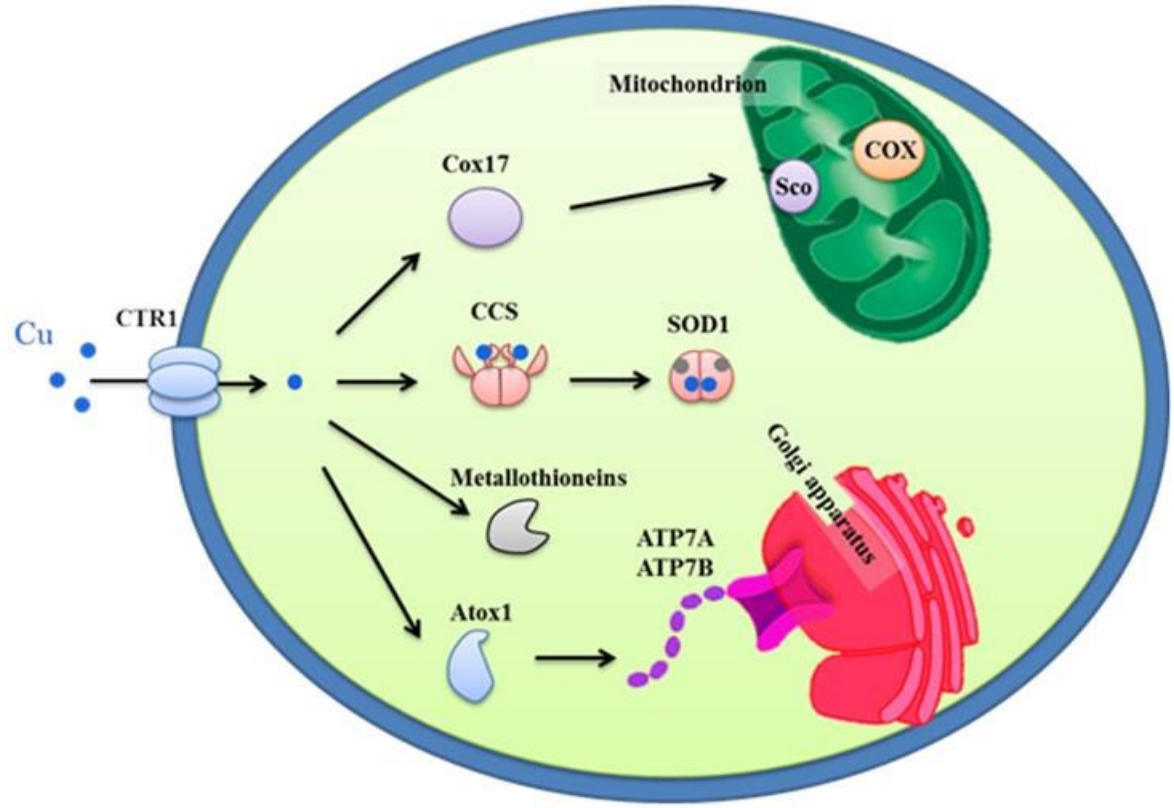

Figure 1. Pathways of copper trafficking within a mammalian cell. The three principal chaperones, Cox17, CCS, and Atox1 are shown along with the respective protein targets, cytochrome *c* oxidase, SOD1 and the Wilson and Menkes transporting ATPases.

1.1.1 Copper-related diseases

Dyshomeostasis of copper has implications in a number of diseases, and deficiencies in copper uptake have a number of detrimental effects. Mutations in ATP7A and ATP7B result in Menkes and Wilson's diseases, respectively.

Patients with WD suffer from brain disorders and liver disease. Copper levels rise and serum Ceruloplasmin levels decrease because of the diminished function of the ATP7B protein, which is directly involved in the vesicular pathway of hepatic copper transport from the liver to bile canaliculi. Pathologic manifestations include liver failure, tremors, slurred speech, and other neurological impairments.

Untreated WD is fatal. The overall therapeutic approach is the generation of a negative copper balance. Some increase the removal of copper from the body, while others prevent the

absorption of copper from the diet. With chelation treatment or liver transplantation, prolonged survival has become the norm.

It is generally agreed that patients with symptoms or signs of hepatic insufficiency or chronic active hepatitis with or without neurologic manifestations should be treated with copper chelators (D-penicillamine (D-Pen) trientine hydrochloride (TETA) or tetrathiomolybdate) and/or zinc salts. Chelating agents directly bind copper and facilitate its excretion whereas zinc interferes with the intestinal uptake of copper and induces the endogenous chelator metallothionein.[16]

Menkes disease is an X-linked recessive disorder associated with copper deficiency due to mutations on the ATP7A gene. Since the ATP7A protein is malfunctioning in the enterocytes, there is a defect in dietary copper absorption and therefore in its distribution in most tissues.

Menkes disease is characterized by neurological defects, growth retardation, hypopigmentation, ‘‘kinky’’ or ‘‘steely’’ hair and deficiencies in a number of cuproproteins. The treatment consists of Cu supplementation by subcutaneous injections of Cu-His.

Light changes in copper homeostasis have strong impact on the brain, leading to the onset of neurological diseases. However, further elucidations are required to clarify the exact mechanisms of these relationships.

Prions are infectious protein particles involved in transmissible spongiform encephalopathies (TSEs) including Creutzfeld-Jakob disease (CJD), chronic wasting disease (CWD), and bovine spongiform encephalopathy (BSE). These fatal neurodegenerative diseases are caused by the misfolding of cellular prion. In its normal cellular form (PrPc) the protein is thought to transport copper into the cell, protect from oxidative stress and buffer copper in the cell. Conversion of the protein to the scrapie form (PrPsc) is induced by interaction with copper and other metal ions such as zinc, iron and manganese and altered metal binding by PrPsc contributes to the pathology. Copper shows an increase in toxicity for PrP knockout mice and exacerbates the disease in a mouse model of familial CJD. Increased copper in the diet of mice raises PrPc levels.[17] Furthermore, when isolated from diseased brain, PrPSc has been found to be bound with Cu^{2+} ions.[18] In addition, oxidative modifications of PrP, generated by copper-catalyzed Fenton reaction, have been linked to prion disease.[19,20] Significantly, copper ion chelation therapy will delay onset of scrapie in mice.[21]

Huntington's disease (HD) is another progressive neurodegenerative disease characterized by a dominant polyglutamine expansion within the N-terminus of huntingtin protein and results in oxidative stress, energetic insufficiency and striatal degeneration. Affected individuals undergo progressive motor, cognitive, and psychiatric deterioration. HD brain has shown an accumulation of copper and iron in the striata of the patients, but the role of these metals in HD pathogenesis is unknown. It has recently hypothesized that increased amounts of copper bound to low affinity sites could contribute to pro-oxidant activities and neurodegeneration.[22] Copper, but not other metal ions, is able to interact with both normal and mutant huntingtin. It also promotes the aggregation of mutant huntingtin fragments probably through the induction of structural changes, obviously metal chelation prevents these effects.

Another highly debilitating progressive neurodegenerative disorder is AD. This latter is characterized by extra cellular deposition of Aβ peptides in senile plaques and intracellular accumulation of hyperphosphorylated tau protein in neuronal cells as neurofibrillary tangles. Generally, AD affects people over 65 or as young as 40–50 years. It is the most prevalent form of dementia and is characterized by severe cognitive impairment due to degeneration of brain cells. For many years, the most popular hypothesis for AD neuropathogenesis was the "Amyloid Cascade Hypothesis," which proposes that all pathology in the AD brain occurs downstream of the excessive accumulation of Aβ in the CNS. Recently, Bush *et al* have posited the "Metal Hypothesis of Alzheimer's Disease," which stipulates that the neuropathogenic effects of Aβ in AD are promoted by (and possibly even dependent on) Aβ-metal interactions.[23] Copper (390 μM), zinc (1055 μM), and iron (940 μM) have been reported to be elevated by several-fold in AD brain as compared with normal age-matched samples (copper [70 μM], zinc [350 μM] and iron [340 μM]). Aβ directly coordinates copper and zinc, but not iron or other metal ions, within the cores of plaques. Both zinc and copper are able to promote the aggregation of oligomers in the synaptic cleft. Moreover, copper and iron can also cause the neurotoxic redox activity of Aβ and induce oxidative cross-linking of the peptide into stable oligomers.

Copper is also associated with cancer and angiogenesis. Serum and tumor tissue copper levels in cancer patients are significantly elevated compared to healthy subjects. The most elevated levels of copper have been documented in cancer patients suffering from breast, cervical, ovarian, lung, prostate, stomach cancer and leukemia.[24,25] Elevated copper levels

have been shown to be directly linked to cancer progression. In fact, copper is important for angiogenesis that is required for invasive tumor growth and metastasis. Angiogenesis is a multi-step process, involving degradation of the endothelial cell basement membrane, endothelial cell migration to the perivascular stroma and capillary sprouting. Avascular tumors are severely limited in their growth because of the lack of an adequate blood supply. Tumors have to perturb the local balance of proangiogenic and antiangiogenic factors in order to trigger angiogenesis. Therefore, tumors overexpress proangiogenic factors, such as vascular endothelial growth factor. It has been recently demonstrated that extracellular translocation of the cytosolic copper occurs during angiogenesis processes *in vitro*,[26] suggesting that the metal coordination by an extracellular protein involved in angiogenesis, such as angiogenin (hAng) and/or vascular endothelial growth factor (VEGF), could play a pivotal role. Copper or its complexes have been shown to directly stimulate angiogenesis in several model systems[27] as well as *in vivo*.[28] Furthermore, copper chelation inhibits angiogenesis in numerous animal and xenograft models.[29] Such findings have led to clinical trials for the treatment of solid tumors by copper chelators with some results of efficacy in disease stabilization, however the molecular basis and the effects that copper ion exerts are still incompletely understood.

Niemann–Pick type C (NPC) is an autosomal recessive disorder characterized by progressive neurological degeneration. The most commonly mutated gene in this pathology, NPC1, is a membrane protein localized in the late endosomes and regulates intracellular cholesterol trafficking. New insight into this disease suggests a possible role of copper. Conflicting results have been reported. Recent findings suggest that ATP7B localizes in the late endosomes where copper is transported to the secretory compartment *via* an NPC1-dependent pathway and incorporated into Ceruloplasmin.[30] Futhermore, it has been observed copper accumulation in the liver[31] and plasma, along with a decrease of copper excretion into the bile of NPC mice.[9]

Copper has been also associated with other diseases such as Parkinson's Disease, diabetes, atherosclerosis, cardiovascular disease and amyotrophic lateral sclerosis. To sum up, it is clear that the regulation of copper homeostasis is essential for the survival and proper functioning of all organisms.

1.2 Zinc

Zinc is essential for all living organisms and is the second most abundant transition metal in both seawater and humans.[32]

The adult human body contains approximately 1.5–2.5 g of zinc, present in all organs, tissues and fluids. The level of free intracellular Zn^{2+} is as low as 0.5 nM and so this makes zinc the most prevalent trace metal found in the cytoplasm. Zinc is a redox inert metal ion and does not participate in oxidation/reduction reactions because of the Zn^{2+} ion has a full d shell. It does not exist in multiple valences under physiological conditions rendering it unique amongst biologically-relevant transition metals. For these reasons, zinc is generally thought to be less toxic than the redox active metals such as copper and iron.

The combination of structural and thermodynamic properties with the abundant bioavailability have led to the incorporation of zinc in a variety of biological systems. Zinc is an element present in more than 300 enzymatic reactions that function in many aspects of cellular metabolism, involving metabolism of proteins, lipids and carbohydrates. Within the zinc proteins a number of distinct functional classes can be identified: for example, matrix metalloproteases (with roles in embryonic development, cell motility, wound healing and reproduction), peptidases (digestive enzymes) and zinc finger proteins (DNA or RNA binding proteins).

Intracellular uptake and efflux of zinc are mediated by two class of mammalian zinc transporters. The first is the ZnT family of transporters, which act to decrease intracellular zinc levels by transporting zinc from the cytoplasm to the lumen of organelles or the extracellular space. The second is the ZIP family responsible for increasing intracellular zinc levels by either transporting the metal from the extracellular space or lumen of organelles into the cytoplasm (Figure 2).

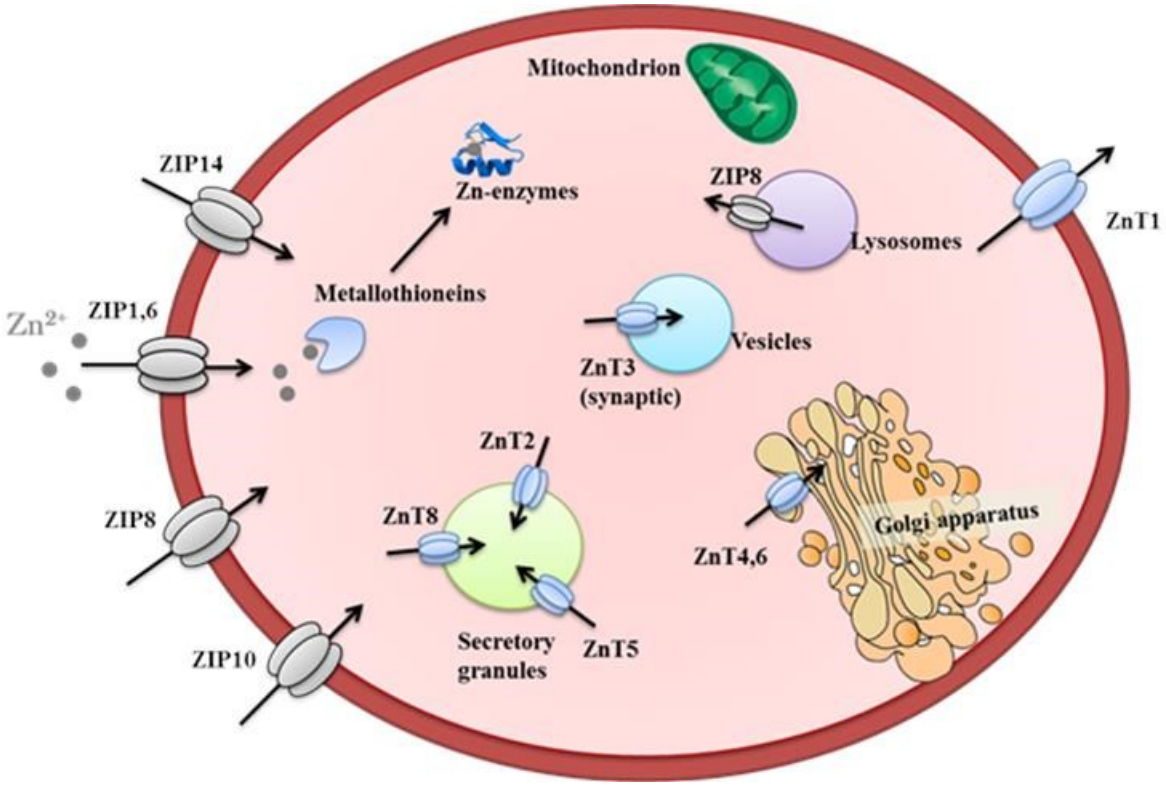

Figure 2. Cellular localization and function of ZIP and ZnT zinc transporter family members in mammalian cells. Arrows indicate the direction of zinc mobilization. ZIP1, 2 and 4 are induced in zinc deficient conditions, whereas ZNT-1 and 2 by zinc accumulation.

1.2.1 Zinc-related diseases

Over one billion people in developing countries are nutritionally deficient in zinc. Its deficiency is associated with a range of pathological states, including skin changes, alopecia, diarrhea, slowed growth, delayed wound healing, hypogonadism, impaired immunity, and brain development disorders, all of which are reversible with zinc supplementation. Zinc deficiency occurs as a result of insufficient dietary zinc uptake (which can be exacerbated by consumption of foods such as cereal grains which are rich in phytates, inhibitors of zinc dietary absorbtion), malabsorption syndromes and other gastrointestinal disorders, chronic liver and renal diseases, excessive alcohol use, malignancy, pancreatic insufficiency, rheumatoid arthritis, and other chronic conditions.[33]

Acute and chronic forms of zinc toxicity have been observed. Acute zinc toxicity is rare and usually due to consumption of contaminated food that can lead to gastrointestinal irritation, fatigue, muscle pain and fever. Chronic zinc toxicity is more common and usually

occurs as a result of prolonged use of oral zinc supplements. Excess zinc can also interfere with other essential transition metals such as copper and iron. [34]

Because of zinc is involved in maintaining of intracellular ion homeostasis and in signal transduction in most cells, it directly affects tumor cells through its regulatory role in gene expression and cell survival.

Levels of zinc in serum and malignant tissues of patients with various types of cancer are altered indicating the involvement of zinc in oncogenesis. Studies of the role of zinc in malignant diseases have contradictory results. It is clear, however, that serum zinc levels are reduced in patients with cancers of the breast, gallbladder, lung, colon, head, neck. Interestingly, while serum zinc levels are low in the setting of most cancers, tumor tissue in breast and lung cancer have elevated zinc levels compared to the corresponding healthy tissues.[35] It has been found that zinc depletion induces cell death *via* apoptosis (or necrosis if apoptotic pathway is blocked) while sufficient zinc levels allow the maintenance of autophagy.[35] Cancer cells have upregulated zinc importers, and frequently increased zinc levels, which allow them to survive.[35]

Besides its role in cancer, zinc is also associated with AD. Zn^{2+} is involved in protein modification, misfolding and aggregation, leading to the precipitation of Aβ.[36] Zinc, released through glutamatergic neurotransmission, is concentrated in the presynaptic bouton by the action of ZnT3 (Figure 3) and it manages to achieve concentrations up to 300 μM in synaptic clefts. Cu^{2+} is released post-synaptically after NMDA-induced activation, which causes the translocation of the Menkes ATPase and its copper release through vesicles to the synaptic cleft. Cu^{2+} concentrations can reach 15 μM.

In the vicinity of the neuron, amyloid-beta comes across Zn^{2+} and forms oligomers of increasing insolubility as the amount of protein-bound-zinc increases. Aβ can bind up to 2.5 moles of Zn^{2+}. The soluble Aβ monomers are constitutively degraded by matrix metalloproteinases (MMPs), neprilysin and insulin degrading enzyme (IDE) but Zn^{2+}-loaded Aβ oligomers are resistant to degradation. Although there has been considerable focus on the toxic nature of amyloid-beta and its oligomers, it is important to note that the latter act as a Zn^{2+} sponge. The net effect of sequestering Zn^{2+} from its physiological targets is the disruption of normal memory events (for example, long-term potentiation) and loss of trophic and metabotropic stimulation of the postsynaptic neuron.[37]

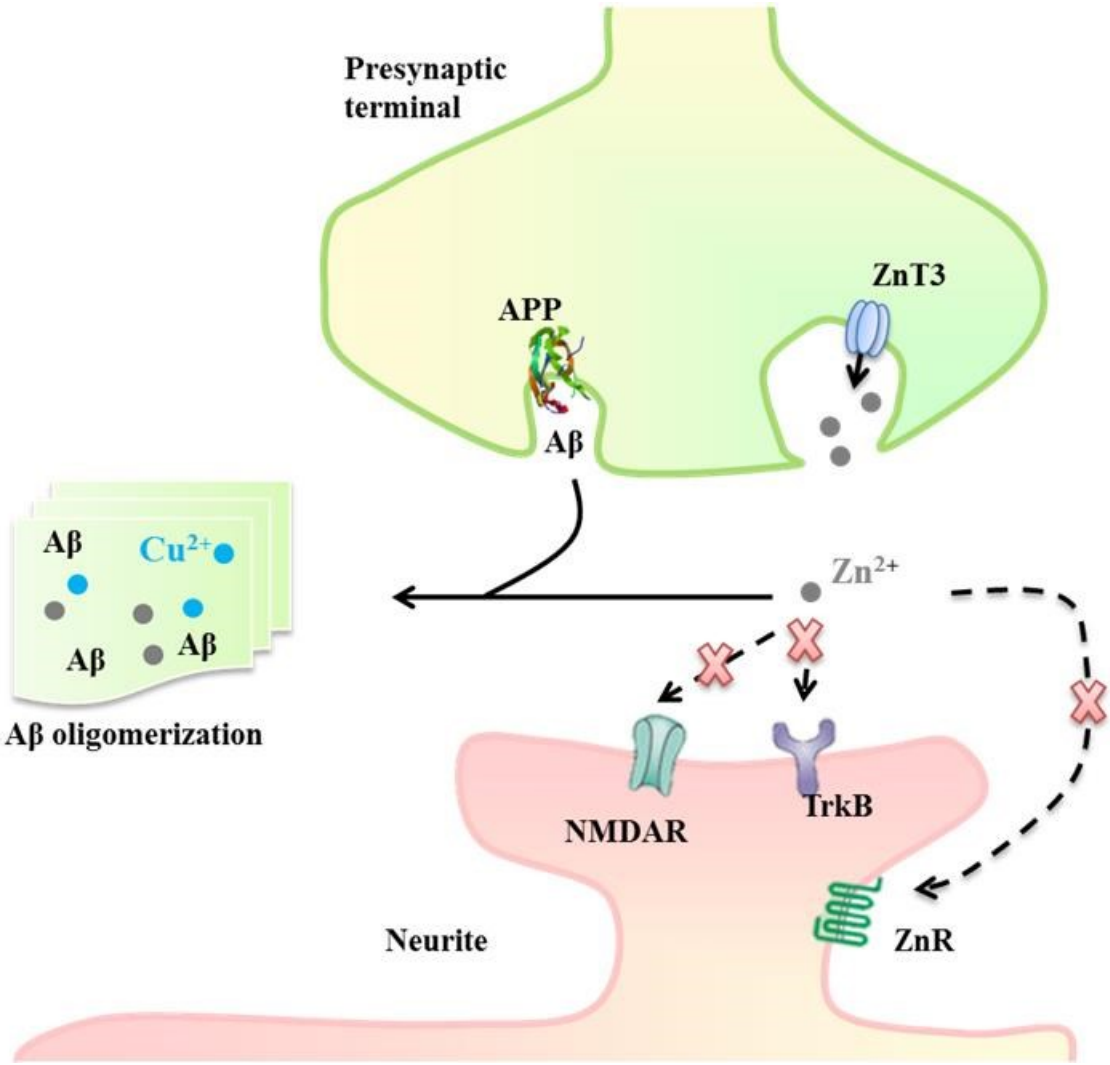

Figure 3. Aβ is released into the synaptic cleft where it has the potential to react with Cu and Zn to form oxidized, crosslinked soluble aggregates and precipitated amyloid.

1.3 Iron

A large amount of cellular enzymes depends on iron for their function and, consequently, this metal is essential for life. The normal iron content of the human body is 3 or 4 grams.

Many of the iron-requiring proteins are involved in enzyme catalysis and electron transport, whereas others are needed for oxygen transport and delivery. Major classes of such proteins include those with heme as the prosthetic group and those with iron–sulfur (Fe–S) clusters. However, the most abundant iron proteins in the body are the hemoglobin and myoglobin. Iron can have two thermodynamically stable oxidation states, ferric iron (Fe^{3+}) and ferrous iron

(Fe^{2+}). This makes it suitable for the catalysis of biochemical reactions, but it also means that it is able to catalyze, similarly to copper, reactions with the production of toxic oxygen radicals.

Thus, individual cells and whole organisms must tightly controlled iron homeostasis.

This latter is a complex process and there are several proteins that respond to the total body burden of iron and to hypoxia, anemia and inflammation. Most iron is delivered to cells bound to plasma transferrin *via* a process that involves transferrin receptor 1, divalent metal-ion transporter 1 and several other proteins (Figure 4). Non-transferrin bound iron can also be taken up efficiently by cells, although the mechanism is not completely clarified. The efflux of iron can occur *via* the iron export protein ferroportin and an iron oxidase. The coupling of an oxidoreductase to a membrane permease is a common feature in membrane iron transport. At the systemic level, iron transport is regulated by the liver-derived peptide hepcidin which acts on ferroportin to control iron release to the plasma (Figure 4).[38]

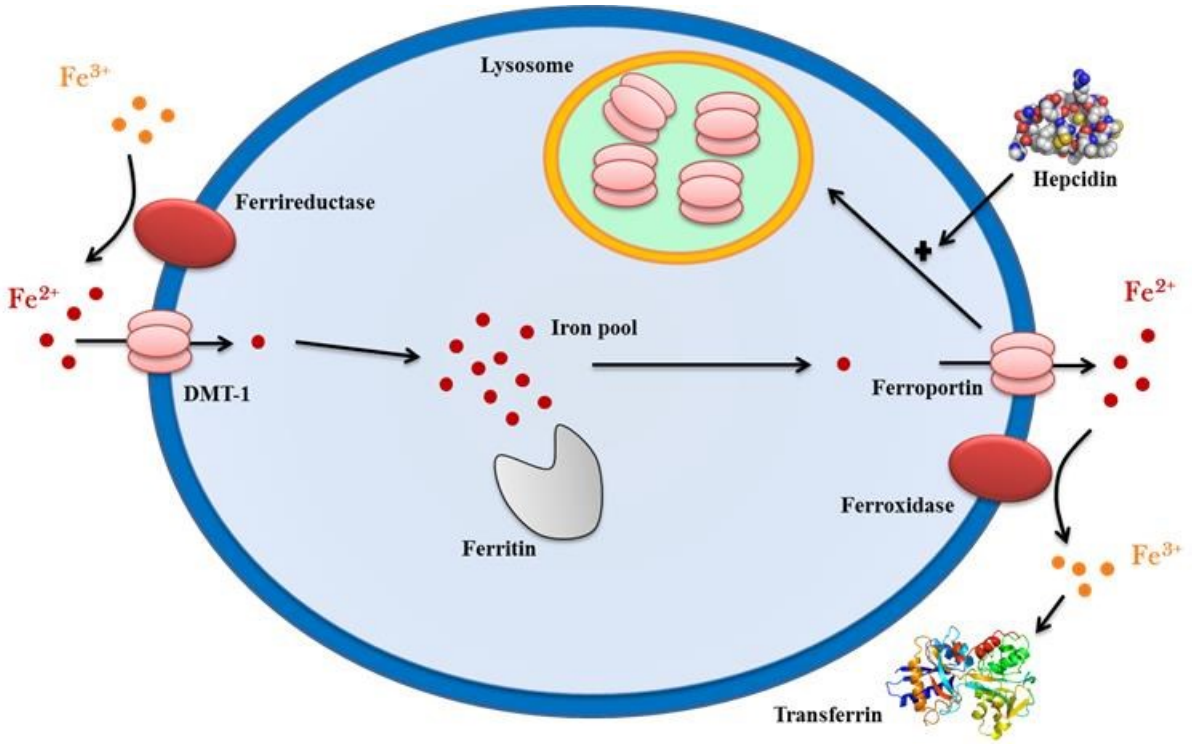

Figure 4. Iron transport in mammalian cells. Arrows indicate the direction of iron mobilization. Hepcidin blocks iron efflux into plasma inducing Ferroportin internalization and degradation in lysosomes.

1.3.1 Iron-related diseases

The most common outcome of systemic iron deficiency is anemia. Anemias are characterized by a deficiency in the number of mature erythrocytes in the circulation, which inevitably lowers the oxygen-carrying capacity of the blood resulting in clinical symptoms such as fatigue, weakness, increased cardiac output as well as increased morbidity and mortality.

On the contrary, there are also iron-overload diseases that can be inherited or acquired, and are typically characterized by the accumulation of iron in the body. Obviously, in these pathology increased levels of oxidative stress have been observed. Among iron-overload diseases, there are hereditary hemochromatoses and β-thalassemia major.[39] The former is characterized by an accelerated rate of intestinal iron absorption and the progressive iron deposition in various tissues. Beta-thalassemia major is a hereditary disease affecting the hemoglobin. The treatment of this disease consists of an opportune transfusion program that prevents death from anemia in childhood and permits a normal growth and development. Nevertheless, transfusion-dependent patients will develop iron overload and require chelation therapy to remove the excess iron.[39]

Iron has been implicated in the onset of a number of neurodegenerative disorders, for example Friedreich's ataxia that is an autosomal recessive disease characterized by degeneration of neurons in the cerebellum. This pathology results in mitochondrial iron accumulation, decreased Fe/S cluster synthesis and an altered antioxidant response. Furthermore, a significant increase in brain iron levels has been found in both PD and AD. The mechanisms responsible for iron accumulation are still unknown in PD. Similarly, how iron is delivered to its major recipients in the cell (e.g. mitochondria) has yet to be elucidated. However, chelation of iron seems to protect from dopaminergic degeneration,[40,41] typical feature of PD.

To sum up, iron is implicated in a large number of diseases and the most mechanisms responsible in the iron-involvement have to be clarified. However, iron overload disorders are successfully treated with chelation therapy.

1.4 Chelation therapy

Metal chelators can be used either to deliver metal ions for medical application (i.e. diagnostic application) or to remove unwanted metals from human body. This latter one is the topic of this section.

The manipulation of the metal distribution in biological systems is very complicated and it requires to consider all possible factors influencing the process.

When a ligand is introduced into a biological system, it is necessary to consider the reactivity and distribution characteristics of all parts of the coordination complex:

- metal ion
- ligand or pro-ligand
- complex

Whereas some neutral chelators are able to permeate biological barriers, other charged systems will achieve significant permeation only upon formation of an uncharged complex. In fact in some cases the corresponding metal complexes are more lipophilic and mobile throughout the biological system than ligands. Metal binding selectivity is very important otherwise one risks affecting the concentrations of other essential metals. In order to design a selective metal ion chelator, one must consider the hard-soft acid-base (HSAB) theory.

Another consideration in ligand design is the *chelate effect* describing the favorable entropy change upon exchange of many monodentate ligands for fewer multidentate ligands binding a given metal ion. The higher denticity the ligand, the more thermodynamically stable will be its complex.

Furthermore, the introduced metal-binding therapeutic system must participate in a series of ligand exchange reactions to form the new, desired complex and so its affinity must be comparable with that of the endogenous ligands. A final consideration must be made about the redox activity of the metal ion in the complexed form; in fact ligands could modify their redox potential promoting production of reactive oxygen species (ROS).

First, an overview of the major compounds for metal ion binding and new strategies to design multifunctional chelator will be discussed, to be followed with the discussion about specific metal chelators or metal ionophores.

The use of small-molecule chelators began in 1941 with the administration of citrate to relieve accidental overexposure to lead. The most obvious medicinal application of metal chelators is in the treatment of metal overload conditions. Among the first used metal chelators, there is D-penicillamine (D-pen, Figure 5) that has been introduced in 1956 for treatment of copper-overloaded WD patients.

Ethylenediaminetetraacetic acid (EDTA, Figure 5) was the next chelator in clinical use (1950s) for treatment of lead toxicity and also used in cases of accidental radionuclide dosing. Later, EDTA was substituted for diethylenetriaminepentaacetic acid (DTPA, Figure 5) in order to remove radionuclide excess. Triethylenetetraamine (TETA, Figure 5), although considered less effective, was introduced in 1980s for use in WD patients intolerant of D-pen.

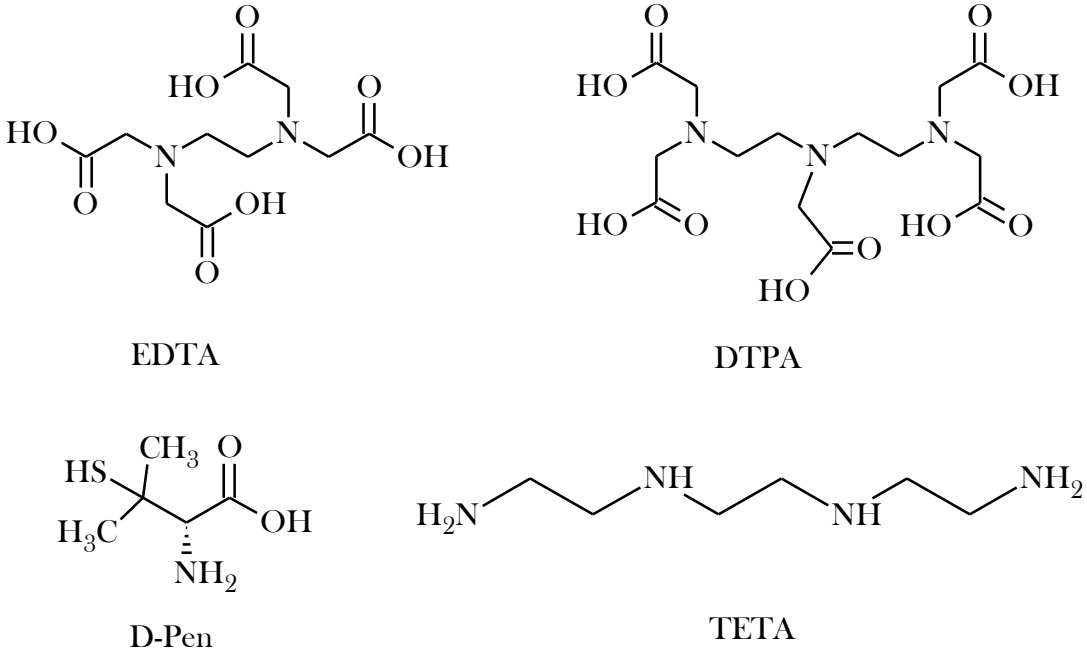

Figure 5. Metal chelators.

Currently, D-Pen is the most widely used treatment across the world; TETA is used in the USA but is hardly accessible in Europe. Tetrathiomolybdate (TM) has been recently used in the USA as a copper chelator for patients who are intolerant to D-Pen and TETA, but it has not approved by FDA.[16] However, D-Pen has severe side effects including bone marrow suppression, anorexia, vomiting and diarrhea. Both TETA and TM have fewer potential side effects, but must still be carefully monitored. Therefore, it is clear that new drugs have to be investigated in order to obtain more efficient and selective therapy in the treatment of WD.

In thalassemia major, iron accumulates in the liver, heart, pancreas and other organs with long-term consequences including fibrosis, cirrhosis, hepatocellular carcinoma, diabetes and heart disease. To prevent this progressive deterioration, iron has to be removed by chelation therapy. Deferoxamine (DFO, Figure 6) a naturally occurring microbial siderophore, is a trihydroxamic acid that efficiently binds Fe^{3+}. It has been used to treat iron overload since the 1970s whereas deferiprone (DFP, Figure 6) has been used orally for the same purpose since the late 1980s.

DFP is currently approved in Europe and in India. It is a bidentate chelator and forms a neutral stable 3:1 ligand iron complex at pH 7.4, which is water soluble and readily excreted by kidneys.[42]

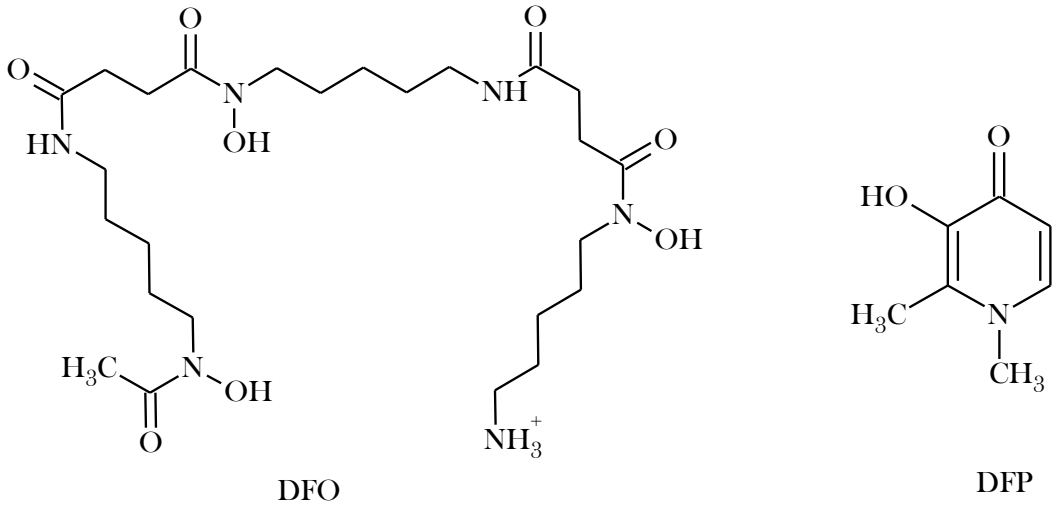

Figure 6. Metal chelators used in the treatment of iron-overload diseases.

Its relative lipophilicity gives it high oral activity and Blood Brain Barrier (BBB) penetration. Because of its side effects, DFP is approved for use only as a second-line treatment after DFO. Nevertheless, deferiprone offers a significant advantage over DFO in its ability to remove cardiac iron and is now in consideration for combination therapy with DFO in iron-overloaded thalassemia patients. Combination therapies are thought to provide higher efficacies and lower toxicities than current monotherapies. Deferiprone and DFO have been used together in iron-overloaded patients; not only was combination therapy well-tolerated, but it caused significant improvement in at least one additional observed end point (such as cardiac function) *vs* treatment with DFO alone.[43] The smaller bidentate chelator acts as a

"shuttle" to first bind the biological metal ion then transfer it to the multidentate chelator, which acts as a "sink" for the ion.

In addition to these properties, the structure of DFP can be easily functionalize by N-substituent variation, which can alter the physicochemical properties of the drug without significant alteration of the metal binding ability. For these reasons, a large amount of derivatives has been synthetized and studied with different applications. Some of these have been applied to the treatment of AD, because of it has been recently demonstrated that deferiprone and a series of its derivatives such as 2-amido-3-hydroxypyridin-4-one are neuroprotective in mouse cortical neuron cultures.[44] Deferiprone prevents neuronal death in cells exposed to AD-related insults such as Fe^{3+}, H_2O_2, and Aβ 1-40.[44]

Other conditions for which chelation therapy and then DFP derivatives have been proposed or tested include cancer. Even if cancer does not involve iron overload, it is a requirement for cell cycle progression and for DNA synthesis; thus, cancer cells have a higher demand for the ion and are particularly susceptible to its depletion. Iron chelators (including DFO and DFP) and other hexadentate naturally occurring siderophores have been investigated as antiproliferatives for cancer therapy as reported by Richardson and coworkers.[45]

However, the chelation of copper has been also proposed in order to have antitumor activity.

Regulation of the copper levels as an anti-cancer strategy is currently under intense investigation and significant efforts were undertaken aiming at the control of the angiogenesis. Obviously, copper chelators utilized in WD were first checked as anti-angiogenic drugs. D-pen, TM, TETA have been shown to inhibit angiogenesis both *in vitro* and *in vivo*.[46-48] Several animal studies have supported the hypothesis of employing copper chelators as anti-angiogenic agent. TETA was used to treat mice bearing hepatocellular carcinoma xenografts showing significant inhibition of the tumor growth associated with suppression of tumor angiogenesis.[49] Analogously, TM displayed encouraging anti-angiogenic and antitumor effects in animal models. Pan *et al.* have reported that copper deficiency induced by tetrathiomolybdate resulted in impairment of tumor growth and angiogenesis in two animal models of breast cancer (an inflammatory breast cancer xenograft model in nude mice and HER2/neu cancer prone transgenic mice).[47]

TM was then selected for clinical trials in humans. In a phase I clinical trial, TM was administrated to patients with metastatic cancer. A reduction of ceruloplasmin without toxicity was observed and five of six patients displayed stable disease.[50] In a following phase II clinical trial in patients with advanced kidney cancer, TM was well tolerated and a significant depletion of copper was observed in all patients. Furthermore, 31% patients exhibited stable disease for at least 6 months.[51]

Amongst the most important metal binding compounds, 8-hydroxyquinolines have recently rekindled interest as promising therapeutic agents in the treatment of diseases related to metal dyshomeostasis and oxidative stress such as cancer, Alzheimer's and Huntington's diseases.

1.4.1 8-hydroxyquinolines (OHQs)

8-Hydroxyquinoline (OHQ) is a quinoline derivative that has been used as a fungicide in agriculture and a preservative in the textile, wood, and paper industries. OHQ possesses a good metal chelating ability and thereof it is widely used for analytical and separation purposes as well as for metal chelation.

Derivatives of OHQ are systems of great interest in the field of inorganic and bioinorganic chemistry. As metal-binding compounds they have recently been viewed with interest as anticancer agents (especially in the presence of Cu^{2+})[52] and as therapeutic agents for Alzheimer's disease (AD).[53] A series of OHQ derivatives, such as 5-chloro-7-iodo-8-hydroxyquinoline or clioquinol (CQ), 5-((4-(prop-2-ynyl)piperazin-1-yl)methyl)quinolin-8-ol (HLA-20, Figure 7), 5-((methyl(prop-2-ynyl)amino)methyl)quinolin-8-ol (M30, Figure 7) and 5-((4-(2-hydroxyethyl)piperazin-1-yl)methyl)quinolin-8-ol (VK-28, Figure 7) have been reported to exert potent antineurodegenerative effects. HLA-20 is a strong Fe^{3+} chelator and radical scavenger with moderate inhibitory effect on monoamine oxidase, MAO-B. VK-28 is a strong iron chelator that can penetrate the mitochondrial membrane and M30 is a multimodal iron chelator that sequesters iron and inhibits MAO-A and MAO-B.[54] In particular, combining the antioxidant chelating moiety of 8-hydroxyquinoline of the brain permeable iron chelator VK-28, with the propargyl moiety found in the MAO inhibitors, HLA-20 became a lead

compound for neuroprotective studies in PD and AD. Among these metal chelators used in neurodegeneration, CQ has reached pilot Phase II of clinical trials in AD patients.

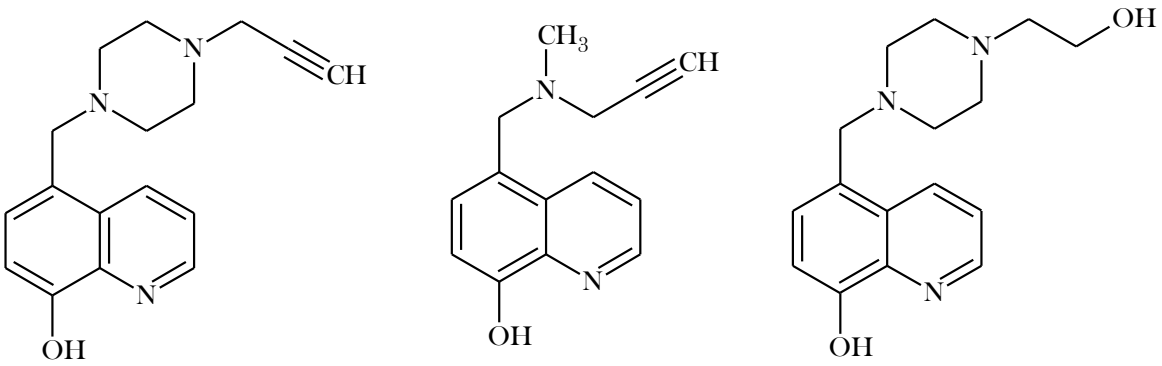

Figure 7. Fe^{3+} chelators with possible application in AD and WD.

Clioquinol (5-chloro-7-iodo-8-hydroxyquinoline, CQ, PBT1, Figure 8) the most successful member of this family, was developed by Ciba–Geigy as an oral antibiotic to treat amoebic dysentery.

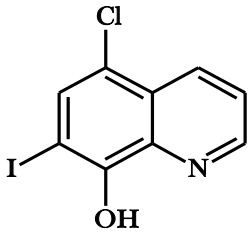

Figure 8. Clioquinol.

In the 1970s, it was associated with a wave of neurotoxic effects in Japan known as subacute myelo-opticoneuropathy (SMON)[55] and was withdrawn from the market. The explanation for such side effects is not clear, but many of these cases may have been related to the ability of CQ to function as a "carrier of heavy metals" to the central nervous system (CNS) or perturbing the homeostasis of vitamin B12. Several recent studies have rekindled interest in CQ as a modulator of metal homeostasis in neurodegenerative disorders, such as AD.[56,57]A pilot phase II study of orally dosed CQ reported that the drug improved the

cognition and behavior in AD patients.[58] Prana Biotechnology, who developed this drug for AD, discovered that the manufacturing process for CQ led to certain mutagenic "di-iodo" impurities and decided to suspend its development.[59]

However, since these results, a new OHQ derivative PBT2 (Prana Biotechnology, phase II completed) was developed. PBT2 (Figure 9) outperforms CQ, avoiding its side effects and offers even better results in the treatment of AD.

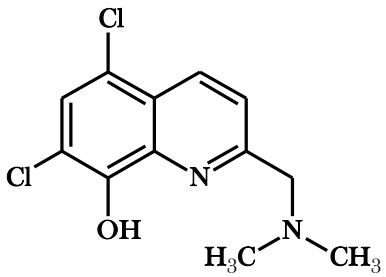

Figure 9. PBT2.

PBT2 has successfully completed phase IIa trials in patients with early Alzheimer's Disease and it is currently in phase IIb trials[60]. Furthermore, PBT2 has been also investigated as a therapeutic agent in Huntington's disease[61] and has recently completed phase IIa clinical trials. The action mechanism of this family of compounds has been investigated and experimental evidence suggests that they could remove copper and other metals from extracellular amyloid.[62] CQ or PBT2 encounter the extracellular pool of metals that are in a dissociable equilibrium with Aβ; e.g. in senile plaques and oligomers, CQ and PBT2 bind the metals (ionic copper or zinc) and facilitate plaque dissociation. The dissociate metal ions may be in a ternary complex with the drug itself or in a complex with dissociated Aβ. These complexes are taken up by neighboring cells, where the elements are separated. The metal ions (copper or zinc) can activate phosphoinositol 3-kinase and JNK and then MMP2 and 3, inducing peptidolytic degradation of Aβ (Figure 10).[23]

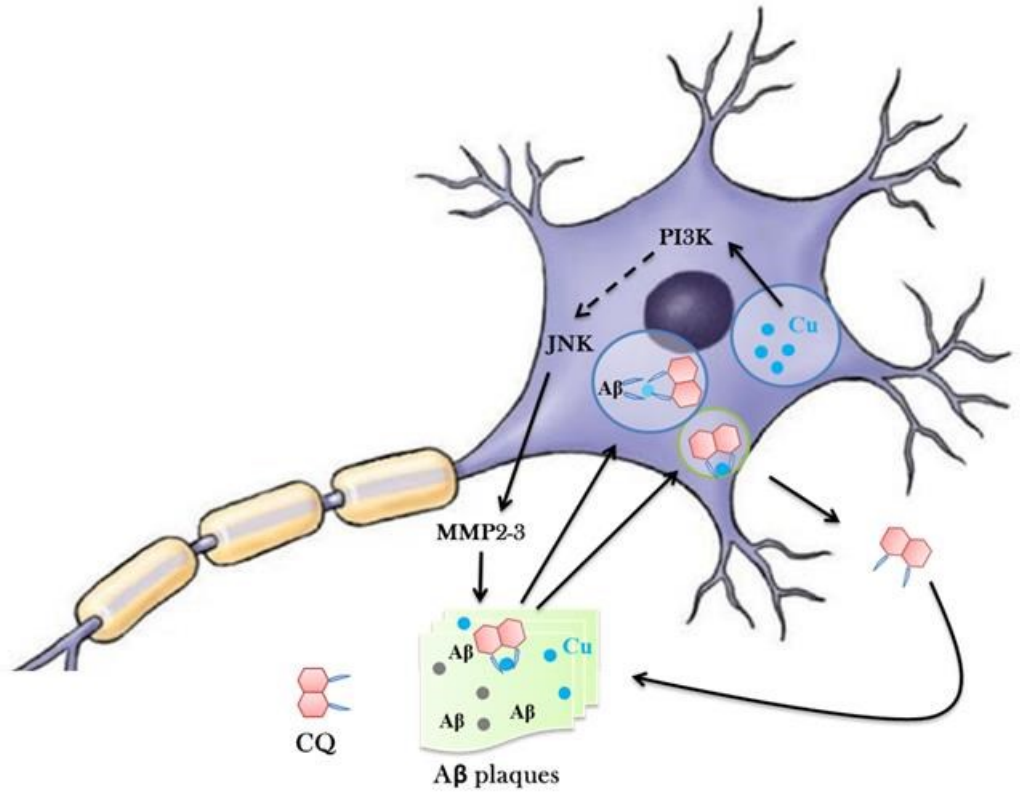

Figure 10. Hypothesized action mechanism of CQ. The figure shows only copper and CQ for clarity, but this mechanism has been also proposed for zinc and PBT2.

Moreover, as for CQ, it directly induces cell death in tumor cells at micromolar concentrations. Currently, CQ is in phase I clinical trial in patients with hematologic malignancy, such as leukemia, myelodysplasia, non-Hodgkin's and Hodgkin's lymphoma and multiple myeloma.[63]

For CQ and other OHQs it has been reported that the interaction with Cu^{2+} ions is a prerequisite for anticancer activity[64] and, although the mechanism of action is not completely understood, experimental evidence suggests that OHQs act as anticancer agents as they are 20S proteasome inhibitors in the presence of Cu^{2+}.[65,66] CQ induces apoptosis in cancer cells through a caspase-dependent apoptotic pathway (Figure 11).[67]

Nevertheless, other mechanism have been reported to explain the cytotoxicity of CQ, such as the induction of the cytoplasmatic clearance of X-linked inhibition of apoptosis protein (Figure 11)[68] and the induction of DNA double strand-breaks.[69]

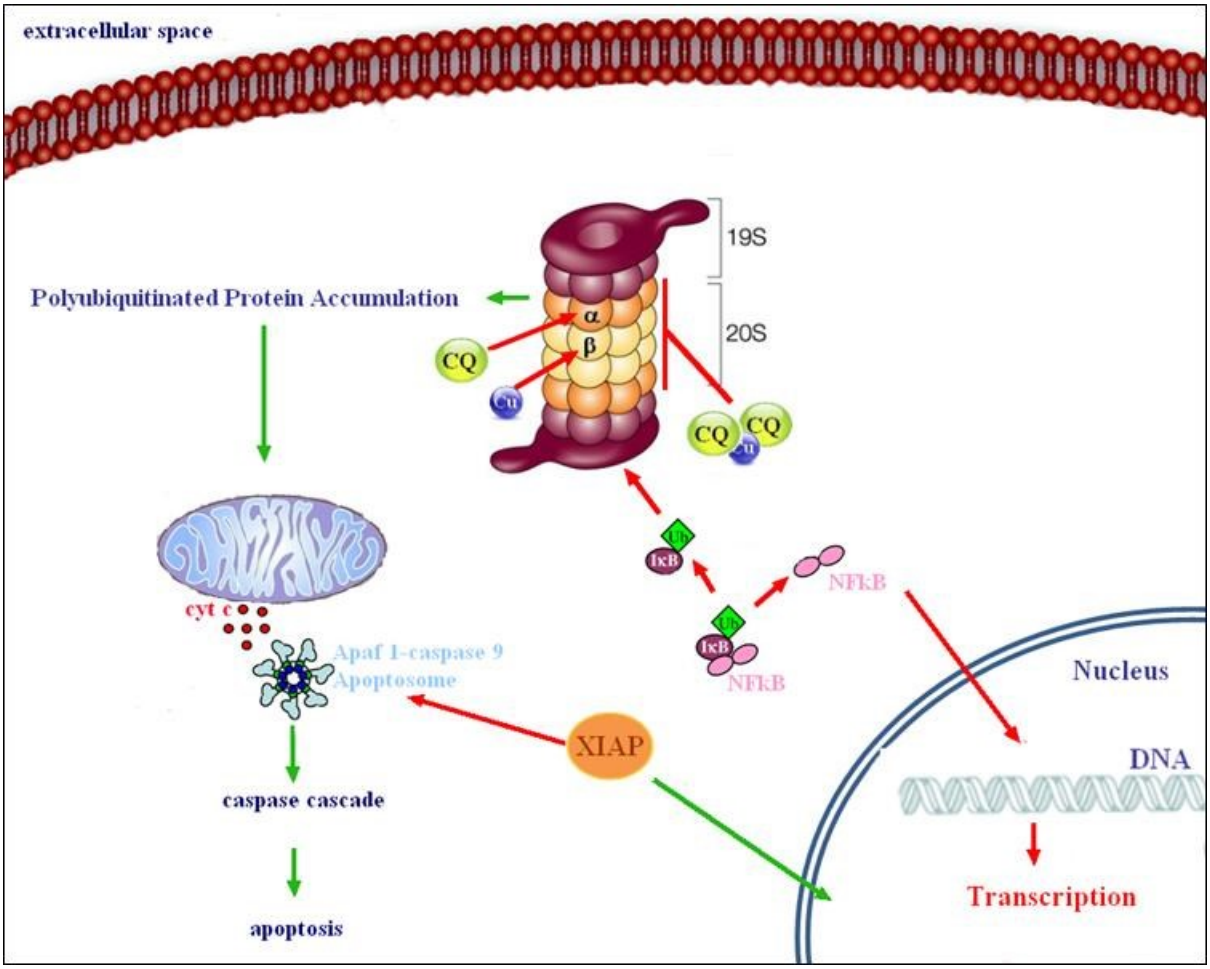

Figure 11. Clioquinol inhibits the proteasome through metal dependent and independent mechanisms. The proposed mechanisms include: (i) Cu^{+} or during its reduction from Cu^{2+} to Cu^{+}, copper interacts with thiol and amino groups outside the active site of the proteasomal enzyme and thereby induces a conformational change in the protein structure causing inhibition of the proteasomal enzymes; (ii) Clioquinol directly inhibits the enzymatic activity of the proteasome by binding to regions of the alpha subunits outside of the active site; (iii) Clioquinol forms a 2:1 complex with copper and this complex inhibits the enzymatic activity of the proteasome.

1.5 Targeting

Although metal chelating agents represent a necessary therapeutic strategy in metal overload diseases such as WD and hemochromatosis, they are associated with severe side-effects. Long-term use of strong chelators that are not selective (e.g. DFO), can be anticipated affecting the homeostasis of numerous biometals and perturb normal physiological functions of essential metal-requiring biomolecules (e.g. metalloenzymes). The ability to target tissues

selectively, through the coupling of chelation agents with targeting moieties, may minimize the toxicity of metal binding agents and enhance their effectiveness.

The concept of site-selective drug delivery or drug targeting has evolved since Nobelist Dr. Paul Ehrlich launched his idea of the "magic bullet", an active chemical substance delivered only at the disease site and left the healthy tissues unharmed, over a century ago. Since then, the goal to develop safer therapeutical agents[70,71] that are efficiently and selectively delivered to the desired site of action without affecting non-target cells has begun an attractive and actively pursued objective in pharmaceutical research.

For example, Mints *et al* have proposed to specifically target intracellular copper in liver because it is the main organ where copper accumulates in WD.[16] Since the pool of intracellular copper is in the +1 oxidation state, they have designed a prochelator that releases the Cu^+ chelator only once inside the reducing medium of the targeted cells. This strategy is represented in Figure 12.

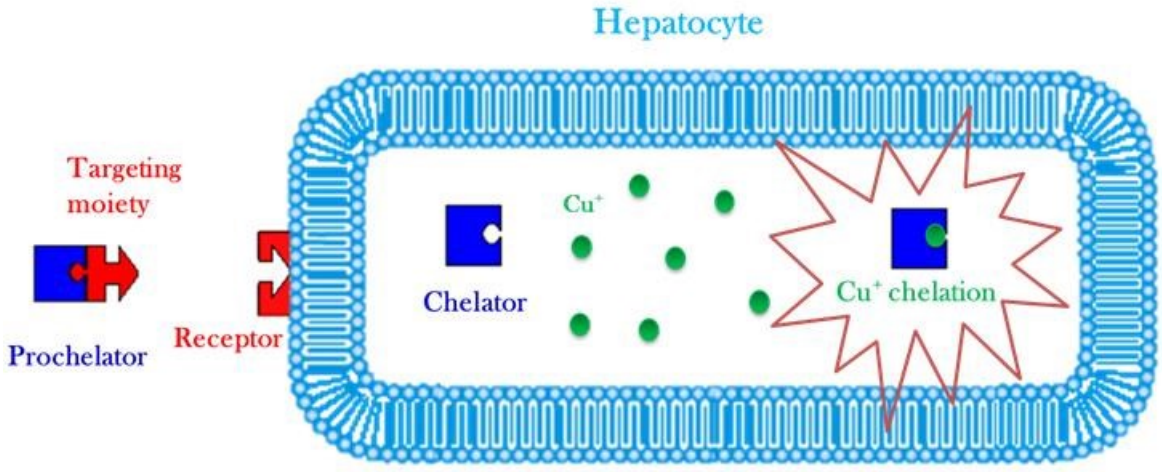

Figure 12. Cu^+ prochelators for the selective targeting of hepatocyte.

In prodrug approach, targeted drug delivery can be obtained by site-specific drug bioactivation or site-directed drug delivery. With site-directed drug delivery, the intact prodrug is primarily transported to the action site; for example, when prodrug is applied directly to the target organ (ocular and dermal drug delivery). Site-directed drug delivery after systemic administration constitutes very challenging task due to various unpredictable barriers in the body, but has demonstrated some success, for example, in brain delivery.[72] With site-specific bioactivation, the prodrug can be widely distributed through the body, but undergoes

bioactivation and exerts its own activity primarily at the desired site. The active agent is typically detached from a carefully designed promoiety, which can act as tissue/organ-selective carrier, or results from a prodrug itself after series of biotransformations in situ.[73]

1.5.1 Prodrug therapy and targeting strategies

Site-selective drug delivery has originated from cancer chemotherapy where drugs are highly reactive and poorly separate their cell-destroying action between healthy cells and tumor cells. Many antitumor drugs possess narrow therapeutic index, indicating that there is only minor difference between the dose needed for therapeutic response and the dose causing potentially life-threatening hazardous adverse effects to the patient.

To overcome the drawbacks of conventional cancer chemotherapy, it has been recently realized that the selectivity of drugs can be substantially increased by conjugating (directly or by using a complex drug delivery system) an anticancer drug with a targeting moiety, which provides two major functional roles. First, it directs the anticancer drug specifically to tumor cells, enhancing drug accumulation in tumor and therefore preventing adverse side effects. Second, it works as a penetration enhancer increasing the drug influx by tumor cells. In these cases non-cytotoxic prodrugs are designed to locally deliver the antitumor agent by tumor-specific activation. This may occur by hypoxic environment of solid tumors, by pH differences, by tumor-associated proteases or by enzyme selectively present in the tumor. In the case of tumor-associated enzyme activation, the active enzyme may be present in the tumor, like in PMT (prodrug monotherapy),[74,75] or targeted to the tumor site such as ADEPT (antibody directed enzyme prodrug therapy). The ADEPT and PMT approaches have been widely investigated as means to deliver drugs specifically to cancerous tissue and have shown promise in both animal studies and clinical trials.[76,77]

1.5.2 Prodrug monotherapy (PMT)

In PMT, prodrugs are designed for direct activation or recognition by tumor-associated factors (a phenotypic difference between tumor and normal tissue). These factors can be a low pH, the overexpression of certain enzymes or receptors in cancer, or the existence of regions in solid tumor where low oxygen tension is present and thereby there is an increased activity of reductive enzymes. In the past, a great number of carrier-linked prodrugs has been

developed with enzyme-specific substrates such as peptides or sugars. An overview of enzymes overexpressed in tumors and examples for respective substrates is given in Table 2.

Because the enzymes that are used for prodrug activation are also present in normal cells, activation of an enzymatically cleavable prodrug can be observed in healthy tissue. This stresses the need to improve tumor uptake through active or passive targeting and to characterize the overexpression of the respective enzymes in the individual tumor.

Table 2. Overview of enzymes that are overexpressed in tumors.

Enzyme	Tumor	Function	Substrate	Ref.
β-galactosidase	Breast, colon	Hydrolysis of galactose moieties	β-Galactose moieties	78
β-glucuronidase	Breast, pancreas	Hydrolysis of glucuronide moieties	β-Glucuronide moieties	79-81
Carboxylesterases		Hydrolysis or transesterification of drugs	Ester or carbamate moieties	82,83
α-mannosidase	Breast, colon	Hydrolysis of mannose moieties	mannose moieties	78
Chatepsin B Chatepsin L	Breast, gastric, colon	Lysosomal degradation of proteins	Arg-Arg, Ala-Leu, Gly-Leu-Phe-Gly.	84
Chatepsin D	Breast, gastric, ovary	Degradation of extracellular matrix	Phe-Ala-Ala-Phe(NO2)-Phe-Val-Leu-OM4P	85
Plasmin		Degradation of blood plasma proteins	D-Ala-Phe-Lys, D-Ala-Trp-Lys, D-Val-Leu-Lys	86
Matrix Metalloproteases		Degradation of extracellular matrix and collagens	Ac-Pro-Leu-Gly-Leu, Gly-Pro-Leu-Gly-Ile-Ala-Gly-Gln	87,88

1.5.3 Two-step prodrug therapies (ADEPT)

Enzyme-activating prodrug therapy is a two-step approach. In the first step, a drug-activating exogenous enzyme is targeted or expressed in tumors. In the second step, a nontoxic prodrug, a substrate of the exogenous enzyme, is administered systemically.

Currently, delivery methods for an enzyme/prodrug strategy can be divided into two major classes:

✓ delivery of genes that encode prodrug-activating enzymes into tumor tissues (GDEPT, VDEPT, etc.);

✓ delivery of active enzymes conjugated to a vehicle that is capable of target tumor tissues (such as an antibody in ADEPT, ligand in LIDEPT).

This introduction focuses only on antibody-directed enzyme prodrug therapy ADEPT (Figure 13).

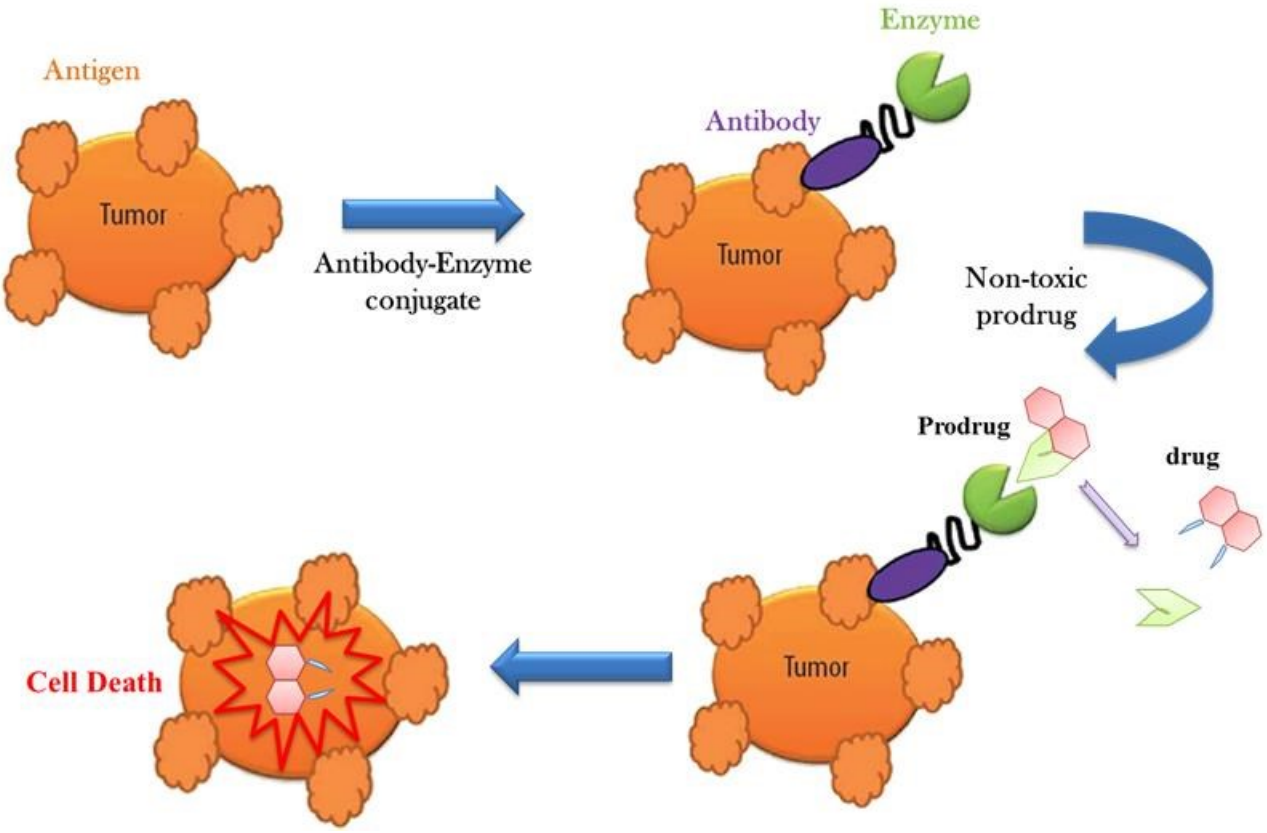

Figure 13. Scheme of antibody-directed enzyme prodrug therapy (ADEPT).

In this approach, a monoclonal antibody is initially employed to selectively deliver an enzyme (for example β-galactosidase) to the tumor cells, which subsequently converts an inactive prodrug to active drug at tumor site. Thus, the selective activation of the prodrug at the tumor site would result in improved antitumor activity with minimal side effects.[89]

Monoclonal antibodies have been used to deliver potent toxins and radionuclides to tumors. Many successful conjugates such as Mylotarg and Zevalin for the treatment of leukemia and

B-cell lymphomas have been developed.[90] However, there are no clinically approved immunoconjugates for the treatment of solid tumor because they suffer from insufficient density of antigens on malignant cells and low cellular internalization. ADEPT approach offers two advantages over chemoimmunoconjugates. The first is the amplification effect since one molecule of enzyme-antibody conjugate, acting as a catalyst, is able to activate a large number of prodrug molecules. The second is the induction of the Bystander effect. The latter occurs when not only the tumor cells that are bound to the antibody enzyme conjugate but as well as the neighboring cells antigen are killed (Figure 14).

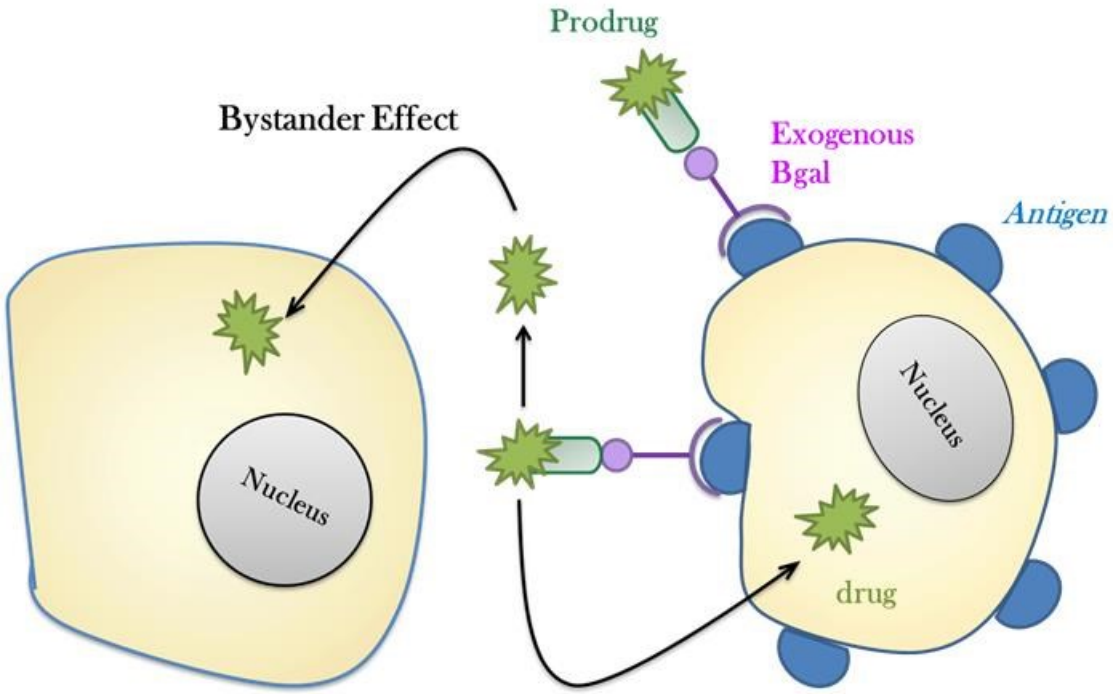

Figure 14. Bystander effect: cells that are killed because they are in close proximity to the targeted cells, rather than being targets themselves.

There are a several general considerations for ADEPT.

The requirements for the prodrug are low cytotoxicity, suitable K_m and k_{cat} parameters and good pharmacokinetic properties. Furthermore, the prodrugs have not to be substrates for endogenous enzymes. Instead, high cytotoxicity and diffusion across cell membrane are pivotal features of the released active drugs.

The target antigen should be either expressed on the tumor cell membrane or secreted into the extracellular matrix of the tumor, and the use of a high affinity monoclonal antibody is

very important. The enzyme should be able to exert its optimal activity at a pH close to that of the tumor extracellular fluid. Because antibody-enzyme conjugate may be immunogenic, circulating host anticonjugate antibodies may interfere with treatment. Ideally, the enzyme system should not have a human homologue to avoid prodrug activation outside the tumor site. However there are many clinical limitations associated with ADEPT. For example, it is difficult to generate effective quantities of active drug since the levels of exogenous enzyme are low. Other drawbacks of ADEPT include cost and difficulties related to development and purification of antibodies, immunogenicity of antibodies, accessibility of tumor to the enzyme/antibody conjugate and the conversion of prodrugs in healthy tissues.[91] For these reasons, a more convenient strategy could be the use of an already present enzyme (PMT).

1.6 Glycoconjugation: approaches to targeting

A good drug is a target-specific agent; it would have high efficiency and few, if any, side effects. Target specificity also means recognition, and this is where carbohydrates come in. While many drugs contain carbohydrates as part of their molecules, other non-saccharidic drugs can be guided by them. Carbohydrates' role is that they provide a guidance mechanism for sick cells, enabling drugs to selectively arrive there.

A few dozen FDA-approved drugs contain carbohydrate moieties as part of their structures. Typically, removal of the sugar eliminates the therapeutic value of the drug.

Among saccharidic drugs there are monosaccharide conjugates that include four groups of systems:

- Anthracycline antibiotics and agents such as Doxorubicin, Daunorubicin, Epirubicin and Idarubicin (Figure 15);
- Nucleotides, nucleosides and their analogs such as Fludarabine Phosphate, Stavudine, Adenosine, Ribavirin;
- Polyene: Amphotericin B;
- Other agents: Etoposide, Lincomycin, Clindamycin, Pentostatin.

The first group (Figure 15) includes cytotoxic anthracycline antibiotics of microbial origin (Doxorubicin and Daunorubicin) or their semi-synthetic derivatives (Epirubicin and

Idarubicin). These drugs are potent neoplastic agents consisting of a naphthacenequinone nucleus linked through a glycosidic bond at ring atom 7 to an amine sugar, daunosamine.

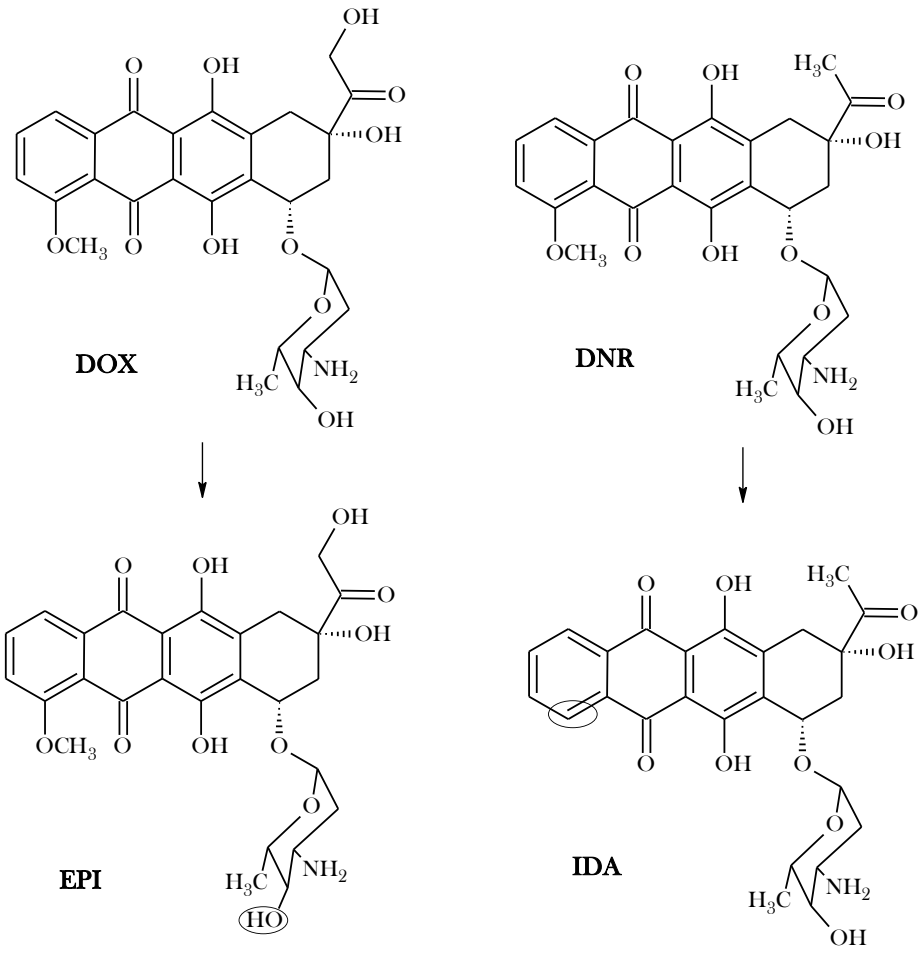

Figure 15. Structures of Doxorubicin (DOX), Daunorubicin (DNR), Epirubicin (EPI) and Idarubicin (IDA).

The second group of monosaccharide drugs is represented by nucleotides and nucleosides and their synthetic analogs. Among them, there are potent neoplastic agents, such as Fludarabine Phosphate (fluorinatedarabinofuranosyladenine 5′-monophosphate) and Gemcitabine (2′-deoxy-2′,2′-difluorocytidine, whose metabolic products inhibit DNA synthesis. The third group, polyenes, is represented by Amphotericin B, which is an antifungal antibiotic of microbial origin. Amphotericin B is a 3-amino-3,6-dideoxy-β-D-mannopyranosyl derivative of an octahydroxypolyene containing seven carbon-carbon double bonds in a macrocyclic 38-member ring.

Finally, the fourth group of monosaccharide drugs contains a number of different compounds, among them Etoposide. It is an anticancer agent which belongs to the topoisomerase inhibitor class (Figure 16).

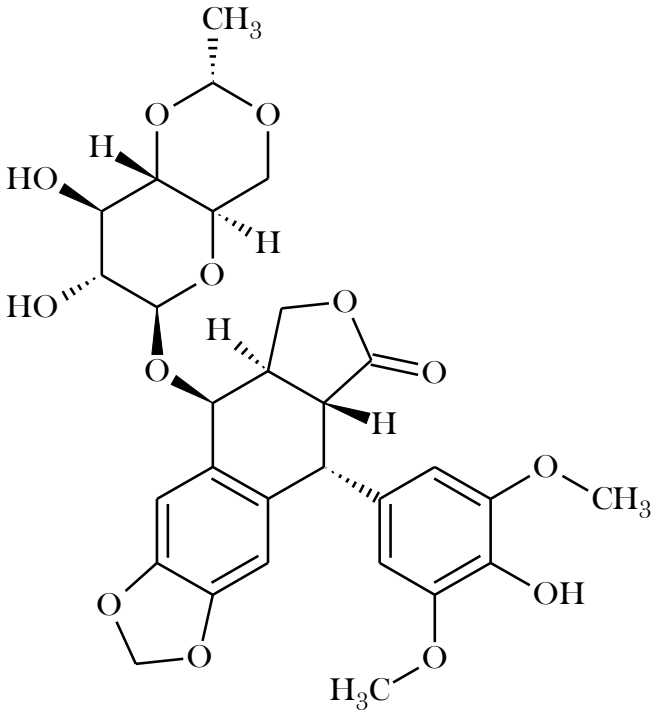

Figure 16. Structure of Etoposide (semi-synthetic β-D-glucopyranoside derivative of podophyllotoxin).

An essential component of these drugs is their sugar moiety. Removal of the sugar residue typically leads to elimination of the drug therapeutic properties. On the other hand, addition of a certain sugar moiety sometimes enhances the recognized potential of the drug at the target level.

For these reasons, it has recently developed the concept of saccharides/anti-tumor conjugates. These compounds contain sugar moieties that allow the binding of the anti-tumor drugs with specific receptors such as glucose transporters or galectin, which transfer the drugs to the tumor cells. The rationale behind the development of glucoconjugates resides on the glucose avidity and elevated glycolysis of tumor cells. Whereas the galactoconjugates could be recognized by lectins which are overexpressed in a number of tumors.[92]

Glucose (Glc) and galactose (Gal) are not the only saccharidic compounds that are used to target cancer cells. Prodrugs of the glucuronic acid that might be activated by glucuronidases

are particularly appealing because the levels of glucuronidase have been reported to be elevated in different tumors. It is possible, therefore, that glucuronide prodrugs may be preferentially activated in tumors. Moreover, glucuronidases have also been used in ADEPT strategy.

Disaccharides (lactose) and oligosaccharides are also used in targeting strategies. Cyclodextrins are also noteworthy among the oligosaccharides applied for targeting.

1.6.1 Gluconjugates

Glucoconjugate approach has been used in an effort to enhance targeting of analgesics,[93] dopamine derivatives,[94] anti-cancer agents,[95] and anti-Alzheimer drugs.[96,97]

Glucoconjugates could target tumors exploiting glucose avidity of cancer cells. It is now clear that the majority of tumor cells *in vivo* and transformed cells *in vitro*, exhibit elevated levels of glucose transporter and elevated rates of glycolysis. This phenomenon was observed for the first time by Otto Warburg.[98] Furthermore, glucose-conjugated compounds can enhance uptake of a drug in cancer cells[99] as tumor cells require a significant amount of glucose and this demand is met by the high density of hexose transporters GLUTs, a family of membrane proteins. Cancer cells generally express higher levels of GLUTs than normal cells. The ratio of GLUT expression in malignant *versus* normal cells is about 100-300.[100] This is because the efficiency of ATP production in normal cells does not satisfy the high energy requirements of cancer cells, so GLUTs are overexpressed in cancer cells to improve glucose uptake. This differential rate of glucose uptake has been used in positron emission tomography (PET), whereby 2-[18F]-2-deoxy-D-glucose (FDG) accumulates in cancer cells and indicates the tumor.[101] It has been reported[102-104] that β-glucosidases have a crucial role in the activation of the glycosylated prodrugs to release the active aglycone moieties. The level of expression of these enzymes into cancer cells remains an essential point to clarify. A good balance between the β-glucosidase activity and the transmembrane glucose transporters may ensure the right and effective activation of glycosylated prodrugs.[105] In practice, high cellular β-glucosidase levels might be effective only when transport proteins are expressed as well.

It has been recently reported the synthesis and preliminary antiproliferative activity of potential DNA bisintercalators that include quinoline and glucose moieties.[106] Binding

experiments have suggested that these compounds could bind DNA by intercalation and glucose moiety could regulate their interaction with DNA. Preliminary MTT assay showed a good anticancer activity of these compounds but experiments of nuclear permeation were not performed.

β-glucosides of curcumin, perillyl alcohol and diethylstilbesterol were also tested in cytotoxicity enzymatic cleavage studies in order to demonstrate the involvement of β-glucosidase and caspases in glucoconjugate antiproliferative activity in colon cancer cell lines.[107] Thus, following glucoconjugate entrapment within cancer cells, they are presumably subject to hydrolysis by specific β-glucosidases to liberate the active aglycone, that exerts its anti-cancer activity.[107]

The glucoconjugates have been also used by various groups to impart elevated brain uptake exploiting the glucose transport system in the BBB (Figure 17).[108]

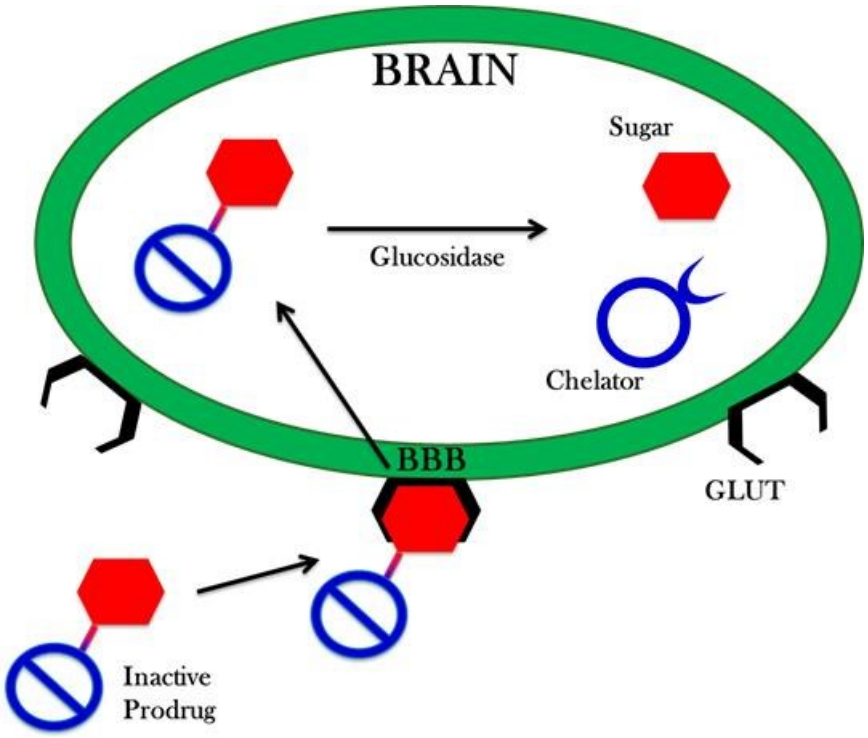

Figure 17. Deferiprone glucoconjugates: possible mechanism of action.

Orvig' s group has recently reported glucosylated tetrahydrosalens (Figure 18) as potential drugs for Alzheimer's therapy.[109,110] These derivatives can be divided in two compound classes: one in which the metal binding site is free[110] and another one in which metal binding

or antioxidant functionality is masked.[109] The molecule in this form is referred to as a prodrug and it requires the cleavage of the carbohydrate moiety to exert its activity. These derivatives are very promising as antioxidant agents and Aβ aggregation inhibitors.

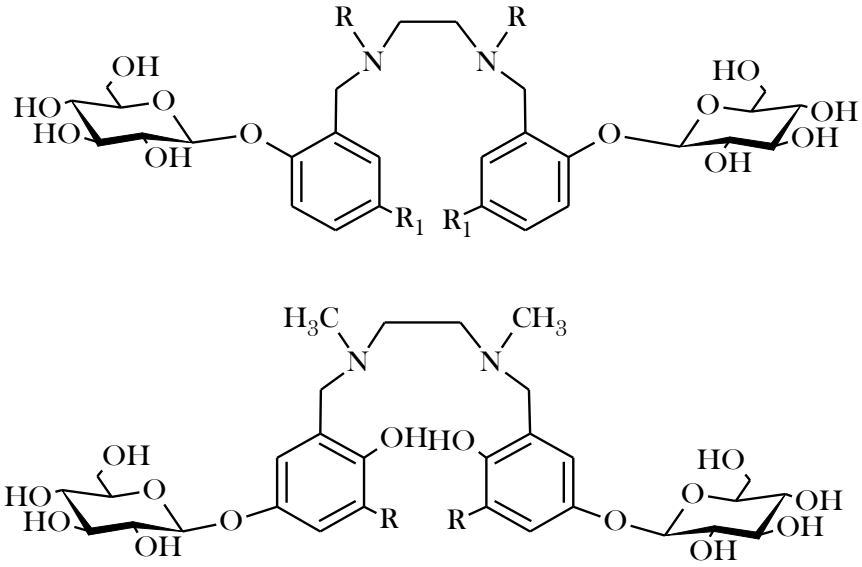

Figure 18. Glucosylated tetrahydrosalens.

The same approach was utilized to design multifunctional pyridinone ligands (Figure 19).[97,111]

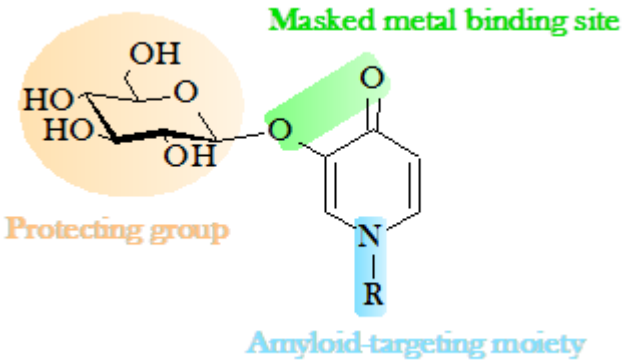

Figure 19. N-aryl-substituted 3-(β-D-glucopyranosyloxy)-2-methyl-4(1H)-pyridinones as agents for Alzheimer's therapy.

1.6.2 Galactoconjugates

There would appear to exist at least two possible rationales for design and use of galactoconjugates: lectin targeting and ADEPT approach.

The concept of lectin-mediated specific drug delivery was proposed by Woodley and Naisbett in 1988. Lectin-based targeting of Drug Delivery Systems (DDSs) may be accomplished *via* two mechanisms: direct lectin targeting and reverse lectin targeting (Figure 20). In the first approach, the DDS has carbohydrate moieties that are recognized and internalized by endogenous cell surface lectins.[112] The reverse lectin targeting utilizes exogenous lectins that recognize endogenous carbohydrate moieties on glycolipids and glycoproteins.[113]

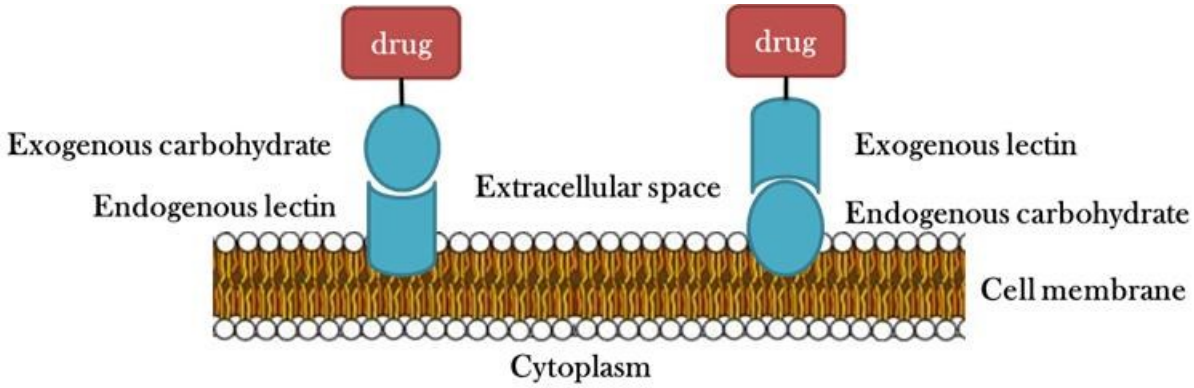

Figure 20. Two types of lectin targeting of DDS might be utilized: direct or reverse lectin targeting. The first approach has found major application in antiviral therapy, immunoactivation, enzyme replacement therapy and gene therapy.

The interest for lectins derives from numerous observations that present a fascinating opportunity to use carbohydrates as a targeting tool for the specific delivery of cytotoxic drugs in cancer therapy. Individual members of the galectin family are clearly implicated in physiological and pathological mechanisms such as inflammation, angiogenesis, immunity[114,115] and cancer.[116,117] The galectins belong to the lectin superfamily. They are β-D-galactoside binding proteins for which fourteen members have been identified in mammals. Natural small saccharides, such as β-D-galactose, D-lactose and N-acetyl-lactosamine, bind to galectins and can inhibit their biological activity. N-acetyl-lactosamine is the most potent natural disaccharide inhibitor of galectin-3 (Figure 21).[118]

Figure 21. High Resolution X-Ray Structure of Carbohydrate Recognition Domain (CRD) of Human Galectin-3 in complex with N-acetyl-lactosamine (LacNAc). hGal-3 is unique because it is a chimera with an N-terminal that is not directly involved in carbohydrate binding. It is localized in the cytoplasm, nucleus and/or extracellular space. It has been shown that h-Gal-3 can be absorbed by cells.[119]

Galectins-1 and -3 are the most extensively studied proteins of the family in the field of cancer biology. Galectin-3 is known for its role in tumorigenesis and progression through regulating cell proliferation, apoptosis, cell adhesion, invasion, angiogenesis and metastasis. In particular, neoplastic progression has been associated with increased galectin-3 expression in malignancies of the head, neck, gastric or anaplastic large cell lymphoma tumors, thyroid and central nervous system (CNS) tumors. Galectin-3 was also shown to have anti-apoptotic effects in galectin-3 cDNA transfected human T cell leukemia Jurkat E6-1 cells.[120] Furthermore galectin-3 was previously shown to play a role in endocytosis of various glycoconjugates.[121,122] Recently, a comprehensive profile of all known human galectins in tumor cell lines from various sources has been published.[123] These data indicate that additional binding sites other than galectin-3 (e.g., galectin-1, -4, -7, or -8) could also be involved in the recognition process. For example, galectin-1 is overexpressed in pancreatic ductal adenocarcinomas compared to normal tissue.[124,125] It is also expressed in the invasive

compartments of tumors in relation to their aggressiveness.[126] Despite the established role of galectins in numerous diseases, there is no clinically proven treatment that targets these proteins, although a number of clinical trials were launched with its inhibitors.[127] However, galectins play an important role as potential biomarkers that may help to identify the disease and serve as a therapeutic target.

Galactoconjugates have been used to target hepatocytes, exploiting the recognition with asialoglycoprotein receptor (ASGP-R), a hepatic lectin expressed exclusively at the surface of Kupffer and parenchymal liver cells. The ASGP-R is a membrane protein randomly distributed over the plasma membrane and is responsible for the clearance of desialylated galactose-terminal glycoproteins from the circulation through receptor-mediated endocytosis. This lectin recognizes terminal galactose (Gal) and, with a higher affinity, N-acetylgalactosamine (GalNAc).

The affinity between lectins and simple monosaccharides is not high (Kd ≈ 0.1–1 mM) but it can be increased (100–1000-fold) by multivalent interactions (cluster glycoside effect). Therefore, this strategy has been applied for the targeting of a Cu^{+} chelating agent to hepatocytes for the treatment of WD. [128129]

Doxorubicin has been conjugated at its sugar part by linking it to a stable D-galactose residue, which was chosen for the important role that galectins play in tumor.[130] The best of six synthesized derivatives, in which D-galactose had the α-anomeric configuration and the two sugar residues were linked *via* 1→6 bond was named Doxo-Galactose. It had a lower toxicity and a higher efficacy compared to the parent doxorubicin when tested on mice bearing lymphocite leukemia P-388. Doxo-Galactose showed 20 to 60 times lower cytotoxicity, using different cell lines, compared to that by doxorubicin.

Non toxic prodrugs and enzyme conjugates have been pursued in more complex prodrug strategies such as PMT and ADEPT (antibody-directed enzyme prodrug therapy).

Lactose and Galactose have been recently conjugated with Geldanamycin (GA), a known anticancer drug. These conjugates can be potentially used for antibody-directed enzyme prodrug therapy (ADEPT). Galactose-GA and Lactose-GA conjugates remained inactive in the absence of exogenous *β*-galactosidase.[131] However, the anticancer activity of galactose-GA conjugate increased by 3- to 40-fold when incubated with β-galactosidase.

These data support the hypothesis that carbohydrate conjugation of GA through the C-17 position produces inactive prodrugs. The inactive carbohydrate-GA prodrugs can be enzyme-specifically activated by β-glucosidase or/and β-galactosidase.

Glycoside prodrugs of daunorubicin (DNR) have been also synthetized and studied by de Graaf *et al.* (Figure 22).[132]

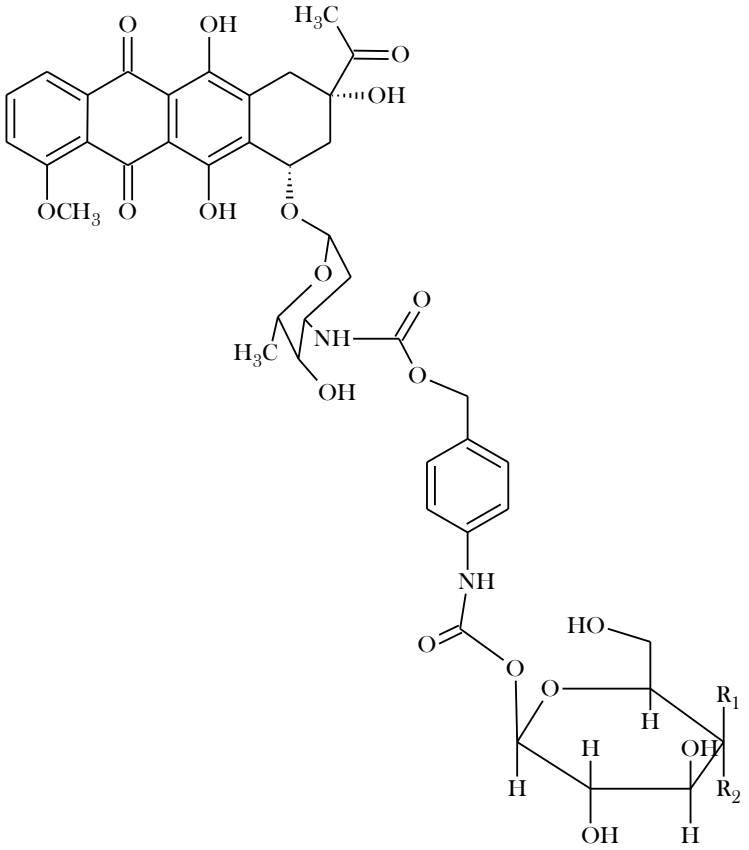

Figure 22. Glycoside prodrugs of Daunorubicin.

In this study, the treatment of OVCAR-3 cells with human β-glycosidase and DNR-Glucose or DNR-Galactose resulted in, respectively, 86 and 81% cell growth inhibition, while the prodrugs alone inhibited growth to only 19 and 1%. Clearly, the prodrugs inhibit cell growth more efficiently in the presence of the enzymes. And so the authors concluded that the endogenous intracellular β-glycosidase is not available for extracellular prodrug activation. This is the reason that renders this compound suitable for ADEPT.

1.6.3 Cyclodextrin conjugates

CyDs are cyclic oligomers of D-(+) glucopyranosyl units linked by 1,4 glycosidic bonds (Figure 23). The natural α-, β- and γ- cyclodextrin consist of six, seven, and eight glucopyranose units, respectively. The OH groups are disposed outside, the primary OHs are around the narrow rim and the secondary 2,3 OHs around the wider rim (Figure 23).

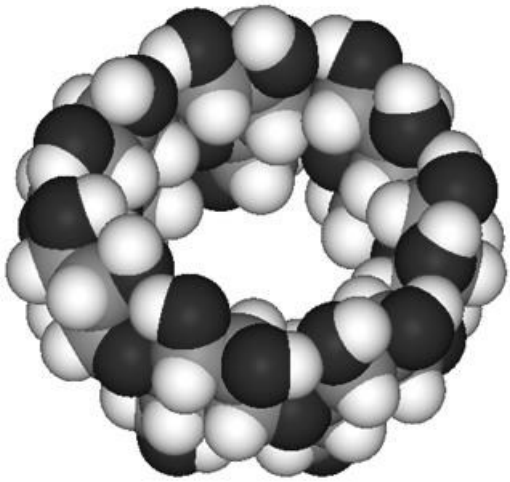

Figure 23. Space filling model of β-cyclodextrin.

The intrinsic nature of CyDs provides them an external hydrophilic surface and a hydrophobic cavity. Cyclodextrin molecules are relatively large with a large number of hydrogen donors and acceptors, and are consequently poorly absorbed through biological membranes. The α- and β-cyclodextrin cannot be hydrolyzed by human salivary and pancreatic amylases, but all three are subjected to fermentation by the intestinal microflora. Hydrophilic cyclodextrins are non-toxic at low to moderate oral dosages.

The presence of the hydrophobic cavity gives the ability of cyclodextrins to form inclusion complexes. As a result, these molecules have found a number of applications in a wide range of fields for example in pharmaceutical field as solubilizers, stabilizers. Furthermore, several cyclodextrins are used extensively to remove cholesterol from food and cultured cells[133] and in 2010, the Food and Drug Administration (FDA) approved the intrathecal and intravenous administration of hydroxypropyl β-cyclodextrin (HPβ-CyD) in six-year-old twin girls suffering from NPC.

CyD-drug conjugates, in which a drug is covalently bound to CyD, have been extensively investigated. The enhanced stability of CyD-drug conjugates is advantageous for oral administration because of a greater chance to cross the stomach and small intestine. However, drug release will be triggered by enzymatic degradation of CyDs in the colon.[134] CyD-drug bioconjugates are reported in the literature as site specific carriers for the colon, being very promising as anti-inflammatory pro-drugs for colon diseases. Modified CyDs can be obtained by functionalizing the OH groups.

Attachment of amino acids,[135-142] peptides[143-149]and aromatic rings [150-157] to cyclodextrins has been reported. The hydrophobic nature and the size variability of the cavity together with the arrangement of the attached molecules have been employed in other studies to obtain a variety of end-products, including enzyme mimics. In addition, the cyclodextrin cavity constitutes a typical scavenger of the OH radicals as reported in the literature[158-160] and could cooperate with the other antioxidant activities shown by attached moieties, rendering these bioconjugates potentially able to react with a cocktail of ROS species.

An example of CyD conjugates with anticancer applications is IT-101(Figure 24).[161] This latter is a polymeric nanoparticle comprised of cyclodextrin-poly(ethylene glycol) copolymer (CDP) conjugated to Camptothecin (a potent anticancer drug), currently in Phase 2a development. IT-101 preclinical and clinical studies confirm that CDP can address not only solubility, formulation, toxicity, and pharmacokinetic challenges associated with administration of CPT, but more importantly, can impart unique biological properties that enhance camptothecin pharmacodynamics and efficacy.

Furthermore, it has been recently reported a novel versatile porphyrin-CyD system suitable for the combined cancer therapy, which is based on the effective drug binding as inclusion complexes with CyD and on known tumor targeting by porphyrin macrocycles.[162] The system allows very efficient combination of photodynamic therapy and chemotherapy. It has been also demonstrated that these conjugates cross the membrane cells.

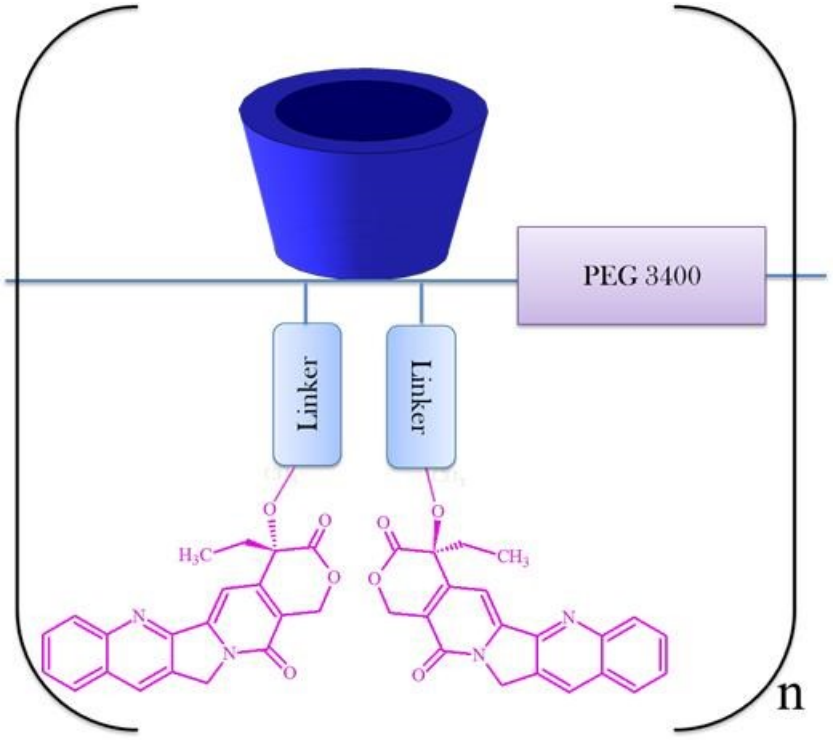

Figure 24. Scheme of IT101, a nanopharmaceutical system comprised of camptothecin conjugated to a linear, cyclodextrin-poly(ethylene glycol) (CD-PEG) copolymer and formulated into nanoparticles.

2. AIMS OF THE RESEARCH

Neurodegenerative diseases and cancer have long been viewed as among the most enigmatic and problematic issues in biomedicine. It is becoming clearer and clearer that the major processes involved are multifactorial in nature, caused by genetic, environmental, and endogenous factors.

The multiple facets of cancer have been well-documented; for example, the presence of elevated levels of copper and oxidative stress. These latter aspects are hallmarks of a vast range of malignancies and thus they could be targets of treatment approaches. Furthermore, the lack of tumor selectivity and limited antitumor activity are the two main limits in the cancer treatment. Finally, targeting one system in the complex cancer cascade may not be sufficient in controlling and/or inhibiting cancer growth.

The design of an appropriate prodrug to selectively deliver a multi-target-directed drug has been one of the primary efforts of this research.

The precise mechanisms responsible for triggering neurodegenerative disorders remain unclear; however, some neurodegenerative diseases (including AD, PD, HD, NPC and ALS) share some multifactorial pathogenic mechanisms and general pathways can be recognized: protein misfolding and aggregation, oxidative stress and free radical formation, metal dyshomeostasis, mitochondrial dysfunction (Figure 25).

The critical involvement of metal ions in oxidative stress, misfolding and aggregation and mitochondrial impairment plays a role in many neurodegenerative diseases, particularly AD. As such, metal ions represent as a promising therapeutic target and they could be a starting point to hit multiple targets.

Considering the multifactorial nature of diseases, it is becoming more and more evident that the next generation of therapies must have multiple functions to combat multiple mechanisms of disease progression.

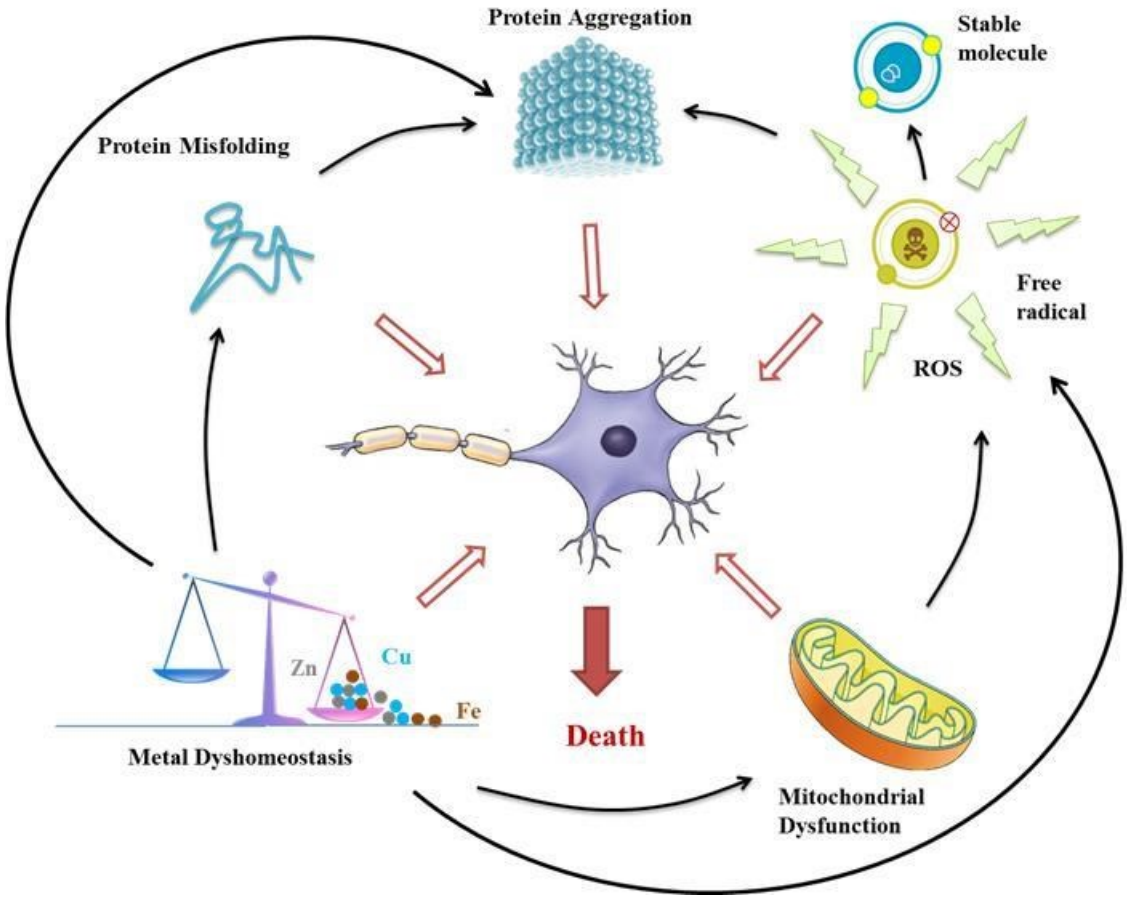

Figure 25. General pathways recognized in neurodegenerative disorders.

Multicomponent therapeutic strategy, which incorporates two or more active ingredients in one drug has been successfully used in current drug cocktails (e.g. chemotherapy). More recently, a new approach has been posited: one-compound-multiple-targets strategy.

Creating multifunctional molecules to interfere with different key target points of neurodegeneration and cancer is the main aim of this research.

OHQ has been chosen as basic molecular scaffold to build selective prodrugs and multifunctional metal-binding compounds. OHQ is an excellent starting point for rational drug development because of its high affinity for Cu^{2+} and Zn^{2+}, low affinity for other common biological ions (such as sodium, potassium, calcium and magnesium) and its antioxidant properties. Furthermore, OHQ structure is amenable to derivatization by different routes, which can improve the chemical-physical properties of the drug.

The research of the best synthetic routes to obtain OHQ bioconjugates has been one of the first purpose of this thesis.

The synthesis, characterization and biological evaluation of new covalent glycoconjugates with OHQs have been the focus of this research (Figure 26). Glycosylation could be a successful strategy in order to improve several features of OHQs. Saccharidic moiety could ameliorate solubility and biological activity of these systems and selectively deliver them in their site of action.

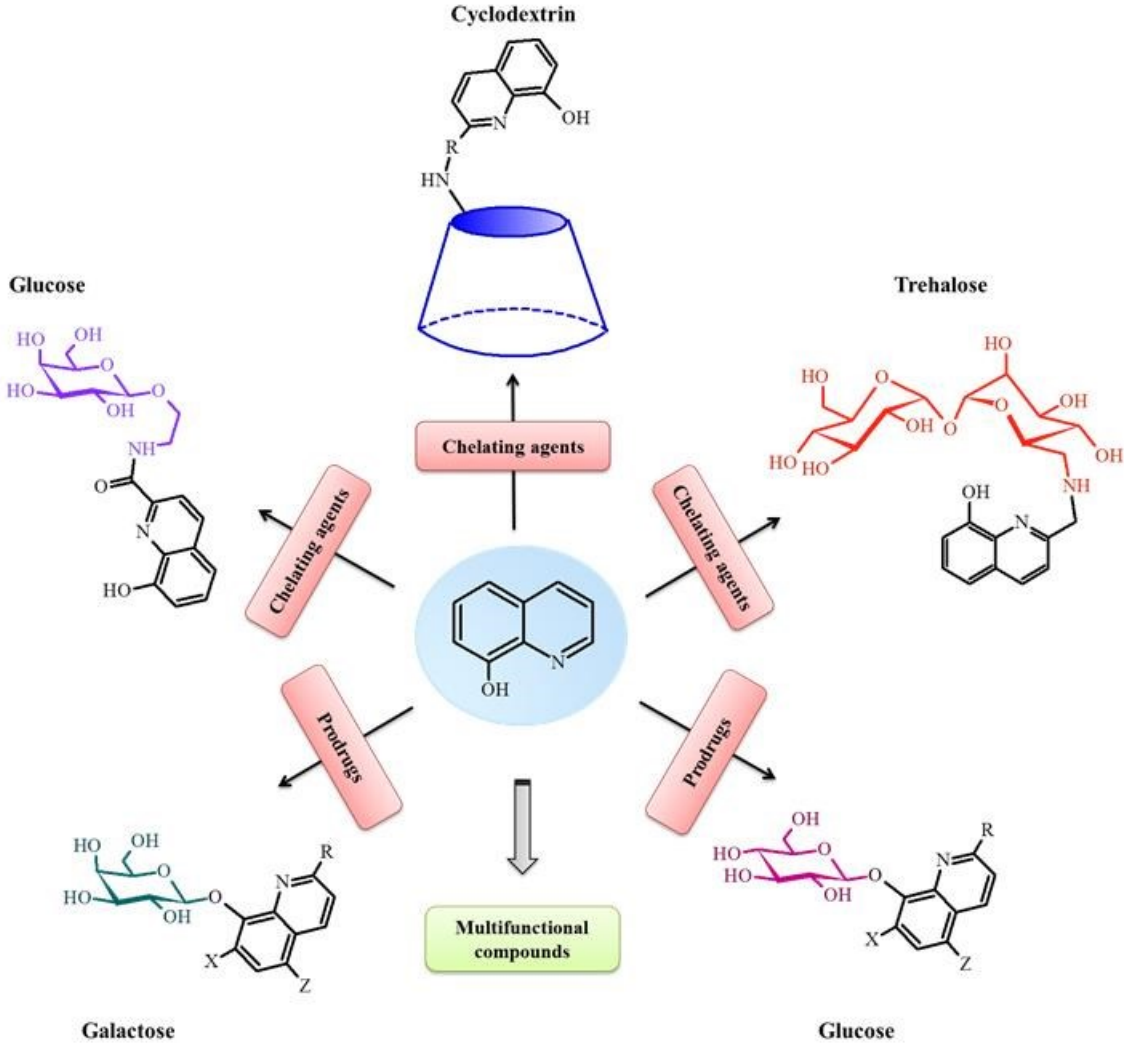

Figure 26. Glycoconjugates of OHQs.

The synthetized glucoconjugates of Cu^{2+} chelating agents would target tumor cells exploiting cancer glucose avidity. Galactoconjugates could exploit ADEPT approach or the lectin system.

As for glucoconjugate and galactoconjugate prodrugs, a series of sub-aims can be identified:

- ✓ Synthesis of a series of glycoconjugate prodrugs
- ✓ Characterization of the compounds
- ✓ Evaluation of the chemical stability
- ✓ Evaluation of the stability to enzymatic cleavage
- ✓ Determination of the antiproliferative activity
- ✓ Understanding of the targets and action mechanisms
- ✓ Analysis of structure-activity relationship

The synthesis and characterization of chelating OHQ conjugates with glucose and trehalose has been another purpose of this research. One of the goals is the comparison of these systems with the glycoconjugates prodrugs that are initially unable to complex metal ions. Thereof, the key points of this topic can be briefly described:

- ✓ Synthesis of chelating monosaccharides and disaccharides
- ✓ Characterization of the compounds
- ✓ Evaluation of the chelating ability
- ✓ Evaluation of the antiproliferative activity

Finally, cyclodextrin conjugates are appealing since their conjugates are employed in cancer therapy and other diseases related to metal dyshomeostasis including Niemann-Pick disease.

The sub-aims for cyclodextrin conjugates can be briefly summarized in:

- ✓ Synthesis of a series of cyclodextrins
- ✓ Characterization of the compounds
- ✓ Evaluation of the stability to α-amylase degradation
- ✓ Evaluation of the chelating ability
- ✓ Evaluation of the antioxidant activity
- ✓ Evaluation of SOD-like activity of the copper complexes
- ✓ Evaluation of the inclusion capacity
- ✓ Evaluation of the ability in inhibiting protein aggregation
- ✓ Determination of the antiproliferative activity
- ✓ Evaluation of the properties in NPC model

3. EXPERIMENTAL SECTION

3.1 Materials

Commercially available reagents were used directly, unless otherwise noted. All quinoline and sugar derivatives were obtained from Sigma-Aldrich. 6-Amino-6-deoxy-β-cyclodextrin, 6-deoxy-6-hydroxylethylamino-β-cyclodextrin and 6-aminoethylamino-6-deoxy-β-cyclodextrin were synthesized by a microwave-assisted procedure starting from the corresponding 6-tosylate derivative as reported elsewhere.[163] 6^A,6^B-Diamino-6^A,6^B-dideoxy-β-cyclodextrin was obtained using the procedure described by Di Blasio *et al*.[164] 2^A(S),3^A(R)-3^A-amino-3^A-deoxy-β-cyclodextrin was previously synthetized as reported elsewhere.[165] 6^A-deoxy-6^A-N-(2-methyl-3-hydroxypyridin-4-one)-β-cyclodextrin (CD6DFP) and 2^A(S),3^A(R)-3^A-N(2-methyl-3-hydroxypyridin-4-one)-3^A-deoxy-β-cyclodextrin (CD3DFP) were provided by Dr. J. Spencer and A. Puglisi (Sussex University).

Thin Layer Chromatography (TLC) was carried out on silica gel plates (Merck 60-F254). Carbohydrates derivatives were detected on TLC by UV and an anisaldehyde test.

The enzymes such as α-amylase, β-galactosidase from bovine liver, β-glucosidase from almonds, β-lactoglobulin A from bovine milk were obtained from Sigma-Aldrich. Cu^{2+} and Zn^{2+} stock solutions were prepared by dissolving the corresponding salt in water and titrating the resulting solutions with standardized EDTA using murexide and eriochrome black T, respectively.[166]

3.2 NMR spectroscopy

^{1}H and ^{13}C NMR spectra were recorded at 25 °C with a Varian UNITY PLUS-500 spectrometer at 499.9 and 125.7 MHz respectively. The NMR spectra were obtained by using standard pulse programs from Varian library. The 2D experiments (COSY, TOCSY, gHSQCAD, gHMBC, ROESY) were acquired using 1K data points, 256 increments and a relaxation delay of 1.2 s. The spectra were referred to the solvent signal. For clarity, the sugar

units in β-CyD derivatives are labelled A–G counter-clockwise starting from the modified ring (denoted as A) and viewing from the upper rim.

3.3 UV-visible and circular dichroism spectroscopy

UV-vis spectra were recorded using an Agilent 8452A diode array spectrophotometer. Circular dichroism measurements were performed with a JASCO model J-810 spectropolarimeter. The spectra represent the average of 10 scans and were recorded at 25 °C, on freshly prepared solutions.

3.4 Mass spectrometry

High resolution mass spectrometry (HRMS) measurements were performed on a Bruker Daltonics, APEX III 4.7 Tesla using an ESI source. ESI-MS measurements were carried out by using a Finnigan LCQ DECA XP PLUS ion trap spectrometer operating in the positive or negative ion mode and equipped with an orthogonal ESI source (Thermo Electron Corporation, USA). Cu^{2+} and Zn^{2+} complexes for ESI-MS studies were prepared by adding a solution of $CuSO_4$ or $ZnSO_4$ to a ligand solution. Different metal ligand ratios were investigated. Sample solutions were injected into the ion source without the addition of any other solvent at a flow rate of 5 μL/ min. For electrospray ionization the drying gas (nitrogen) was heated at 260 °C. The capillary exit and skimmer voltage were varying in order to optimize the signal responses. Scanning was performed from *m/z* = 100 to 2000. Xcalibur software was used for the elaboration of mass spectra. The assignments of the peaks in ESI-MS spectra were done by comparing the experimental isotopic patterns with the corresponding simulated profiles. Each species is indicated with the *m/z* value of the first peak of its isotopic cluster.

3.5 Competition experiments

Spectrophotometric competition titrations were carried out at 25 ^{o}C in buffered aqueous solution (pH 7.4, 3-morpholinopropane-1-sulfonic acid, MOPS) using an Agilent 8453 diode-

array spectrophotometer. Increasing amounts of the competing ligand (EDTA solution 5.0 ÷ 9.0 × 10^{-4} M) were added with a precision burette (Hamilton, 1 mL) into the measuring cell containing a known volume of the ML (M = Cu^{2+} or Zn^{2+}; L = CD6HQ or CDNHQ) complex solution. Typically, a solution of the metal ion (7.0 × 10^{-4} ÷ 1.0 × 10^{-3} M) was added to a solution of either ligand CD6HQ or CDNHQ (3.0 ÷ 5.0 × 10^{-5} M) to have a metal/ligand (M/L) ratio of 1:1 in the cell. Addition, equilibration time and data recording were controlled by a homemade software. 60-70 scans were recorded for each titration run. Three independent runs were collected for each metal-ligand system. Data from the competition experiments were used, along with the conditional formation constants of Cu-EDTA (log K = 15.9) and Zn-EDTA (log K = 13.6) complexes, to determine the stability constants of the complex species for each metal-ligand system. The conditional constants of EDTA metal complexes were calculated at pH 7.4 from the reported values[167] and held constant in the analysis. UV-vis spectra were handled with the software Hyperquad[168] which allows for a multi-wavelength treatment of the data and the simultaneous refinement of data from different titrations. The species distribution was calculated by the program Hyss.[167]

3.6 Trolox equivalent antioxidant capacity assay

The antioxidant capacity of the tested compounds was determined by 2,2'-azino-bis-(3-ethylbenzothiazoline-6-sulphonic acid) diammonium salt (ABTS) radical cation decolorisation assay[64] using 6-hydroxy-2,5,7,8-tetramethylchroman-2-carboxylic acid (Trolox) as a standard. Briefly, the radical cation $ABTS^{+\bullet}$ was generated by a reaction between ABTS (7.00 mM) and persulfate (2.45 mM) in water. After a 16 h incubation (dark, room temperature) the resulting solution was diluted in a cuvette with phosphate buffer (10 mM, pH 7.4) such that the absorbance of the solution at 734 nm was 0.70 ± 0.02. This radical solution was combined with antioxidant samples, in varying concentrations, and allowed to react for 6 min. All samples were diluted to provide 20–80% inhibition of the blank absorbance. The absorbance values were measured for 6 min. Solution absorbance was plotted *vs* compound concentration; each resultant slope was normalized with respect to that obtained for Trolox to give the Trolox-equivalence (TEAC) value for each time point (1, 3, 6 min). All determinations were

carried out at least three times and in triplicate at each separate concentration of the samples in order to obtain consistent data with statistical error.

3.7 SOD-like activity (NBT assay)

Superoxide radical anions were enzymatically generated by the xanthine–xanthine oxidase (XO/XOD) system and spectrophotometrically detected monitoring the formation of reduced nitro blue tetrazolium (NBT) at 550 nm. The reaction mixture was composed by NBT 250 μM, XO 50 μM, catalase 30 μg/mL in phosphate buffer 10 mM, at pH 7.4. An appropriate amount of XOD was added to 2.0 mL reaction mixture to produce a ΔA_{550} nm min^{-1} of 0.024. This corresponded to a $O_2^{\bullet-}$ production rate of 1.1 μmol min^{-1}. The NBT reduction rate was measured in the presence and in the absence of the investigated complex for 500 s. All measurements were carried out at 25.0 ± 0.2 °C using a thermostated cuvette (light path, 1 cm) in which solutions were magnetically stirred. In separate experiments urate production by XOD was spectrophotometrically monitored at 295 nm, ruling out any inhibition of XOD activity. The I_{50} (the concentration which causes the 50% inhibition of NBT reduction) of Cu^{2+} and Fe^{3+} complexes was determined. Three determinations were carried out. The metal complexes were prepared adding a solution of Cu^{2+} and Fe^{3+} salts to a ligand water solution in 1:1 ratio.

3.8 ThT fluorescence measurements

Fluorescence emission spectra of Thioflavin T (ThT) undergo a red shift upon incorporation into β-sheet amyloid structures. The reaction mixture contained a final concentration of 0.08 mM β-lactoglobulin (BLG), 0.24 mM ThT, 0.080 mM $ZnSO_4$ in 10 mM MOPS buffer (pH 7.0). The ThT fluorescence signal was measured (excitation wavelength, 440 nm; emission wavelength, 480 nm), at 60 °C in a quartz cell (light path, 1 cm) by an LS55 spectrofluorimeter (PerkinElmer) thermostated with a programmable refrigerated circulating bath (Julabo F25HE). Excitation and emission bandwidths were set to 4 nm. Fluorescence experiments were carried out for 400 min.

3.9 Dynamic light scattering measurements

Dynamic light-scattering (DLS) measurements were carried out using a Zetasizer Nano ZS (Malvern Instruments, UK) equipped for backscattering at 173° with a 633 nm He–Ne laser. Protein solutions (0.08 mM) were buffered at pH 7.0 (MOPS, 10 mM). Each DLS measurement was run using automated, optimal measurement times and laser attenuation settings. Metal-mediated aggregation was studied using Cu^{2+} and Zn^{2+} stock solution in order to obtain Zn^{2+}-BLG and Cu^{2+}-BLG ratios of 1 and 0.2, respectively. Temperature scanning was realized by increasing the temperature of 1.5 or 2 °C with an equilibration time of 5 min. A measurement of 10 runs were carried out for each temperature. Scattering measurements as a function of time of Zn^{2+}-BLG and Cu^{2+}-BLG were performed, recording size data every 5 min at 60 °C and 75 °C, respectively. As for the measurements carried out in presence of CyD derivatives, these latter compounds were added in equimolar amount to metals. The recorded correlation functions and measured protein mobilities were converted into size, using Dispersion Technology Software (DTS). The software gives multiple aspects and interpretations of the data collected for the sample such as intensity, volume, and number distribution graphs as well as statistical analysis for each. Through Mie theory with the use of the input parameter of sample refractive index, it is possible to convert the intensity distribution to volume and number distributions.

3.10 *In vitro* stabilities of glycoconjugates

The compounds were incubated at 37 °C in Phosphate Buffer Saline (pH 7.4) to monitor their stabilities through TLC, ESI-MS and UV-Vis spectroscopy. Furthermore, the compound stability was evaluated at pH 4.0 and 11.0.

3.11 Glucosidase cleavage assay

A screen using almond β-glucosidase was performed to assess the potential of the OHQ glucosides to act as substrates for glucosidases. Glycoconjugates were incubated at 37 °C for 2 h. TLC and ESI-MS monitoring of the glucosidase reactions were used to determine whether the OHQ glycosides showed any sign of being cleaved by the enzyme.

3.12 Galactosidase cleavage assay

A screen using β-galactosidase from *Escherichia Coli* was performed to assess the potential of the OHQ galactosides to act as substrates for the enzyme. Galactoconjugates were incubated at 37 °C and pH 7.4 in the presence of the enzyme. TLC and ESI-MS monitoring of the galactosidase reactions were used to determine whether the glycosides showed any sign of being cleaved by the enzyme. Enzymatic cleavage was also monitored by UV-vis spectroscopy. β-galactosidase (1.1×10^{-8} M) was incubated in the assay solution (phosphate buffer, 10 mM, pH 7.4) in the presence of the galactoconjugates (6.0×10^{-5} M) and UV-vis spectra were recorded every 8 or 64 s.

3.13 Amylase cleavage assay

CyD derivatives (5.0×10^{-5} M) were incubated with α-amylase at 37 °C in a solution of ammonium acetate buffer (10 mM, pH 7.0). Hydrolysis was monitored by ESI-MS for 96 h.

3.14 Determination of half-lives of the glucoconjugates

β-glucosidase (1.0×10^{-6} M) was incubated in the assay solution in the presence of the glucoconjugates (5.0×10^{-5} M) at 37 °C. Samples (2.0 mL) were removed at selected times over 4 h and were immediately added with a solution of NaOH until the pH value of the solution reached 11.0 in order to stop enzymatic activity. Furthermore at this pH the released drug showed a shift of the bands because of the deprotonation of phenolic group and so it was possible to quantify the released drug by UV-vis spectroscopy. Calibration curves of the free ligands for absorbance against their concentrations were obtained at pH 11.0. All assays were performed in triplicate.

3.15 Determination of antiproliferative activity (MTT assay)

All glycosides and their parent compounds were firstly dissolved in dimethylsulfoxide (DMSO) at the concentration of 100 mM and then further diluted in fetal calf serum (FCS, final concentration DMSO 2-4%).

Human cell lines A2780 (ovary, adenocarcinoma), A549 (lung, carcinoma), Hep-G2 (liver, carcinoma), MDA-MB-231 (breast, carcinoma) Panc-1 and Capan-1 (pancreas adenocarcinoma) were plated at appropriate concentrations in 180 μL into flat-bottomed 96-well microtiter plates. After 6–8 h they were treated with 20 μL containing five 1 : 10 fold concentrations of the compounds diluted in FCS in the presence or absence of Cu^{2+} and Zn^{2+} (20 μM $CuCl_2$ and 50 μM $ZnCl_2$). After 72 h, the plates were processed and IC_{50}s values calculated on the basis of the analysis of single concentration–response curves. For IC_{50}s higher than 100 μM, the final mean IC_{50} value was extrapolated using the mean concentration–response curve. Each experiment was repeated 4–6 times.

For the evaluation of antiproliferative activity of the galactoconjugates in the presence of β-galactosidase, A2780 and Hep-G2 cells were treated with GalOHQ (10 μM), GalAHQ (2 or 10 μM) or GalClHQ (10 μM) in the presence or not of 2U/well β-galactosidase.

As for cyclodextrin-quinoline conjugates, A2780, A549, Panc-1, and Capan-1 cells were also plated in the presence of 0.4, 0.8 and 1.6 U × mL^{-1} α -amylase and treated, 6–8 h later, as described before.

3.16 Inhibition assay of glucosidase activity

Antiproliferative activity assay was performed in the presence of Cu^{2+} ions and 100 μM of 2,5-dideoxy-2,5-imino-D-mannitol (DMDP), a known β-glycosidase inhibitor. The same experiment was also carried out without DMDP for comparison.

3.17 Microscopy visualization of apoptotic cells after DAPI staining

A2780, A549 and MDA-MB-231 were plated in 24-well plates at their optimal densities/well in 1 mL complete medium for 6-8 h. ClHQ, Cl_2HQ and their glucosylated counterparts were then added in order to reach the IC_{50} concentration determined by the MTT assay. After 72 h, floating and adherent cells were harvested, washed twice with cold PBS, fixed with 60 µL of ethanol (70 %) in PBS and maintained at 4 °C until analysis. Just before microscopy examination 5 µL of 10 µg/mL 4'-6-diamidino-2-phenylindole (DAPI) in water were added to the samples, and the percentage of apoptotic segmented nuclei/cells evaluated.

3.18 Evaluation of apoptosis by annexin-V staining

The triggering of apoptosis was also evaluated for the glycosylated compounds GluClHQ and $GluCl_2HQ$ in A2780, and A549 cells. Cells were treated with the specific IC_{50} of each compound in the presence or absence of Cu^{2+} salt (20 µM). After three days, floating and adherent cells were harvested, washed with cold PBS and early and late apoptotic cells determined by double staining with FITC-annexin-V/PI (rh Annexin-V/FITC Kit, Bender MedSystem GmbH, Vienna, Austria). The subsequent analysis was performed by flow cytometry as described elsewhere.[169]

3.19 Molecular docking

The crystal structure of human cytosolic β-glucosidase was obtained from the RCSB Protein Data Bank, code 2JFE. The 3D structure was visualized and modified with Pymol v1.1.r1 as follows. Water and NAG molecules were removed, hydrogen atoms were added and the resulting structure was saved in the pdb format. Ligands were built using CORINA[170] and saved in the mol2 format. AutoDock Vina[171] and FLAP UI version 0.43.0[172] were used to perform docking studies. The active site in AutoDock was defined by the coordinates of Cα of the catalytic residue Glu165 (33 (X), 51 (Y) and 38 (Z)).[173] To ensure a correct docking process, the search space was defined to encompass all flexible residues as a box with dimensions of 30.0 × 30.0 × 30.0 Å. Ligand Explorer v.3.9 was used to visualize the interactions of bound ligands in the protein.

3.20 Synthesis of 8-quinolinyl-tetra-*O*-acetyl-β-D-glucopyranoside

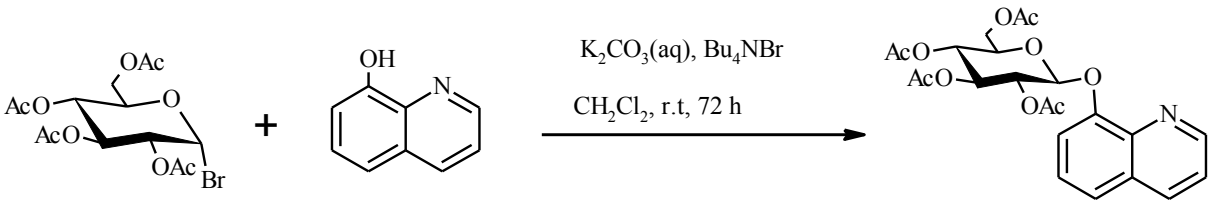

8-hydroxyquinoline (90 mg, 0.62 mmol) and K_2CO_3 (0.86 g, 6.2 mmol) were added to water (50 mL) and dissolved with heating. Chloroform (50 mL) was added to this aqueous solution, followed by acetobromoglucose (0.63g, 1.55 mmol) and tetrabutylammonium bromide (0.2 g, 0.62 mmol). The resulting mixture was vigorously stirred for 72 h. The two-phase system was separated, and the aqueous phase was washed repeatedly with chloroform.

The combined organic extracts were dried with Na_2SO_4, filtered, and evaporated under vacuum. The resulting dark oil was purified by column chromatography (eluent: AcOEt/hexane 1:1) to afford a white solid.

Yield: 40 %.

TLC: Rf = 0.20 (AcOEt/n-hexane 1:1).

ESI-MS: *m/z* = 476.0 $[P+H]^+$, 498.1 $[P+Na]^+$, 950.5 $[2P+H]^+$, 972.6 $[2P+Na]^+$.

^{1}H NMR (500 MHz, $CDCl_3$) δ (ppm): 9.01 (m, 1H, H-2), 8.26 (d, 1H, $J_{4,3}$ = 6.7 Hz, H-4), 7.63 (m, 1H, H-6), 7.52 (m, 3H, H-3, H-5, H-7), 5.55 (d, 1H, $J_{1,2}$ = 7.8 Hz, H-1 of Glc), 5.47 (m, 1H, H-2 of Glc), 5.39 (t, 1H, J = 9.3 Hz, H-3 of Glc), 5.23 (t, 1H, J = 9.6 Hz, H-4 of Glc), 4.27 (dd, 1H, $J_{6a,6b}$ = 12.3 Hz, $J_{6a,5}$ = 4.9 Hz, H-6a of Glc), 4.21 (dd, 1H, $J_{6b,6a}$ = 12.3 Hz, $J_{6b,5}$ = 2.5 Hz, H-6b of Glc), 3.88 (ddd, 1H, $J_{5,4}$ = 9.9 Hz, $J_{5,6a}$ = 4.9 Hz, $J_{5,6b}$ = 2.5 Hz, H-5 of Glc), 2.12-2.04 (m, 12H, CH_3).

3.21 Synthesis of 8-quinolinyl-β-D-glucopyranoside (GluOHQ)

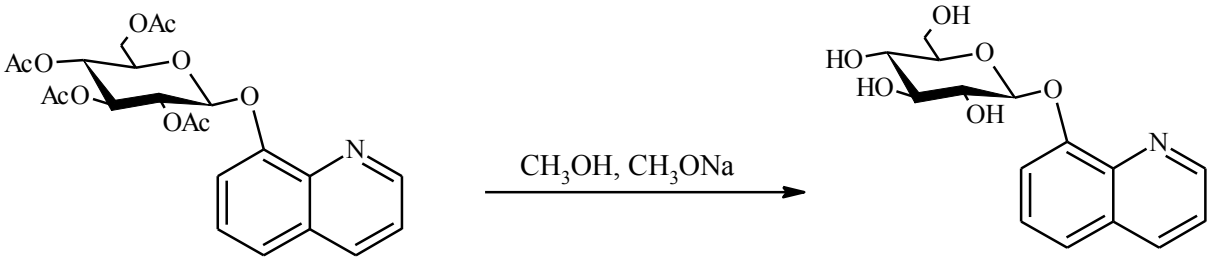

Peracetylated glucoside (70 mg, 0.15 mmol), absolute methanol (15 mL), and NaOMe (0.1 mL, 0.5 N MeOH solution) were placed in a flask. The reaction was stirred at r.t. for 24 h and evaporated under vacuum. Ion exchange CM Sephadex (form NH_4^+) was used to remove salts.

Yield: 65 %.

TLC: Rf = 0.36 (PrOH/AcOEt/H_2O/NH_3 4:4:1:1).

ESI-MS: *m/z* = 308.0 $[P+H]^+$, 330.1 $[P+Na]^+$, 636.7 $[2P+Na]^+$.

UV-vis: (H_2O) λ/nm (ε M^{-1} cm^{-1}) 236 (29734), 298 (3165).

^{1}H NMR (500 MHz, D_2O) δ (ppm): 8.79 (d, 1H, $J_{2,3}$ = 3.5 Hz, H-2), 8.43 (d, 1H, $J_{4,3}$ = 8.5 Hz, H-4), 7.65 (d, 1H, $J_{5,6}$ = 8.1 Hz, H-5), 7.61 (m, 1H, H-3), 7.55 (m, 1H, H-6), 7.45 (m, 1H, H-7), 5.30 (d, 1H, $J_{1,2}$ = 7.8 Hz, H-1 of Glc), 3.89 (m, 1H, H-3 of Glc), 3.78-3.58 (m, 4H, H-2, H-4, Hs-6 of Glc), 3.50 (m, 1H, H-5 of Glc).

3.22 Synthesis of 5-chloro-7-iodo-8-quinolinyl-tetra-*O*-acetyl-β-D-glucopyranoside

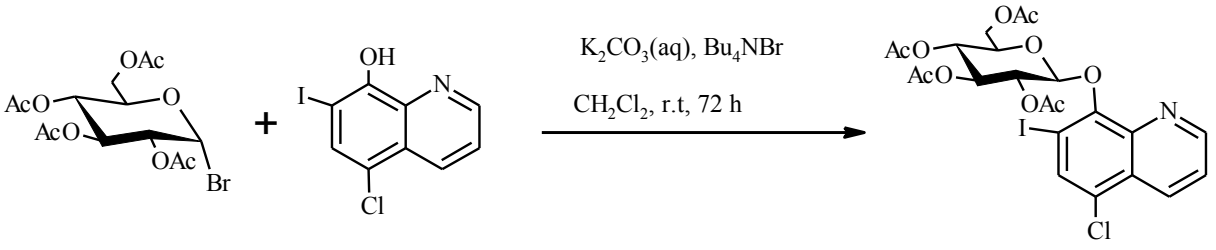

5-Chloro-7-iodo-8-hydroxyquinoline (230 mg, 0.75 mmol) and K_2CO_3 (1.04 g, 7.5 mmol) were added to water (50 mL) and methanol (25 mL). Dichloromethane (50 mL) was added to this aqueous solution, followed by acetobromoglucose (774 mg, 1.88 mmol) and tetrabutylammonium bromide (242 mg, 0.75 mmol). The resulting mixture was vigorously stirred for 72 h. The two-phase system was separated, and the aqueous phase was washed repeatedly with dichloromethane. The combined organic extracts were dried with Na_2SO_4, filtered and evaporated *in vacuo*. The crude product was purified by column chromatography (eluent: AcOEt/hexane 3:2).

Yield: 58 %.

TLC: Rf = 0.56 (AcOEt/n-hexane 1:1).

ESI-MS: *m/z* = 635.8 $[P+H]^+$, 657.8 $[P+Na]^+$, 673.8 $[P+K]^+$.

^{1}H NMR (500 MHz, $CDCl_3$) δ (ppm): 8.92 (dd, 1H, $J_{2,3}$ = 4.1 Hz, $J_{2,4}$ = 1.6 Hz, H-2), 8.54 (dd, 1H, $J_{4,3}$ = 8.6 Hz, $J_{4,2}$ = 1.6 Hz, H-4), 7.99 (s, 1H, H-6), 7.56 (dd, 1H, $J_{3,4}$ = 8.6 Hz, $J_{3,2}$ = 4.1 Hz, H-3), 6.28 (d, 1H, $J_{1,2}$ = 7.9 Hz, H-1 of Glc), 5.51 (dd, 1H, $J_{2,3}$ = 9.3 Hz, $J_{2,1}$ = 7.9 Hz, H-2 of Glc), 5.37 (t, 1H, J = 9.3 Hz, H-3 of Glc), 5.27 (t, 1H, J = 9.7 Hz, H-4 of Glc), 4.15 (dd, 1H, $J_{6a,6b}$ = 12.2 Hz, $J_{6a,5}$ = 4.9 Hz, H-6a of Glc), 4.02 (dd, 1H, $J_{6b,6a}$ = 12.2 Hz, $J_{6b,5}$ = 4.9 Hz, H-6b of Glc), 3.68 (m, 1H, H-5 of Glc), 2.12 (s, 3H, CH_3), 2.07 (s, 3H, CH_3), 2.03 (s, 3H, CH_3), 1.94 (s, 3H, CH_3).

^{13}C NMR (125 MHz, $CDCl_3$) δ (ppm): 149.7 (C-2), 135.4 (C-6), 133.4 (C-4), 122.1 (C-3), 100.7 (C-1 of Glc), 72.9 (C-3 of Glc), 72.2 (C-2 of Glc), 71.8 (C-5 of Glc), 68.6 (C-4 of Glc), 61.7 (C-6 of Glc), 20.9-20.6 (CH_3).

3.23 Synthesis of 5-chloro-7-iodo-8-quinolinyl-β-D-glucopyranoside (GluCQ)

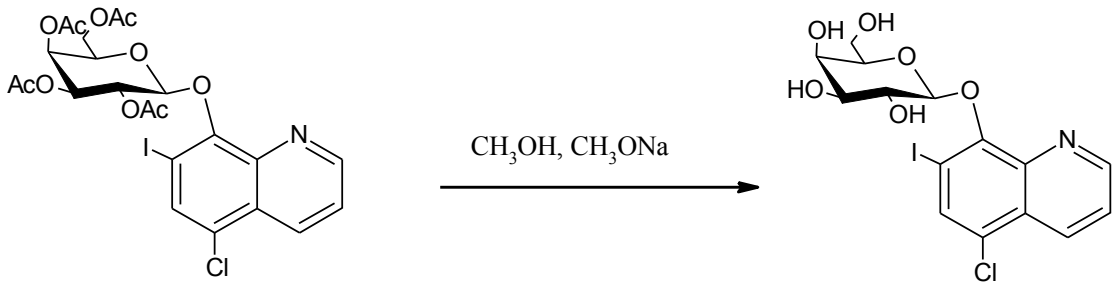

Peracetylated glucoside (100 mg, 0.16 mmol) was dissolved in absolute methanol (8 mL). NaOMe (2 mL, 0.1 N, MeOH solution) was added to this mixture. After 20 min, a solid precipitated, however the mixture was stirred overnight to complete the deacetylation. The product was collected by filtration, washed with cool methanol and dried.

Yield: 70 %.

TLC: Rf = 0.48 ($PrOH/AcOEt/H_2O/NH_3$ 4:4:1:1).

ESI-MS: *m/z* = 467.9 $[P+H]^+$, 489.9 $[P+Na]^+$, 956.4 $[2P+Na]^+$, 972.4 $[2P+K]^+$.

UV-Vis: (EtOH) λ/nm (ε/M^{-1} cm^{-1}) 208 (27326), 248 (33527), 299 (4457).

^{1}H NMR (500 MHz, CD_3OD) δ (ppm): 8.94 (dd, 1H, $J_{2,3}$ = 4.2 Hz, $J_{2,4}$ = 1.5 Hz, H-2), 8.67 (dd, 1H, $J_{4,3}$ = 8.6 Hz, $J_{4,2}$ = 1.5 Hz, H-4), 8.12 (s, 1H, H-6), 7.73 (dd, 1H, $J_{3,4}$ = 8.6 Hz, $J_{3,2}$ = 4.2 Hz, H-3), 5.52 (d, 1H, $J_{1,2}$ = 7.9 Hz, H-1 of Glc), 3.80-3.72 (m, 2H, H-2, H-6 of Glc), 3.69-3.64 (m, 1H, H-6 of Glc), 3.51-3.40 (m, 2H, H-3, H-4 of Glc), 3.21 (m, 1H, H-5 of Glc).

^{13}C NMR (125 MHz, CD_3OD) δ (ppm): 150.1 (C-2), 135.6 (C-6), 133.8 (C-4), 122.6 (C-3), 105.3 (C-1 of Glc), 77.0 (C-3 and C-5 of Glc), 74.7 (C-2 of Glc), 69.8 (C-4 of Glc), 61.2 (C-6 of Glc).

3.24 Synthesis of 5-chloro-8-quinolinyl-β-D-glucopyranoside (GluClHQ)

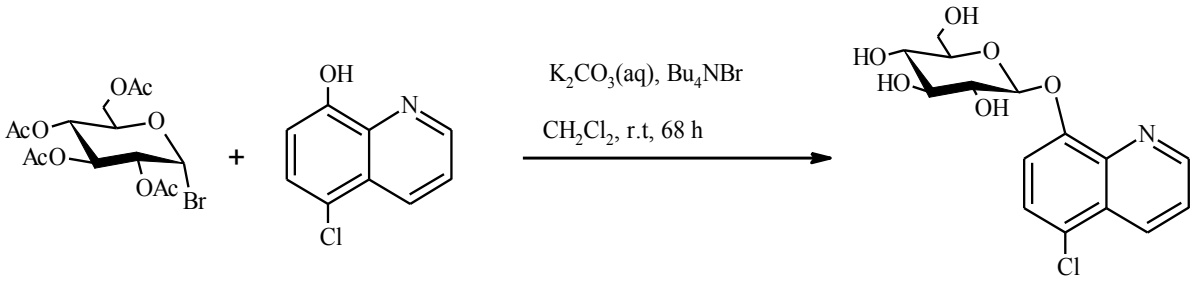

5-chloro-8-hydroxyquinoline (135 mg, 0.75 mmol, ClHQ) and K_2CO_3 (1.04 g, 7.5 mmol) were added to water (50 mL) and methanol (40 mL). Dichloromethane (100 mL) was added to this aqueous solution, followed by acetobromoglucose (773 mg, 1.88 mmol) and tetrabutylammonium bromide (242 mg, 0.75 mmol). The resulting mixture was vigorously stirred for 68 h. A solid precipitated, and the deacetylated product was collected by filtration, washed with cool methanol and dried.

Yield: 68 %.

TLC: Rf = 0.51 (PrOH/AcOEt/H_2O/NH_3 4:4:1:1).

ESI-MS: *m/z* = 341.8 $[P+H]^+$, 363.9 $[P+Na]^+$, 704.6 $[2P+Na]^+$.

UV-Vis: (CH_3OH) λ/nm (ε/M^{-1} cm^{-1}): 243 (25600), 317 (3360).

CD (CH_3OH) λ/nm (Δε): 197.8 (-4.24), 311.4 (-0.70).

^{1}H NMR (500 MHz, CD_3OD) δ (ppm): 8.97 (dd, 1H, $J_{2,3}$ = 4.3, $J_{2,4}$ = 1.6 Hz, H-2), 8.71 (dd, 1H, $J_{4,3}$ = 8.6, $J_{4,2}$ = 1.6 Hz, H-4), 7.75 (dd, 1H, $J_{3,4}$ = 8.6 Hz, $J_{3,2}$ = 4.3 Hz, H-3), 7.67 (d, 1H, $J_{6,7}$ = 8.5 Hz, H-6), 7.51 (d, 1H, $J_{7,6}$ = 8.5 Hz, H-7), 5.09 (d, 1H, $J_{1,2}$ = 7.8 Hz, H-1 of Glc), 3.97 (dd, 1H, $J_{6a,6b}$ = 12.1 Hz, $J_{6a,5}$ = 2.2 Hz, H-6a of Glc), 3.81 – 3.64 (m, 2H, H-2 and H-6b of Glc), 3.60-3-54 (m, 2H, H-3 and H-5 of Glc), 3.45 (dd, 1H, *J* = 9.6 Hz, *J* = 9.0 Hz, H-4 of Glc).

^{13}C NMR (125 MHz, CD_3OD) δ (ppm): 153.2 (C-8), 151.1 (C-2), 140.9 (C-9), 135.1 (C-4), 128.4 (C-6, C-5), 125.0 (C-10), 124.1 (C-3), 114.5 (C-7), 103.3 (C-1 of Glc), 78.6 (C-5 of Glc), 77.4 (C-3 of Glc), 74.7 (C-2 of Glc), 71.6 (C-4 of Glc), 63.0 (C-6 of Glc).

3.25 Synthesis of 5,7-dichloro-8-quinolinyl-β-D-glucopyranoside ($GluCl_2HQ$)

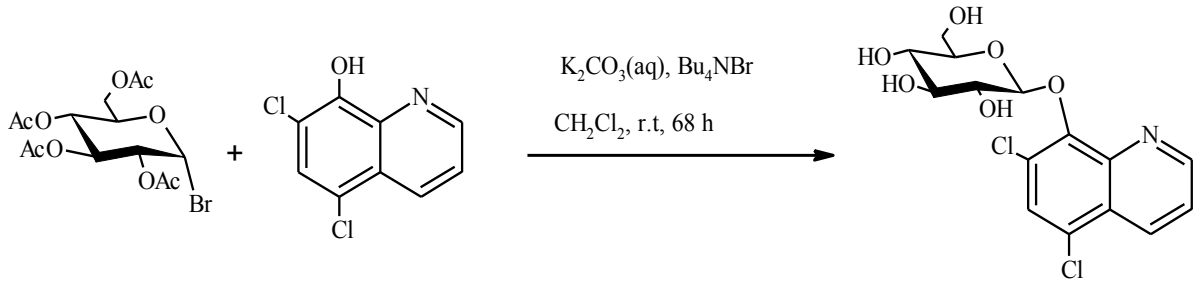

5,7-dichloro-8-quinolinol (160 mg, 0.75 mmol, Cl_2HQ) and K_2CO_3 (1.04 g, 7.5 mmol) were added to water (50 mL) and methanol (40 mL). Dichloromethane (100 mL) was added to this aqueous solution, followed by acetobromoglucose (773 mg, 1.88 mmol) and tetrabutylammonium bromide (242 mg, 0.75 mmol). The resulting mixture was vigorously stirred for 68 h. A solid precipitated, and the deacetylated product was collected by filtration, washed with cool methanol and dried.

Yield: 61 %.

TLC: Rf = 0.52 (PrOH/AcOEt/H_2O/NH_3 4:4:1:1).

ESI-MS: *m/z* = 375.8 $[P+H]^+$, 397.9 $[P+Na]^+$, 772.5 $[2P+Na]^+$.

UV-Vis: (CH_3OH) λ/nm (ε/M^{-1} cm^{-1}) : 207 (20900), 242 (24800), 302 (3020).

CD (CH_3OH) λ/nm (Δε): 206.6 (-5.10), 240.2 (-10.77), 318.0 (0.73).

^{1}H NMR (500 MHz, CD_3OD) δ (ppm): 8.98 (dd, 1H, $J_{2,3}$ = 4.3 Hz, $J_{2,4}$ = 1.5 Hz, H-2), 8.68 (dd, 1H, $J_{4,3}$ = 8.6 Hz, $J_{4,2}$ = 1.6 Hz, H-4), 7.82 (s, 1H, H-6), 7.72 (dd, 1H, $J_{3,4}$ = 8.6 Hz, $J_{3,2}$ = 4.3 Hz, H-3), 5.34 (d, 1H, $J_{1,2}$ = 7.8 Hz, H-1 of Glc), 3.77 (dd, 1H, $J_{6a,6b}$ = 11.9 Hz, $J_{6a,5}$ = 2.4 Hz, H-6a of Glc), 3.72 (dd, 1H, $J_{2,3}$ = 8.8 Hz, $J_{2,1}$ = 7.8 Hz, H-2 of Glc), 3.66 (dd, 1H, $J_{6b,6a}$ = 11.9 Hz, $J_{6b,}$ = 5.3 Hz, H-6b of Glc), 3.50-3.42 (m, 2H, H-4 and H-3 of Glc), 3.23 (ddd, 1H, $J_{5,4}$ = 9.4, $J_{5,6b}$ = 5.3, $J_{5,6a}$ = 2.3 Hz, H-5 of Glc).

^{13}C NMR (125 MHz, CD_3OD) δ (ppm): 152.3 (C-2), 143.4 (C-8), 144.1 (C-9), 135.6 (C-4), 130.0 (C-6), 129.2 (C-7), 128.5 (C-5), 127.8 (C-10), 124.2 (C-3), 107.3 (C-1 of Glc), 78.6 (C-5 of Glc), 78.4 (C-3 of Glc), 72.2 (C-2 of Glc), 71.3 (C-4 of Glc), 62.7 (C-6 of Glc).

3.26 Synthesis of 2-methyl-8-quinolinyl-β-D-glucopyranoside (GluMeHQ)

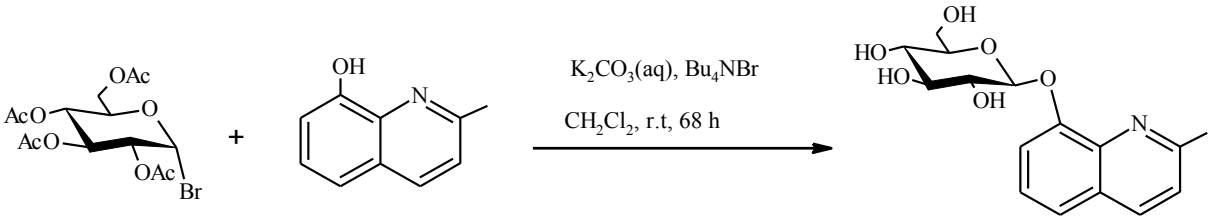

2-methyl-8-quinolinol (119 mg, 0.75 mmol, MeHQ) and K_2CO_3 (1.04 g, 7.5 mmol) were added to water (50 mL) and methanol (40 mL). Dichloromethane (100 mL) was added to this aqueous solution, followed by acetobromoglucose (773 mg, 1.88 mmol) and tetrabutylammonium bromide (242 mg, 0.75 mmol). The resulting mixture was vigorously stirred for 68 h. The two-phase system was separated, and the aqueous phase was washed repeatedly with dichloromethane. The aqueous phase was partially evaporated under vacuum to remove residual organic solvents and then a white solid precipitated. The product was collected by filtration washed with cool methanol and dried.

Yield: 57 %.

TLC: Rf = 0.44 (PrOH/AcOEt/H_2O/NH_3 4:4:1:1).

ESI-MS: *m/z* = 321.9 $[P+H]^+$, 344.0 $[P+Na]^+$, 359.9 $[P+K]^+$, 664.7 $[2P+Na]^+$, 680.8 $[2P+K]^+$.

UV-Vis: (CH_3OH) λ/nm (ε/M^{-1} cm^{-1}): 204 (31700), 240 (32200), 297 (3110).

CD (CH_3OH) λ/nm (Δε): 196.8 (-2.68), 312.6 (-0.34).

^{1}H NMR (500 MHz, CD_3OD) δ (ppm): 8.24 (d, 1H, $J_{4,3}$ = 8.4 Hz, H-4), 7.56 (dd, 1H, $J_{5,6}$ = 6.8 Hz, $J_{5,7}$ = 2.7 Hz, H-5), 7.48 (m, 3H, H-3, H-6 and H-7), 5.05 (d, 1H, $J_{1,2}$ = 7.8 Hz, H-1 of Glc), 3.96 (dd, 1H, $J_{6a,6b}$ = 12.1 Hz, $J_{6a,5}$ = 2.2 Hz, H-6a of Glc), 3.75 (dd, 1H, $J_{6a,6b}$ = 12.1 Hz, $J_{6b,5}$ = 15.0 Hz, H-6b of Glc), 3.73 (t, 1H, H-2 of Glc), 3.56 (m, 2H, H-5 and H-3 of Glc), 3.46 (t, 1H, *J* = 18 Hz, H-4 of Glc), 2.77 (s, 3H, CH_3).

^{13}C NMR (125 MHz, CD_3OD) δ (ppm): 154.5 (C-2), 148.0 (C-8), 133.2 (C-9), 134.7 (C-4), 123.6 (C-6, C-10), 120.3 (C-3), 118.9 (C-5), 111.5 (C-7), 105.3 (C-1 of Glc), 77.0 (C-3 and C-5 of Glc), 74.7 (C-2 of Glc), 69.8 (C-4 of Glc), 61.2 (C-6 of Glc), 20.8 (CH_3).

3.27 Synthesis of 2-methyl-8-quinolinyl-β-D-galactopyranoside (GalMeHQ)

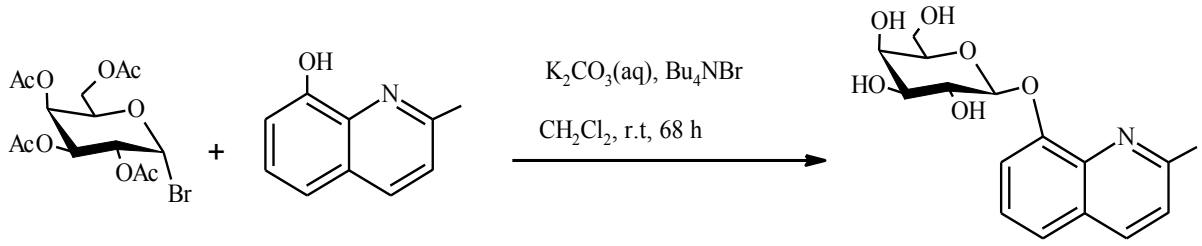

2-methyl-8-quinolinol (230 mg, 1.44 mmol) and K_2CO_3 (1.99 g, 14.4 mmol) were added to water (70 mL) and methanol (30 mL). Dichloromethane (100 mL) was added to this aqueous solution, followed by acetobromogalactose (773 mg, 1.88 mmol) and tetrabutylammonium bromide (464 mg, 1.44 mmol). The resulting mixture was vigorously stirred for 68 h. The two-phase system was separated, and the aqueous phase was washed repeatedly with dichloromethane. The aqueous phase was partially evaporated under vacuum to remove residual organic solvents and then a white solid precipitated. The product was collected by filtration washed with cool methanol and dried.

Yield: 55 %.

TLC: Rf = 0.78 (MeOH).

ESI-MS: *m/z* = 321.9 $[P+H]^+$, 344.0 $[P+Na]^+$, 664.7 $[2P+Na]^+$.

CD (CH_3OH) λ/nm (Δε/mdeg $M^{-1}cm^{-1}$): 224 (-2.70), 243 (+1.67).

^{1}H NMR (500 MHz, CD_3OD) δ (ppm): 8.23 (d, 1H, $J_{4,3}$ = 8.5 Hz, H-4), 7.56 (dd, 1H, $J_{5,6}$ = 7.9 Hz, $J_{5,7}$ = 1.3 Hz, H-5), 7.48 (m, 3H, H-3, H-6 and H-7), 4.99 (d, 1H, $J_{1,2}$ = 7.8 Hz, H-1 of Gal), 4.08 (dd, 1H, $J_{2,3}$ = 9.8 Hz, $J_{2,1}$ = 7.8 Hz, H-2 of Gal), 3.95 (d, 1H, $J_{4,3}$ = 3.4 Hz, H-4 of Gal), 3.82 (m, 3H, Hs-6 and H-5 of Gal), 3.68 (dd, 1H, $J_{3,2}$ = 9.8 Hz, $J_{3,4}$ = 3.4 Hz, H-3 of Gal), 2.77 (s, 3H, CH_3).

^{13}C NMR (125 MHz, CD_3OD) δ (ppm): 137.3 (C-4), 126.2 (C-6), 123.3 (C-3), 121.9 (C-5), 114.1 (C-7), 102.5 (C-1 of Gal), 76.1 (C-5 of Gal), 72.5 (C-3 of Gal), 71.4 (C-2 of Gal), 68.9 (C-4 of Gal), 61.5 (C-6 of Gal), 23.0 (CH_3).

3.28 Synthesis of 2-amino-8-quinolinyl-β-D-galactopyranoside (GalAHQ)

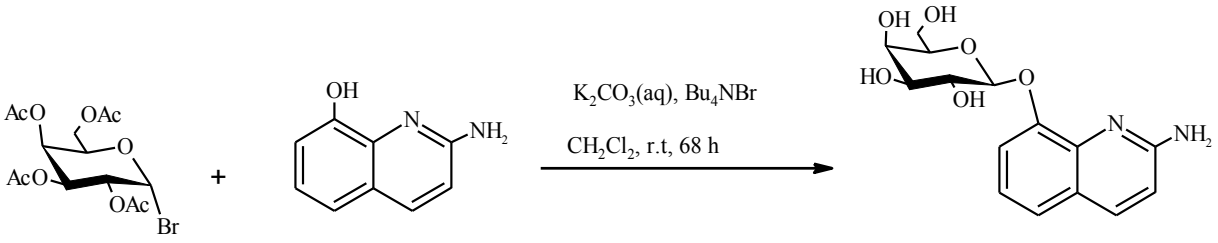

2-amino-8-quinolinol (230 mg, 1.44 mmol, AHQ) and K_2CO_3 (1.99 g, 14.4 mmol) were added to water (70 mL) and methanol (30 mL). Dichloromethane (100 mL) was added to this aqueous solution, followed by acetobromogalactose (773 mg, 1.88 mmol) and tetrabutylammonium bromide (464 mg, 1.44 mmol). The resulting mixture was vigorously stirred for 68 h. The two-phase system was separated, and the aqueous phase was washed repeatedly with dichloromethane. The aqueous phase was partially evaporated under vacuum to remove residual organic solvents and then a white solid precipitated. The product was collected by filtration washed with cool methanol and dried.

Yield: 62 %.

TLC: Rf = 0.76 (MeOH).

ESI-MS: *m/z* = 322.9 $[P+H]^+$, 345.0 $[P+Na]^+$, 666.8 $[2P+Na]^+$.

CD (CH_3OH) λ/nm (Δε/mdeg $M^{-1}cm^{-1}$): 241 (-6.56), 261 (+2.94), 334 (-0.61).

^{1}H NMR (500 MHz, CD_3OD) δ (ppm): 7.93 (d, 1H, $J_{4,3}$ = 8.9 Hz, H-4), 7.39 (d, 1H, $J_{5,6}$ = 7.9 Hz, H-5), 7.35 (m, 1H, H-7), 7.15 (t, 1H, $J_{6,5}$ = 7.9 Hz, H-6), 6.85 (d, 1H, $J_{3,4}$ = 8.9 Hz, H-3), 4.88 (d, 1H, $J_{1,2}$ = 7.8. Hz, H-1 of Gal), 4.01 (dd, 1H, $J_{2,3}$ = 9.8 Hz, $J_{2,1}$ = 7.8 Hz, H-2 of Gal), 3.93 (d, 1H, $J_{4,3}$ = 3.4 Hz, H-4 of Gal), 3.82 (m, 2H, Hs-6 of Gal), 3.73 (m, 1H, H-5 of Gal), 3.65 (dd, 1H, $J_{3,2}$ = 9.8 Hz, $J_{3,4}$ = 3.4 Hz, H-3 of Gal).

^{13}C NMR (125 MHz, CD_3OD) δ (ppm): 138.3 (C-4), 121.7 (C-6), 121.5 (C-7), 114.5 (C-5), 112.1 (C-3), 103.2 (C-1 of Gal), 75.7 (C-5 of Gal), 73.1 (C-3 of Gal), 70.8 (C-2 of Gal), 68.7 (C-4 of Gal), 61.0 (C-6 of Gal).

3.29 Synthesis of 5-chloro-8-quinolinyl-β-D-galactopyranoside (GalClHQ)

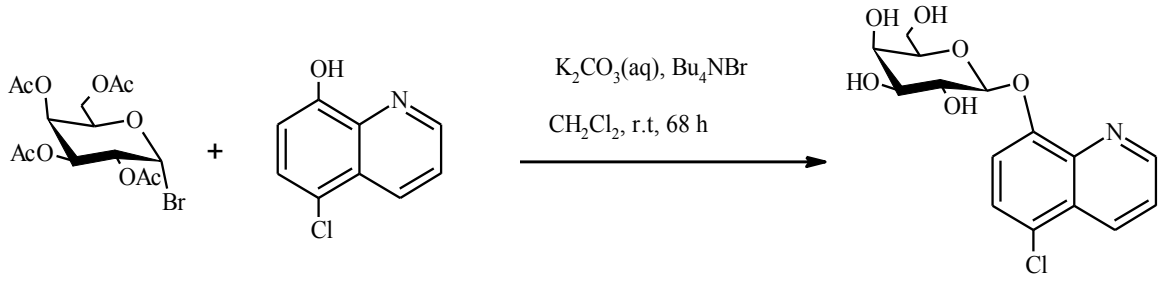

5-chloro-8-hydroxyquinoline (258 mg, 1.44 mmol) and K_2CO_3 (1.99 g, 14.4 mmol) were added to water (70 mL) and methanol (30 mL). Dichloromethane (100 mL) was added to this aqueous solution, followed by acetobromogalactose (773 mg, 1.88 mmol) and tetrabutylammonium bromide (464 mg, 1.44 mmol). The resulting mixture was vigorously stirred for 68 h. A solid precipitated, and the deacetylated product was collected by filtration, washed with cool methanol and dried.

Yield: 50%.

TLC: Rf = 0.75 (MeOH).

ESI-MS: *m/z* = 341.9 $[P+H]^+$, 363.9 $[P+Na]^+$, 704.6 $[2P+Na]^+$.

CD (CH_3OH) λ/nm (Δε/mdeg $M^{-1}cm^{-1}$): 217 (-1.29), 244 (+ 1.52), 260 (-0.41).

^{1}H NMR (500 MHz, CD_3OD) δ (ppm): 8.96 (dd, 1H, $J_{2,3}$ = 4.3 Hz, $J_{2,4}$ = 1.5 Hz, H-2), 8.69 (dd, 1H, $J_{4,3}$ = 8.6 Hz, $J_{4,2}$ = 1.5 Hz, H-4), 7.74 (dd, 1H, $J_{3,4}$ = 8.6 Hz, $J_{3,2}$ = 4.3 Hz, H-3), 7.67

(d, 1H, $J_{6,7}$ = 8.5 Hz, H-6), 7.53 (d, 1H, $J_{7,6}$ = 8.5 Hz, H-7), 5.04 (d, 1H, $J_{1,2}$ = 7.7 Hz, H-1 of Gal), 4.07 (dd, 1H, $J_{2,1}$ = 7.7 Hz, $J_{2,3}$ = 9.9 Hz, H-2 of Gal), 3.96 (d, 1H, $J_{4,3}$ = 3.4 Hz, H-4 of Gal), 3.83 (m, 3H, Hs-6 and H-5 of Gal), 3.69 (dd, 1H, $J_{3,2}$ = 9.9 Hz, $J_{3,4}$ = 3.4 Hz, H-3 of Gal).

^{13}C NMR (125 MHz, CD_3OD) δ (ppm): 149.2 (C-2), 133.3 (C-4), 122.4 (C-3), 126.6 (C-6), 112.9 (C-7), 102.1 (C-1 of Gal), 76.0 (C-5 of Gal), 72.7 (C-3 of Gal), 70.5 (C-2 of Gal), 68.7 (C-4 of Gal), 61.1 (C-6 of Gal).

3.30 Synthesis of 5-nitro-8-quinolinyl-tetra-O-acetyl-β-D-galactopyranoside

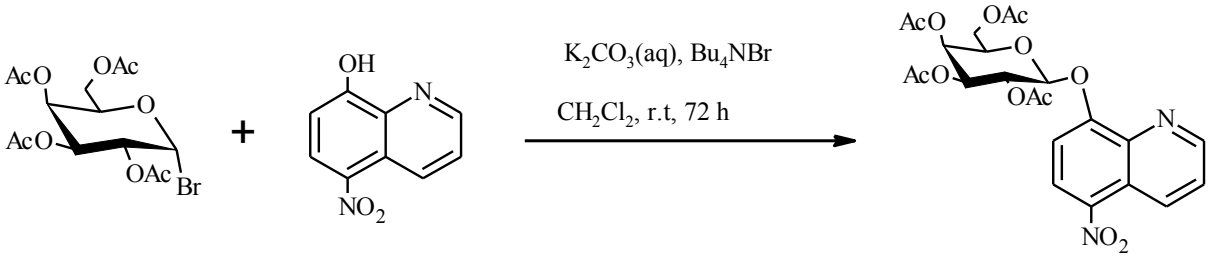

5-nitro-8-hydroxyquinoline (230 mg, 1.21 mmol, NHQ) and K_2CO_3 (1.67 g, 12.1 mmol) were dissolved in water (250 mL). Dichloromethane (250 mL) was added to this aqueous solution, followed by acetobromogalactose (600 mg, 1.46 mmol) and tetrabutylammonium bromide (390 mg, 1.21 mmol). The resulting mixture was vigorously stirred for 72 h. The two-phase system was separated, and the aqueous phase was washed repeatedly with dichloromethane. The combined organic extracts were dried with Na_2SO_4, filtered, and evaporated under vacuum. The crude product was purified by column chromatography (eluent: AcOEt/hexane 3:2).

Yield: 62 %.

ESI-MS: *m/z* = 521.0 $[P+H]^+$, 544.0 $[P+Na]^+$, 1062.9 $[2P+Na]^+$.

^{1}H NMR (500 MHz, $CDCl_3$) δ (ppm): 9.19 (dd, 1H, $J_{4,3}$ = 8.9 Hz and $J_{4,2}$ = 1.6 Hz, H-4), 9.06 (dd, 1H, $J_{2,3}$ = 4.2 Hz and $J_{2,4}$ = 1.6 Hz, H-2), 8.47 (d, 1H, $J_{6,7}$ = 8.8 Hz, H-6), 7.72 (dd, 1H, $J_{3,4}$ = 8.9 Hz, $J_{3,2}$ = 4.2 Hz, H-3), 7.47 (d, 1H, $J_{7,6}$ = 8.8 Hz, H-7), 5.77 (dd, 1H, $J_{2,3}$ = 10.4 Hz, $J_{2,1}$ = 7.9 Hz, H-2 of Gal), 5.52 (m, 2H, H-1 and H-4 of Gal), 5.22 (dd, 1H, $J_{3,2}$ = 10.4 Hz, $J_{3,4}$

= 3.4 Hz, H-3 of Gal), 4.29-4.09 (m, 3H, H-5 and Hs-6 of Gal), 2.20 (s, 3H, CH_3), 2.10-2.03 (m, 9H, CH_3).

3.31 Synthesis of 5-nitro-8-quinolinyl-β-D-galactopyranoside (GalNHQ)

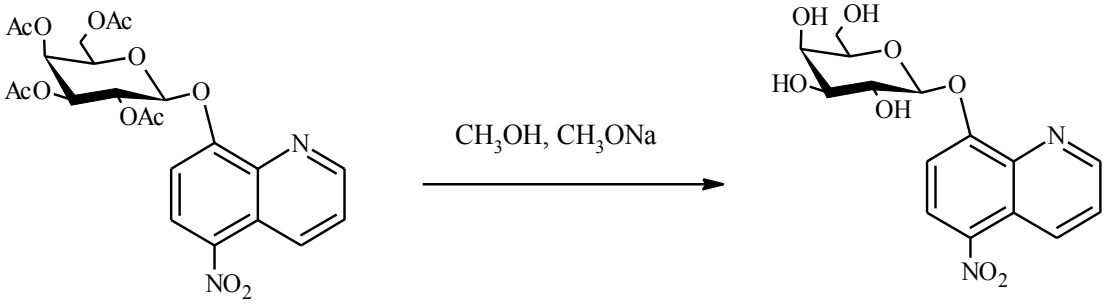

Peracetylated galactoside (100 mg, 0.19 mmol) was dissolved in 8 mL of absolute methanol. To this mixture 2 mL of NaOMe (0.1 N, MeOH solution) were added. The mixture was stirred for 3 h and the deacetylated product precipitated and was collected by filtration, washed with cool methanol and dried.

Yield: 94 %.

TLC: Rf = 0.74 (MeOH).

ESI-MS: *m/z* = 352.9 $[P+H]^+$, 375.0 $[P+Na]^+$, 726.7 $[2P+Na]^+$.

^{1}H NMR (500 MHz, CD_3OD) δ (ppm): 9.23 (dd, 1H, $J_{4,3}$ = 8.9 Hz, $J_{4,2}$ = 1.2 Hz, H-4), 9.03 (dd, 1H, $J_{2,3}$ = 4.2 Hz, $J_{2,4}$ = 1.2 Hz, H-2), 8.54 (d, 1H, $J_{6,7}$ = 8.9 Hz, H-6), 7.86 (dd, 1H, $J_{3,4}$ = 8.9 Hz, $J_{3,2}$ = 4.2 Hz, H-3), 7.61 (d, 1H, $J_{7,6}$ = 8.9 Hz, H-7), 5.21 (d, 1H, $J_{1,2}$ = 7.8 Hz, H-1 of Gal), 4.11 (dd, 1H, $J_{2,3}$ = 9.9 Hz, $J_{2,1}$ = 7.8 Hz, H-2 of Gal), 3.98 (d, 1H, $J_{4,3}$ = 3.4 Hz, H-4 of Gal), 3.87 (m, 2H, H-5 and H-6a of Gal), 3.80 (dd, 1H, $J_{6b,6a}$ = 10.6 Hz, $J_{6b,5}$ = 4.1 Hz, H-6b of Gal), 3.72 (dd, 1H, $J_{3,2}$ = 9.9 Hz, $J_{3,4}$ = 3.4 Hz, H-3 of Gal).

^{13}C NMR (125 MHz, CD_3OD) δ (ppm): 158.2 (C-8), 150.2 (C-2), 138.7 (C-9), 132.9 (C-4), 127.2 (C-6), 124.5 (C-3), 122.7 (C-10), 110.4 (C-7), 101.7 (C-1 of Gal), 76.0 (C-5 of Gal), 72.6 (C-3 of Gal), 70.2 (C-2 of Gal), 68.6 (C-4 of Gal), 60.9 (C-6 of Gal).

3.32 Synthesis of 5,7-dichloro-8-quinolinyl-β-D-galactopyranoside ($GalCl_2HQ$)

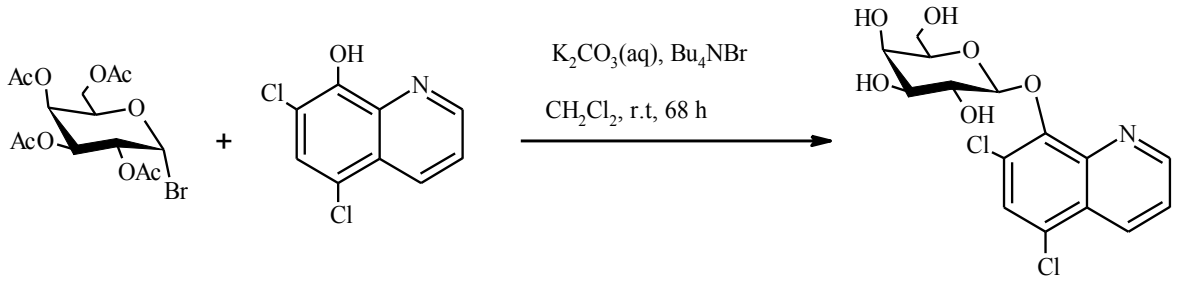

5,7-dichloro-8-quinolinol derivative (308 mg, 1.44 mmol) and K_2CO_3 (1.99 g, 14.4 mmol) were added to water (70 mL) and methanol (30 mL). Dichloromethane (100 mL) was added to this aqueous solution, followed by acetobromogalactose (773 mg, 1.88 mmol) and tetrabutylammonium bromide (464 mg, 1.44 mmol). The resulting mixture was vigorously stirred for 68 h. A solid precipitated, and the deacetylated product was collected by filtration, washed with cool methanol and dried.

Yield: 64%.

TLC: Rf = 0.79 (MeOH).

ESI-MS: *m/z* = 375.9 $[P+H]^+$, 397.9 $[P+Na]^+$, 772.5 $[2P+Na]^+$.

CD (CH_3OH) λ/nm (Δε): 243 (-8.49), 321 (+1.18).

^{1}H NMR (500 MHz, CD_3OD) δ (ppm): 8.98 (dd, 1H, $J_{2,3}$ = 4.3 Hz, $J_{2,4}$ = 1.5 Hz, H-2), 8.70 (dd, 1H, $J_{4,3}$ = 8.6 Hz, $J_{4,2}$ = 1.5 Hz, H-4), 7.84 (s, 1H, H-6), 7.73 (dd, 1H, $J_{3,4}$ = 8.6 Hz, $J_{3,2}$ = 4.3 Hz, H-3), 5.24 (d, 1H, $J_{1,2}$ = 7.8 Hz, H-1 of Gal), 4.05 (dd, 1H, $J_{2,3}$ = 9.7 Hz, $J_{2,1}$ = 7.8 Hz, H-2 of Gal), 3.85 (d, 1H, $J_{4,3}$ = 3.2 Hz, H-4 of Gal), 3.72 (dd, 1H, $J_{6a,6b}$ = 11.2 Hz, $J_{6,5}$ = 6.1 Hz, H-6a of Gal), 3.64 (m, 2H, H-6b and H-3 of Gal), 3.48 (m, 1H, H-5 of Gal).

^{13}C NMR (125 MHz, CD_3OD) δ (ppm): 150.5 (C-2), 147.7 (C-8), 137.2 (C-9), 135.2 (C-4), 133.2 (C-6), 128.0 (C-7), 127.4 (C-5), 126.0 (C-10), 123.4 (C-3), 106.1 (C-1 of Gal), 79.6 75.8 (C-5 of Gal), 74.0 (C-3 of Gal), 71.7 (C-2 of Gal), 68.6 (C-4 of Gal), 60.1 (C-6 of Gal).

3.33 Synthesis of 5-chloro-7-iodo-8-quinolinyl-tetra-O-acetyl-β-D-galactopyranoside

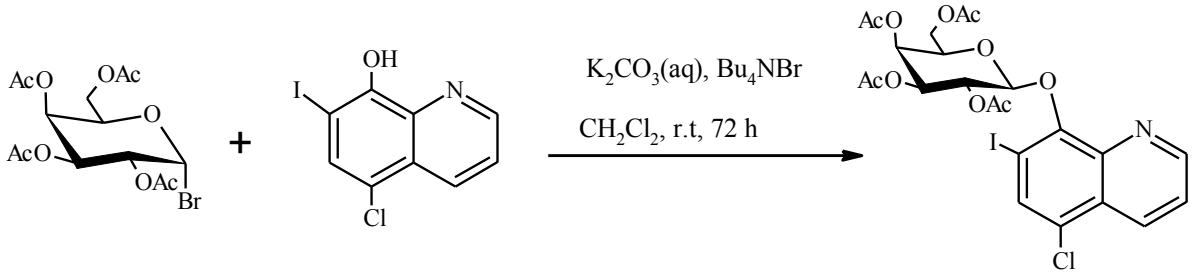

5-Chloro-7-iodo-8-hydroxyquinoline (230 mg, 0.75 mmol) and K_2CO_3 (1.04 g, 7.5 mmol) were added to 75 mL water and methanol. Dichloromethane (75 mL) was added to this aqueous solution, followed by acetobromogalactose (650 mg, 1.58 mmol) and tetrabutylammonium bromide (242 mg, 0.75 mmol). The resulting mixture was vigorously stirred for 72 h. The two-phase system was separated, and the aqueous phase was washed repeatedly with dichloromethane. The combined organic extracts were dried with Na_2SO_4, filtered, and evaporated under vacuum. The crude product was purified by column chromatography (eluent: AcOEt/hexane = 3:2) to afford a white solid.

Yield: 42 %.

ESI-MS: *m/z* = 635.8 $[P+H]^+$, 657.8 $[P+Na]^+$, 673.8 $[P+K]^+$.

^{1}H NMR (500 MHz, $CDCl_3$) δ (ppm): 8.96 (d, 1H, $J_{2,3}$ = 4.0 Hz, H-2), 8.56 (dd, 1H, $J_{4,3}$ = 8.5 Hz, $J_{4,2}$ = 1.1 Hz, H-4), 8.01 (s, 1H, H-6), 7.58 (dd, 1H, $J_{3,4}$ = 8.5 Hz, $J_{3,2}$ = 4.0 Hz, H-3), 6.15 (d,1H, $J_{1,2}$ = 8.0 Hz, H-1 of Gal), 5.70 (dd, 1H, $J_{2,3}$ = 10.4 Hz, $J_{2,1}$ = 8.0 Hz, H-2 of Gal), 5.41 (dd, 1H, $J_{4,5}$ = 4.9 Hz, $J_{4,3}$ = 3.8 Hz, H-4 of Gal), 5.19 (dd, 1H, $J_{3,2}$ = 10.4 Hz, $J_{3,4}$ = 3.8 Hz, H-3 of Gal), 4.14 (m, 1H, H-6a of Gal), 4.04 (m, 1H, H-6b of Gal), 3.87 (t, 1H, J = 6.8 Hz, H-5 of Gal), 2.23 (s, 3H, CH_3), 2.13 (s, 3H, CH_3), 2.04 (s, 3H, CH_3), 1.89 (s, 3H, CH_3).

^{13}C NMR (125 MHz, $CDCl_3$) δ (ppm): 149.8 (C-2), 135.7 (C-6), 133.8 (C-4), 122.2 (C-3), 101.4 (C-1 of Gal), 70.9 (C-3 of Gal), 70.8 (C-5 of Gal), 69.7 (C-2 of Gal), 66.8 (C-4 of Gal), 60.8 (C-6 of Gal), 20.9-20.3 (CH_3).

3.34 Synthesis of 5-chloro-7-iodo-8-quinolinyl-β-D-galactopyranoside (GalCQ)

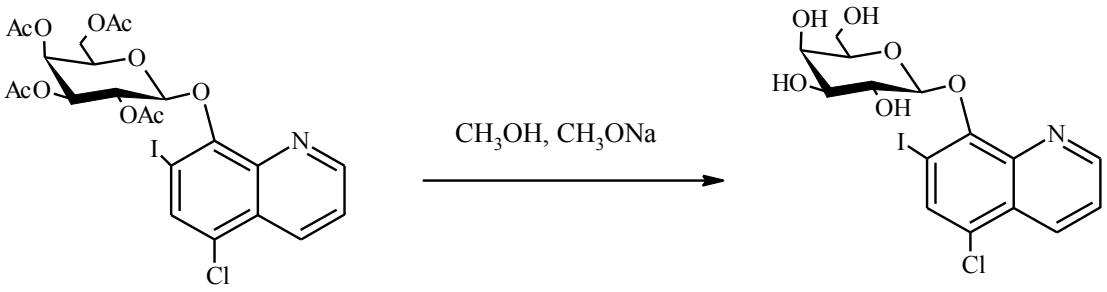

Peracetylated galactoside (100 mg, 0.16 mmol) was dissolved in 8 mL of absolute methanol. To this mixture 2 mL of NaOMe (0.1 N, MeOH solution) were added. After 20 min, a solid precipitated, however the mixture was stirred overnight to complete the deacetylation. The product was collected by filtration, washed with cool methanol and dried.

Yield: 50 %.

TLC: Rf = 0.79 (MeOH).

ESI-MS: *m/z* = 467.9 $[P+H]^+$, 489.9 $[P+Na]^+$, 956.7 $[2P+Na]^+$.

CD (CH_3OH) λ/nm (Δε/mdeg $M^{-1}cm^{-1}$): 226 (-3.24), 246 (-6.00), 320 (+2.16).

^{1}H NMR (500 MHz, CD_3OD) δ (ppm): 8.94 (d, 1H, $J_{2,3}$ = 4.0 Hz, H-2), 8.68 (d, 1H, $J_{4,3}$ = 7.9 Hz, H-4), 8.13 (s, 1H, H-6), 7.74 (dd, 1H, $J_{3,4}$ = 7.9 Hz, $J_{3,2}$ = 4.0 Hz, H-3), 5.35 (d, 1H, $J_{1,2}$ = 7.8 Hz, H-1 of Gal), 4.08 (m, 1H, H-2 of Gal) 3.86 (m, 1H, H-4 of Gal), 3.74 (dd, 1H, $J_{6a,6b}$ = 11.2 Hz, $J_{6a,5}$ = 6.1 Hz, H-6a of Gal), 3.66 (dd, 1H, $J_{6b,6a}$ = 11.2 Hz, $J_{6b,5}$ = 6.1 Hz, H-6b of Gal), 3.59 (dd, 1H, $J_{3,2}$ = 9.6 Hz, $J_{3,2}$ = 3.4 Hz, H-3 of Gal), 3.44 (m, 1H, H-5 of Gal).

^{13}C NMR (125 MHz, CD_3OD) δ (ppm): 151.2 (C-2), 136.6 (C-4), 134.2 (C-6), 123.4 (C-3), 105.1 (C-1 of Gal), 75.8 (C-5 of Gal), 74.8 (C-3 of Gal), 71.8 (C-2 of Gal), 68.6 (C-4 of Gal), 60.3 (C-6 of Gal).

3.35 Synthesis of 2'-[(8-hydroxyquinolyl)-2-carboxyl]aminoethyl]-β-D-glucopyranoside (GlcHQ)

GlcHQ was synthetized by a three-step procedure.

3.35.1 I step: synthesis of 2'-(Fmoc-amino)ethyl-2,3,4,6-tetra-O-acetyl-β-D-glucopyranoside

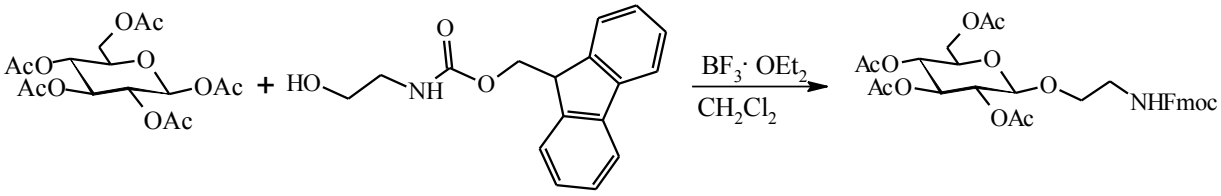

Boron trifluoride diethyl etherate (1.8 mL) was added dropwise to a solution of β-D-glucose pentaacetate (1.67 g, 4.3 mmol) and 9-fluorenylmethyl-*N*-(2-hydroxyethyl)carbamate (1.3 g, 4.6 mmol) in 20 mL of CH_2Cl_2 at 0 °C. After a few minutes, the mixture was heated at room temperature and stirred for 48 h. The reaction was then quenched with water and extracted with CH_2Cl_2. The CH_2Cl_2 layer was collected, dried with Na_2SO_4, and concentrated *in vacuo*. The crude product was purified by silica gel chromatography using ethyl acetate/hexane (3:2) as the eluent.

Yield: 74 %.

TLC: Rf = 0.42 (AcOEt: Hex 3:2).

Positive ion ESI-MS: *m/z* = 613.9 $[P+H]^+$, 636.1 $[P+Na]^+$, 651.9 $[P+K]^+$.

^{1}H NMR (500 MHz, $CDCl_3$) δ (ppm): 7.79 (t, 2H, $J_{4,3} = J_{5,6}$ = 6.7 Hz, H-4 and H-5 of Fmoc), 7.61 (t, 2H, $J_{1,2} = J_{8,7}$ = 6.5 Hz, H-1 and H-8 of Fmoc), 7.43 (m, 2H, H-3 and H-6 of Fmoc), 7.34 (m, 2H, H-2 and H-7 of Fmoc), 5.22 (t, 1H, *J* = 9.6 Hz, H-3 of Glc), 5.05 (t, 1H, *J* = 9.7 Hz, H-4 of Glc), 4.98 (m, 1H, H-2 of Glc), 4.56 (m, 1H, H-9 of Fmoc), 4.49 (m, 1H, CH_2 of Fmoc), 4.36 (d, 1H, $J_{1,2}$ = 7.9 Hz, H-1 of Glc), 4.31-4.03 (m, 3H, CH_2 of Fmoc and Hs-6), 3.79 (m, 1H, OCH_2 of en), 3.71 (m, 1H, OCH_2 of en), 3.59 (m,1H, H-5 of Glc), 3.38 (m, 2H, CH_2N of en), 2.11-2.00 (m, 12H, CH_3).

3.35.2 II step: synthesis of 2'-aminoethyl-β-D-glucopyranoside

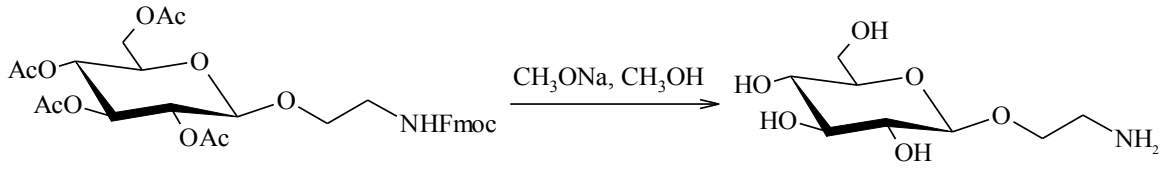

2′-(Fmoc-amino)-ethyl-2,3,4,6-tetra-O-acetyl-β-D-glucopyranoside (1.0 g, 1.63 mmol) was stirred in methanol (25 mL) with sodium methoxide (MeOH solution, 2.4 mL, 0.5 M) at room temperature overnight. The reaction mixture was concentrated *in vacuo*; the resulting residue was dissolved in water and the aqueous solution was extracted with CH_2Cl_2. The aqueous layer was lyophilized and the product was used without further purification.

Yield: 85 %.

ESI-MS: *m/z* = 224.0 $[P+H]^+$, 246.0 $[P+Na]^+$, 446.7 $[2P+H]^+$, 468.7 $[2P+Na]^+$.

3.35.3 III step: synthesis of GlcHQ

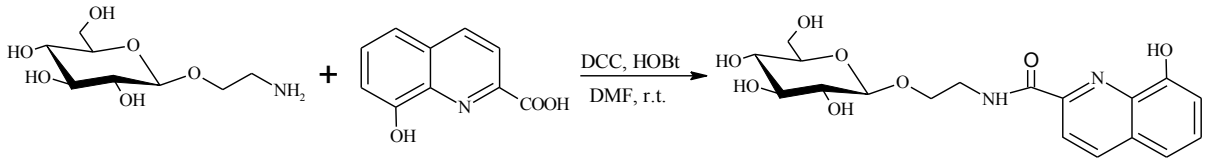

To a suspension of 8-hydroxyquinoline-2-carboxylic acid (127 mg, 0.67 mmol) in dry DMF (10 mL) were added 1-hydroxybenzotriazole monohydrate (91 mg, 0.67 mmol) and DCC (138 mg, 0.67 mmol). After 0.5 h, 2′-aminoethyl-β-D-glucopyranoside (150 mg, 0.67 mmol) was added. The reaction mixture was stirred for 48 h at room temperature.

Yield: 68 %.

TLC: Rf = 0.70 (MeOH).

Positive ion ESI-MS (CH_3OH): *m/z* = 394.9 $[P+H]^+$, 417.1 $[P+Na]^+$, 433.1$[P+K]^+$, 810.7 $[2P+Na]^+$, 827.1 $[2P+K]^+$.

Negative ion ESI-MS (CH_3OH): *m/z* = 393.1 $[P-H]^-$, 808.9 $[2P-2H+Na]^-$.

^{1}H NMR (500 MHz, CD_3OD) δ (ppm): 8.41 (d, 1H, $J_{4,3}$ = 8.6 Hz, H-4), 8.19 (d, 1H, $J_{3,4}$ = 8.6 Hz, H-3), 7.54 (t, 1H, *J* = 7.9 Hz, H-6), 7.41 (d, 1H, $J_{5,6}$ = 7.7 Hz, H-5), 7.16 (d, 1H, $J_{7,6}$ = 7.5

Hz, H-7), 4.37 (d, 1H, $J_{1,2}$ = 7.8 Hz, H-1 of Glc), 4.13 (m, 1H, CH_2), 3.84 (m, 3H, CH_2, H-5 of Glc), 3.69 (m, 2H, CH_2, H-4 of Glc), 3.40-3.17 (m, 4H, H-3, Hs-6, H-2 of Glc).

3.36 Synthesis of 6-deoxy-6-(8-hydroxyquinolyl)-2-methylamino]-α,α'-trehalose (THRHQ)

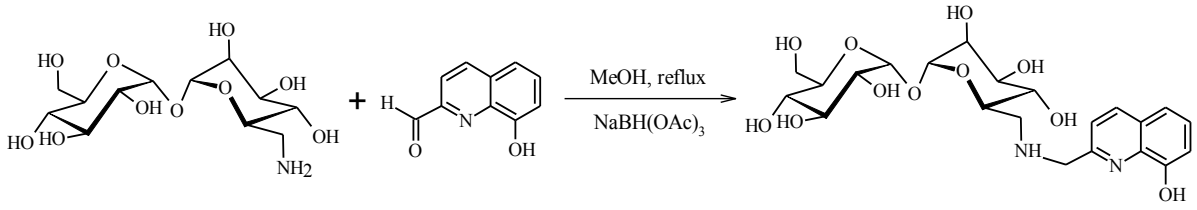

8-Hydroxy-2-quinolinecarboxaldehyde (13 mg, 0.075 mmol) was added to 6-amino-6-deoxy-α,α'-trehalose (25 mg, 0.074 mmol) in anhydrous methanol (8 mL). After 7 h, sodium triacetoxyborohydride (31 mg, 0.15 mmol) was added. The reaction was refluxed overnight and then the solvent was evaporated *in vacuo*. The crude product was purified by ion-exchange chromatography on Sephadex CM-25 (linear gradient of NH_4HCO_3 from 0 to 0.25).

Yield: 83 %.

TLC: 0.54 (AcOEt: PrOH: H_2O: NH_3 4:3:2:1).

Positive ion ESI-MS: *m/z* = 499.1 $[P+H]^+$, 521.1 $[P+Na]^+$, 996.6 $[2P+H]^+$, 1018.7 $[2P+Na]^+$.

^{1}H NMR (500 MHz, D_2O) δ (ppm): 8.17 (d, 1H, $J_{4,3}$ = 8.4 Hz, H-4), 7.37 (m, 2H, H-3 and H-6), 7.24 (d, 1H, $J_{5,6}$ = 7.8 Hz, H-5), 6.98 (d, 1H, $J_{7,6}$ = 7.4 Hz, H-7), 5.11 (m, 2H, Hs-1 of TH), 4.04 (m, 2H, CH_2Ar), 3.89 (m, 1H, H-5A of TH), 3.74 (m, 4H, Hs-3, H-5B, H-6B of TH), 3.66 (dd, 1H, $J_{6B,6'B}$ = 11.9 Hz and $J_{6'B,5}$ = 4.9 Hz, H-6'B of TH), 3.55 (dd, 1H, $J_{2A,3A}$ = 9.9 Hz and $J_{2A,1A}$ = 3.0 Hz, H-2A of TH), 3.51 (dd, 1H, $J_{2B,3B}$ = 9.9 Hz and $J_{2B,1B}$ = 3.5 Hz, H-2B of TH), 3.34 (t, 1H, *J* = 9.4 Hz, H-4B of TH), 3.22 (m, 1H, H-4A of TH), 2.98 (d, 1H, $J_{6A,6'A}$ = 12.5 Hz, H-6A of TH), 2.76 (m, 1H, H-6'A of TH).

^{13}C NMR (125 MHz, D_2O) δ (ppm): 156.2 (C-2), 155.6 (C-8), 139.1 (C-9), 137.4 (C-4), 128.8 (C-10), 127.5 (C-6), 120.7 (C-3), 116.1 (C-5), 112.6 (C-7), 93.2 (Cs-1 of TH), 73.1-71.4 (Cs-3, C-4A, C-5B of TH), 71.0 (Cs-2 of TH), 70.3 (C-5A of TH), 69.6 (C-4B of TH), 60.5 (C-6B of TH), 53.4 (CH_2Ar), 49.0 (C-6A of TH).

3.37 Synthesis of 6^A-deoxy-6^A-[[(8-hydroxyquinolyl)-2-carboxyl]amino]-β-cyclodextrin (CD6HQ)

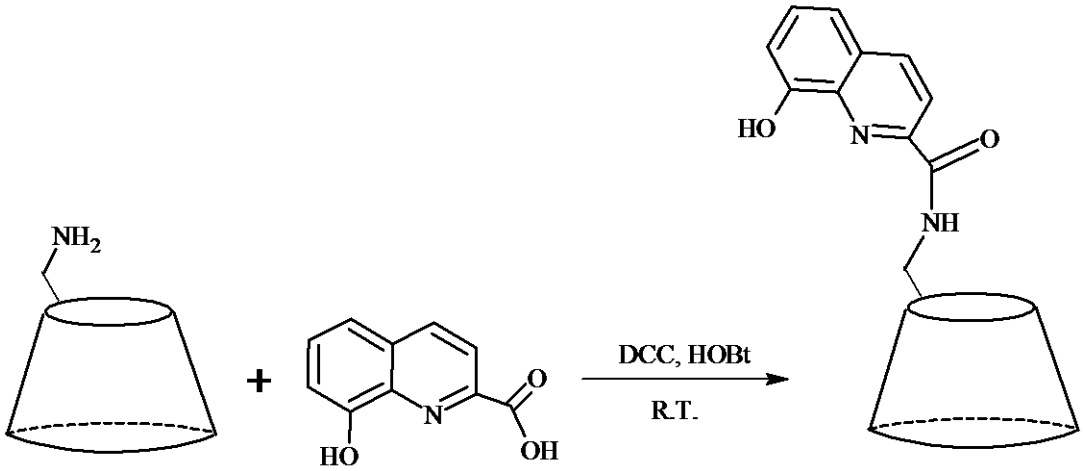

HOBt (24 mg, 0.175 mmol) and DCC (36 mg, 0.175 mmol) were added to a suspension of 8-hydroxyquinoline-2-carboxylic acid (33 mg, 0.175 mmol) in dry DMF (7 mL). After 0.5 h, 6-amino-6-deoxy-β-cyclodextrin (198 mg, 0.175 mmol) was added. The reaction mixture was stirred for 48 h at room temperature. Then the solution was added to acetone (200 mL) and the resulting precipitate was collected by filtration. The crude product was purified by reversed-phase (C-18) flash chromatography (eluent: $H_2O \rightarrow MeOH$) to give the product as a white solid.

Yield: 53 %.

TLC: Rf = 0.35 (AcOEt: PrOH: H_2O: NH_3 4:3:2:1).

ESI-MS: *m/z* = 664.1 $[P+H+Na]^{2+}$, 672.2 $[P+H+K]^{2+}$, 1305.2 $[P+H]^+$, 1327.4 $[P+Na]^+$, 1343.3 $[P+K]^+$.

HRMS: *m/z* = 675.1985 $[P+2Na]^{2+}$, 1327.4068 $[P+Na]^+$.

UV-Vis (MOPS, 5mM, pH 7.4) λ/nm (ε): 255 (24592), 307 (1683), 348 (1167).

CD (H_2O) λ/nm (Δε): 254.5 (-9.9).

^{1}H NMR (500 MHz, D_2O) δ (ppm): 8.17 (d, 1H, $J_{4,3}$ = 8.5 Hz, H-4), 7.91 (d, 1H, $J_{3,4}$ = 8.5 Hz, H-3), 7.36 (m, 1H, H-6), 7.27, (d, 1H, $J_{5,6}$ = 8.2 Hz, H-5), 7.09 (d, 1H, $J_{7,6}$ = 7.5Hz, H-7), 5.10 (d, 1H, $J_{1F,2F}$ = 3.8 Hz, H-1F of CyD), 5.03 (d, 1H, $J_{1,2}$ = 3.7 Hz, H-1 of CyD), 5.01-4.97 (m, 2H, Hs-1 of CyD), 4.94 (d, 1H, $J_{1G,2G}$ = 3.8 Hz, H-1G of CyD), 4.92 (d, 1H, $J_{1B,2B}$ = 3.6 Hz,

H-1B of CyD), 4.80 (d, 1H, $J_{1A,2A}$ = 3.4 Hz, H-1A of CyD), 4.14 (d, 1H, $J_{6F,6'F}$ = 13.1 Hz, H-6F of CyD), 4.13-3.35 (m, 38H, H-3, H-5, H-6, H-4, H-2 of CyD), 3.31 (m, 1H, H-5A of CyD), 3.12 (m, 1H, H-6B of CyD), 2.86 (d, 1H, $J_{6A,6'A}$ = 11.5 Hz, H-6A of CyD).

^{13}C NMR (125 MHz, D_2O) δ (ppm): 165.9 (C=O), 152.4 (C-10), 146.5 (C-2), 137.5 (C-4), 136.4 (C-9), 129.7 (C-6), 118.7 (C-3), 118.2 (C-5), 111.9 (C-7), 102.5-101.0 (Cs-1 of CyD), 83.7 (C-4A of CyD), 81.7-79.9 (Cs-4 of CyD), 74.0-70.5 (Cs-3, Cs-5, Cs-2 of CyD), 61.0-58.5 (Cs-6 of CyD), 40.3 (C-6 of CyD).

3.38 Synthesis of 6^A-deoxy-6^A-[[(8-hydroxyquinolyl)-2-carboxyl]ethylamino]-β-cyclodextrin (CDOHQ)

CDOHQ was synthetized starting from 6-deoxy-6-hydroxylethylamino-β-cyclodextrin that was obtained as follows.

3.38.1 Synthesis of 6-deoxy-6-hydroxylethylamino-β-cyclodextrin

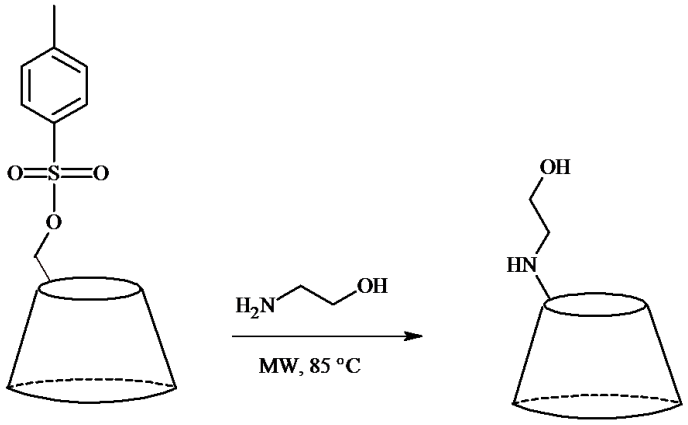

An excess of ethanolamine (5 mL) was reacted with 6-tosyl-β-CD (400 mg, 0.31 mmol) in a sealed tube yielding the product *via* the microwave procedure (30 min, 200 W, 85 °C) reported elsewhere.[163] After cooling, the solution was added to acetone (200 mL) and the resulting precipitate was collected by filtration.

Yield: 89 %.

TLC: Rf = 0.46 (PrOH: AcOEt: H_2O: NH_3 5:2:3:3).

HRMS: *m/z* = 1178.4246 $[P+H]^+$.

^{1}H NMR (500 MHz, D_2O): 5.08 (m, 7H, Hs-1 of CyD), 4.03–3.79 (m, 26H, Hs-3, Hs-5, Hs-6 of CyD), 3.76–3.53 (m, 15H, Hs-2, Hs-4, β–CyD–NH–CH_2–CH_2–OH), 3.45 (t, 1H, *J* = 9.5 Hz, H-4A of CyD), 3.09 (d, 1H, $J_{6A,6A'}$ = 10.6 Hz, H-6A of CyD), 2.83 (m, 1H, H-6'A of CyD), 2.78–2.71 (m, 2H, CyD–NH–CH_2–CH–OH).

^{13}C NMR (125 MHz, D_2O): 102.0 (Cs-l of CyD), 83.8 (C-4A of CyD), 81.3 (Cs-4 of CyD), 73.2 (Cs-2 of CyD), 72.2 (Cs-5 of CyD), 71.9 (Cs-3 of CyD), 70.6 (C-5A of CyD), 60.3 (Cs-6 and CyD–NH–CH_2–CH_2–OH), 50.3 (C-6A of CyD), 49.4 (CyD–NH–CH_2–CH_2–OH).

3.38.2 Synthesis of CDOHQ

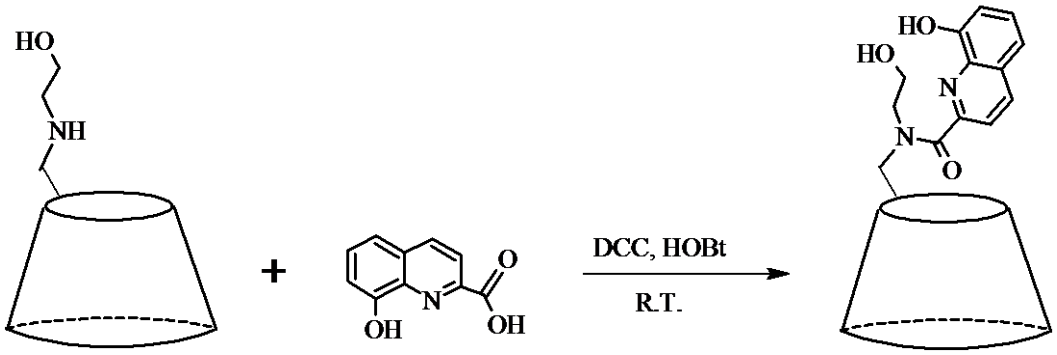

8-hydroxyquinoline-2-carboxylic acid (29 mg, 0.153 mmol) was dissolved in dry DMF (7 mL). HOBt (20.7 mg, 0.153 mmol) and DCC (31.6 mg, 0.153 mmol) were added. This mixture was stirred at room temperature for 30 min. 6-deoxy-6-hydroxylethylamino-β-cyclodextrin (180 mg, 0.153 mmol) was added to the solution and the reaction was carried out at room temperature for 60 h and was followed by TLC. Acetone was added until the precipitation of the CyD derivative was complete. The precipitate was collected by filtration and purified by reversed-phase (C18) flash chromatography (eluent: H_2O→MeOH) to give the product as a white solid.

Yield: 37 %.

TLC: 0.32 (AcOEt: PrOH: H_2O: NH_3 4:3:2:1).

ESI-MS: *m/z* = 686.2 $[P+H+Na]^{2+}$, 697.2 $[P+2Na]^{2+}$, 1349.3 $[P+H]^+$, 1371.5 $[P+Na]^+$, 1387.3 $[P+K]^+$.

HRMS: *m/z* = 1371.4266 $[P+Na]^+$.

UV-Vis (MOPS, 5mM, pH 7.4) λ/nm (ε): 250 (24688), 307 (1983).

CD (H_2O) λ/nm (Δε): 227.0 (+15.9), 251.5 (-29.8), 275 (+3.6).

^{1}H NMR (500 MHz, D_2O) δ (ppm): 8.37 (d, 1H, $J_{4,3}$ = 8.6 Hz, H-4), 7.74 (d, 1H, $J_{3,4}$ = 8.6 Hz, H-3), 7.60 (m, 1H, H-6), 7.39 (d, 1H, $J_{5,6}$ = 8.1 Hz, H-5), 7.36 (d, 1H, $J_{7,6}$ = 7.6 Hz, H-7), 5.5 (t, 1H, 5A), 5.10 (d, 1H, H-1A of CyD), 5.15-4.74 (m, 4H, Hs-1 of CyD), 4.77 (m, 2H, H-1B, H-1X of CyD), 4.34-3.02 (m, 39H, H-2, H-3, H-4, H-5, H-6 of CyD), 3.07 (m, 1H, H of CH_2 α to NCO), 2.97 (t, 1H, H of CH_2 in β to NCO), 2.82 (m, 1H, H of CH_2 α to NCO), 2.73 (d, 1H, H of CH_2 β to NCO), 2.59 (d, 1H, H-3X of CyD), 1.96 (m, 1H, H-3B of CyD).

^{13}C NMR (125 MHz, D_2O) δ (ppm): 171.7 (C=O), 152.5 (C-8), 151.6 (C-2), 137.5 (C-4), 135.9 (C-9), 129.1 (C-6), 128.8 (C-10), 121.1 (C-3), 117.8 (C-5), 111.9 (C-7), 102.2-100.4 (Cs-1 of CyD), 84.5 (C-4A of CyD), 81.4-80.0 (Cs-4 of CyD), 73.7-70.8 (other Cs of CyD), 60.3- 58.6 (Cs-6 of CyD), 51.2 (CH_2 α to NCO), 50.5 (CH_2 β to NCO).

3.39 Synthesis of 6^A-deoxy-6^A-[[(8-hydroxyquinolyl)-2-carboxyl]aminoethylamino]-β-cyclodextrin (CDNHQ)

CDNHQ was synthetized starting from 6-deoxy-6-aminoethylamino-β-cyclodextrin that was obtained as follows.

3.39.1 Synthesis of 6-deoxy-6-aminoethylamino-β-cyclodextrin

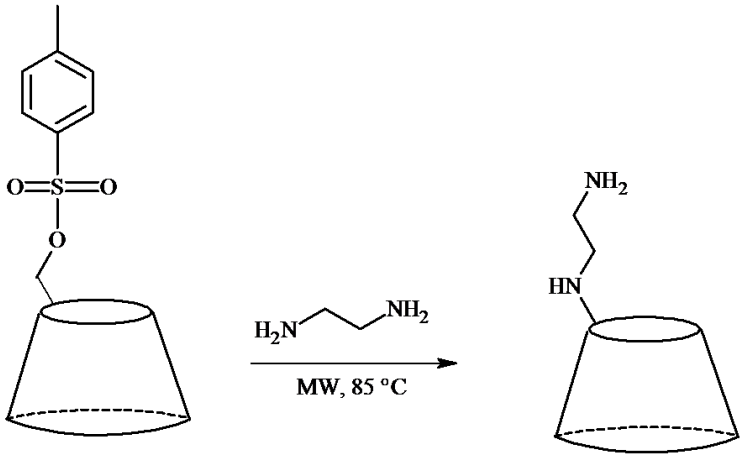

The synthesis of 6-deoxy-6-aminoethylamino-β-cyclodextrin was performed under microwave irradiation (200 W). In brief, 6-tosyl-β-CyD (400 mg, 0.31 mmol) was dissolved in neat ethylendiamine (5 mL) and the reaction was carried out at 85 °C for 30 min. After cooling, the solution was added to acetone (200 mL) and the resulting precipitate was collected by filtration.

Yield: 88 %.

TLC: Rf = 0.26 (PrOH: AcOEt: H_2O: NH_3 5:2:3:3).

HRMS: *m/z* = 1177.4339 $[P+H]^+$.

^{1}H NMR (500 MHz, D_2O): 4.97 (s, 7H, Hs-1 of CyD), 3.90–3.71 (m, 26H, Hs-3, Hs-5, Hs-6 of CyD), 3.60–3.43 (m, 13H, Hs-2, Hs-4 of CyD), 3.35 (t, 1H, $J_{3,4} = J_{4,5}$ = 9.17 Hz, H-4A of CyD), 2.95 (d, 1H, $J_{6A,6A'}$ = 11.0 Hz, H-6A of CyD), 2.76–2.55 (m, 5H, H-6A', β– CD–CH_2–CH_2–NH_2).

^{13}C NMR (125 MHz, D_2O): 102.0 (Cs-l of CyD), 84.0 (C-4A of CyD), 81.2 (Cs-4 of CyD), 73.1 (Cs-2 of CyD), 72.1 (Cs-5 of CyD), 71.9 (Cs-3 of CyD), 70.5 (C-5A of CyD), 60.4 (C-6 of CyD), 50.2 (C-6A of CyD), 49.3 (–NH–CH_2–), 39.7(–CH_2–NH_2).

3.39.2 Synthesis of CDNHQ

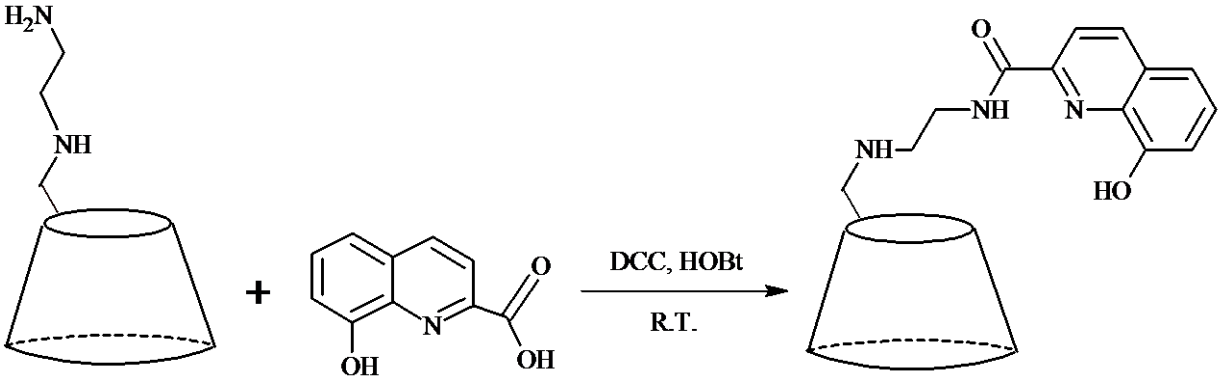

8-hydroxyquinoline-2-carboxylic acid (32 mg, 0.170 mmol) was dissolved in dry DMF (7 mL). HOBt (23 mg, 0.170 mmol) and DCC (35 mg, 0.170 mmol) were added. This mixture was stirred at room temperature for 30 min. 6-aminoethylamino-6-deoxy-β-cyclodextrin (200 mg, 0.170 mmol) was added to the solution and the reaction mixture was stirred at room temperature for 60 h. Acetone was added until the precipitation of the CyD derivative was

complete. The precipitate was collected by filtration and purified by reversed-phase (C18) flash chromatography (eluent: $H_2O \rightarrow MeOH$) to give the product.

Yield: 35 %.

TLC: Rf = 0.48 (PrOH: AcOEt: H_2O: NH_3 4:3:2:1).

ESI-MS: *m/z* = 685.7 $[P+H+Na]^{2+}$, 696.7 $[P+2Na]^{2+}$, 1348.4 $[P+H]^{+}$, 1370.4 $[P+Na]^{+}$.

CD (H_2O) λ/nm (Δε): 255.5 (-1.46).

HRMS: *m/z* = 1348.4844 $[P+H]^{+}$.

UV-Vis (MOPS, 5mM, pH 7.4) λ/nm (ε): 256 (29935), 345 (1500).

^{1}H NMR (500 MHz, D_2O) δ (ppm): 8.20 (bs, 1H, H-4), 7.89 (bs, 1H, H-3), 7.32 (bs, 1H, H-6), 7.23 (bs, 1H, H-5), 7.02 (bs, 1H, H-7), 4.94 (m, 7H, Hs-1 of CyD), 3.90-3.42 (m, 41H, other Hs of CyD and CH_2 α to the amide group), 3.32 (m, 1H, H-4A), 3.03 (bs, 1H, H-6A), 2.88 (bs, 2H, CH_2 β to the amide group), 2.79 (bs, 1H, H-6'A).

^{13}C NMR (125 MHz, D_2O) δ (ppm): 137.7 (C-4), 129.3 (C-6), 118.5 (C-3), 117.4 (C-5), 111.9 (C-7), 101.7 (Cs-1 of CyD), 83.8-80.7 (Cs-4 of CyD), 74.3-69.2 (Cs-2, Cs-3, Cs-5), 60.8-59.2 (Cs-6), 48.9 (C-6A), 47.5 (CH_2 β to the amide group), 38.4 (CH_2 α to the amide group).

3.40 Synthesis of 2^{A}(S),3^{A}(R)-3^{A}-[[(8-hydroxyquinolyl)-2-carboxyl]amino]-3^{A}-deoxy-β-cyclodextrin (CD3HQ)

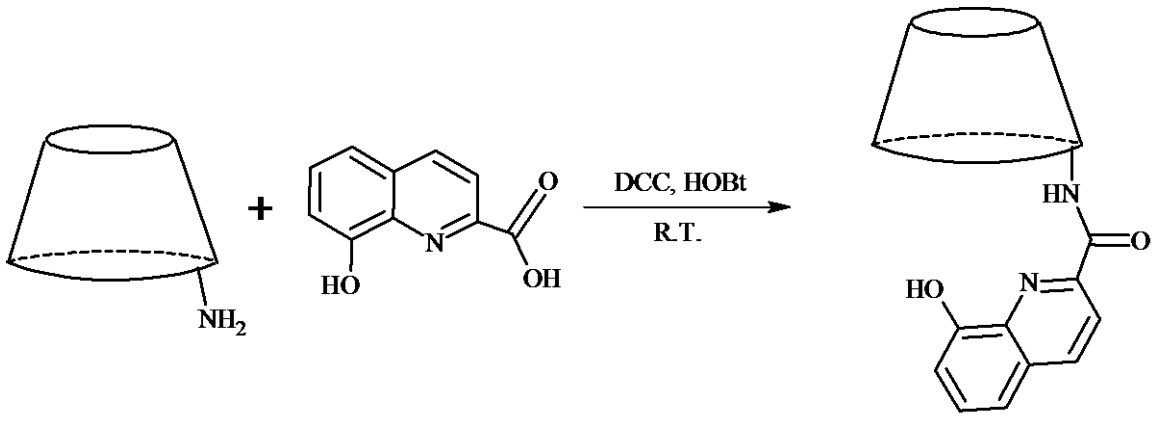

To a suspension of 8-hydroxyquinoline-2-carboxylic acid (17 mg, 0.09 mmol) in dry DMF (7 mL) were added HOBt (14 mg, 0.09 mmol) and DCC (18 mg, 0.09 mmol). After 0.5 h, 3^{A}-deoxy-3^{A}-amino-β-cyclodextrin (100 mg, 0.09 mmol) was added. The reaction mixture was

stirred for 48 h at room temperature. Then the solution was added to acetone (200 mL) and the resulting precipitate was collected by filtration. The crude product was suspended in water, filtered off, purified by ion-exchange chromatography on Sephadex CM-25 and then further dialyzed with a Float-A-Lyzer G2 (0.5-1 kD) device.

Yield: 65 %.

TLC: Rf = 0.30 (AcOEt: PrOH: H_2O: NH_3 4:3:2:1).

ESI-MS: *m/z* = 664.1 $[P+H+Na]^{2+}$, 672.2 $[P+H+K]^{2+}$, 1305.2 $[P+H]^{+}$, 1327.4 $[P+Na]^{+}$, 1343.3 $[P+K]^{+}$.

UV-Vis (H_2O, pH 6.5) λ/nm (ε): 203 (28097), 256 (32304), 308 (2279), 348 (1512).

^{1}H NMR (500 MHz, D_2O) δ (ppm): 8.40 (d, 1H, $J_{4,3}$ = 8.4 Hz, H-4), 8.09 (d, 1H, $J_{3,5}$ = 8.5 Hz, H-3), 7.56 (bs, 1H, H-6), 7.44 (bs, 1H, H-5), 7.21 (bs, 1H, H-7), 5.03 (d, 1H, $J_{1F,2F}$ = 3.4 Hz, H-1F of CyD), 4.98 (d, 1H, $J_{1,2}$ = 3.6 Hz, H-1 of CyD), 4.97 (d, 1H, $J_{1G,2G}$ = 3.4 Hz, H-1G of CyD), 4.95 (bs, 1H, H-1A of CyD), 4.93 (d, 1H, $J_{1B,2B}$ = 3.8 Hz, H-1B of CyD), 4.89 (bs, 1H, H-1 of CyD), 4.84 (bs, 1H, H-1Z of CyD), 4.72 (m, 1H, H-3A of CyD), 4.22 (bs, 1H, H-2A of CyD), 4.16 (bs, 1H, H-4A of CyD), 4.02 (m, 1H, H-3F of CyD), 3.94-3.38 (m, 36H, Hs-2, Hs-3, Hs-4, Hs-5, Hs-6 of CyD), 3.29 (bs, 2H, H-3Z and H-4 of CyD).

3.41 Synthesis of $6^A,6^B$-dideoxy-$6^A,6^B$-di[[(8-hydroxyquinolyl)-2-carboxyl]amino]-β-cyclodextrin (ABCD6HQ)

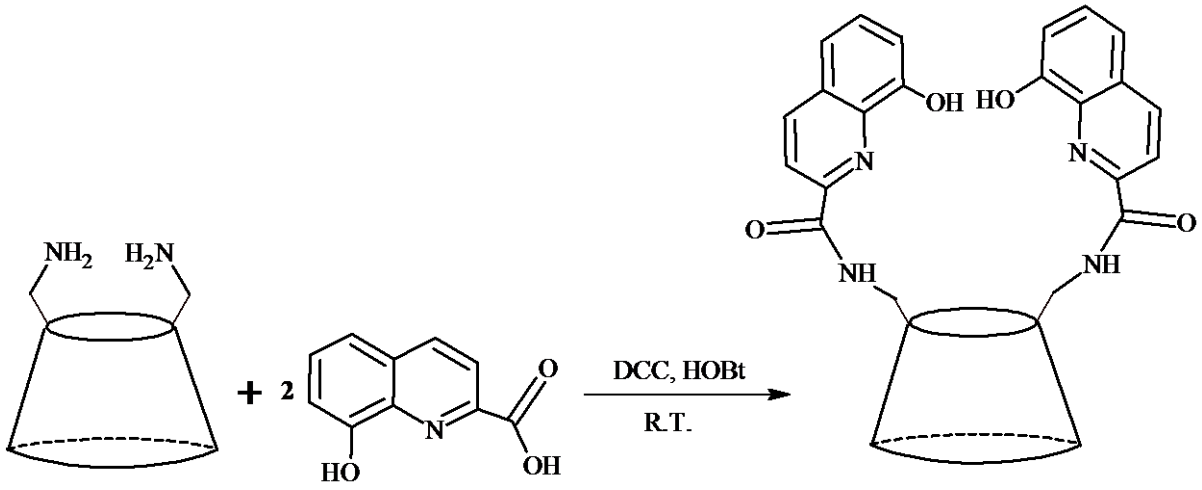

To a suspension of 8-hydroxyquinoline-2-carboxylic acid (5 mg, 0.025 mmol) in dry DMF (3 mL) were added HOBt (4 mg, 0.025 mmol) and DCC (5 mg, 0.025 mmol). After 1 h, 6^A,6^B-diamino-6^A,6^B-dideoxy-β-cyclodextrin (10 mg, 0.009 mmol) was added. The reaction mixture was stirred for 48 h at room temperature. The solvent was evaporated to dryness *in vacuo*. The crude product was suspended in water, filtered off, purified by ion-exchange chromatography on Sephadex CM-25 (eluent: water) and then further dialyzed with a Float-A-Lyzer G2 (0.5-1 kD) device to give the product (white solid).

Yield: 73 %.

TLC: Rf = 0.33 (AcOEt: PrOH: H_2O: NH_3 4:3:2:1).

Positive ion ESI-MS: *m/z* = 738.1 $[P+2H]^{2+}$, 749.1 $[P+H+Na]^{2+}$, 757.1 $[P+H+K]^{2+}$, 1475.2 $[P+H]^+$, 1497.2 $[P+Na]^+$, 1513.3 $[P+K]^+$.

Negative ion ESI-MS: *m/z* = 736.1 $[P-2H]^{2-}$, 1473.3 $[P-H]^-$.

CD (H_2O) λ/nm (Δε): 209.5 (-14.14), 254.5 (30.32), 269.0 (-17.08).

UV-Vis (H_2O, pH 6.5) λ/nm (ε): 201 (64675), 253 (64915), 307 (4615), 350 (3070).

^{1}H NMR (500 MHz, CD_3OD) δ (ppm): 8.17 (d, 1H, $J_{4,3}$ = 8.6 Hz, H-4), 7.89 (d, 1H, $J_{4,3}$ = 8.5 Hz, H-4'), 7.55 (m, 3H, H-3, H-3', H-6'), 7.40 (dd, 1H, *J* = 8.3 Hz, *J* = 1.0 Hz, H-5), 7.15, (dd, 1H, *J* = 7.6 Hz, *J* = 1.1 Hz, H-7), 6.98 (m, 1H, H-6'), 6.85 (dd, 1H, *J* = 7.6 Hz, *J* = 1.1 Hz, H-5'), 6.49 (m, 1H, H-7'), 5.13 (d, 1H, $J_{1A,2A}$ = 3.7 Hz, H-1A of CyD), 5.09 (d, 1H, $J_{1G,2G}$ = 3.6 Hz, H-1G of CyD), 5.06 (d, 1H, $J_{1E,2E}$ = 3.7 Hz, H-1E of CyD), 5.04 (d, 1H, $J_{1F,2F}$ = 3.6 Hz, H-1F of CyD), 4.98 (d, 1H, $J_{1D,2D}$ = 3.7 Hz, H-1D of CyD), 4.79 (d, 1H, $J_{1B,2B}$ = 3.8 Hz, H-1B of CyD), 4.74 (d, 1H, $J_{1C,2C}$ = 3.6 Hz, H-1C of CyD), 4.56 (m, 1H, H-6A of CyD), 4.25-4.10 (m, 3H, H-5A, H-6G, H-3G of CyD), 4.08-3.84 (m, 12H, H-3A, H-5B, H-6B, H-6'G, H-5E, H-3E, H-6E, H-6'E, H-5F, H-3F, H-6F, H-6'F of CyD), 3.81 (t, 2H, *J* = 9.4 Hz, H-3B and H-3D of CyD), 3.75 (t, 1H, *J* = 9.4 Hz, H-3C of CyD), 3.68-3.23 (m, 22H, H-2, H-4, H-6'A, H-6D, H-6'D, H-5C, H-6C, H-6'B, H-5G, H-5D of CyD), 2.51 (d, 1H, $J_{6C,6'C}$ = 10.8 Hz, H-6'C of CyD).

^{13}C NMR (125 MHz, CD_3OD) δ (ppm): 165.6 (C=O bound to the A ring), 164.1 (C=O bound to the B ring), 153.8 (C-8), 153.5 (C-2), 152.9 (C-8'), 146.1 (C-10), 147.2 (C-2'), 136.9 (C-4), 136.6 (C-6), 129.6 (C-10'), 128.9 (C-3'), (128.4 C-6'), 118.5 (C-4'), 118.0 (C-3), 117.5 (C-5), 116.8 (C-7'), 111.2 (C-7), 111.0 (C-5'), 103.0 (C-1G of CyD), 102.9 (C-1A of CyD), 102.6 (C-1D of CyD), 102.5 (C-1C of CyD), 102.3 (C-1E and C-1F of CyD), 101.5 (C-1B of CyD),

85.7 (C-4B of CyD), 85.1 (C-4A of CyD), 81.7 (C-4E of CyD), 81.3 (C-4G and C-4F of CyD), 81.1 (C-4D of CyD), 80.3 (C-4C of CyD), 74.6-71.2 (Cs-2, Cs-3, Cs-5 of CyD), 69.2 (C-5B of CyD), 60.4 (C-6E, C-6F, C-6G of CyD), 59.8 (C-6D of CyD) 58.8 (C-6C of CyD), 41.2 (C-6A of CyD), 40.4 (C-6B of CyD).

3.42 Synthesis of 6^A-deoxy-6^A-[(8-hydroxyquinolyl)-2-methylamino]-β-cyclodextrin (CD6RHQ)

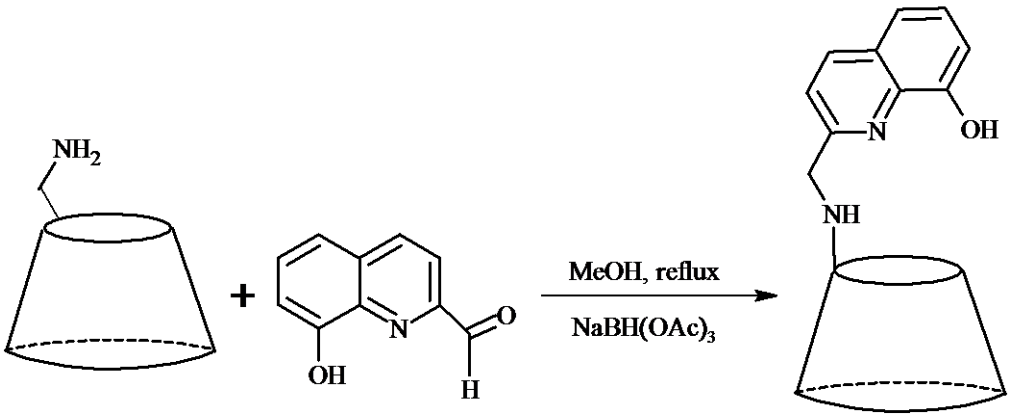

8-Hydroxy-2-quinolinecarboxaldehyde (9 mg, 0.05 mmol) was added to 6^A-deoxy-6^A-amino-β-cyclodextrin (60 mg, 0.05 mmol) in anhydrous methanol (7 mL). After 12 h, sodium triacetoxyborohydride (22 mg, 0.10 mmol) was added. The reaction was refluxed under stirring for 24 h. After the solvent was evaporated *in vacuo* and the solid obtained was washed with acetone. The crude product was purified by ion-exchange chromatography on Sephadex CM-25 (linear gradient of NH_4HCO_3 from 0 to 0.2).

Yield: 60 %.

TLC: Rf = 0.19 (PrOH: AcOEt: H_2O: NH_3 4:3:2:1).

Positive ion ESI-MS: *m/z* = 657.1$[P+H+Na]^{2+}$, 668.2 $[P+2Na]^{2+}$, 1291.3 $[P+H]^+$, 1313.4 $[P+Na]^+$.

Negative ion ESI-MS: *m/z* = 644.0 $[P-2H]^{2-}$, 1289.3 $[P-H]^-$.

UV-Vis (H_2O, pH 6.5) λ/nm (ε): 201 (29142), 244 (29812), 308 (2316).

^{1}H NMR (500 MHz, D_2O) δ (ppm): 8.19 (d, 1H, $J_{4,3}$ = 8.4 Hz, H-4), 7.53 (m, 2H, H-3 and H-6), 7.44 (d, 1H, $J_{5,6}$ = 8.2 Hz, H-5), 7.25 (d, 1H, $J_{7,6}$ = 7.5 Hz, H-7), 4.97 (m, 2H, H-1B and H-

1X of CyD), 4.95-4.87 (m, 5H, Hs-1 of CyD), 4.09 (m, 3H, CH_2Ar and H-5A of CyD), 3.92-3.22 (m, 38H, Hs-2, Hs-3, Hs-4, Hs-5, Hs-6 of CyD), 3.20 (m, 1H, H-4A of CyD), 2.93 (d, 1H, $J_{6A,6A'}$ = 12.4 Hz, H-6A of CyD), 2.83 (m,1H, H-6A' of CyD).

3.43 Synthesis of 2^A(S),3^A(R)-3^A-[(8-hydroxyquinolyl)-2-methylamino]-3^A-deoxy-β-cyclodextrin (CD3RHQ)

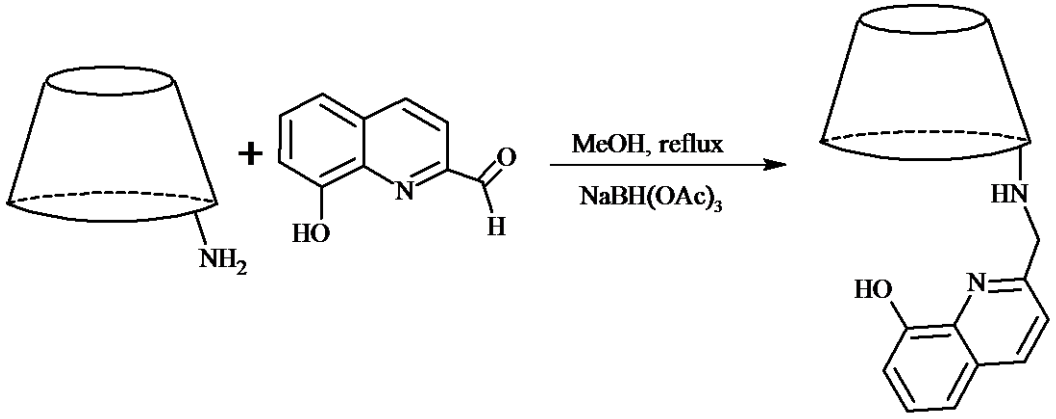

8-Hydroxy-2-quinolinecarboxaldehyde (9 mg, 0.05 mmol) was added to 3^A-deoxy-3^A-amino-β-cyclodextrin (60 mg, 0.05 mmol) in anhydrous methanol (15 mL). After 12 h, sodium triacetoxyborohydride (22 mg, 0.010 mmol) was added. The reaction was refluxed under stirring for 24 h. The solvent was evaporated *in vacuo* and the solid obtained was washed with acetone. The crude product was purified by ion-exchange chromatography on Sephadex CM-25 (linear gradient of NH_4HCO_3 from 0 to 0.2).

Yield: 70 %.

TLC: 0.17 (PrOH: AcOEt: H_2O: NH_3 4:3:2:1).

Positive ion ESI-MS: *m/z* = 657.2 $[P+H+Na]^{2+}$, 668.2 $[P+2Na]^{2+}$,1291.3 $[P+H]^+$, 1313.4 $[P+Na]^+$.

Negative ion ESI-MS: *m/z* = 1289.3 $[P-H]^-$.

UV-Vis (H_2O, pH 6.5) λ/nm (ε): 201 (25467), 243 (23957), 304 (1865).

^{1}H NMR (500 MHz, CD_3OD) δ (ppm): 8.20 (d, 1H, $J_{4,3}$ = 8.5 Hz, H-4), 7.51 (d, 1H, $J_{3,4}$ = 8.5 Hz, H-3), 7.40 (t, 1H, *J* = 7.8 Hz, H-6), 7.35 (dd, 1H, $J_{5,6}$ = 8.2 Hz, $J_{5,7}$ = 1.2 Hz, H-5), 7.09 (dd, 1H, $J_{7,6}$ = 7.5 Hz, $J_{7,5}$ = 1.2 Hz, H-7), 5.04 (d, 1H, $J_{1,2}$ = 4.0 Hz, H-1 of CyD), 5.02 (d, 1H,

$J_{1,2}$ = 3.8 Hz, H-1 of CyD), 5.00 (d, 1H, $J_{1G,2G}$ = 3.9 Hz, H-1G of CyD), 4.97 (d, 1H, $J_{1F,2F}$ = 3.5 Hz, H-1 of CyD), 4.94 (m, 2H, H-1B and H-1E of CyD), 4.76 (d, 1H, $J_{1A,2A}$ = 7.0 Hz, H-1A of CyD), 4.24 (m, 2H, H-5A and benzylic CH_2), 4.13 (d, 1H, $J_{CH,CH}$ = 15.3 Hz, benzylic CH_2), 4.02 (dd, 1H, $J_{6B,6'B}$ = 12.9 Hz, $J_{6B,5}$ = 3.8 Hz, H-6B of CyD), 3.97 (m, 1H, H-4A of CyD), 3.95-3.71 (m, 25H, H-2A, Hs-3, Hs-5, Hs-6, of CyD), 3.63 (m, 2H, H-4B and H-6'A of CyD), 3.56-3.43 (m, 11H, Hs-2 and Hs-4 of CyD), 2.96 (dd, 1H, $J_{3A,2A}$ = 10.5 Hz, $J_{3A,4A}$ = 3.5 Hz, H-3A of CyD).

^{13}C NMR (125 MHz, CD_3OD) δ (ppm): 157.5 (C-2), 152.5 (C-8), 138.5 (C-4), 137.6 (C-9), 128.1 (C-10), 128.9 (C-6), 123.1 (C-3), 119.6 (C-5), 112.6 (C-7), 104.1 (C-1A of CyD), 103.5-101.2 (Cs-1 of CyD), 82.9-80.9 (Cs-4 of CyD), 80.4 (C-4B of CyD), 77.9 (C-5A of CyD), 77.1 (C-4A of CyD), 74.6-70.9 (Cs-2, Cs-3, Cs-5 of CyD), 61.4-59.8 (Cs-6 of CyD), 59.6 (C-6A of CyD), 59.0 (C-3A of CyD), 51.4 (benzylic CH_2).

3.44 Synthesis of 6^A-deoxy-6^A-[(8-benzyloxyquinolyl)-2-methylamino]-β-cyclodextrin (CD6RHQBn)

CD6RHQBn was synthetized starting from 2-carboxaldehyde-8-benzyloxyquinoline and 6^A-deoxy-6^A-amino-β-cyclodextrin, the former was obtained by a two-step procedure as follows.

3.44.1 Synthesis of 2-methyl-8-benzyloxyquinoline (HQBn)

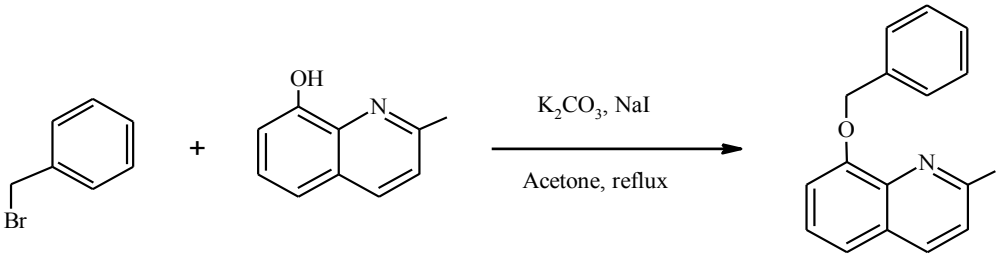

8-Hydroxyquinaldine (1 g, 6.25 mmol), benzyl bromide (1.11 mL, 9.4 mmol), anhydrous K_2CO_3 (1.72 g,12.5 mmol), and a catalytic amount of NaI (9 mg) were suspended in acetone (80 mL), and heated at reflux until complete consumption of the 8-hydroxyquinaldine (12 h, TLC: CH_2Cl_2/MeOH 99:1). The reaction mixture was evaporated to dryness and the residue

dissolved in CH_2Cl_2/H_2O 1:1 (300 mL). The organic layer was separated and dried over anhydrous $MgSO_4$, filtered and evaporated. The yellow oil was purified by flash chromatography on silica gel column (CH_2Cl_2/MeOH 99:1) and then dried under vacuum to give the product as white crystals.

Yield: 91 %.

TLC: Rf = 0.86 (CH_2Cl_2/MeOH 99:1).

^{1}H NMR (500 MHz, $CDCl_3$) δ (ppm): 2.83 (s, 3H, CH_3), 5.48 (s, 2H, CH_2-O), 7.03 (dd, 1H, $J_{7,6}$ = 7.6 Hz, $J_{7,5}$ = 1.5 Hz, H-7), 7.28–7.42 (m, 6H, H-3, H-5, H-6, Hs of Bn), 7.54 (d, 2H, J = 7.3 Hz, Hs of Bn), 8.02 (d, 1H, $J_{4,3}$ = 8.4 Hz, H-4).

^{13}C NMR (125 MHz, $CDCl_3$): 25.4 (CH_3), 70.7 (CH_2-O), 110.9 (C-7), 120.0 (C-5), 122.6 (C-3), 125.8 (C-6), 127.0 (C of Bn), 127.7 (C of Bn), 128.7 (C of Bn), 136.2 (C-4), 137.2 (C-9), 158.1 (C-8, C-2).

HRMS: m/z = 250.1214 $[P+H]^+$.

3.44.2 Synthesis of 2-carboxaldehyde-8-benzyloxyquinoline (HQBnA)

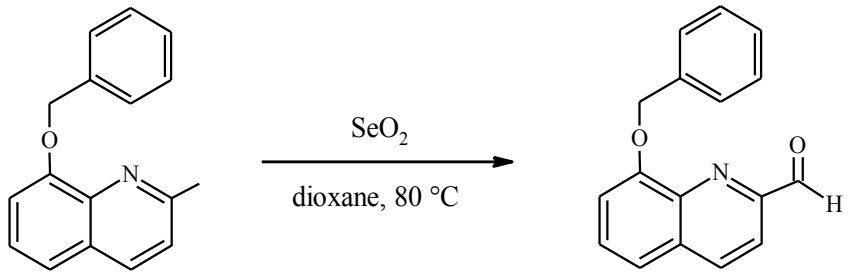

2-Methyl-8-benzyloxyquinoline (0.5 g, 2 mmol) and SeO_2 (0.25 g, 2.25 mmol) were suspended in dioxane (10 mL). The white solid quickly dissolved and the color of the suspension turned orange in a few minutes. The reaction mixture was then heated at 80 °C under an inert atmosphere. After 2 h, the suspension turned brown and the reaction was carried out for 24 h. Selenium was filtered through Celite, and washed with dichloromethane. The yellow filtrate was evaporated, dried under vacuum for 12 h, dissolved in CH_2Cl_2 (100 mL), and kept at RT for 24 h. The red selenium precipitate was removed by filtration and the filtrate evaporated to dryness. The crude product was purified by flash chromatography (silica gel, CH_2Cl_2) to give the aldehyde as a yellow solid.

Yield: 96 %.

TLC: Rf = 0.86 (CH_2Cl_2).

^{1}H NMR (500 MHz, $CDCl_3$) δ (ppm): 5.51 (s, 2H, CH_2), 7.17 (d, 1H, $J_{7,6}$ = 7.8 Hz, H-7), 7.34 (t, 1H, H of Bn),7.40 (t, 2H, Hs of Bn), 7.46 (t, 1H, J = 8.2 Hz, H-6), 7.59-7.53 (m, 3H, H-5, Hs of Bn), 8.08 (d, 1H, $J_{3,4}$ = 8.2 Hz, H-3), 8.26 (d, 1H, $J_{4,3}$ = 8.3 Hz, H-4), 10.32 (s, 1 H, HC=O).

^{13}C NMR (125 MHz, CD_3OD) δ (ppm): 71.14 (CH_2), 111.2 (C-7), 118.1 (C-3), 119.9 (C-6), 127.0 (Cs of Bn), 128.0 (C of Bn), 128.7 (Cs of Bn), 129.5 (C-5), 131.4 (C-10), 136.4 (C of Bn), 137.2 (C-4), 140.3 (C-9), 151.6 (C-2), 155.2 (C-8), 193.9 (C=O).

3.44.3 Synthesis of CD6RHQBn

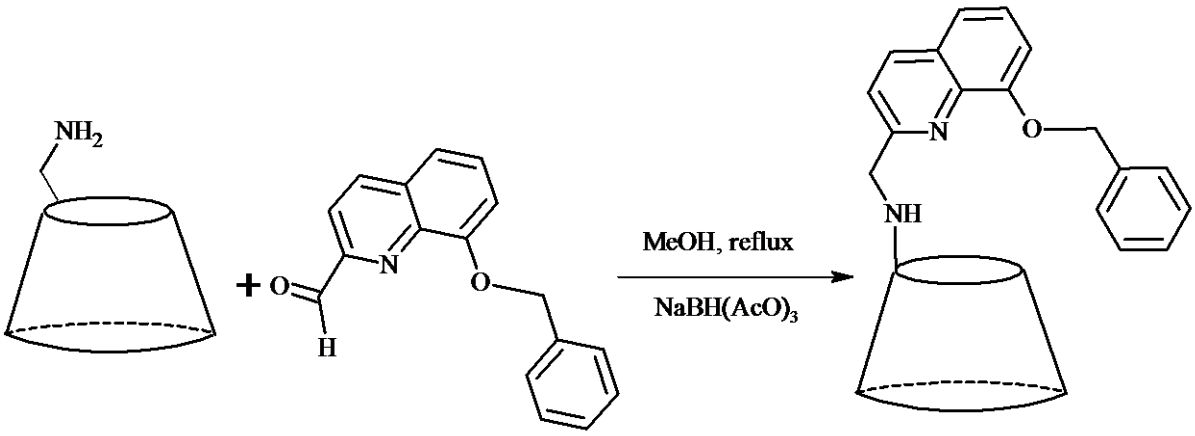

2-carboxaldehyde-8-benzyloxyquinoline (32 mg, 0.12 mmol) was added to 6^A-deoxy-6^A-amino-β-cyclodextrin (140 mg, 0.12 mmol) in anhydrous methanol (about 15 mL). After 12 h, triacetoxy sodium borohydride (52 mg, 0.24 mmol) was added. The reaction was refluxed under stirring for 24 hand then the solvent was evaporated *in vacuo*. The solid obtained was washed with acetone. The crude product was purified by reversed-phase flash chromatography (eluent: H_2O→MeOH) to give the product as a white solid.

Yield: 60 %.

TLC: Rf = 0.50 (PrOH: AcOEt: H_2O: NH_3 4:3:2:1).

HRMS: 1381.4927 $[P+H]^+$.

^{1}H NMR (500 MHz, CD_3OD) δ (ppm): 8.25 (d, 1H, $J_{4,3}$ = 8.5 Hz, H-4), 7.60 (d, 2H, *J* = 7.5 Hz, Hs of Bn), 7.56-7.38 (m, 6H, H-6, H-5, H-3, Hs of Bn), 7.20 (d, 1H, $J_{7,6}$ = 7.6 Hz, H-7), 5.40 (s, 2H, CH_2 of Bn), 5.02-4.86 (m, 7H, Hs-1 of CyD), 4.21 (d, 1H, *J* = 15.6 Hz, CH_2-N-CyD), 4.10 (d, 1H, *J* = 15.6 Hz, CH_2-N-CyD), 4.06 (t, 1H, H-5A of CyD) 3.98-3.34 (m, 39H, H-3, H-5, H-2, H-4, H-6 of CyD), 3.09 (d, 1H, *J* = 11.4 Hz, H-6X of CyD), 2.83 (m, 1H, H-6'A of CyD).

^{13}C NMR (125 MHz, CD_3OD) δ (ppm): 158.2 (C-2), 153.6 (C-8), 139.4 (C-9), 137.0 (C of Bn), 136.7 (C-4), 128.7 (C-10), 128.5 (C of Bn), 127.8 (C of Bn), 127.0 (C of Bn), 126.1 (C-6), 121.0 (C-3), 119.9 (C-5), 110.8 (C-7), 102.9-102.3 (Cs-1 of CyD), 84.8 (C-4A of CyD), 82.0-81.0 (Cs-4 of CyD), 74.0-72.0 (Cs-3, Cs-2, Cs-5 of CyD), 71.1 (C-5A of CyD), 70.7 (CH_2 of Bn), 61.0-59.5 (C-6 of CyD), 53.8 (CH_2-N-CyD), 49.8 (C-6A of CyD).

4. RESULTS AND DISCUSSION

The results in this section are divided into four distinct parts. More precisely, the first part describes glucose-bearing OHQ prodrugs (systems in which the metal binding site is protected) and their chemical and biological features in relation to their target enzyme (β-glucosidase), analyzing the structure-activity relationship. The second part presents a description of OHQ galactoconjugates and their behavior in the presence of the enzyme β-galactosidase in order to evaluate their suitability for ADEPT approach. The third part presents other new monosaccharide and disaccharide-appended OHQ systems, that differ from glycoconjugate prodrugs because they are able to complex metal ions. Finally, the last part gives a detailed description of cyclodextrin conjugates and their multiple functions such as metal-chelating and inclusion abilities, antioxidant and antiaggregant properties.

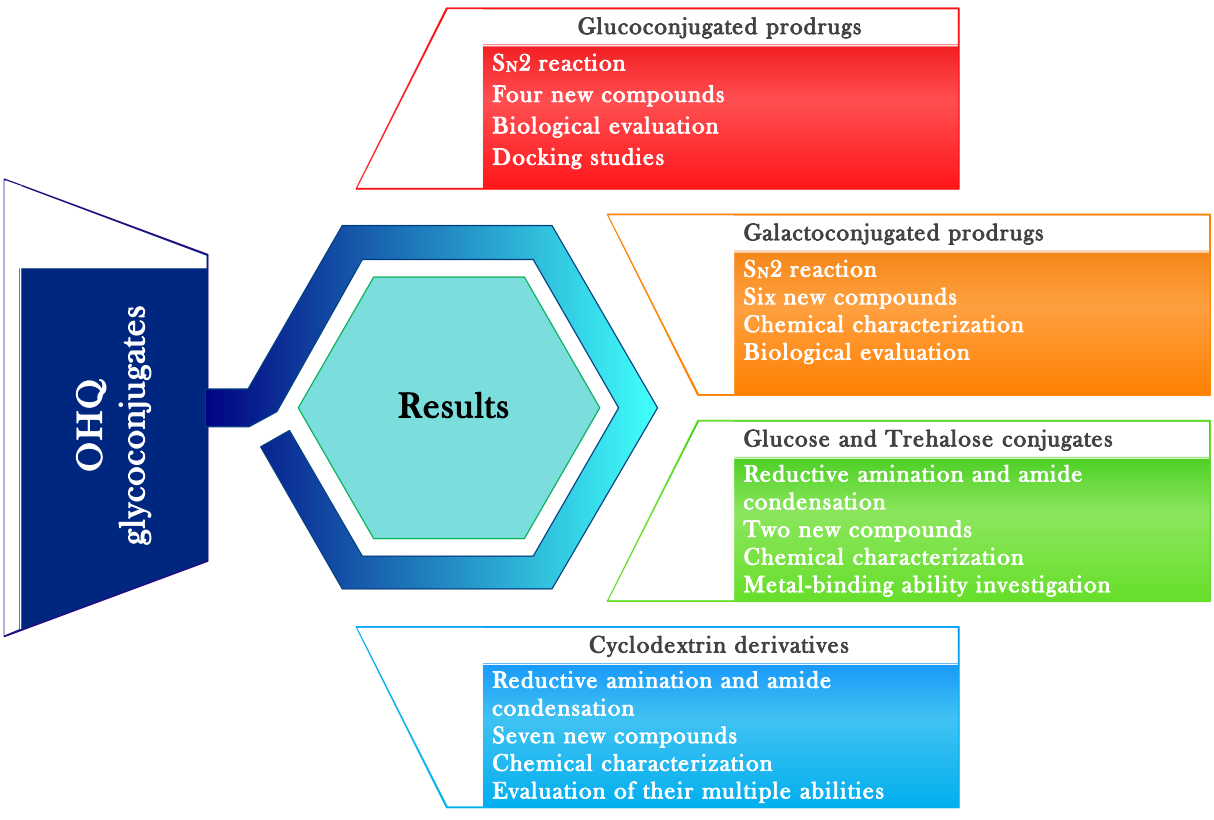

Figure 27. Schematic overview of the chapters of this section and highlights concerning the four classes of compounds.

First of all, a brief overview of the explored synthetic routes to synthetize OHQ conjugates is discussed in order to give a better understanding (Figure 28).

The most convenient syntheses have exploited S_N2 reaction (in which the phenolic group of OHQs acts as nucleophile), amide condensation starting from 8-hydroxyquinoline-2-carboxylic acid and reductive amination using 8-hydroxyquinoline-2-carboaldehyde. Any attempt to synthetize new compounds starting from 2-amino-8-hydroxyquinoline failed (low yield), indicating that NH_2 group is deactivated to take part in nucleophilic substitution and amide condensation. Wohl-Ziegler reaction in the presence of N-bromosuccinimide has not even allowed to obtain the desired product in satisfactory yield.

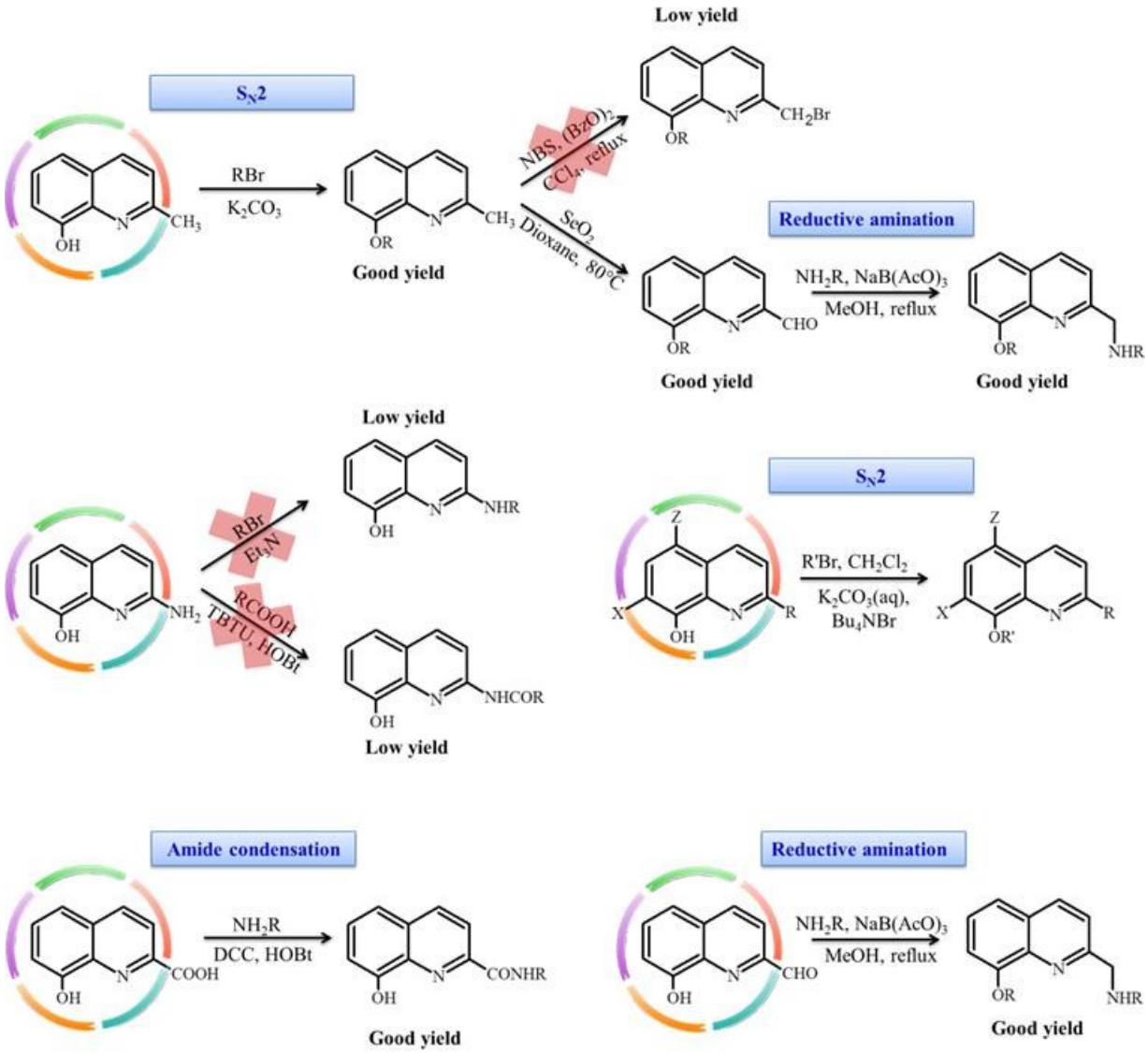

Figure 28. Synthetic routes to obtain OHQ conjugates. Starting materials are highlighted.

4.1 Glucosylated prodrugs

4.1.1 Synthesis and characterization

Although numerous works concerning aromatic O-glycosylation reveal increasing interest in the recent years, there are no precedents for O-glycosylation of CQ and other OHQ derivatives. The new compounds GluCQ, $GluCl_2HQ$, GluClHQ, GluMeHQ (Figure 29) were achieved through a facile one-pot reaction in good yields using a modified Michael procedure.

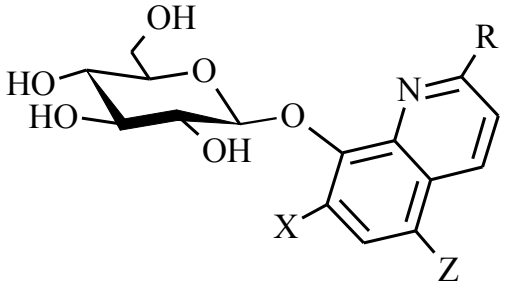

Compound	X	Z	R
GluOHQ	H	H	H
GluMeHQ	H	H	CH_3
GluClHQ	H	Cl	H
$GluCl_2HQ$	Cl	Cl	H
GluCQ	I	Cl	H

Figure 29. Glucoconjugates of OHQ derivatives.

Glycosidic bonds were formed through an SN_2 reaction under basic conditions using glycosyl bromide. Briefly, the quinoline compounds were dissolved in a water/methanol solution of K_2CO_3 and then a solution of glycosyl bromide in CH_2Cl_2 was added together with a phase transfer catalyst (tetrabutylammonium salt). This reaction produced the β-anomer of the glycosides. The pure products were isolated by precipitation. All novel compounds were characterized by ^1H NMR, ^{13}C NMR spectroscopy and ESI-MS. The ESI spectra of glucoconjugates show at least three peaks due to proton and sodium adduct ion and the dimeric sodium adduct ion (e.g. Figure 30 reports ESI-MS spectrum of GluMeHQ).

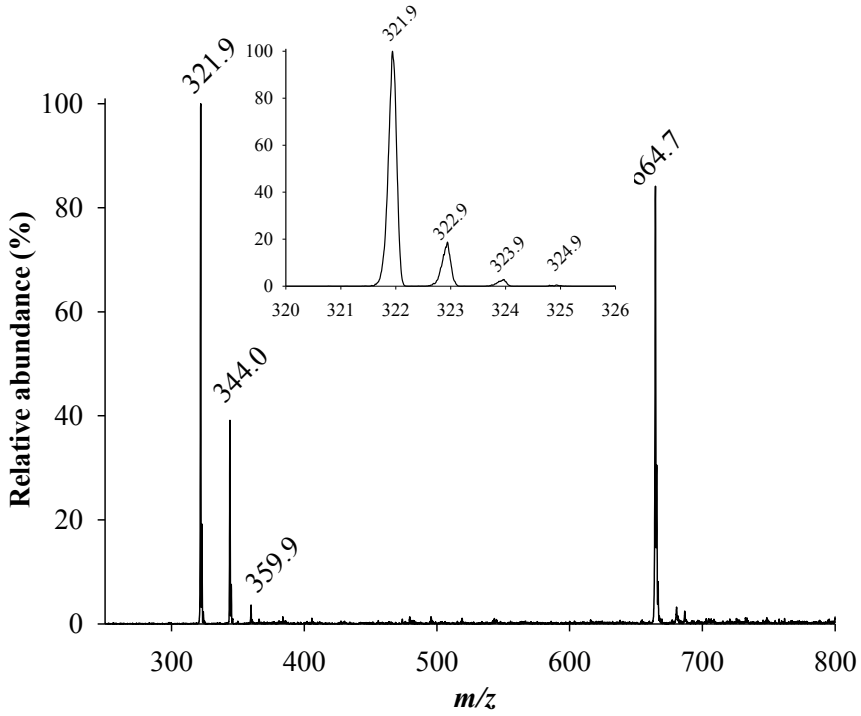

Figure 30. ESI-MS spectrum of GluMeHQ in water.

Furthermore, the zoom scan spectra of the halogenated compounds show typical isotopic patterns due to the halogen atoms (e.g. Figure 31 reports the spectrum of GluCQ).

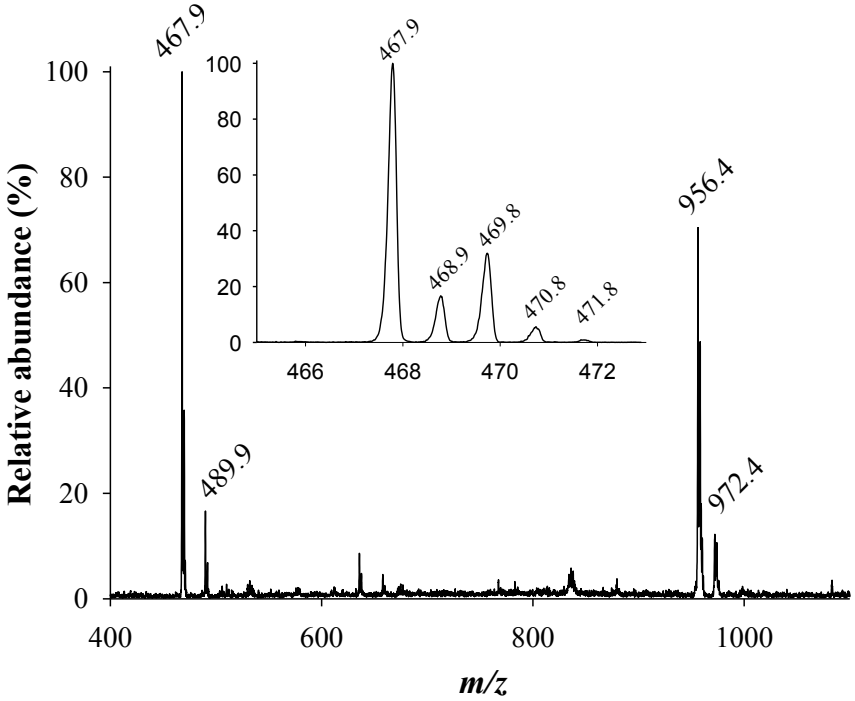

Figure 31. ESI-MS spectrum of GluCQ in water.

The ^{1}H NMR spectra, assigned by multidimensional NMR experiments (COSY, TOCSY, gHSQCAD, gHMBCAD), are reported in Figure 32. In all the spectra the signals due to the quinoline moiety and the signals due to the sugar moiety can be seen. The $J_{1,2}$ values of the glucose ring (about 7.8 Hz) confirm the β configuration for all derivatives. The H-1 of the glucose moiety is downfield shifted because of the deshielding effect of the aromatic ring as reported for similar compounds and resonates at about 5.1 ppm.[174] The presence of halogen at C-7 position in GluCQ and $GluCl_2HQ$ further shifts the H-1 downfield at 5.52 and 5.34 ppm, respectively. The glucose protons of GluCQ and $GluCl_2HQ$ are more shifted upfield compared to the other glucoconjugates suggesting a different orientation of the aromatic ring. The disposition of the aromatic ring respect to the sugar unit affects the chemical shifts especially of glucose H-5 and H-6.

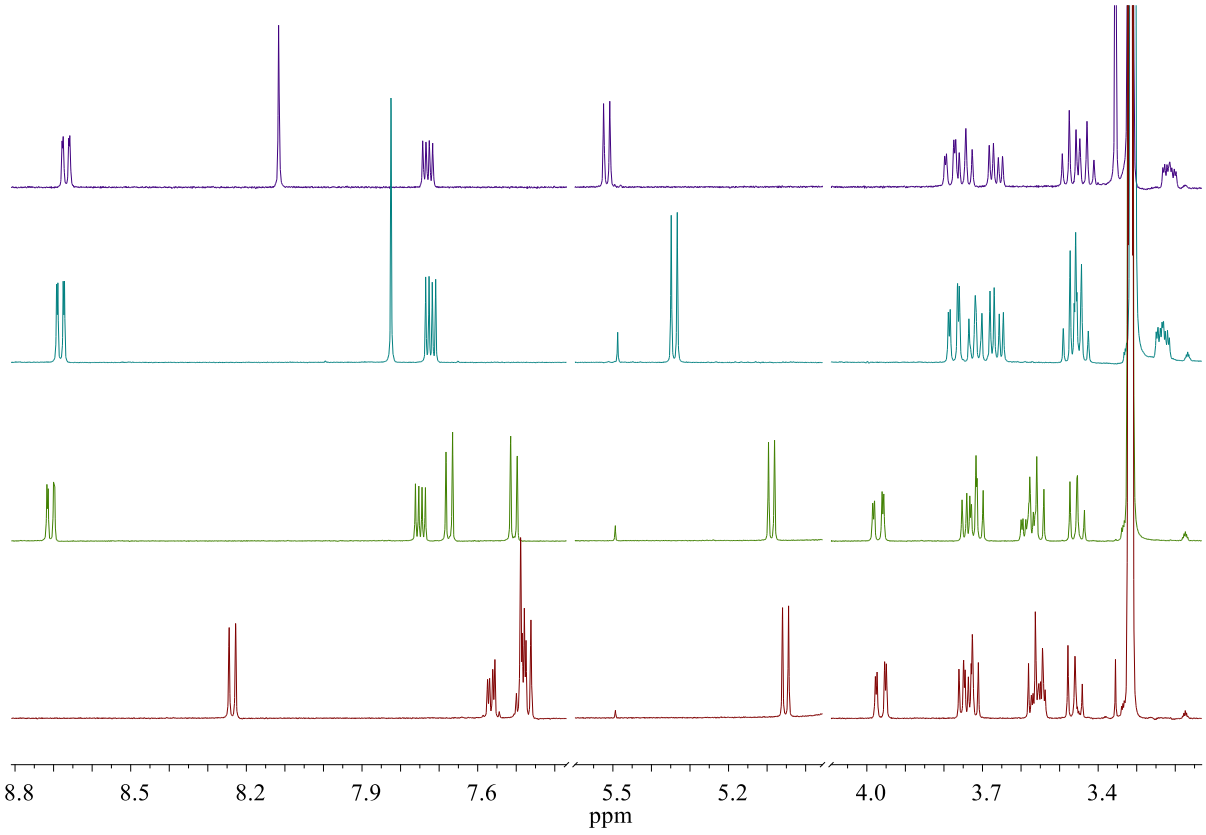

Figure 32. NMR spectra of the glucoconjugates at 500 MHz in CD_3OD: GluCQ (violet), $GluCl_2HQ$ (light blue), GluClHQ (green), GluMeHQ (red).

CD spectra of the four new compounds were also recorded in methanol as well as CD spectrum of GluOHQ that was synthetized for comparison. CD data are consistent with NMR

results. The presence of glucose moiety induces chirality in the π-π* region of the aromatic ring. GluOHQ, GluClHQ and GluMeHQ have similar CD spectra that show a slight negative band at 310 nm and a more intense negative band at 200 nm. The CD spectrum of $GluCl_2HQ$ is significantly different and displays a positive band at 300 nm and two intense negative bands at 240 and 206 nm, respectively (Figure 33). The Δε values of $GluCl_2HQ$ spectrum are higher than those of the other compounds, suggesting a different orientation of the aromatic ring respect to the sugar moiety in this case. This could be due to the presence of 7-substituent (a chlorine atom) given that a similar trend is observed for GluCQ. However, this latter compound shows a less intense negative band at about 240 nm.

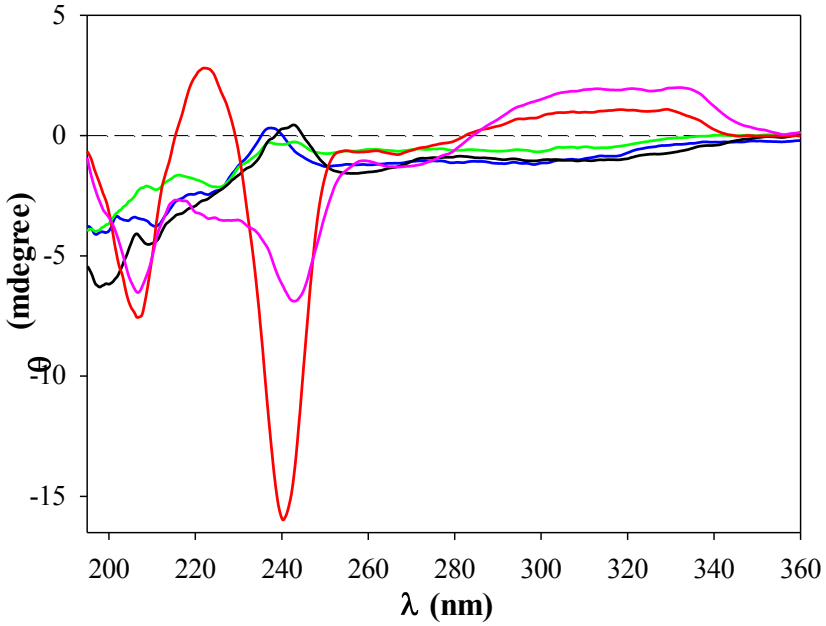

Figure 33. CD spectra of GluOHQ (blue), GluMeHQ (green), GluClHQ (black) , $GluCl_2HQ$ (red) and GluCQ (pink) in methanol at room temperature.

4.1.2 Copper complexes

Cu^{2+} complexes of CQ and OHQ have been investigated by different techniques.[175] The coordination properties of MeHQ, ClHQ and Cl_2HQ were also investigated by ESI-MS. A picture of the metal–ligand complexes formed in solution can be obtained by means of the mass spectrometric data. The ESI-MS spectra in the positive mode of the L (ligand) solutions containing copper sulphate (1 equivalent) were recorded. The experiments were carried out at

different pH, from 4.0 to 10.0. The formation of complex species was observed for pH values greater than 5. In Table 3 the pseudo-molecular ions of the observed species complexes are reported. The assignments of the peaks in ESI-MS spectra were done by comparing the experimental isotopic patterns with the corresponding simulated profiles. The CuL species shows the presence of a water molecule. As expected, the three compounds can form different complex species with Cu^{2+}. These data are in agreement with data previously reported in literature for similar compounds.

Table 3. ESI-MS characterization of the Cu^{2+} complexes of MeHQ, ClHQ, Cl_2HQ ([Cu^{2+}] = [ligand] = 3.0 × 10^{-5} M). L is a hydroxyquinolinate derivative.

Ligand	Assignment	Calcd (*m/z*)	Found (*m/z*)
MeHQ	$[LH + H]^+$	160.1	160.1
	$[CuL + H_2O]^+$	239.0	238.9
	$[CuL_2 + H]^+$	380.1	379.9
	$[CuL_2 + Na]^+$	402.0	401.9
	$[CuL_2 + K]^+$	418.0	418.0
	$[Cu_2L_3]^+$	600.0	599.8
ClHQ	$[LH + H]^+$	180.0	180.1
	$[CuL + H_2O]^+$	292.9	292.8
	$[CuL_2 + H]^+$	419.9	419.9
	$[CuL_2 + Na]^+$	441.9	441.9
	$[Cu_2L_3]^+$	659.9	659.9
Cl_2HQ	$[LH + H]^+$	214.0	214.0
	$[CuL + H_2O]^+$	274.9	274.9
	$[CuL_2 + H]^+$	487.9	487.8
	$[CuL_2 + Na]^+$	509.8	487.8
	$[Cu_2L_3]^+$	762.8	762.7

4.1.3 Chemical and enzymatic stability

Chemical stabilities of the synthesized compounds were assessed by several techniques such as mass spectrometry, UV-vis spectroscopy and chromatography.

Glucoconjugates are very stable in the range of investigated pH values (pH 4.0-11.0) and temperatures (25-37 °C). No decomposition was detected after 24 h under these conditions. In

particular, the incubation of prodrugs at 37 °C in PBS (phosphate-buffered saline, pH 7.4) revealed that the prodrugs were stable for at least 1 week.

In order to evaluate the ability of prodrugs to release the active moiety in the presence of specific enzyme, hydrolysis was carried out with β-glucosidase and monitored by several techniques, especially UV-vis spectroscopy (Figure 34). Almond β-glucosidase, commercially available, was used as enzyme model. The UV-vis spectra were recorded at different times to follow the hydrolysis at pH 7.4. When the glucoconjugates are hydrolyzed the OHQ moiety is released and new bands due to the free oxine appear. The last spectrum is the same of OHQ derivatives at pH 7.4. For comparison the same assay was repeated for the prodrugs in the absence of glucosidase and no modification of the bands was observed.

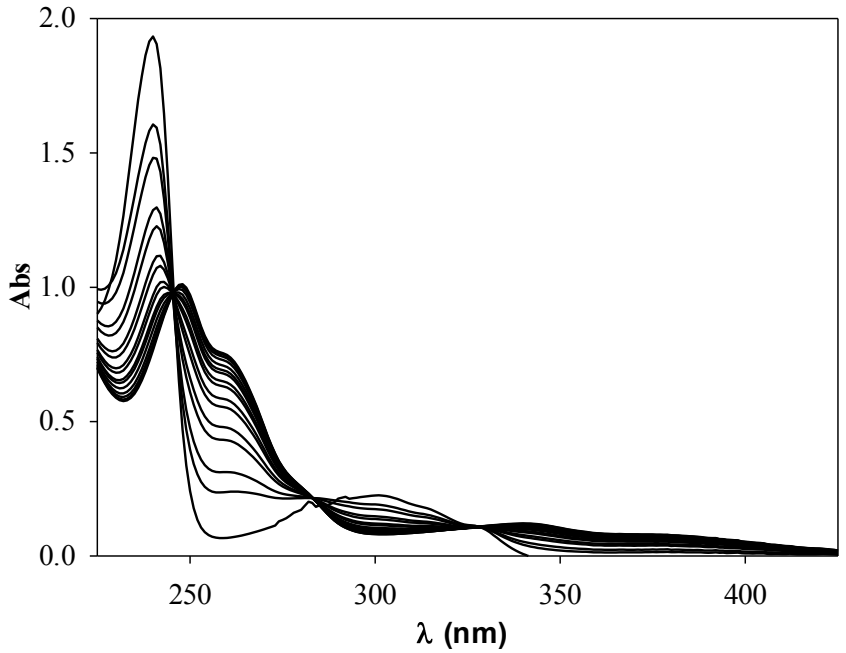

Figure 34. Enzymatic kinetic assay of $GluCl_2HQ$ (6×10^{-5} M) in the presence of glucosidase (1.1×10^{-6} M) at pH 7.4 (phosphate buffer 5 mM). UV-vis spectra were recorded every 9 min.

However, the glucoconjugates showed different behavior in the presence of β-glucosidase (Figure 34). To quantify the rate and extent of glucoconjugate hydrolysis, another UV-vis experiment was performed. In this case the glucoconjugates were incubated with β-glucosidase and samples of this solution were removed at selected times over 4 h and were immediately added with a solution of NaOH (final pH = 11.0) in order to stop enzymatic

activity. Furthermore, the released drug shows a shift of the bands at this pH because of the deprotonation of phenolic group and so it is possible to quantify it by measures of absorbance at λ_{max} value. The glycosidic bond of $GluCl_2HQ$ and GluClHQ was rapidly cleaved (within 40 min) showing that the glucoside trigger is readily accessible for the enzyme, despite the presence of bulky aromatic moieties. Oxine was expelled significantly faster from $GluCl_2HQ$ and GluClHQ than from GluCQ and GluOHQ. On the contrary, GluMeHQ did not show significant cleavage within 2 h. However GluMeHQ was partially cleaved in longer times. Half-lives of prodrugs in the presence of β-glucosidase are reported in Table 4.

Table 4. Half-lives of prodrugs in the presence of almond β-glucosidase (1.0×10^{-6} M) at 37 °C (pH 7.0).

	$GluCl_2HQ$	GluClHQ	GluMeHQ	GluCQ	GluOHQ
$t_{1/2}$ (min)	9.5	26.5	>600	130.5	145

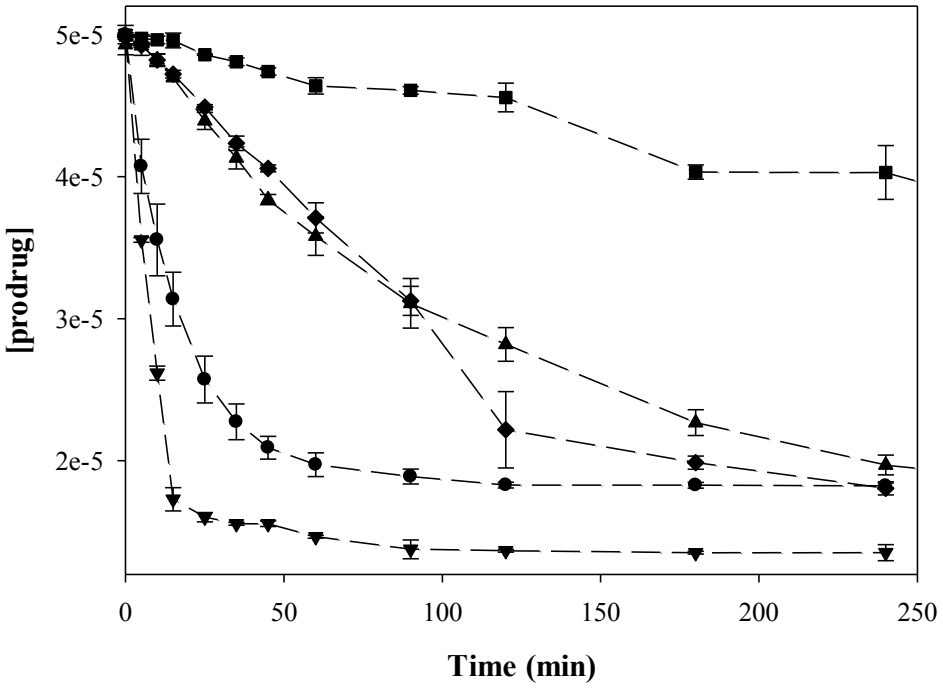

Figure 35. Hydrolysis of prodrugs in the presence of almond β-glucosidase (1.0×10^{-6} M) at 37 °C (pH 7.0). GluClHQ (●), $GluCl_2HQ$ (▼), GluMeHQ (■), GluCQ (♦), GluOHQ (▲).

4.1.4 Biological activities

Antiproliferative activity of OHQ compounds

All compounds were evaluated for their cytotoxic effect on several cancer cell lines. These measurements were carried out at Department of Integrated Oncological Therapies, IRCCS AOU S. Martino-IST (Genoa). To compare the cytotoxicity of CQ and OHQ with their glucoconjugated analogs, A2780 and A549 cells were treated with increasing concentrations of the compounds in the presence or absence of Cu^{2+} (20 µM) or Zn^{2+} (50 µM). These metal ions were not toxic for the cells at the tested concentrations. Cell viability was analyzed and IC_{50} values of compounds are reported in Table 5 and Figure 36.

Table 5. Summary of IC_{50}s (µM) of GluOHQ, GluCQ and their parent compounds on A2780, A549 cells.

Cell line	OHQ			GluOHQ		
		Zn^{2+}	Cu^{2+}		Zn^{2+}	Cu^{2+}
A2780	2.2 ± 0.4	2.2 ± 0.2	0.3 ± 0.1	66 ± 3	68 ± 3	5.6 ± 0.4
A549	5.3 ± 0.5	5.6 ± 0.9	0.54 ± 0.03	96 ± 5	97 ± 4	7 ± 1
Cell line	**CQ**			**GluCQ**		
		Zn^{2+}	Cu^{2+}		Zn^{2+}	Cu^{2+}
A2780	55 ± 3	53 ± 4	6.0 ± 0.4	119 ± 1	104 ± 22	57 ± 12
A549	65 ± 11	60 ±6	7.2 ± 0.4	79 ± 4	74 ± 6	65 ± 5

The antiproliferative activity of each compound was significantly enhanced by the addition of Cu^{2+} up to 14-fold (in case of GluOHQ). On the contrary, the Zn^{2+} did not affect the IC_{50} of compounds. In particular, OHQ and its glucosylated analog were more active than CQ and its derivative. The increase of glucoconjugate activity in the presence of Cu^{2+} ions could be explained considering the hydrolysis of glucose derivatives. In fact, these latter are molecules that cannot chelate copper. However, glucoconjugates of OHQ and CQ were less active than their parent compounds.

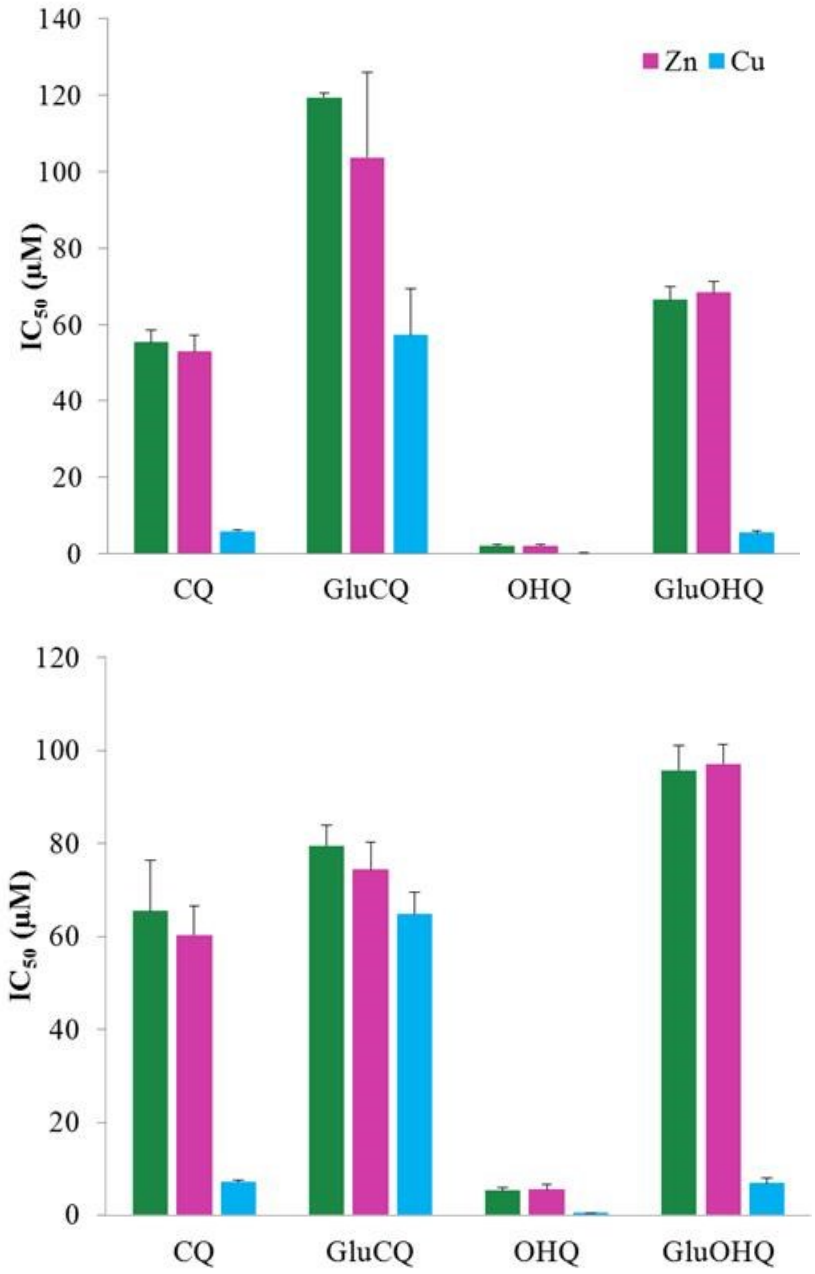

Figure 36. IC_{50} (µM) of CQ, OHQ and their glucoconjugates in the presence or absence of copper (or zinc) for 72 h on A2780 (up) and A549 cells (down).

GluClHQ, $GluCl_2HQ$, and GluMeHQ were also tested for their antiproliferative activity in the absence or presence of Cu^{2+} ions.

A different behavior was observed for these derivatives. GluClHQ and $GluCl_2HQ$ displayed an antiproliferative activity nearly similar to that of their parent compounds. On the contrary, GluMeHQ did not show activity (IC_{50}>100 µM) in the presence or absence of

Cu^{2+} ion whereas its unglycosylated counterpart show a good antiproliferative activity. The presence of Cu^{2+} ions also makes GluClHQ and $GluCl_2HQ$ more active as confirmed by the data of antiproliferative activity against A2780, A549 and MDA-MB-231 human cancer cells. In fact, Cu^{2+} caused a deep reduction of IC_{50}s for both the active compounds GluClHQ (mean reduction, 90 ± 7%) and $GluCl_2HQ$ (mean reduction, 63 ± 30%) (Table 6). Furthermore, GluClHQ had a higher mean antiproliferative activity compared to $GluCl_2HQ$. A similar increase of activity in the presence of the Cu^{2+} ions was also observed for ClHQ and Cl_2HQ (Table 6). As regard to the target cell lines, in nearly all conditions the breast cancer cell line MDA-MB-231 was the least sensitive of those studied to the compound activity. It is noteworthy that ClHQ is the most active compound of the series with IC_{50} ranging between 5.1 ± 0.9 µM and 19 ± 6 µM.

Table 6. Summary of IC_{50}s (µM) of $GluCl_2HQ$, GluMeHQ, GluClHQ and their parent compounds on A2780, A549 and MDA-MB-231 cells.

Cell line	Cl_2HQ		$GluCl_2HQ$	
		Cu^{2+}		Cu^{2+}
A2780	25 ± 3	2.5 ± 0.3	25 ± 2	3.1 ± 0.2
A549	24 ± 2	1.7 ±0.4	32 ± 7	6 ± 1
MDA-MB-231	25 ± 3	5 ± 1	35 ± 3	28.1 ± 0.9
Cell line	**MeHQ**		**GluMeHQ**	
		Cu^{2+}		Cu^{2+}
A2780	8 ± 2	4.1 ± 0.2	>100	>100
A549	25 ± 3	4.6 ± 0.3	>100	>100
MDA-MB-231	51 ± 3	5.3 ± 0.1	>100	49 ± 2
	ClHQ		**GluClHQ**	
		Cu^{2+}		Cu^{2+}
A2780	5.1 ± 0.9	0.47 ± 0.03	4.1 ± 0.5	0.36 ± 0.07
A549	5.9 ± 0.9	0.4 ± 0.2	5 ± 1	0.56 ± 0.03
MDA-MB-231	19 ± 6	0.59 ± 0.07	55 ± 5	5.2 ± 0.2

The numbers express the mean ± SD of 4-8 data.

Glucosidase inhibition assay

In order to verify that the glucosidase is crucial for enzymatic activation of the glucoconjugates, antiproliferative experiments were performed in the presence of Cu^{2+} ions and the known β-glucosidase inhibitor DMDP. Interestingly, after treatment with DMDP, the activity of GluClHQ and $GluCl_2HQ$ decreased significantly by 10-fold, while DMDP did not influence the activity of ClHQ and Cl_2HQ (Figure 37). Obviously, DMDP has no effect on cell growth at the used concentration. The results strongly suggest that the anticancer activity of the glucoconjugates is achieved through cleavage of glucose moiety by β-glucosidase within the cells.

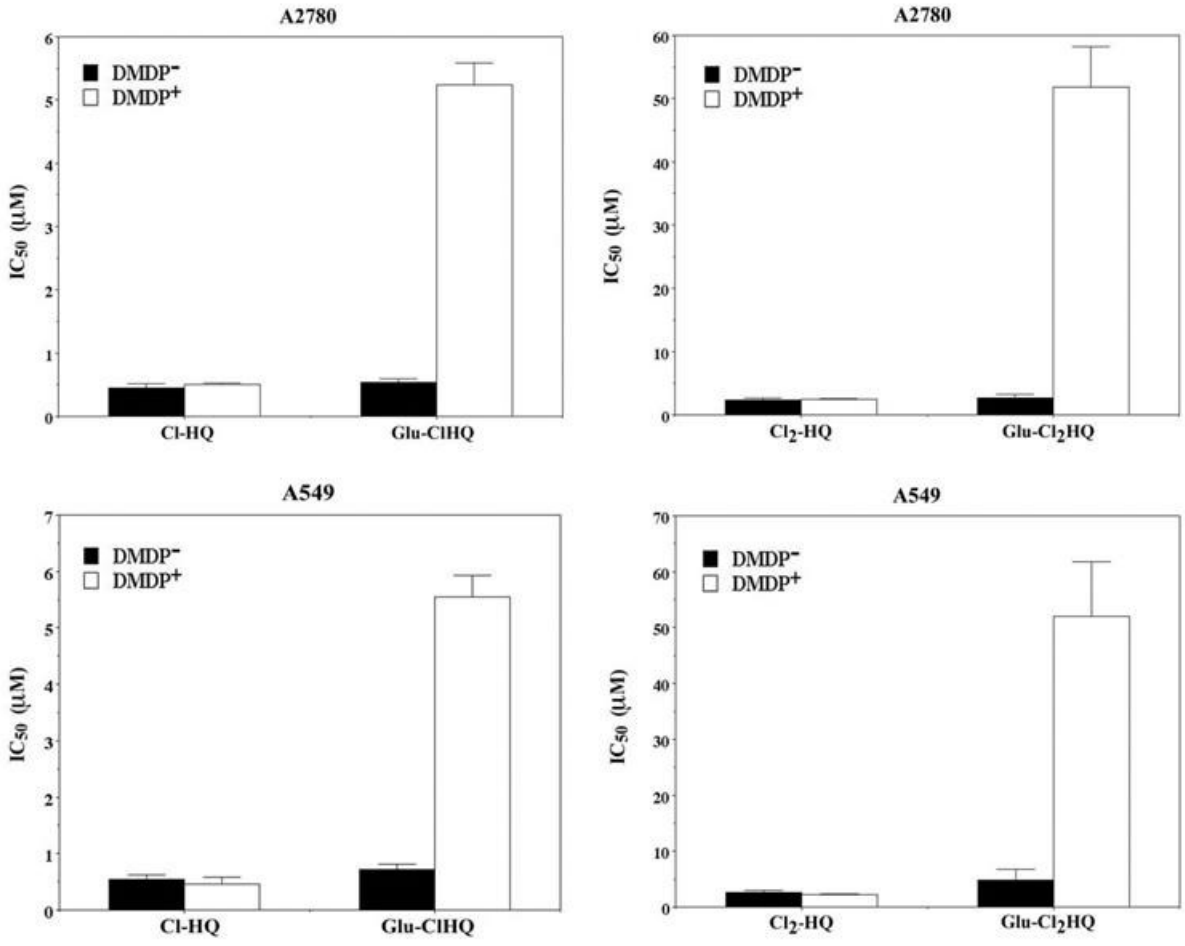

Figure 37. Histograms represent the mean IC_{50}s of ClHQ, Cl_2HQ and their glucoconjugates in the presence or absence of the β-glucosidase inhibitor DMDP (100 μM).

Identification of apoptotic cells by DAPI and annexin V/PI stainings

GluClHQ, $GluCl_2HQ$ and their parent compounds were analyzed by DAPI staining for the triggering of apoptosis, they were chosen because of their pharmacologically significant antiproliferative activity (higher than that of the other compounds). These compounds showed a pharmacologically relevant apoptotic activity that was higher when the Cu^{2+} ions were present in culture, except Cl_2HQ that did not show significant differences in terms of apoptotic cells in the presence or absence of Cu^{2+} ions (Table 7).

Table 7. Triggering of apoptosis by glucoconjugates as evaluated by nuclear morphological analysis after DAPI staining.

	ClHQ		GluClHQ	
		Cu^{2+}		Cu^{2+}
A2780	6 ± 3	33 ± 14	7 ± 5	27 ± 14
A549	5 ± 4	14 ± 6	4 ± 2	23 ± 4
MDA-MB-231	3 ± 2	65 ± 7	3 ± 2	67 ± 5
	Cl_2HQ		$GluCl_2HQ$	
		Cu^{2+}		Cu^{2+}
A2780	69 ± 26	60 ± 16	14 ± 2	24.5 ± 0.7
A549	10 ± 6	7 ± 3	15 ± 4	38 ± 15
MDA-MB-231	3 ± 1	2 ± 1	2 ± 1	34 ± 12

[a] Each cell line was treated with the IC_{50} concentration, as calculated by the MTT assay.
[b] The means ± SD (4-9 data) express the percentage of apoptotic cells.

In order to confirm the previous data, GluClHQ and $GluCl_2HQ$ were also analyzed for their ability to trigger apoptosis by the annexin V/PI staining. Once used at their IC_{50}s these compounds confirmed the previous results obtained by the microscopy observation of nuclear morphology after DAPI staining. In particular, these results showed that a higher early and/or late apoptotic activity was developed in the presence of Cu^{2+} ions (Figure 38).

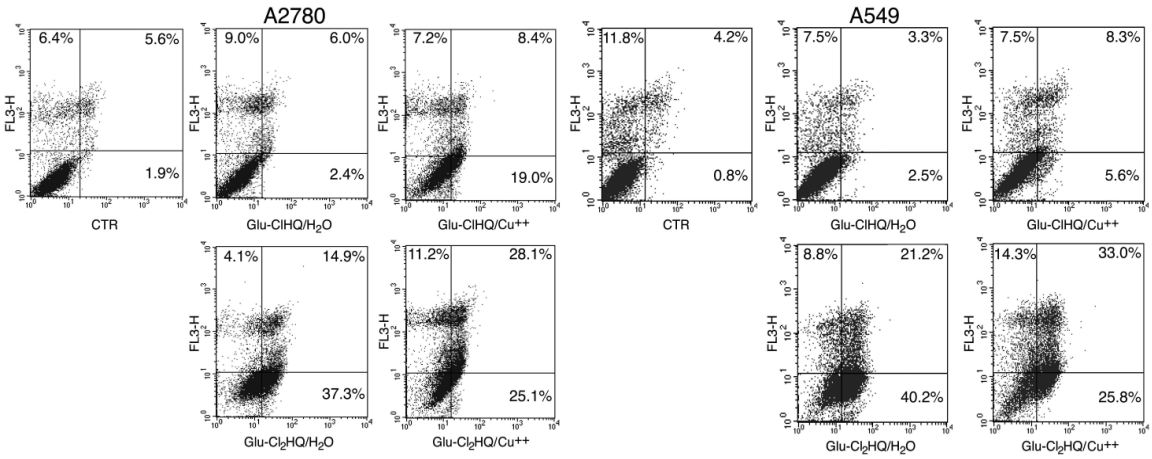

Figure 38. Scatter plots of A2780 and A549 cells labeled with Annexin-V/PI after three days culture. The tested compounds were GluClHQ and $GluCl_2HQ$ in the presence or absence of Cu^{2+} ions.

4.1.5 Docking studies

It will be shown that the docking simulation can be a useful tool for elucidating the different observed half-lives of the glucoconjugates and thereof their different antiproliferative activity. The preferred orientation of ligands in 3D space into the protein binding site determines the activity of that ligand, therefore, the ligand–protein binding modes and interactions are crucial to understand the catalytic activity. Since, the 3D structure of human β-glucosidase has been determined, the 3D coordinates of human cytosolic β-glucosidase[173] (hCBG, PDB code 2JFE) were taken and this protein has been used as the target protein.

The crystallographic structure of hCBG shows that the active site of the enzyme is located on the bottom of a deep pocket (Figure 39 A-B). It can be divided into two parts; the recognition site for the glucose moiety located at the bottom of the active site and the binding site for the aglycone at the entrance of the pocket. The active site is shaped as an oval or slit-like pocket with a cluster of hydrophobic amino acid side chains (in yellow in Figure 39 B) lining the walls of the aglycone binding slot, whereas hydrophobic, polar and charged residues are present in the sugar binding moiety. 2JFE provides useful 3D structural information for performing molecular docking studies. Investigated compounds were therefore docked to the binding cavity of 2JFE to evaluate their binding mode and affinity (kcal/mol). To do that among the plethora of docking softwares, AutoDock Vina[171] was selected since it was recently used to model OHQs in docking studies.[176] The performances of AutoDock Vina were

evaluated by reproducing the crystal structure of the complex of the maize β-glucosidase (ZMGlu1) with the non-hydrolysable inhibitor p-nitrophenyl-β-D-thioglucoside (PDB code: 1E1F). In this validation step particular attention was paid to check the position of the glucose moiety at the bottom of the active site close to the two catalytic residues (Glu165 and Glu373 shown in Figure 39 for hCBG). The orientation of the sugar moiety of the substrate was in fact used as a filter to evaluate docking results. In particular, the best poses of any ligand (= the most stable) provided that their glucose moiety was located at the bottom of the active site. This was verified for the three best poses of all compounds. Results (Figure 39 D) indicated that GluMeHQ has the best affinity for the binding site (-8.4 kcal/mol for the best pose), whereas $GluCl_2HQ$ shows the lowest affinity (-7.04 kcal/mol for the best pose). The three remaining compounds show intermediate values. FLAP[172] analysis confirmed this trend.

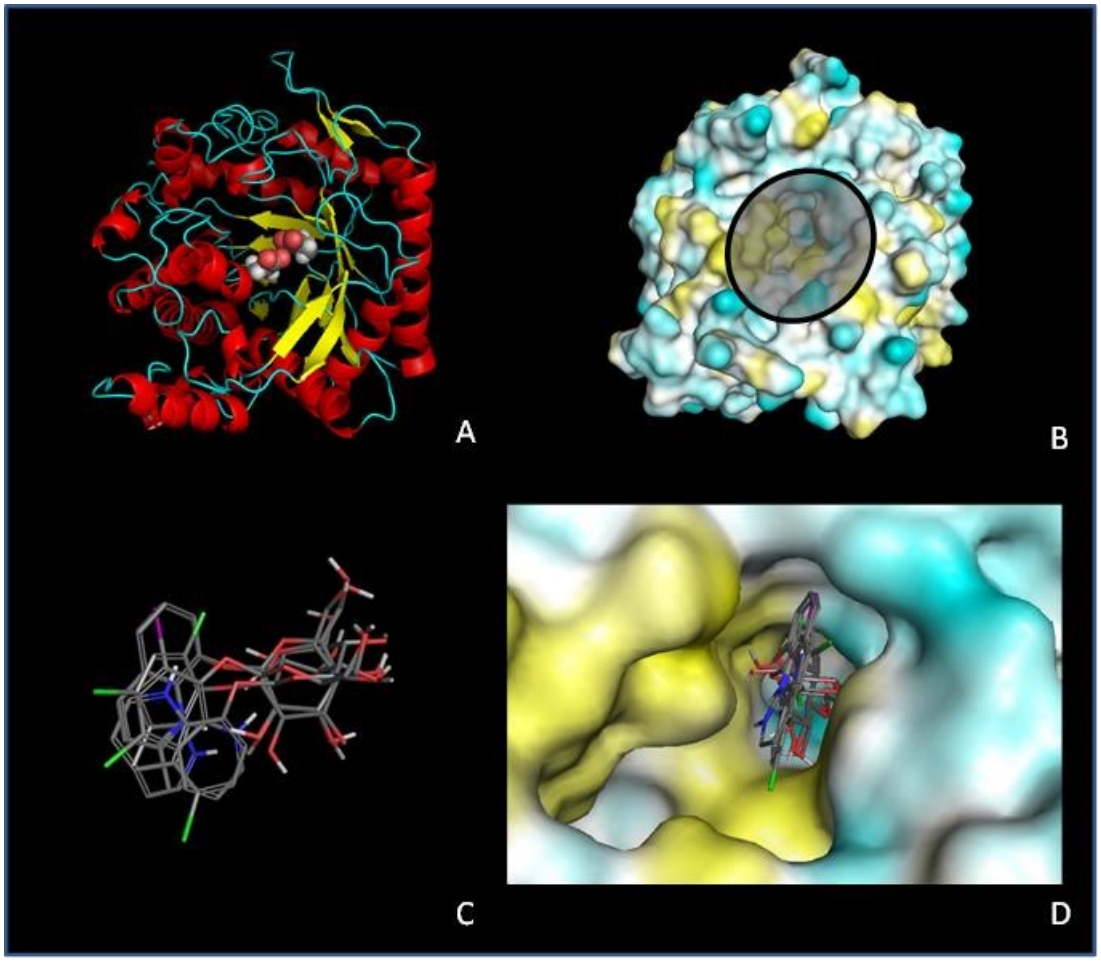

Figure 39. A) The crystallographic structure of human cytosolic β-glucosidase (hCBG, PDB code 2JFE); B) the active site of hCGB; the two catalytic residues (Glu165 and Glu373) are highlighted; C) The best poses of the five docked structures as obtained with AutoDock Vina abd; D) The best poses of the five docked structures in the active site (hydrophobic residues in yellow; hydrophilic residues in light blue).

4.2 Galactosylated prodrugs

4.2.1 Synthesis and characterization

The galactoconjugates (Figure 40) were synthetized in good yields with a straightforward procedure similar to that of glucoconjugates. The β-anomers were the compounds of interest in this study. For this reason, α-anomer glycosyl bromide was used as starting material. Briefly, the quinoline compounds were dissolved in a water/methanol solution of K_2CO_3 and then a dichloromethane solution of galactosyl bromide was added together with a phase transfer catalyst.

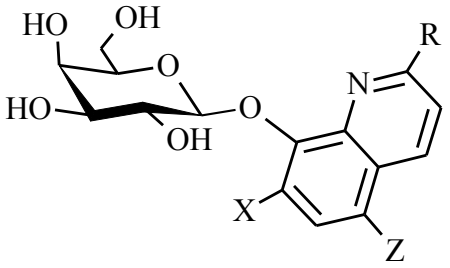

Compound	X	Z	R
GalOHQ	H	H	H
GalMeHQ	H	H	CH_3
GalAHQ	H	H	NH_2
GalNHQ	H	NO_2	H
GalClHQ	H	Cl	H
$GalCl_2HQ$	Cl	Cl	H
GalCQ	I	Cl	H

Figure 40. Galactoconjugates of OHQs.

The products were fully characterized by NMR, ESI-MS and CD. The ESI spectra of galactoconjugates (Figure 41 and Figure 42) show at least three peaks due to proton and sodium adduct ions and the dimeric sodium adduct ion as similarly observed for the glucoconjugates.

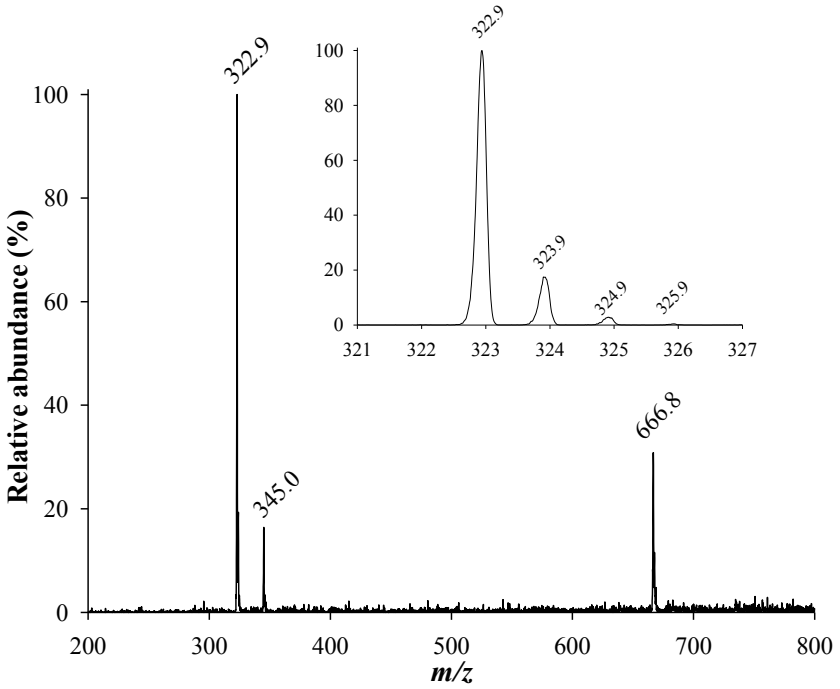

Figure 41. ESI-MS spectrum of GalAHQ in water.

Furthermore, the zoom scan spectra of the halogenated compounds show typical isotopic patterns due to the presence of the halogen atoms (Figure 42).

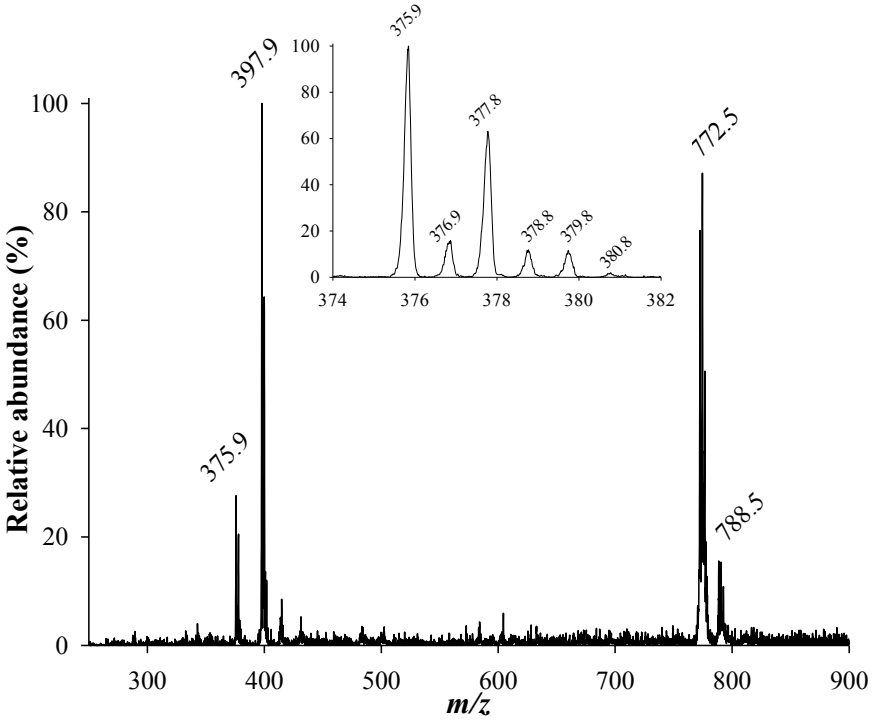

Figure 42. ESI-MS spectrum of $GalCl_2HQ$ in water.

The ^{1}H NMR spectra, assigned by 2D NMR experiments, are reported in Figure 43. The signals due to the quinoline moiety and the signals due to the sugar moiety can be seen identified in all spectra. The $J_{1,2}$ values of the glucose ring (about 7.8 Hz) confirm the β configuration for all derivatives. The H-1 of the galactose moiety is downfield shifted at about 5.1 ppm because of the deshielding effect of the aromatic ring as reported for similar compounds.[177] The presence of a halogen atom (chlorine or iodine) at C-7 position in $GalCl_2HQ$ and GalCQ further shifts the H-1 downfield at about 5.3 ppm.

As for GalMeHQ, GalAHQ, GalClHQ and GalNHQ, the signals due to the sugar moieties are superimposable except for a slight upfield shift in the case of GalAHQ.

The aliphatic protons of $GalCl_2HQ$ and GalCQ are more shifted upfield compared to the other galactoconjugates. The disposition of the aromatic ring respect to the sugar unit affects the chemical shifts especially of galactose H-4, H-5 and H-6. In particular, H-5 resonates at upper fields than H-3 in $GalCl_2HQ$ and GalCQ, this behavior is opposite to that of the other galactoconjugates.

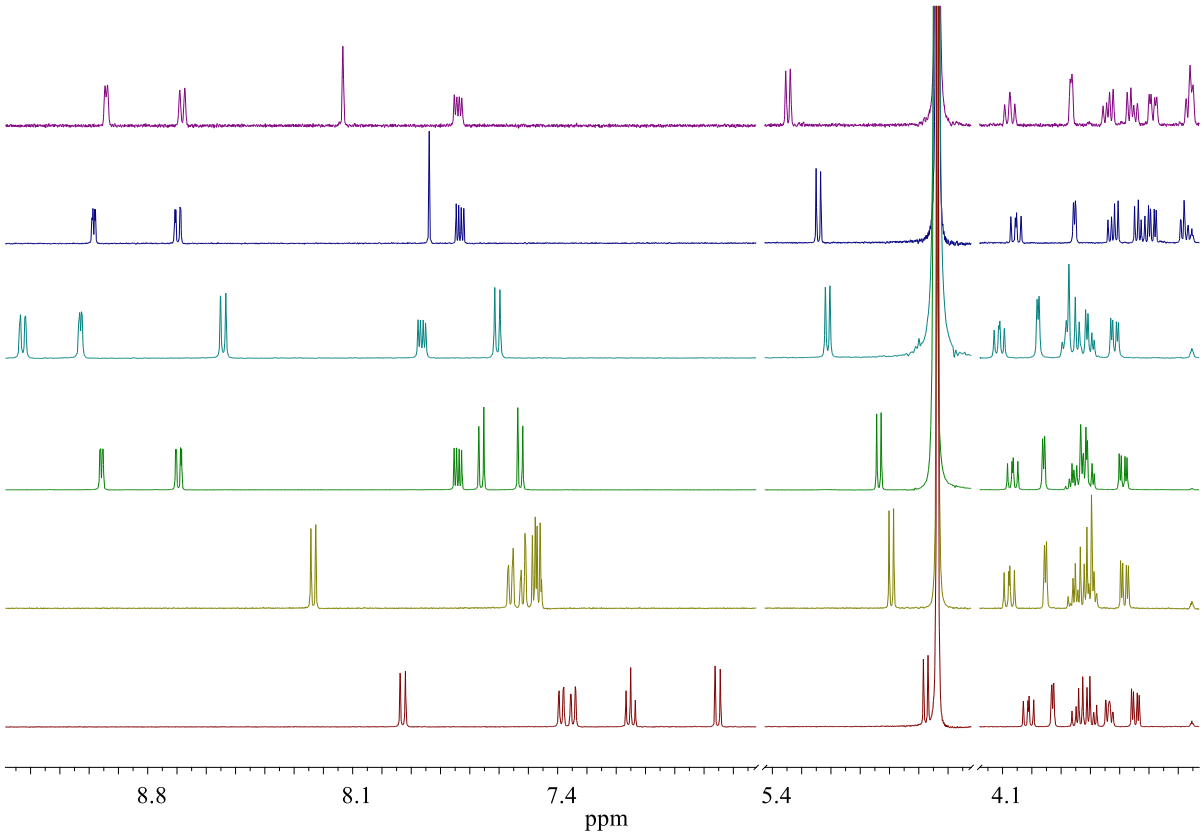

Figure 43. ^{1}H NMR spectra of GalCQ (violet), $GalCl_2HQ$ (blue), GalNHQ (light blue), GalClHQ (green), GalMeHQ (light green) and GalAHQ (red).

CD spectra of the new compounds were also recorded in methanol (Figure 44). The presence of the galactose moiety induces chirality in the π–π* region of the aromatic ring due to the dipole–dipole coupling between the quinoline ring and the sugar moiety.[178]

GalOHQ, GalMeHQ and GalClHQ have similar CD spectra showing two slight negative bands at 220 and 305 nm and a more intense positive band at 241 nm. CD spectra of $GalCl_2HQ$, GalCQ, GalAHQ are significantly different, the former compounds display a positive band at 320 nm and an intense negative band in the region between 280-210 nm. The presence of a 7-substituent halogen atom could preferentially orient the aromatic ring with respect to the sugar moiety, as observed in the case of the glucose derivatives. As for GalAHQ, its CD spectrum shows a negative band at 339 nm and 241 nm and a positive band at 261 nm. In this case the presence of ortho NH_2 group could influence the reciprocal disposition of sugar and aglycone moieties.

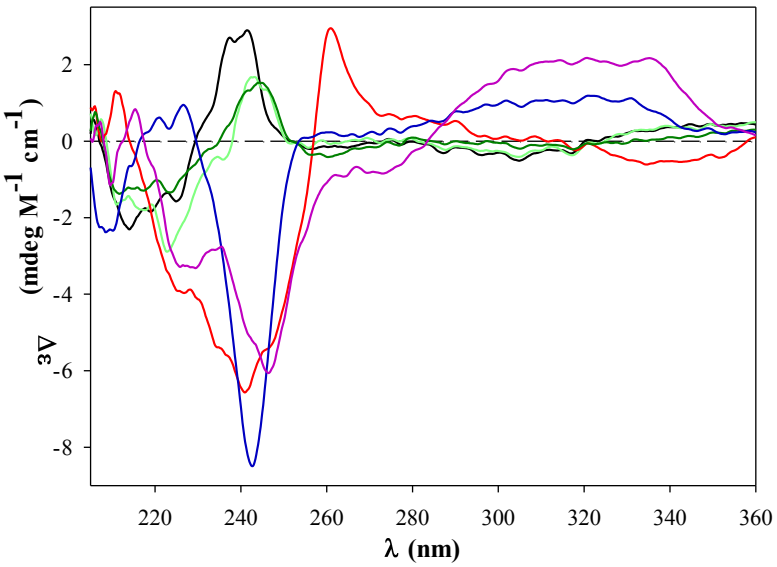

Figure 44. CD spectra of GalCQ (violet), $GalCl_2HQ$ (blue), GalClHQ (green), GalMeHQ (light green) and GalAHQ (red) in methanol at room temperature.

Copper Complexes

The galactosides are not able to complex metal ions with the same affinity of their parent compounds as the pyridine ring can complex Cu^{2+} only with a log K_1 of 2.6.[167] The galactose moiety has to be cleaved before metal chelation and therefore O-glycosylation could prevent of systemic chelation of essential metal ions.

The chelating properties of GalAHQ were evaluated by ESI-MS because it possesses a NH_2 group that could participate in the complexation of metal ions. The ESI-MS spectra in the positive mode of the ligand solutions containing copper sulfate were recorded. The assignments of the peaks in ESI-MS spectra were done by comparing the experimental isotopic patterns with the corresponding simulated profiles. The $CuLH_{-1}$ species was observed for GalAHQ. These data support the argument that NH_2 group can complex the metal ion. The deprotonated 2-OH of sugar could assist the complexation.

Because of the enzymatic hydrolysis allows the release of the compounds with a free metal binding site, the chelating ability of the released compounds was evaluated. The data for ClHQ, Cl_2HQ and MeHQ are previously reported (Section: copper complexes in Glucosylated prodrugs) whereas the obtained data for AHQ and NHQ are shown in Table 8. Methanol was added to facilitate the solubilization of their copper complexes. AHQ and NHQ are able to complex Cu^{2+} ions. The main species for both compounds is the CuL species that shows the presence of a water or methanol molecule owing to its unsaturated character of the coordination shell. AHQ can also form complexes with the ML_2 stoichiometry.

Table 8. ESI-MS characterization of Cu^{2+} complexes of AHQ and NHQ where L is a hydroxyquinolinate derivative. Cu^{2+} complexes of GalAHQ are also reported where L refers to the compound without charges.

Ligand	Assignment	Calcd (*m/z*)	Found (*m/z*)
AHQ	$[LH + H]^+$	161.1	161.1
	$[CuL + H_2O]^+$	240.0	239.8
	$[CuL + CH_3OH]^+$	254.0	253.8
	$[CuL_2 + H]^+$	382.0	382.0
	$[CuL_2 + H + H_2O]^+$	400.1	400.2
NHQ	$[LH + H]^+$	191.0	191.0
	$[CuL + H_2O]^+$	270.0	269.9
GalAHQ	$[L + H]^+$	323.1	323.0
	$[Cu^{II}LH_{-1}]^+$	384.0	383.9
	$[Cu^{I}LH_{-1}+H]^+$	385.0	384.9

4.2.2 Chemical and enzymatic stability

Chemical stabilities of the synthesized compounds were assessed by several techniques such as mass spectrometry, UV-vis spectroscopy and chromatography.

Galactose conjugates are very stable in the investigated conditions (37 °C, phosphate-buffered saline, pH 7.4). No decomposition was detected after 72 h under these conditions. The systems are also stable in the presence of $CuSO_4$.

In order to evaluate the ability of prodrugs to release the active moiety in the presence of β-galactosidase, cleavage assays were performed. The prodrugs were hydrolyzed by the enzyme as observed by ESI-MS and UV-vis experiments. In Figure 45 Figure 46, the Uv-vis spectra of $GalCl_2HQ$ and GalNHQ in the presence of β-galactosidase are reported. In these cases, the spectral changes which occur upon the hydrolysis are very evident because the phenolic group of Cl_2HQ and NHQ is partially deprotonated at pH 7.4 as Cl_2HQ has pK1 and pK2 values of 2.6 and 7.3 whereas the pK1 and pK2 values of NHQ are 2.6 and 6.4, respectively.[167] Other enzymes such as β-glucosidase and α-amylase did not affect the prodrug stability, although it has been reported that the former is able to hydrolyzed several galactoconjugates. These data suggest that the galactoconjugates could be specifically cleaved by β-galactosidase as desirable for ADEPT approach.

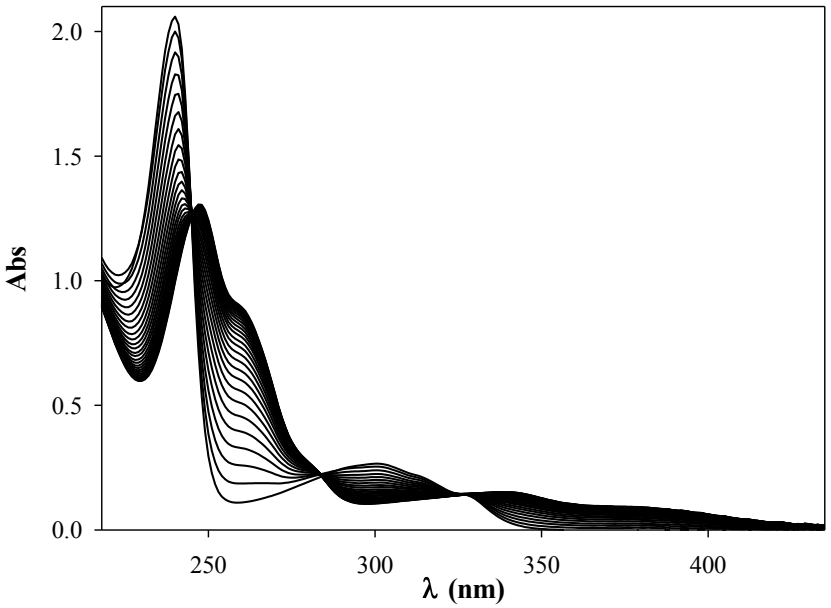

Figure 45. Enzymatic kinetic assay of $GalCl_2HQ$ in the presence of β-galactosidase (pH 7.4). UV-vis spectra were recorded every 64 s.

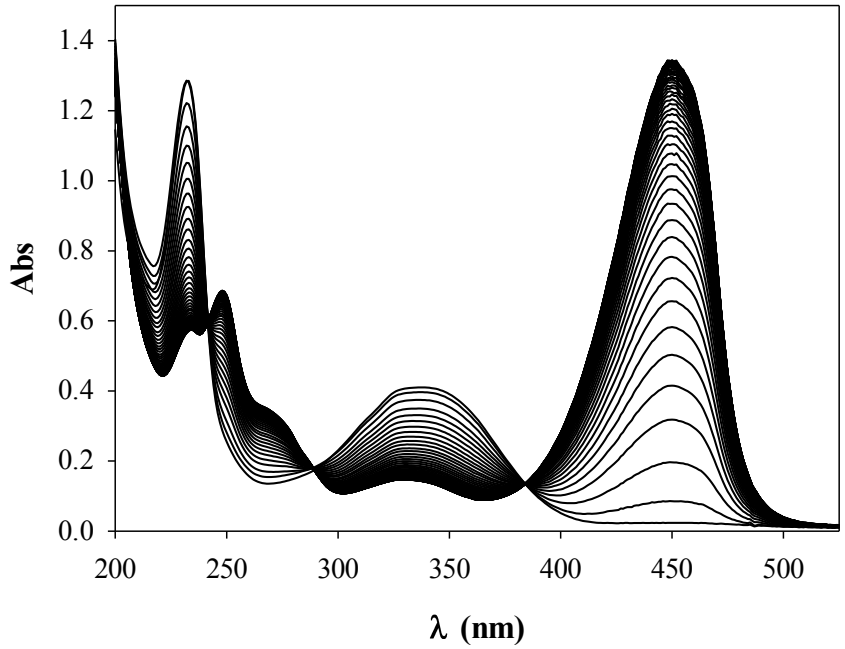

Figure 46. Enzymatic kinetic assay of GalNHQ in the presence of β-galactosidase (pH 7.4). UV-vis spectra were recorded every 8 s.

4.2.3 Antiproliferative activity

The antiproliferative activity of galactococonjugates was tested in the presence and absence of Cu^{2+}. Three different cell lines, A2780, A549 and Hep-G2 (Table 9) were selected to probe the antiproliferative activity. A2780 and A549 cancer cell lines are representative of the most common cancer types whereas Hep-G2 was tested because of it has been found that some galactoconjugates could be suitable for use in PMT of hepatocellular carcinoma.[179]

The simple OHQs were also tested for comparison (Table 9). It is noteworthy that AHQ displayed a very significant activity in the presence of Cu^{2+}, much higher than that of CQ.

Parent compounds showed a good antiproliferative activity against the tested cell lines, in particular in the presence of Cu^{2+}. In general galactosides did not show significant level of antiproliferative activity except GalAHQ and GalNHQ when administrated with Cu^{2+}. These compounds had an increased activity in the presence of Cu^{2+} ions that was pharmacologically relevant (arbitrary <30 μM) only when A2780 ovarian cancer cells were used. These data are in agreement with the behavior observed in the case O-alkylated derivatives of OHQ and CQ as they are not able to strongly complex Cu^{2+} and then exert a good anticancer activity. In the

case of A2780 cells, the presence of Cu^{2+} produces an increased activity perhaps due to a partial hydrolysis of the prodrugs. It has been reported that galactosidase is a lysosomal enzyme and that its concentration depends on the tumor type.[180] A2780 cells could contain the amount of galactosidase needed to partially activate the prodrug, thus only GalAHQ and GalNHQ that are more rapidly cleaved by β-galactosidase could be suitable for PMT approach in this type of tumor where β-galactosidase is overexpressed.

As for Hep-G2 cell line, galactoconjugates did not show a different trend (the antiproliferative activity of the quinoline galactoconjugates does not result higher) compared to the other cell lines even if Hep-G2 cells possess ASGP-receptors that could internalized galactose derivatives through endocytosis. Probably the affinity of these galactoconjugates for this receptor is too low and as a consequence of these results they are not good candidates for PMT. Probably, OHQ galactoconjugates are not easily internalized because of β-galactosidase is expressed in all tested cell lines and in particular hepatocellular carcinoma cell line have higher levels of the enzyme compared to normal liver tissues. The low-lipophilic nature of the molecule arising from the sugar moiety is anticipated to be the reason of this behavior preventing the passive transport of the molecule across the cell membrane, and thereby preventing the interaction of the prodrug with the endogenous enzyme. As for glucoconjugates, the antiproliferative activity and the possibility of exploiting them for PMT approach are probably ascribed to their recognition and then transport by mean of an active system (e.g. GLUT).

However, some galactoconjugates were tested by MTT assay in the presence of β-galactosidase in order to verify if they are suitable for at least ADEPT approach. When the cell lines were treated with GalOHQ, GalAHQ or GalMeHQ in the presence of β-galactosidase (Figure 47). The antiproliferative activity significantly increased, in particular in the presence of Cu^{2+} (Figure 47). This confirmed that for the activation of the galactoconjugates is necessary the formation of the aglycone through the action of the galactosidase and the following complexation of the Cu^{2+}. The different activity of the galactosides can be related to a different hydrolysis of the substrates in the presence of the enzyme as reported in the case of the analogous glucosides.

Table 9. Summary of IC_{50}s (μM) of galactosides and their parent compound on A2780, A549, and Hep-G2 human tumor cells.

	OHQ		GalOHQ	
		Cu^{2+}		Cu^{2+}
A2780	2.2 ± 0.4	0.3 ± 0.1	>100	>100
A549	5.3 ± 0.5	0.54 ± 0.03	>100	>100
Hep-G2	9 ± 2	0.50 ± 0.02	>100	50 ± 2
	MeHQ		**GalMeHQ**	
		Cu^{2+}		Cu^{2+}
A2780	8 ± 2	4.1 ± 0.2	>100	>100
A549	25 ± 3	4.6 ± 0.3	>100	>100
Hep-G2	12 ± 3	5.0 ± 0.3	>100	>100
	AHQ		**GalAHQ**	
		Cu^{2+}		Cu^{2+}
A2780	4 ± 1	0.54 ± 0.01	103 ± 26	4 ± 2
A549	7 ± 1	0.58 ± 0.03	>100	46 ± 10
Hep-G2	7.6 ± 0.3	0.51 ± 0.02	>100	52 ± 2
	ClHQ		**GalClHQ**	
		Cu^{2+}		Cu^{2+}
A2780	5.1 ± 0.9	0.47 ± 0.03	>100	70 ± 6
A549	5.9 ± 0.9	0.4 ± 0.2	>100	>100
Hep-G2	10 ± 3	5.1 ± 0.1	>100	>100
	Cl_2HQ		**GalCl_2HQ**	
		Cu^{2+}		Cu^{2+}
A2780	25 ± 3	2.5 ± 0.3	>100	80 ± 7
A549	24 ± 2	1.7 ± 0.4	>100	>100
Hep-G2	65 ± 7	5.7 ± 0.3	>100	>100
	CQ		**GalCQ**	
		Cu^{2+}		Cu^{2+}
A2780	55 ± 3	6.0 ± 0.4	>100	>100
A549	65 ± 10	7.1 ± 0.4	>100	>100
Hep-G2	-	-	-	-
	NHQ		**GalNHQ**	
		Cu^{2+}		Cu^{2+}
A2780	6.4 ± 0.3	2.6 ± 0.8	52 ± 4	5.4 ± 0.8
A549	19 ± 4	4.9 ± 0.6	86 ± 18	10 ± 5
Hep-G2	19 ± 6	5.3 ± 0.4	>100	92 ± 22

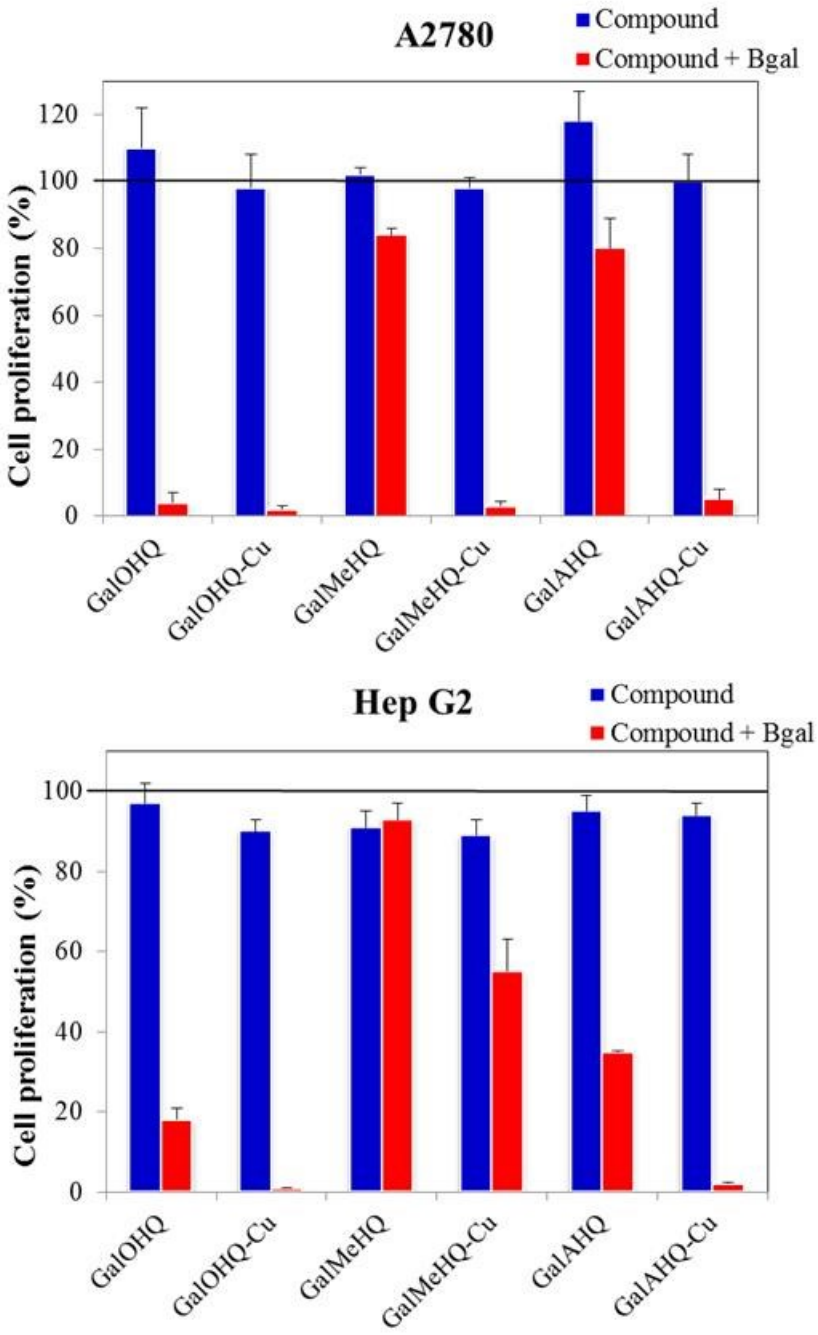

Figure 47. Antiproliferative activity of GalOHQ, GalAHQ or GalMeHQ towards A2780 and Hep-G2 in the presence or absence of β-galactosidase (2U/well). Final concentration of galactosides is 10 µM, except GalAHQ used at 2 µM when administered to A2780 cells.

4.3 Chelating OHQ conjugates with monosaccharides and disaccharides

4.3.1 Synthesis and characterization

A chelating glucoconjugate of 8-hydroxyquinoline (GlcHQ) was also synthetized and characterized in order to compare its chemical and biological properties to those of glucoconjugated prodrugs previously described. GlcHQ was synthesized by a multistep procedure as follows: Lewis acid mediated glycosylation of glucose pentaacetate with Fmoc-protected aminoethanol gave GluFmoc. The Fmoc and acyl protecting groups were removed simultaneously to give 2′-aminoethyl-β-D-glucopyranoside, which was then coupled to 8-hydroxyquinoline-2-carboxylic acid (Figure 48). After purification, the isolated product was characterized by ESI-MS and NMR.

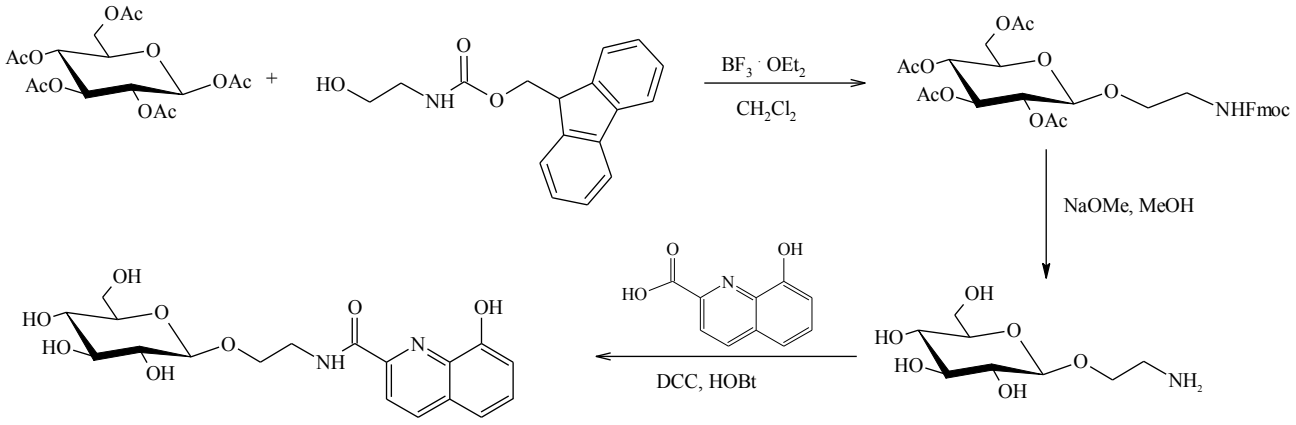

Figure 48. Synthesis of GlcHQ.

Positive ion ESI-MS spectrum confirmed the identity of the product. Peaks due to singly charge ion adducts with proton, sodium and potassium were detected at 394.9, 417.1 and 433.1 *m/z*. Furthermore the dimeric sodium and potassium adducts are also evident at 810.7 and 827.1 *m/z*. In the negative mode, the base peak can be assigned to the singly charged $[P-H]^-$, presumably due to the deprotonation of the phenolic group.

^{1}H NMR spectrum displays peaks due to the quinoline moiety, the glucose units and the ethylenic chain (Figure 49). The former resonate in the aromatic region δ = 8.5-7.1 ppm.

Anomeric proton of the sugar resonates at 4.37 ppm as a doublet with coupling constants of 7.8 Hz, indicating the β-anomer. On the contrary of glucoconjugated prodrugs, the

anomeric proton is not downfield shifted owing to the ring current because the presence of the spacer (ethylenic chain) prevents this effect. The other sugar protons and the diastereotopic ethylenic protons appear in the range δ = 4.2-3.1 ppm.

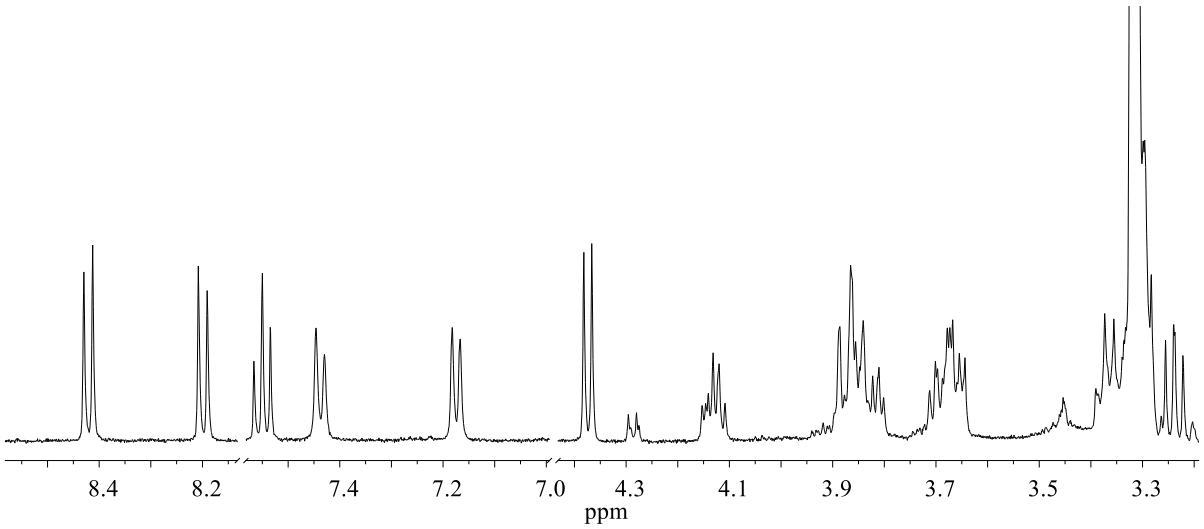

Figure 49. ^{1}H NMR spectrum of GlcHQ in D_2O at 500 MHz.

8-hydroxyquinoline was also conjugated with trehalose (Figure 50). Trehalose is a natural alpha-linked disaccharide formed by an α,α-1,1-glucoside bond between two α-glucose units. Trehalose possesses interesting biological properties including antioxidant and antiaggregant activity.

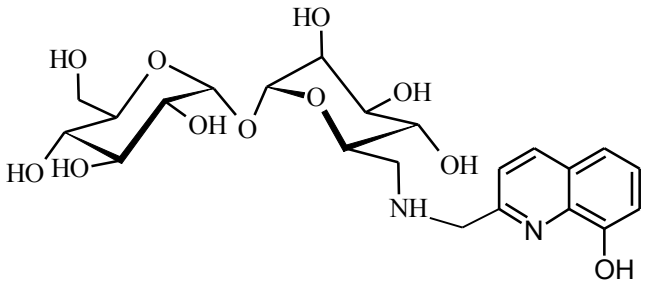

Figure 50. Trehalose-OHQ conjugate.

THRHQ was synthetized by a stepwise reductive amination. In brief, the reaction of the aldehyde with 6-amino-6-deoxy-α,α'-trehalose involved the preformation of the intermediate imine that was reduced by $NaBH(OAc)_3$. The final product was isolated through ion-exchange chromatography and was obtained in excellent yield. Characterization and unequivocal structural assignments were achieved by a combination of techniques including ESI-MS and NMR. The ESI mass spectrum of THRHQ in aqueous solution is essentially constituted by

peaks due to singly charged ions at *m/z* 499.1 and 521.1 attributable to $[THRHQ+H]^+$ and $[THRHQ+Na]^+$ ions and singly charge dimeric proton and sodium ion adducts at 996.6 and 1018.7 *m/z*.

As for NMR characterization, the two glucose rings of trehalose (A and B refer to the functionalized and the unfunctionalized glucose rings) become inequivalent due to the functionalization and their signals are assigned by 2D NMR experiments such as COSY, TOCSY, HSQC and HMBC. Aromatic protons are evident in the range 8.17-6.98 ppm (Figure 51).

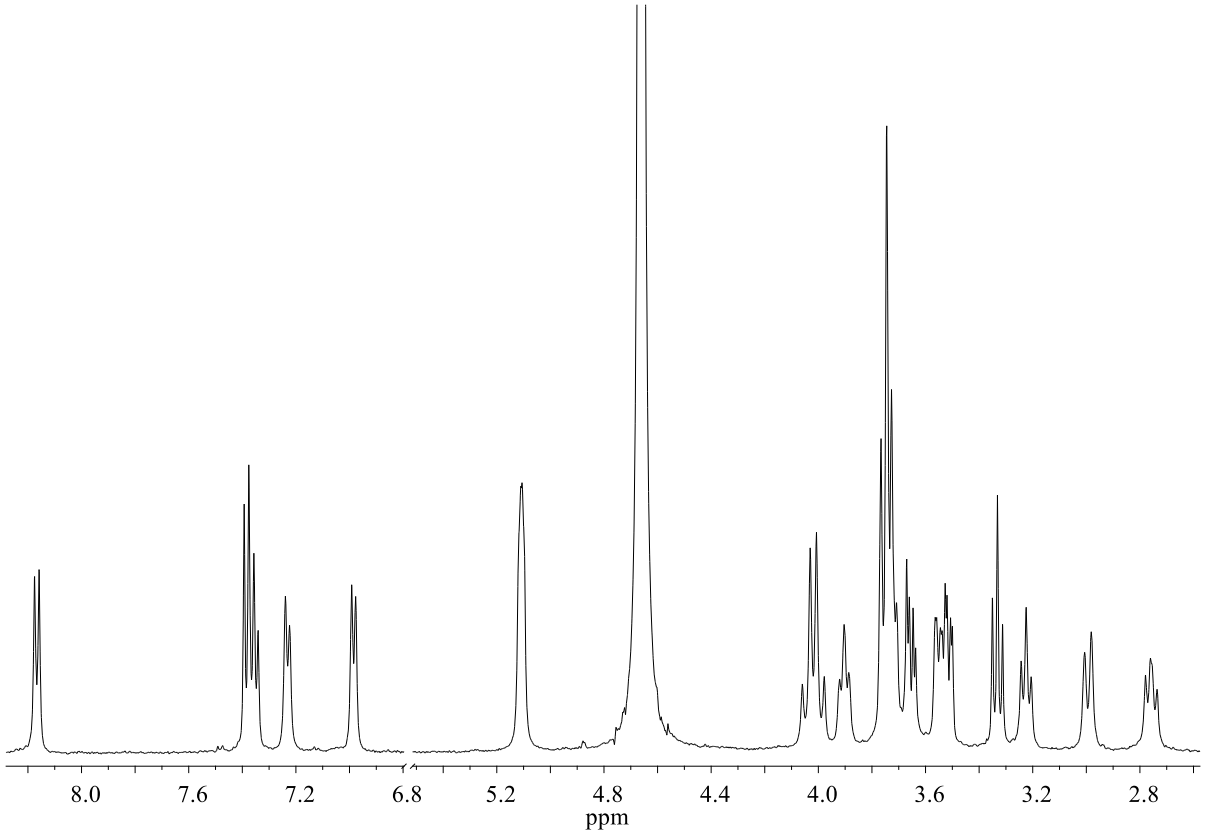

Figure 51. ^{1}H NMR spectrum of THRHQ in D_2O at 500 MHz.

Using TOCSY and HSQC spectra (Figure 52 and Figure 53), both spin systems of glucose rings were fully assigned. Hs-1 appear together at 5.11 ppm. The diastereotopic Hs-6 of the A ring are detected at 2.98 and 2.76 ppm and the H-5A signal is downfield shifted at 3.89 ppm. The H-2A and H-2B are overlapped, while the H-4B and H-4A resonate at 3.34 and 3.22 ppm, respectively. The diastereotopic protons of the benzylic CH_2 show up at 4.04 ppm.

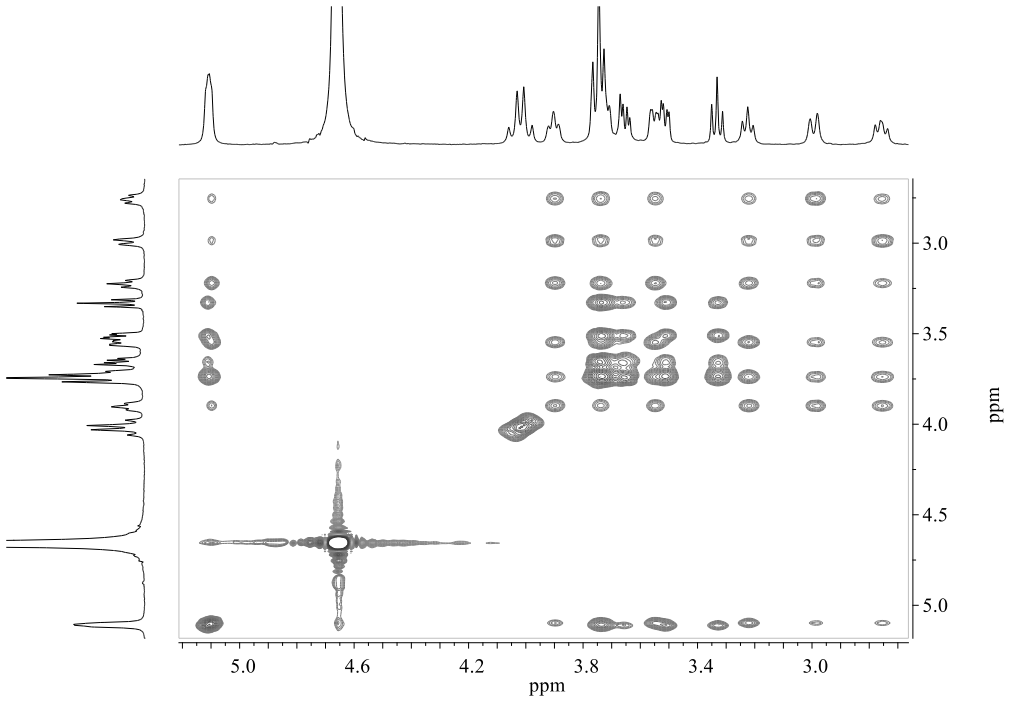

Figure 52. TOCSY spectrum of THRHQ in D_2O at 500 MHz.

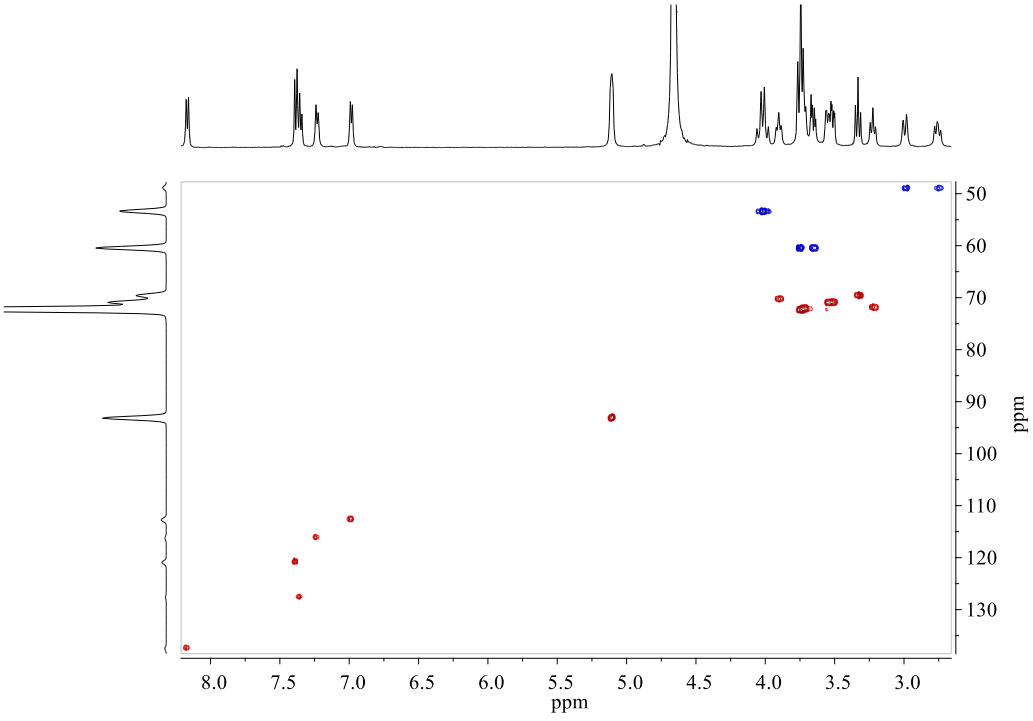

Figure 53. HSQCAD spectrum of THRHQ in D_2O at 500 MHz.

4.3.2 Metal complexes

In Table 10 the ESI-MS characterizations of the Cu^{2+} complexes with GlcHQ and THRHQ are reported.

Table 10. ESI-MS characterization of the Cu^{2+} complexes of ([L] = 5.0×10^{-5} M, [Cu^{2+}] = 1.25×10^{-5} M, 2.5×10^{-5} M and [Cu^{2+}] = 5.0×10^{-5} M) at pH 7.0. L is a hydroxyquinolinate derivative.

Ligand	Assignment	Calcd (*m/z*)	Found (*m/z*)
GlcHQ	$[LH+H]^+$	395.1	395.1
	$[LH+Na]^+$	417.1	417.1
	$[CuL]^+$	456.1	455.9
	$[CuL-H+Na]^+$	478.0	477.9
	$[CuL_2+Na]^+$	872.2	872.0
	$[Cu_2L_2-H]^+$	911.1	910.9
	$[Cu_2L_2-2H+Na]^+$	933.1	932.9
THRHQ	$[LH+H]^+$	499.2	499.1
	$[LH+Na]^+$	521.2	521.2
	$[CuL]^+$	560.1	559.9
	$[CuL-H+Na]^+$	582.1	582.1
	$[CuL_2+H]^+$	1058.3	1058.1
	$[CuL_2+Na]^+$	1080.3	1080.0
	$[Cu_2L_2-H]^+$	1119.2	1119.1
	$[Cu_2L-2H+Na]^+$	1141.2	1141.0

The ESI-MS experiments were carried out at different pH (5.0-9.0) and various ratios M/L (from 1.5 to 0.2). The formation of complex species was observed at pH > 5. In addition to the peak of the ligand new peaks due to singly charged species $[CuL]^+$ and $[CuL-H+Na]^+$ and single charged dimeric species appear in the presence of Cu^{2+}. CuL^+ is the main species over the explored pH range (pH 5-9). In comparison with similar systems and taking account of the mass spectrometry data, a main species ML (with the metal ion bound to N of py ring, phenolate and amino group) could be hypothesized. ML_2 species are essentially observed for $[Cu^{2+}]/[L] \leq 0.5$ (Figure 54). A dinuclear dimeric species is also observed at *m/z* = 910.9 and 1119.1 for GlcHQ and THRHQ, respectively.

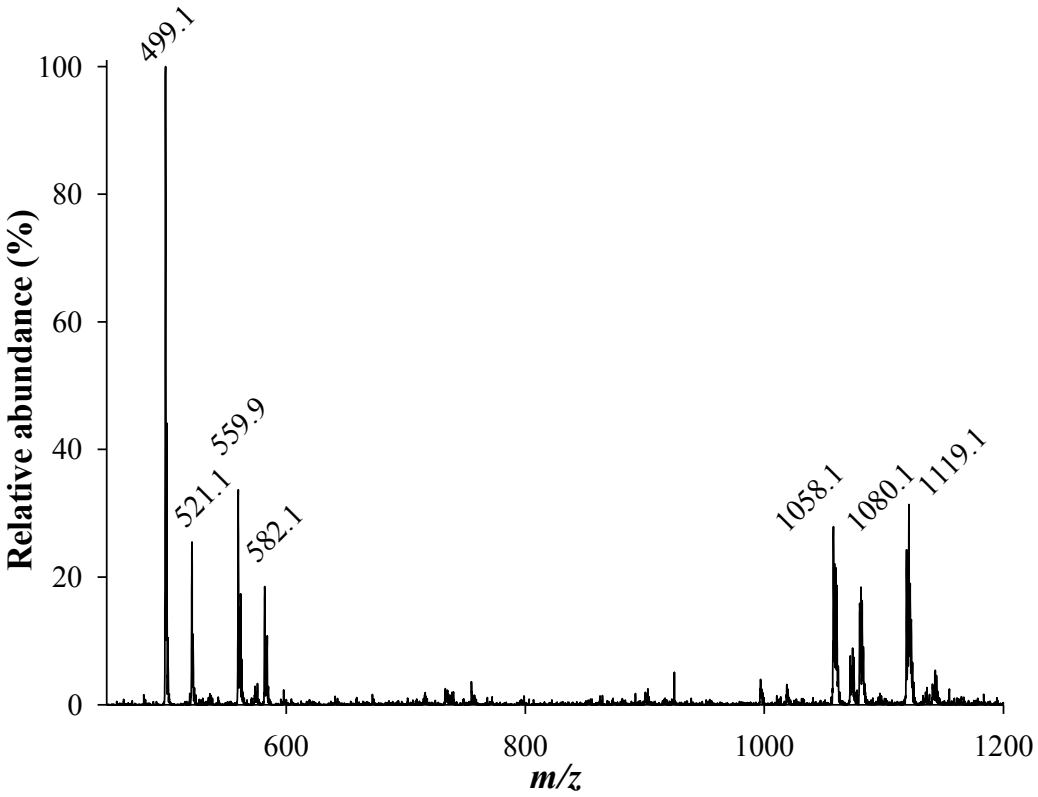

Figure 54. ESI-MS spectrum of a Cu^{2+}-THRHQ solution (ratio Cu^{2+}/L = 0.25) at pH 7.0.

ESI-MS spectra were also recorded in the presence of different amount of Zn^{2+} at different pH (Table 11). The detected species are similar to those of copper, suggesting the involvement of the same groups in the metal coordination. However, the relative intensity of the peaks due to the zinc complexes is much lower than that of copper complexes, suggesting a minor affinity of the ligand for this metal ion as expected in keeping with Irving-Williams series.

Table 11. ESI-MS characterization of the Zn^{2+} complexes of ([L] = 5.0×10^{-5} M, [Zn^{2+}] = 1.25×10^{-5} M, 2.5×10^{-5} M and [Zn^{2+}] = 5.0×10^{-5} M) at pH 7.0. L is a hydroxyquinolinate derivative.

Ligand	Assignment	Calcd (*m/z*)	Found (*m/z*)
GlcHQ	$[LH+H]^+$	395.1	395.1
	$[LH+Na]^+$	417.1	417.1
	$[ZnL]^+$	457.1	456.9
	$[ZnL_2+H]^+$	851.2	851.0
	$[ZnL_2+Na]^+$	873.2	873.0
	$[Zn_2L_2-H]^+$	913.1	912.9
THRHQ	$[LH+H]^+$	499.2	499.1
	$[LH+Na]^+$	521.2	521.2
	$[ZnL]^+$	561.1	560.9
	$[ZnL_{2+}H]^+$	1059.3	1059.1
	$[ZnL_2+Na]^+$	1081.3	1081.1
	$[Zn_2L_2-H]^+$	1121.2	1121.1

4.4 New cyclodextrin-bearing 8-hydroxyquinoline ligands

4.4.1 Synthesis and characterization

Monofunctionalized β-CyDs via an amide bond

CD6HQ, CDOHQ and CDNHQ (Figure 55) were synthesized by an amide condensation reaction starting from the respective cyclodextrin derivatives and 8-hydroxyquinoline-2-carboxylic acid in the presence of typically used activating agents.[181]

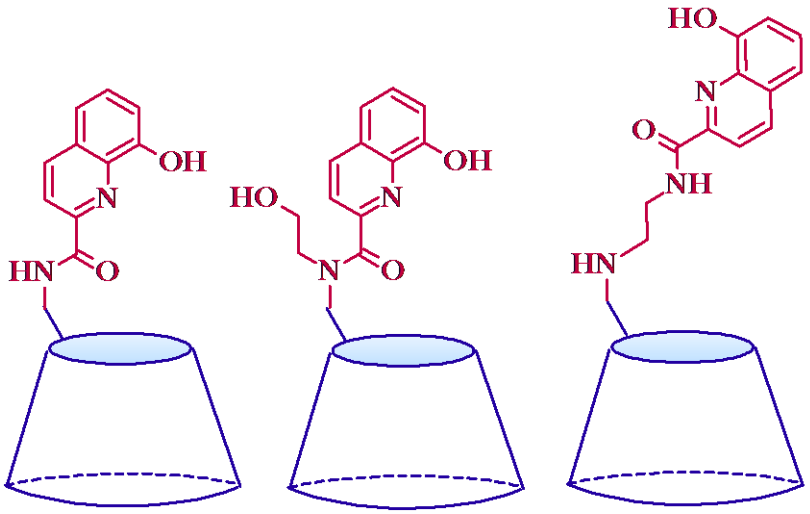

Figure 55. Schematic representation of monofunctionalized CyDs *via* an amide bond.

The products were isolated by reversed-phase flash chromatography. Multinuclear NMR spectroscopy and MS experiments confirmed the identity of the products.

The 1D NMR spectra of the products were assigned by 2D experiments. The ^{1}H NMR spectrum of CD6HQ displays signals due to the quinoline ring and cyclodextrin moieties, the former resonating in the aromatic region between 8.17 and 7.09 ppm (Figure 56).

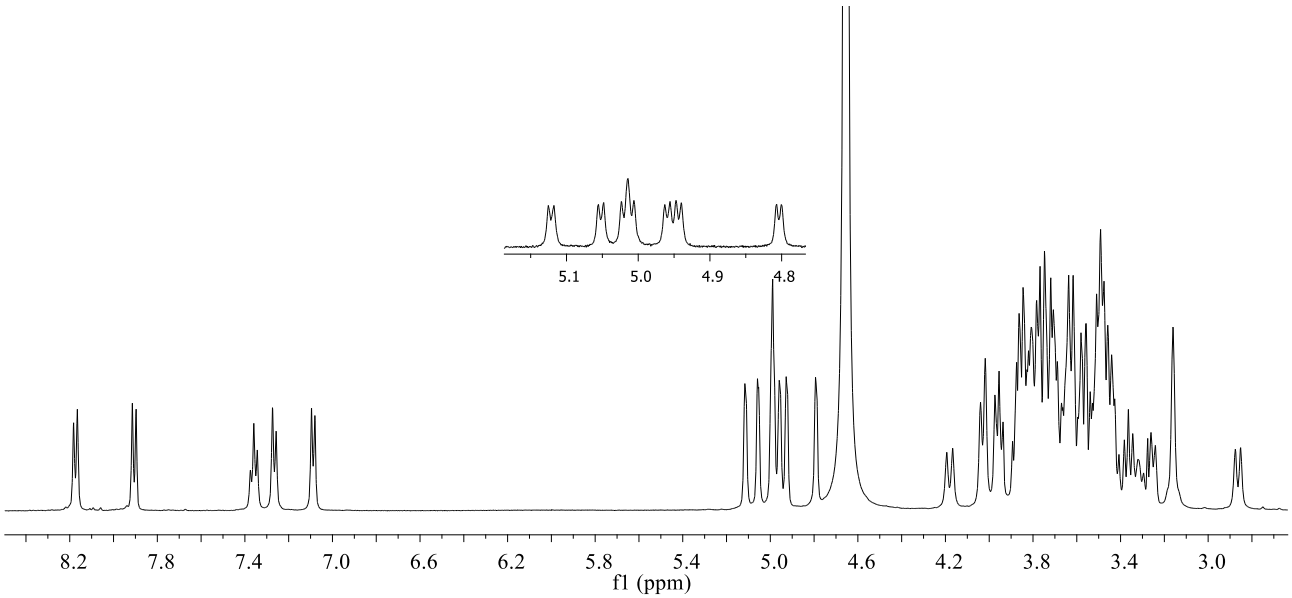

Figure 56. ^{1}H NMR of CD6HQ in D_2O at 500 MHz.

The Hs-1 of the CyD moiety are divided into six groups (Figure 56: inset) as a consequence of functionalization. Some H-6 of CyD are spread due to the functionalization. The well evident different effects on the Hs-6 are due to the aromatic ring current effect as reported for other aromatic derivatives.[182] This behavior suggests the self-inclusion of the aromatic moiety into the cavity. A similar effect can be seen in the ^{13}C NMR spectra (Figure 57).

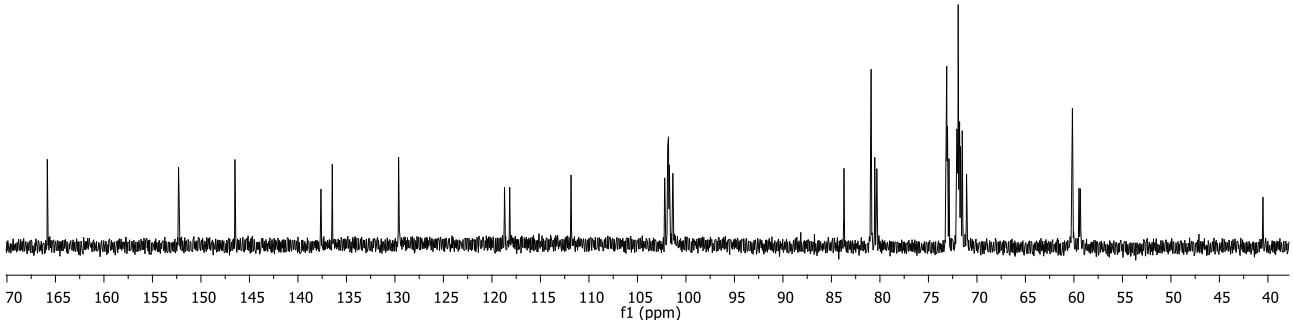

Figure 57. ^{13}C NMR spectrum of CD6HQ (D_2O, 125 MHz).

ROESY spectra were carried out (Figure 58). Aromatic H-4, H-3, H-7 show cross correlations with the H-5, H-3 and H-6 of CyD. Aromatic H-3 and H-4 show also correlations with the 6B proton. These spectra confirm the self-inclusion of quinoline ring into the cavity. NMR spectra were also carried out in the presence of 1-adamantanol (ADM), a competitive guest for cyclodextrin cavity. ROESY spectra show that ADM was included in the cavity and

the OHQ ring moved towards the upper rim. Hs-6B were shifted upfield and cross peaks between H-6B and aromatic proton appear in the ROESY spectra.

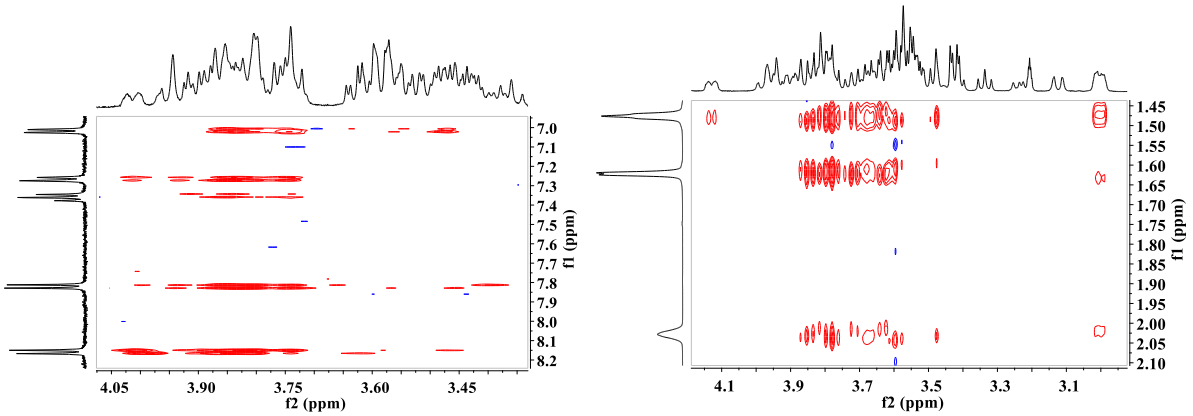

Figure 58. ROESY spectra of CD6HQ (left) and a 1:2 mixture of CD6HQ and ADM (right).

The ^{1}H NMR spectrum of CDOHQ is reported in Figure 59. The NMR spectrum does not change with CDOHQ concentration.

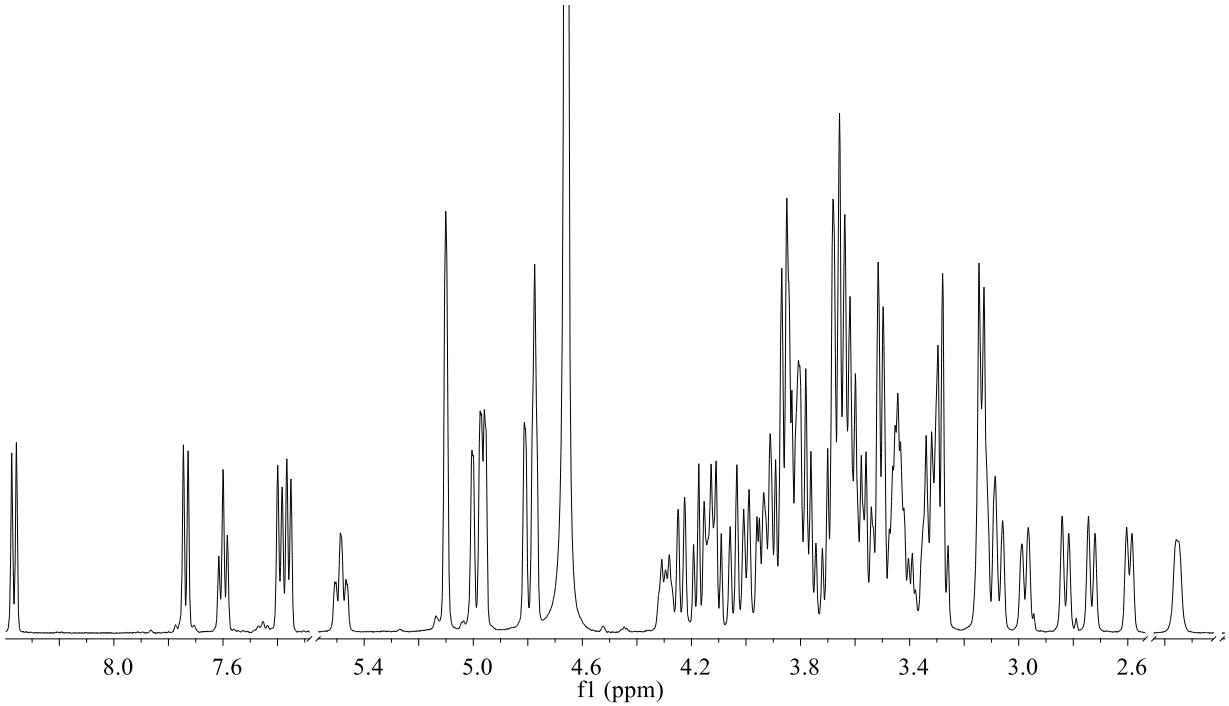

Figure 59. ^{1}H NMR of CDOHQ in D_2O at 500 MHz.

The diastereotopic protons of the ethylenic chain are easily assigned by HSQC (Figure 60) and appear at 3.10, 2.97, 2.82, 2.73 ppm, whereas the protons of the aromatic rings resonate in the range δ = 8.37-7.36 ppm.

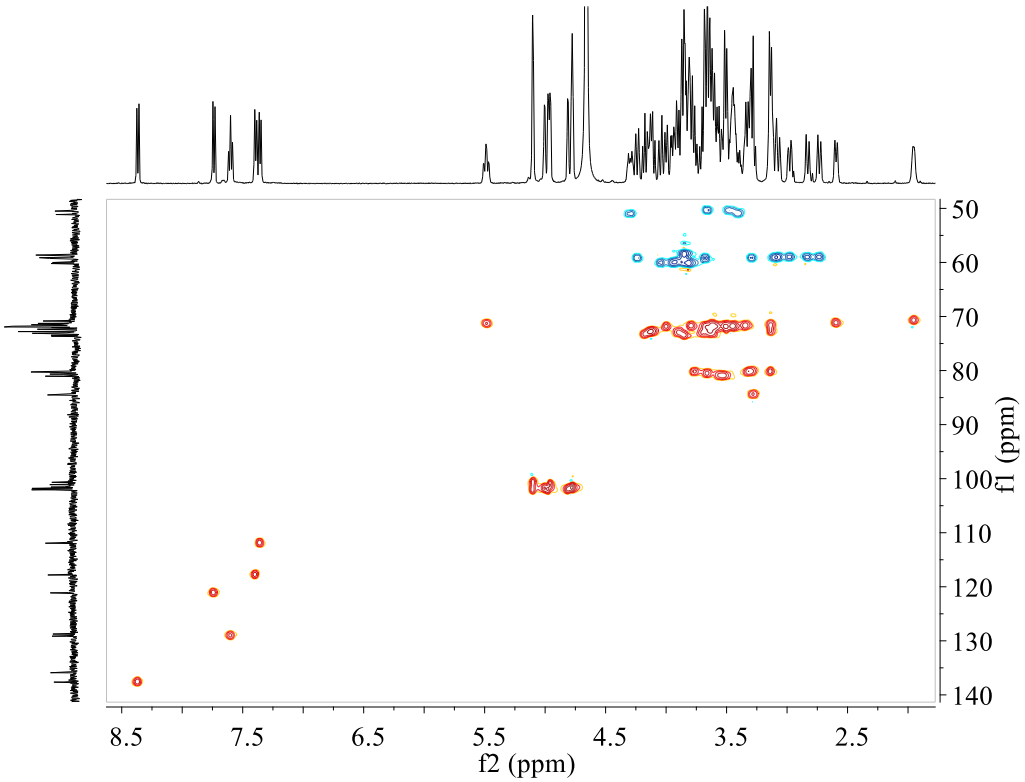

Figure 60. HSQCAD spectrum of CDOHQ (D_2O, 500MHz).

In these spectra the spreading of the different sugar protons can be also observed. The H-1 protons of cyclodextrin moiety are divided into five groups, the H-5, H-3 and H-6 are clearly spread. A triplet assigned to the 5A proton can be observed downfield at 5.5 ppm. The signals at 2.00 ppm and 2.60 ppm can be assigned to H-3B and H-3X. In this system a spreading of H-3 protons can be seen in comparison to CD6HQ, suggesting a deeper inclusion of the moiety. The effect of self-inclusion conformation is more evident compared to CD6HQ.

The ROESY spectra of CDOHQ were also carried out and confirm the inclusion of quinoline moiety in CyD cavity showing correlations between the H-4, H-5, H-6 and H-7 of quinoline moiety and the H-3, H-5 region of CyD. The presence of an ethylenic linker confers rigidity to the system. The chain is probably involved in H bond formation with the upper rim protons, as suggested by the different chemical shifts of the ethylenic chain protons.

The ^{1}H NMR spectrum of CDNHQ (Figure 61) shows immediately a different conformation of the aromatic moiety with respect to the CyD, the presence of ethylendiamine chain does not favor the self-inclusion of the aromatic moiety. In the spectra the protons of the functionalized ring can be identified. No correlation is shown in the ROESY spectra.

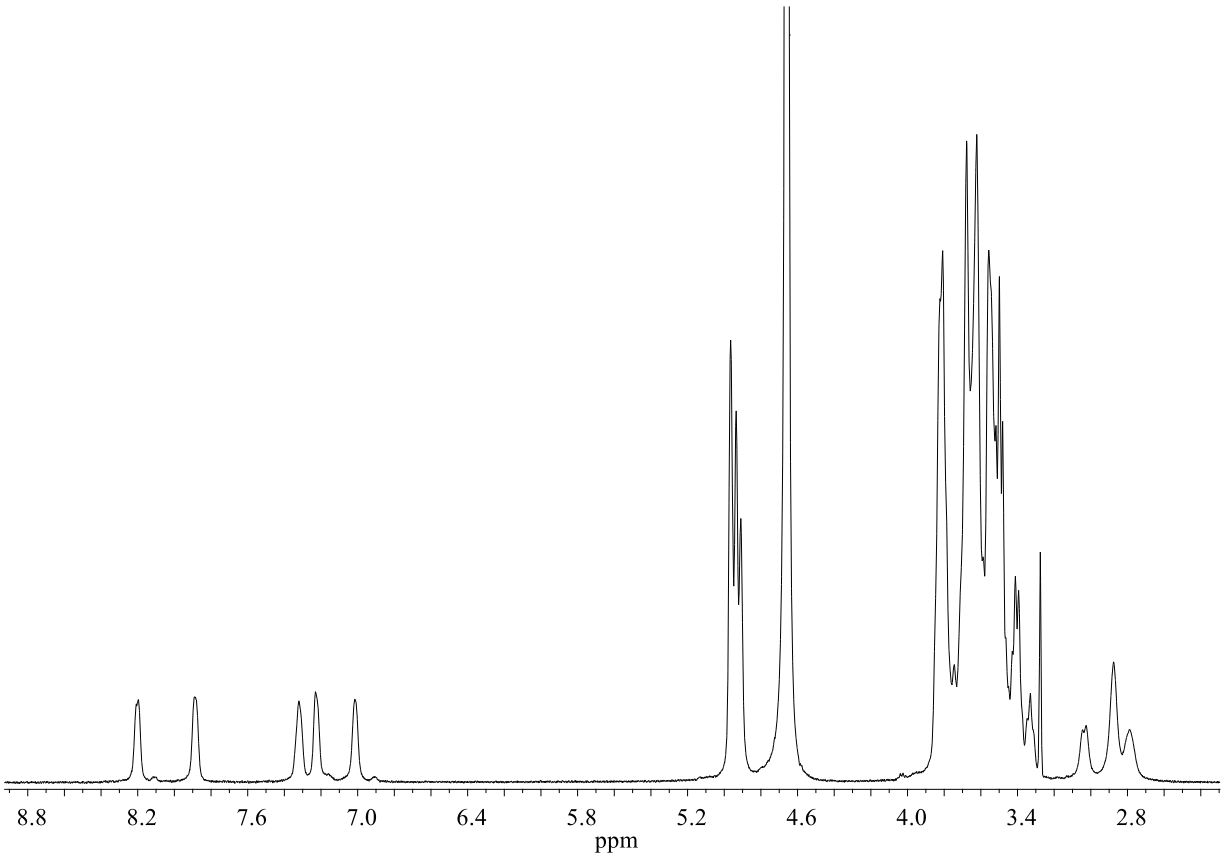

Figure 61. ^{1}H NMR of CDNHQ in D_2O at 500 MHz.

The ligands were characterized by CD spectroscopy in order to further investigate the interaction of quinoline ring with the β-CyD cavity. The CD spectrum at pH 6.8 of CD6HQ shows an intense negative band at 255 nm and a small positive band at 220 nm. These bands in the absorption region of the OHQ rings are due to the dipole–dipole coupling between the quinoline ring moiety and the β-CyD cavity. This behavior has been generally reported for functionalized CyDs and is due to the interaction of the functionalizing moiety[183,184] with CyD. In this case the inclusion of the side chain can be proposed on the basis of NMR and CD data. The CD spectrum of CD6HQ is influenced by pH as well as its UV spectrum owing to the deprotonation of phenolic group of the quinoline moiety. At basic pH, another band at 283 nm appears whereas the band at 255 nm decreases its intensity. Furthermore, the spectrum is affected by the presence of ADM (Figure 62), in keeping with the self-inclusion. The intensity of the band enhances with increasing concentrations of ADM suggesting a modification of the orientation of the quinoline moiety with respect to the cyclodextrin. In the literature the signs and intensities of the ICD signals in the host-guest complex formation have been summarized

by the Harata's and Kodaka's rules. When the cavity of CD6HQ is available the quinoline moiety is self-included in the cavity and the quinoline long axis is inclined slightly away from cyclodextrin sevenfold axis as observed for similar systems.[185] This hypothesis is in keeping with the NMR results. When ADM was added the quinoline moved out the cavity. The quinoline moiety would be in a lid-type conformation as reported for alike systems.[186,187]

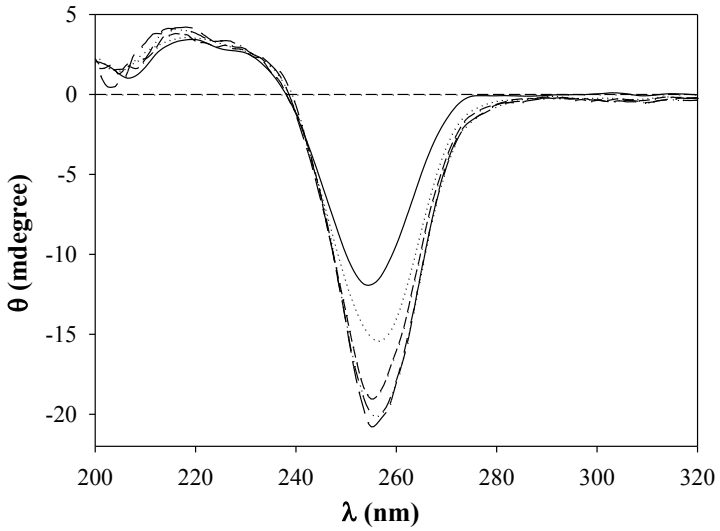

Figure 62. CD spectra of CD6HQ (4×10^{-5} M) with increasing concentrations of ADM (2×10^{-5} to 4×10^{-4} M).

As for CDOHQ, its CD spectrum shows two positive bands at 273 and 226 nm and a more intense negative band at 251 nm. The presence of the CyD moiety induces chirality in the π–π* region of the aromatic ring. A stronger induced circular dichroism (ICD) is observed compared to CD6HQ. This is in keeping with the NMR results which suggest a deeper inclusion of the moiety. The spectrum is affected by the presence of ADM (Figure 63). In fact a decrease of the bands with increasing concentrations of ADM suggests a changed disposition of the quinoline moiety with respect to β-CyD cavity, in keeping with the interaction of the aromatic rings with the cavity.

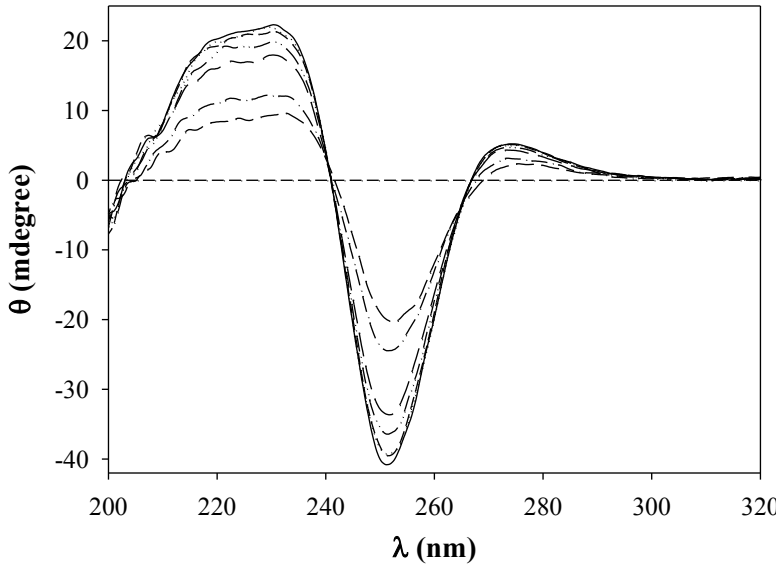

Figure 63. CD spectra of CDOHQ (4×10^{-5} M) in the presence of increasing concentrations of ADM (3.2×10^{-5} to 2×10^{-3} M).

The CD spectrum varies linearly with concentration of the conjugate, ranging from 2×10^{-6} M to 9×10^{-5} M, confirming the intramolecular interaction of the aromatic moiety. Even when a large excess of ADM was added, the dichroic band is partially maintained. The quinoline moiety could be in a lid-type disposition as suggested by the similarity of the CD spectra of CD6HQ and CDOHQ in the presence of ADM.

As for CDNHQ, the circular dichroism spectra show only a very weak band at 256 nm, in agreement with the absence of interactions of the aromatic moiety with the cavity. Only slight changes were observed when ADM was added, in keeping with the disposition outside the cavity of the quinoline moiety. In this case the self-inclusion is ruled out because of the presence of the ethylenic spacer that moves away the quinoline moiety from the upper rim of CyD.

A CyD derivative functionalized at the lower rim (Figure 64) was also obtained and studied in comparison with the other CyD derivatives functionalized at the upper rim *via* an amidation.

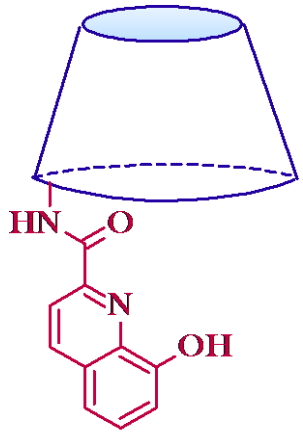

Figure 64. Schematic representation of CD3HQ.

CD3HQ was synthesized starting from 2^A(S),3^A(R)-3^A-amino-3^A-deoxy-β-cyclodextrin obtained by the diaxial opening of 2,3-manno-epoxide. The coupling of the former with 8-hydroxyquinoline-2-carboxylic acid using DCC and HOBt, allowed to afford the desired compound. In the ^{1}H NMR (Figure 65), H-1 signal is split into 7 peaks as monosubstituted cyclodextrins lack the C7 symmetry of free or symmetrically substituted CyDs. Furthermore, 2^A(S),3^A(R)-CyDs have an altrose instead of a glucose unit because of their synthetic mechanism.

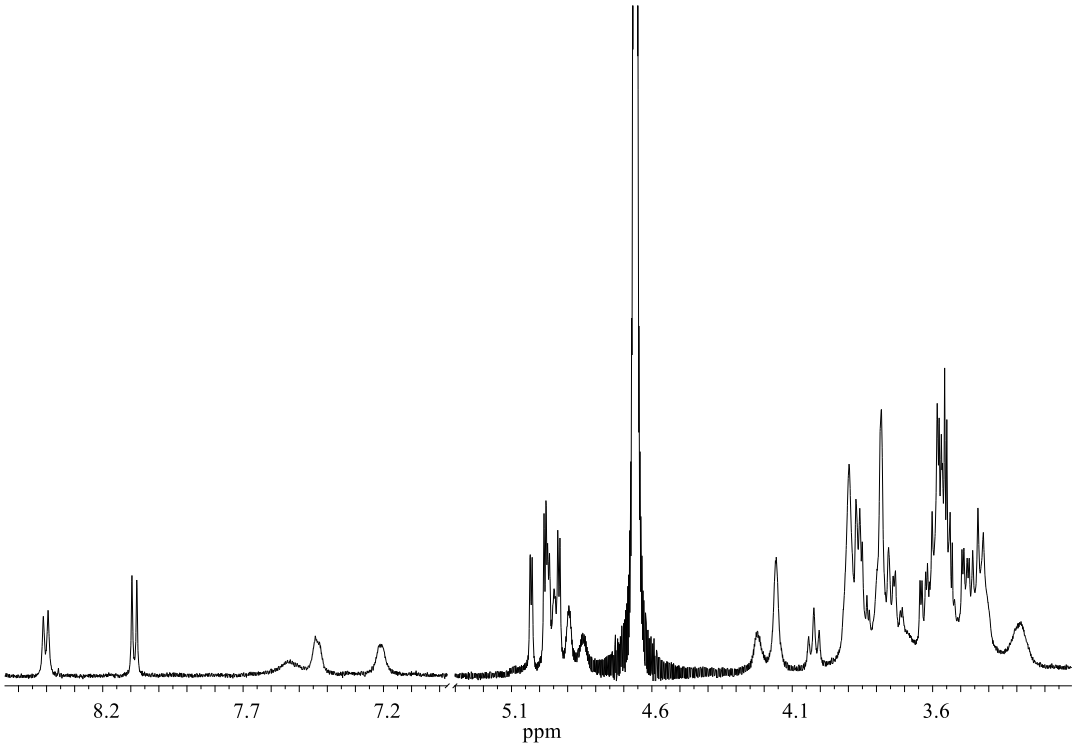

Figure 65. ^{1}H NMR spectrum of CD3HQ in D_2O at 500 MHz.

Using TOCSY and COSY spectra (Figure 66 and Figure 67), the spin systems were assigned to the protons of one particular glucose residue. NMR spectrum evidences the downshift of H-3A and H-2A that resonate at 4.72 and 4.22 ppm. H-4A is also shifted downfield at 4.16 ppm whereas H-5A and H-6A resonate at 3.91 and 3.58 ppm. These large shifts of A protons could be due to the anisotropic deshielding effect of the carbonyl group and aromatic moiety. ^{1}H NMR also shows the downfield shift of H-3F at 4.02 ppm and the upfield shift of H-4 and H-3Z at 3.29 ppm. Aromatic protons of quinoline moiety resonate in the aromatic region between 8.40 and 7.21 ppm.

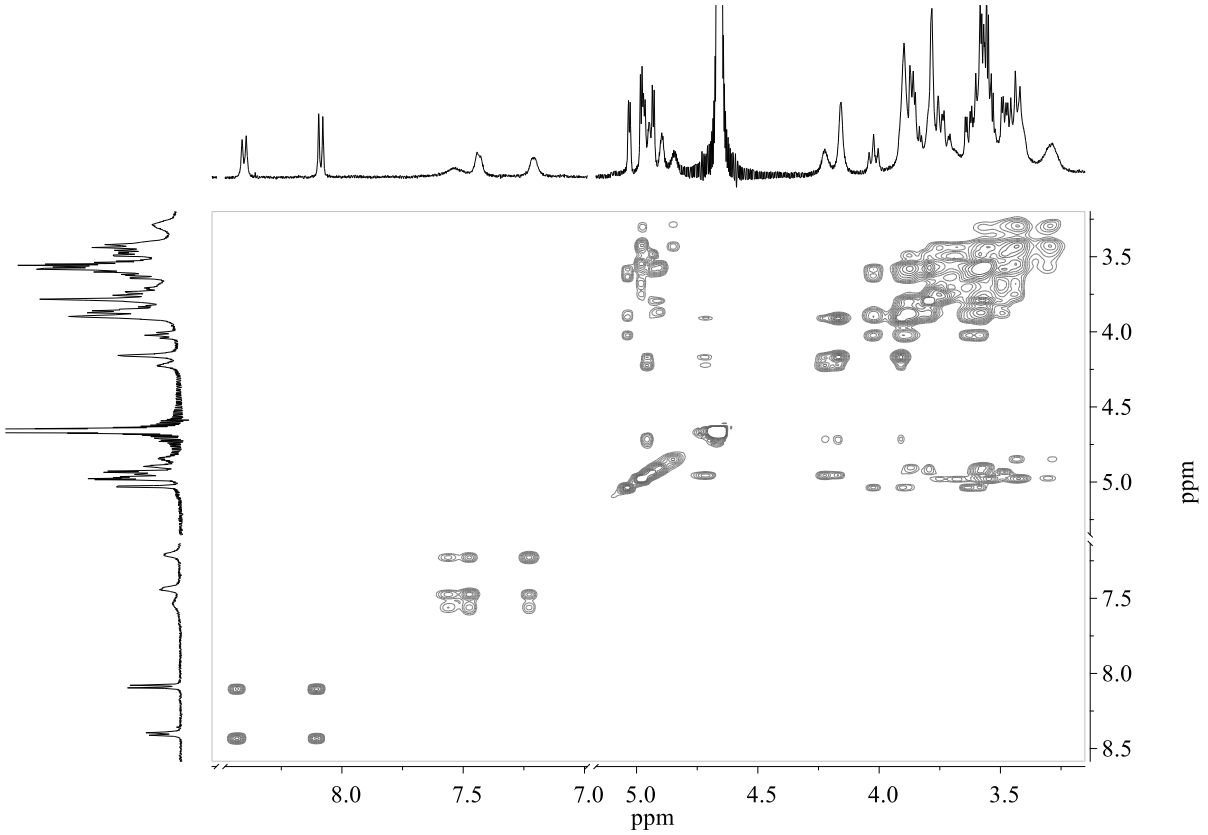

Figure 66. TOCSY spectrum of CD3HQ in D_2O at 500 MHz.

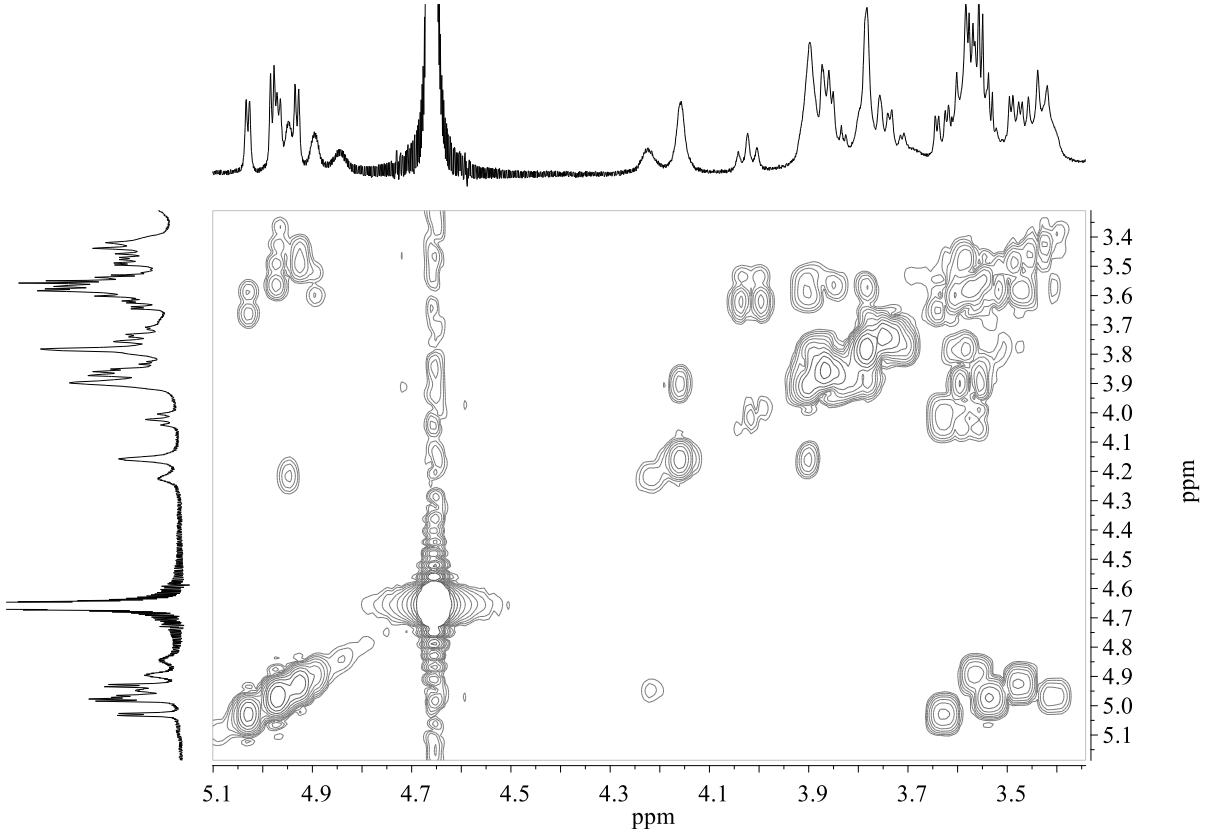

Figure 67. COSY spectrum of CD3HQ in D_2O at 500 MHz.

ROESY spectra allow to assign some glucose units. It is possible to attribute the doublet at 4.97 ppm to H-1G whereas H-1B resonates at 4.93 ppm.

The analysis of the ROESY spectrum also reveals the presence of through-space proximities between the quinoline aromatic and some CyD protons, essentially H-3 and H-5. Since these protons are pointed towards the interior of the cavity, it can deduced that an inclusion complex of the pendant is formed. Intense cross peaks were detected between the aromatic H-7 and H-3F, H-5 and other protons of CyD. Aromatic H-4, H-5, H-6 also display correlations with H-3F and CyD protons resonating at 3.87 and 3.57 ppm. NOE signals between H-3 and inner CyD protons are not evident suggesting that the former does not penetrate the cavity even though was closely located in the outer layer of the CyD. This behavior could be explained by the proximity of H-3 to the functionalization site. Taken together, ROESY data suggest that the most hydrophobic part of the phenolic ring is nearer or inside the CyD cavity as showed by the strong NOE signals of H-7, H-6 and H-5.

CD3HQ was also characterized by CD spectroscopy in order to further investigate the interaction of quinoline ring with the β-CyD cavity. The CD spectrum at pH 6.8 of CD3HQ shows a positive band at 252 nm and two small negative bands at 233 and 265 nm. These bands in the absorption region of the OHQ are due to the dipole–dipole coupling between the quinoline ring moiety and the β-CyD cavity. It is worth mentioning that in CD spectrum the signs of the bands are opposite to those of CD6HQ suggesting that the orientation between quinoline moiety and CyD cavity in CD3HQ is opposite to that of CD6HQ. The CD spectrum of CD3HQ is deeply influenced by pH as well as its UV spectrum owing to the deprotonation of phenolic group of the quinoline moiety. At basic pH, a negative band at 271 nm and a positive band at 243 nm appear.

Furthermore, the spectrum is affected by the presence of ADM (Figure 68). Titration of ADM into the solution of CD3HQ elicited the hyperchromic and bathochtomic shifts of the band at 252 nm, with corresponding isosbestic points near 248 and 273 nm. The band enhancement with increasing concentrations of ADM indicates a modification of the orientation of the quinoline moiety with respect to the cyclodextrin.

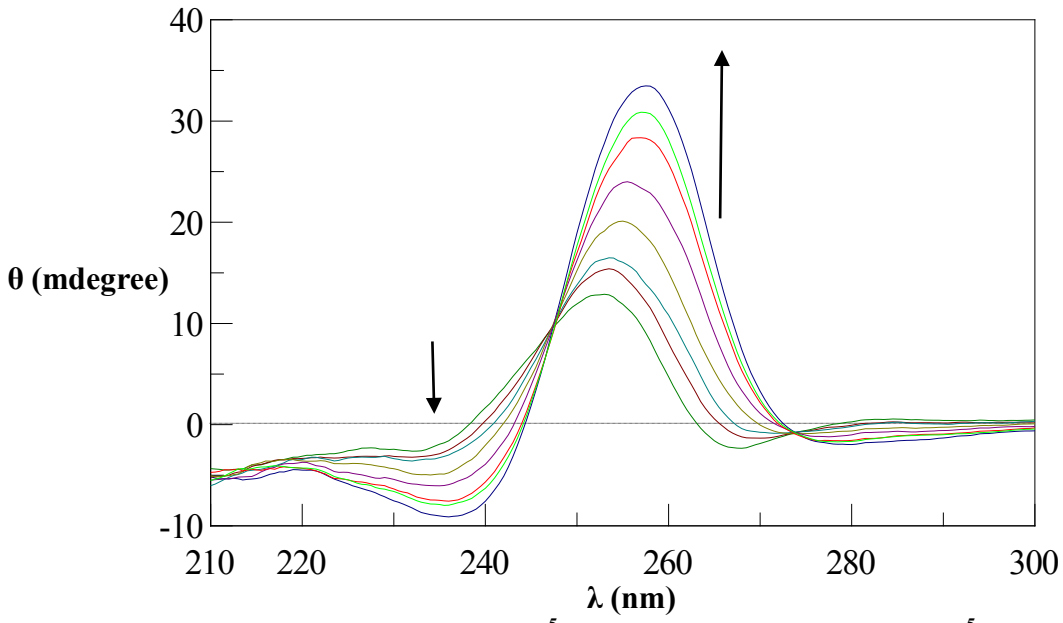

Figure 68. CD spectra of CD3HQ (4×10^{-5} M) in the presence of ADM (2×10^{-5} M to 8×10^{-4} M).

Monofunctionalized CyDs via an amine bond

CD6RHQ and CD3RHQ (Figure 69) were synthetized by a stepwise reductive amination. In brief, the reaction of the aldehyde with the primary amine (mono-6-amino-cyclodextrin or mono-3-amino-cyclodextrin, respectively) involved the preformation of the intermediate imine followed by reduction to give a secondary amine.

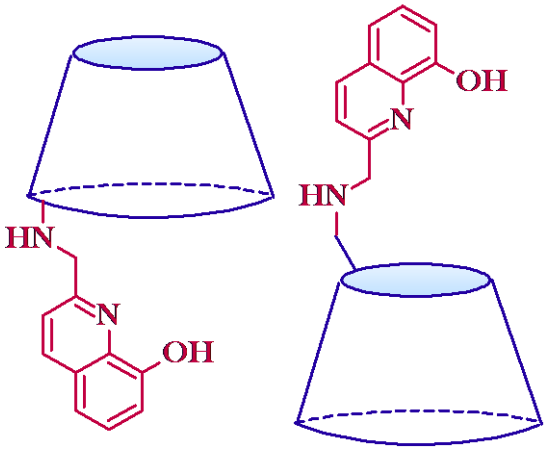

Figure 69. Schematic representation of CD6RHQ and CD3RHQ.

$NaBH(OAc)_3$ was used as reducing agent because gave consistently higher yields and no side products. The imine Shiff bases were not isolated but characterized by positive ion ESI-MS in methanol in order to avoid their hydrolysis. Mass spectra display two peaks at 1289.3 and 1311.3 *m/z* due to the proton $[P+H]^+$ and sodium $[P+ Na]^+$ adducts, respectively.

The products were fully characterized by ^1H NMR, ^{13}C NMR and ESI-MS. Characterization and unequivocal structural assignments were achieved by a combination of techniques including ESI-MS, UV-vis, NMR. The ESI-MS spectrum of CD3RHQ in aqueous solution at pH 6.4 is essentially constituted by peaks due to singly charged (at *m/z* 1291.3 and 1313.4 attributable to $[CD3RHQ+H]^+$ and $[CD3RHQ+Na]^+$ ions) and doubly charged ions (at *m/z* values between 657.1 and 668.2 as $[CD3RHQ+M]^{2+}$ with M = different combinations of H, Na ions).

No signal due to both unreacted starting materials are present in the spectrum. However, the ligands CD3RHQ and CD6RHQ have the same molecular mass as and then their MS spectra are exactly coincident.

NMR spectra of CD6RHQ confirm the identity of the compound (Figure 70).

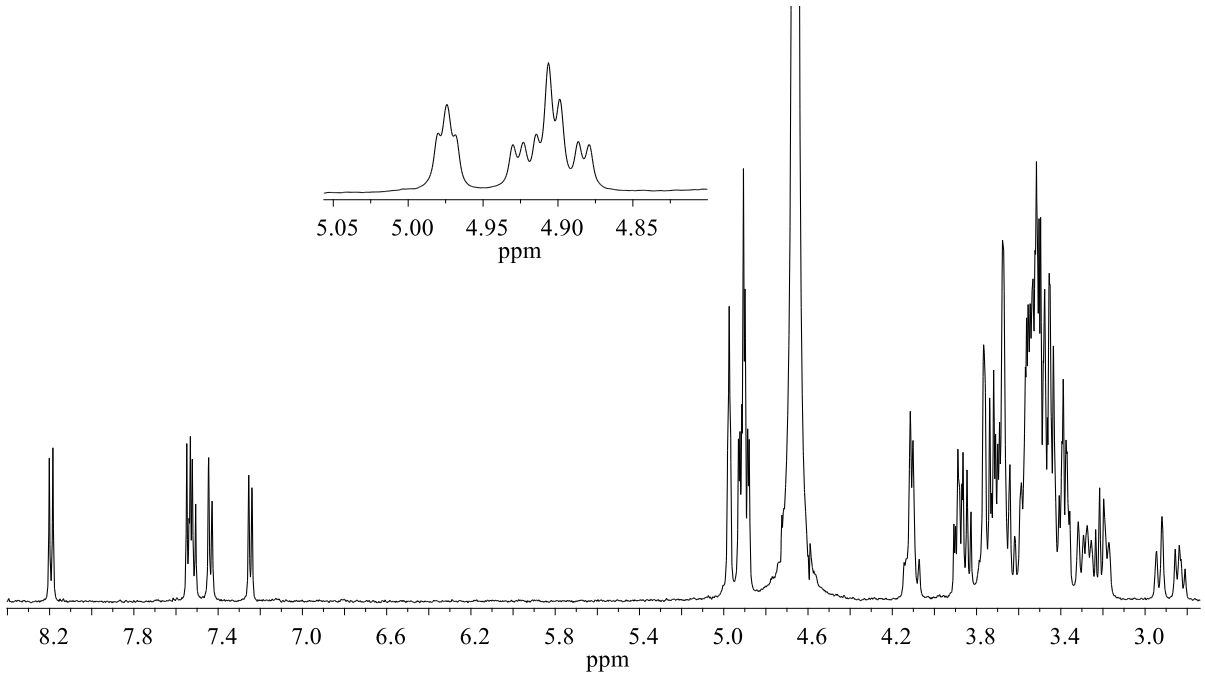

Figure 70. ^{1}H NMR spectrum of CD6RHQ in D_2O at 500 MHz.

The signals of the conjugate in the ^{1}H NMR spectrum were assigned by various 2D NMR experiments (COSY, TOCSY, HSQCAD, HMBC, ROESY). The signals due to the cyclodextrin and quinoline protons are evident. In particular, H-4 of quinoline moiety resonates at lower fields and H-7 at higher fields compared to the other aromatic protons and the benzylic protons resonate at 4.09 ppm. The Hs-1 of the CyD moiety are spread out into four groups as a consequence of the conjugation. Some protons of A ring are significantly shifted because of the functionalization as well revealed by TOCSY (Figure 71). In particular, the diastereotopic H-6A and H-6'A are shifted upfield at 2.83 and 2.93 ppm. H-5A and H-4A resonate at 4.09 and 3.20 ppm, respectively. In this system, the spreading of these protons suggests the inclusion of the aromatic moiety in the CyD cavity.

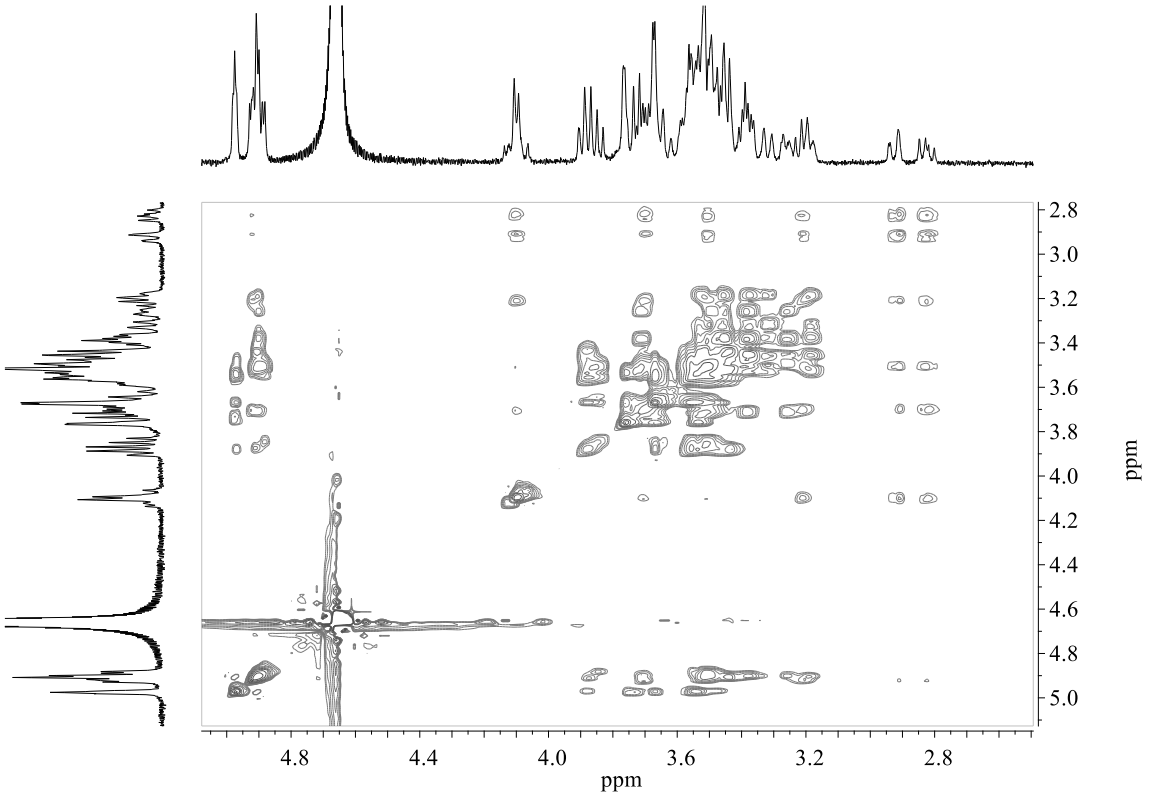

Figure 71. TOCSY spectrum of CD6RHQ in D_2O at 500 MHz.

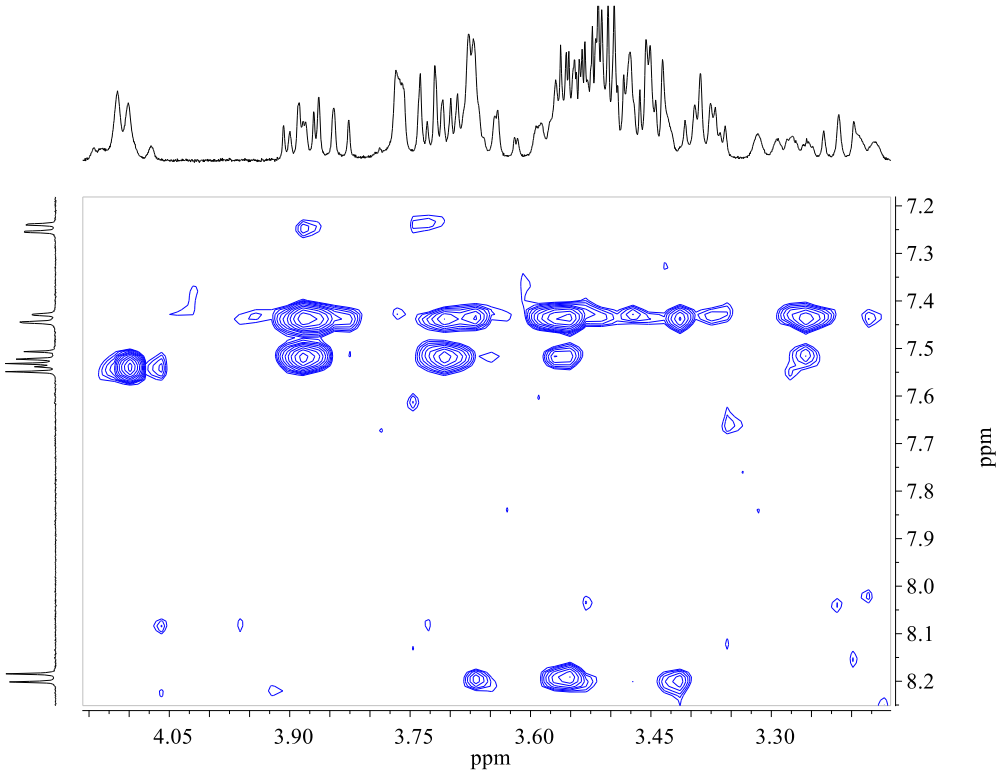

Figure 72. ROESY spectrum of CD6RHQ in D_2O at 500 MHz.

ROESY spectrum (Figure 72) is also consistent with the inclusion. It shows that there are correlation peaks between aromatic protons and inner protons of CyD, indicating that aromatic moiety is included in CyD cavity. In particular, H-3 of quinoline moiety shows two cross peaks corresponding to correlations with benzylic CH_2 and H-6A due to the proximity as it is nearer to the functionalization site than the other quinoline protons. Furthermore H-3 does not correlate with any inner CyD proton suggesting that is outside the cavity as expected taking into account the structural features of the conjugate. Aromatic H-7 and H-4 protons display only few NOE correlations with CyD protons compared to with H-5 and H-6. These results suggest a partial penetration of the phenolic ring into the cavity, although OH group remains outside and easily available for metal binding.

^{1}H NMR spectra of CD3RHQ were carried out in D_2O and CD_3OD at 500 MHz. It is worth noting that all peaks are broadened when the spectrum is recorded in D_2O. The result could indicate that the proton movements are restricted probably because the polar nature of water molecules promotes the intramolecular and intermolecular hydrophobic interactions leading to aggregate formation. This effect is lost in CD_3OD. NMR spectra recorded in methanol enable to confirm the identity of the compound (Figure 73). Assignments were achieved by 2D experiments including COSY, TOCSY, ROESY, HSQC and HMBC.

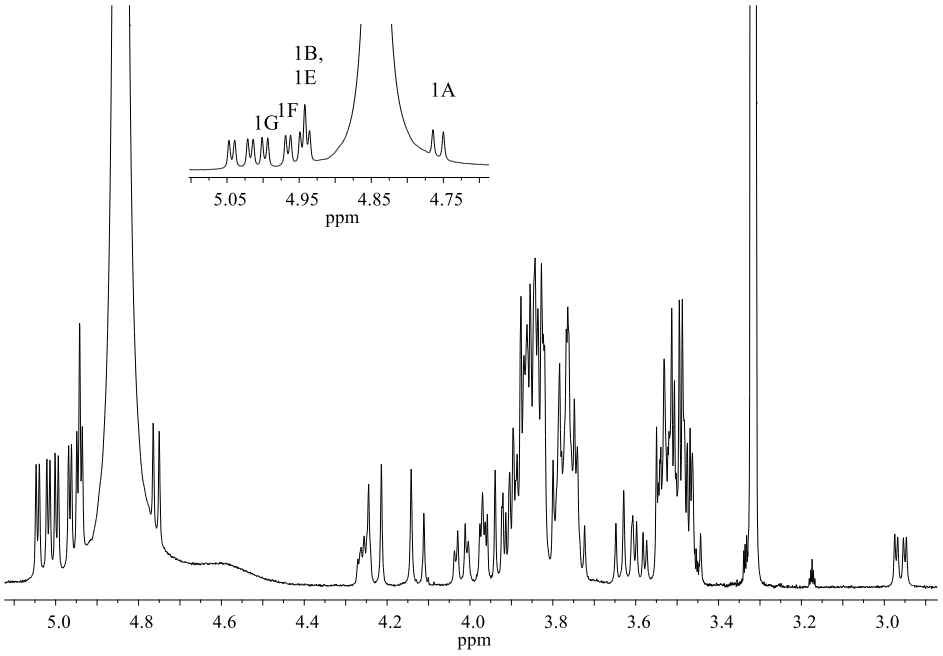

Figure 73. ^{1}H NMR spectrum (aliphatic region) of CD3RHQ in CD_3OD at 500 MHz.

The ^{1}H NMR spectrum of CD3RHQ shows signals due to the quinoline moiety in the aromatic region (δ = 7.0-8.3 ppm). The peaks attributable to CyD moiety resonate in the aliphatic region between 2.9 and 5.0 ppm. In the H-1 region 6 groups of signals appear because of the asymmetry introduced by the conjugation. H-1A proton is easily assigned (4.76 ppm) by HMBC, observing the presence of cross peaks between the diastereotopic benzylic protons at 4.24 and 4.13 ppm and C-3A at 59.0 ppm (Figure 74).

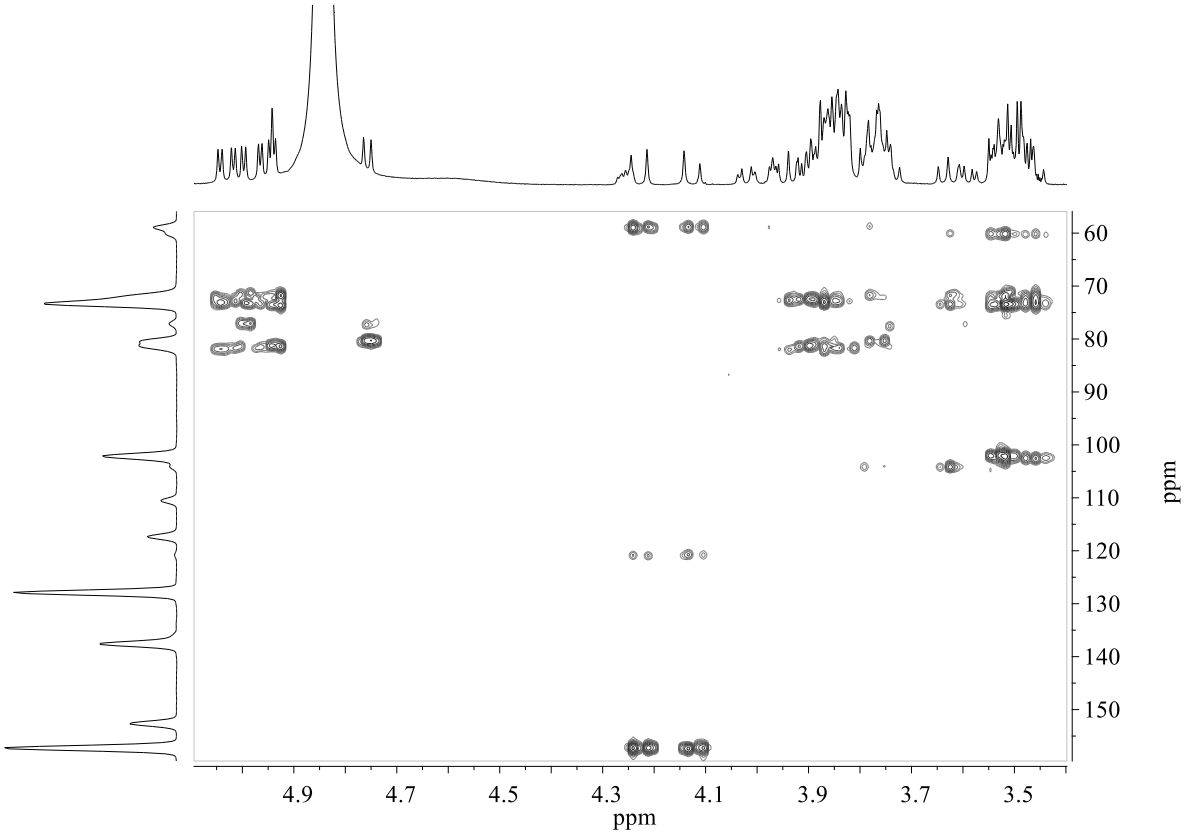

Figure 74. HMBC (aliphatic region) of CD3RHQ in CD_3OD at 500 MHz.

ROESY spectra also allow to identify the H-1G and H-1B protons, in fact they show a cross peak between H-1A and H-4B, indicating the two glucose units adjoin. Another cross peak between H-4A and H-1G is evident, identifying the G ring spin system. NMR spectra exhibit an appreciable downfield shift of the resonances due to the H-4A and H-5A at 4.25 and 3.97 ppm. In particular, the signals due to the functionalized A ring are strongly influenced as a consequence of the 3-functionalisation. Besides H-4A and H-5A, it is possible to identify all protons of A ring through COSY (Figure 75) and TOCSY experiments. H-2A resonates at

3.78 ppm, thereof it is considerably shifted downfield as well. H-3A appears as doublet doublets with vicinal coupling constants $J_{3A,2}$ = 10.5 Hz, $J_{3A,4}$ = 3.5 Hz and, on the contrary, is strongly shifted upfield at 2.96 ppm upon the functionalization. Finally, the diastereotopic H-6A and H-6'A are shifted upfield at 3.73 and 3.59 ppm.

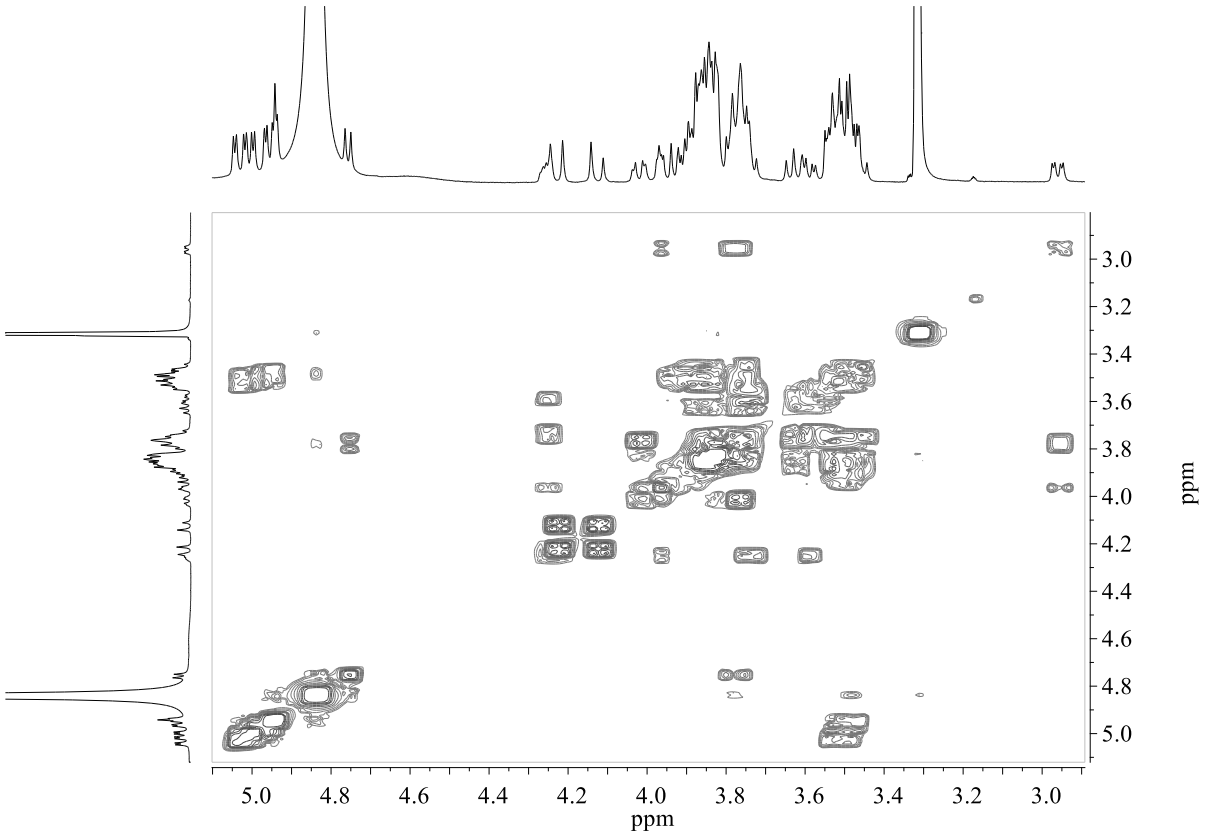

Figure 75. COSY spectrum of CD3RHQ in CD_3OD at 500 MHz.

The B ring is also significantly influenced by the ring effect of the quinoline moiety, the 4B and 6B protons appear downfield at 3.63 and 4.02 ppm, respectively.

The vicinal coupling constant values between H-1A and H-2A ($J_{1A,2A}$ = 7.0 Hz) and between H-2A and H-3A ($J_{2A,3A}$ = 10.5 Hz) indicates that 1A, 2A, 3A protons are axial because of ^3J depend on the dihedral angle defined by the intervening bonds according to Karplus relation.[188] Furthermore, the coupling constant value for H-3A with H-4A ($J_{3A,4A}$ = 3.5 Hz) indicates an equatorial orientation of the H-4A proton. These data, compared to the calculated J for β-glucose rings, suggest that the altrose residue is in $^1C_4 \leftrightarrows {}^0S_2 \leftrightarrows {}^4C_1$ conformational equilibrium shifted towards the $^1C_4$ conformation, as typically described for

this class of compounds.[189] As a consequence of the synthetic route followed to functionalize CyDs on the lower rim, the configuration inversions of C-2 and C-3 occur and an altrose unit replaces a glucose unit in the CyD molecule.

^{13}C NMR spectrum shows that C-1A resonates at higher chemical shift than those of the other Cs-1. All carbons of the A ring differ from the carbons of the other rings and can be easily identified. In particular, C-3A appears at 59 ppm, considerably shifted upfield in respect with other Cs-3. This behavior could be easily explained by the direct involvement in the functionalization of CyD. Finally the benzylic carbon resonates at 51.4 ppm and quinoline carbons are in the aromatic region δ = 157.5-112.6 ppm.

Another monofunctionalized CyD *via* an amine bond (CD6RHQBn) was obtained. In this compound the phenolic group is protected by a benzyl group. CD6RHQBn was designed in order to compare this system to CD6RHQ and to understand the role of the phenolic group in the activity of this compound. CD6RHQBn was synthetized in a similar way to the other two derivatives. The starting material 2-carboxaldehyde-8-benzyloxyquinoline was synthetized by a route of two steps as reported elsewhere.[190,191] The aldehyde was obtained by oxidation of 8-benzyloxy-2-methylquinoline (prepared by O-alkylation of commercially available 8-hydroxyquinaldine) using selenium dioxide (Figure 76).

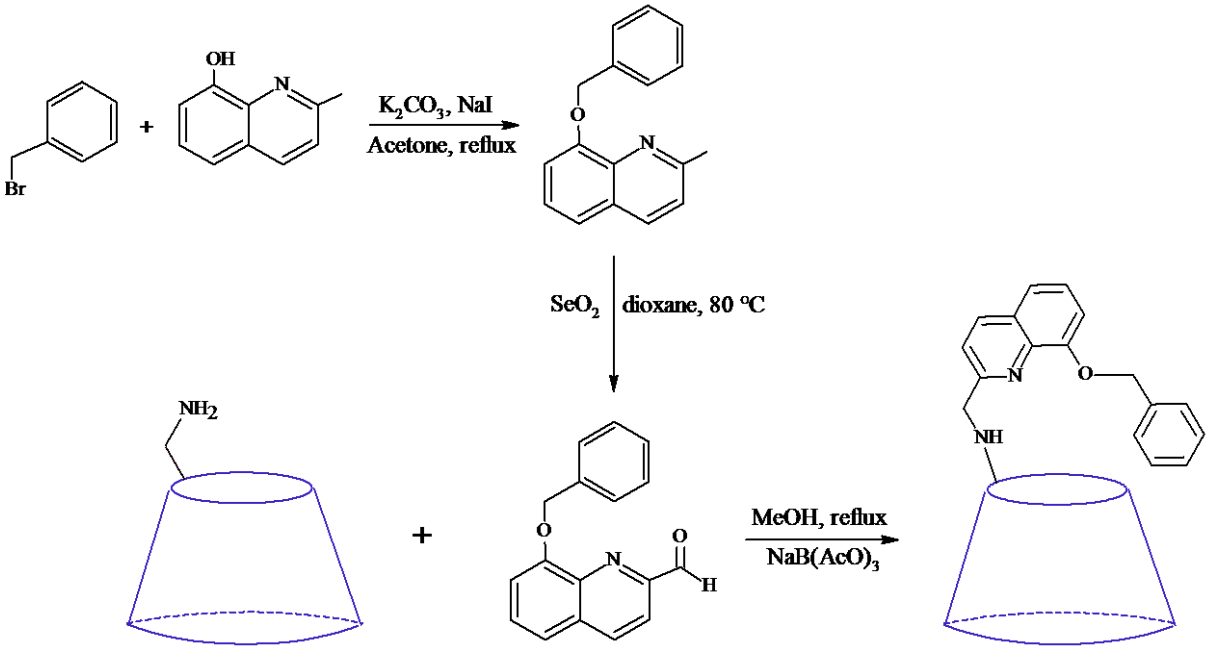

Figure 76. Synthesis of CD6RHQBn.

The product CD6RHQBn and all the intermediate compounds were fully characterized by ^{1}H NMR, ^{13}C NMR, COSY, TOCSY, HSQCAD and HRMS.

NMR spectra were recorded in two different solvents CD_3OD and D_2O because of the compound has a good solubility in both solvents (Figure 77).

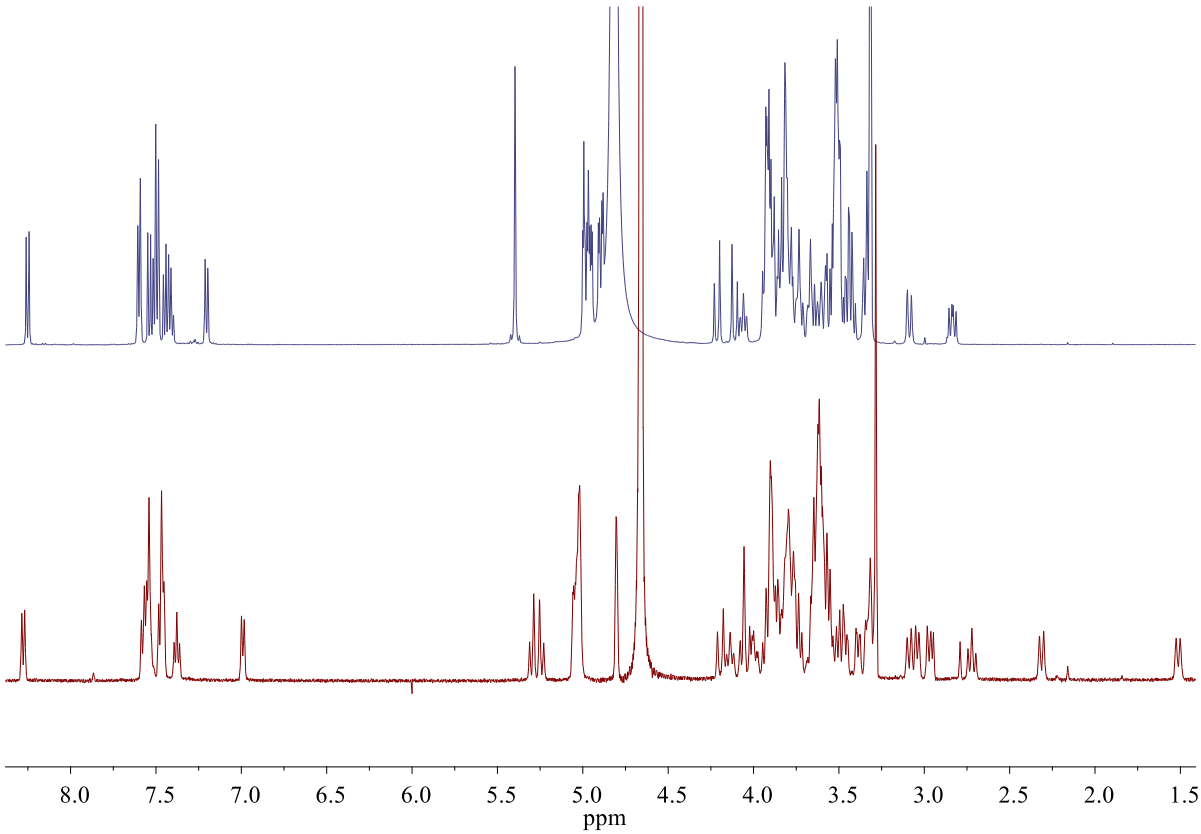

Figure 77. ^{1}H NMR spectrum of CD6RHQBn at 500 MHz in CD_3OD (blue) and D_2O (red).

The signals due to the cyclodextrin protons, the signals of the quinoline moiety and benzylic group are evident. In particular, H-4 of quinoline moiety resonates at lower fields and H-7 at higher fields compared to the other aromatic protons as typically observed in similar compounds. The protons in α to the aminic group are diastereotopic and resonate at 4.21 and 4.10 ppm as a doublet with a coupling constant of 15.6 Hz in CD_3OD. The benzylic protons resonate at 5.40 ppm as a singlet in CD_3OD whereas these protons appear diastereotopic in D_2O and resonate at about 5.3 ppm. In both solvents, some diastereotopic H-6 protons are shifted upfield because of the conjugation with quinoline moiety. It is also noteworthy that the

spreading of H-6 is more evident in deuterium oxide where H-6X protons resonate at 1.51 and 2.31 ppm. Some Hs-5 protons of CyD are also shifted upfield. The different proton resonances in D_2O can be attributable to the self-inclusion of the aromatic moiety in CyD cavity. The self-inclusion is also suggested by CD spectra in water. CD6RHQBn possesses an intense positive CD signal at 242 nm and the intensity of this band decreased upon the addition of increasing amounts of ADM, indicating the displacement of the aromatic moiety from the CyD cavity due to the inclusion of ADM.

However, ^{13}C NMR spectrum of the compound is not significantly different in CD_3OD (Figure 78) and D_2O.

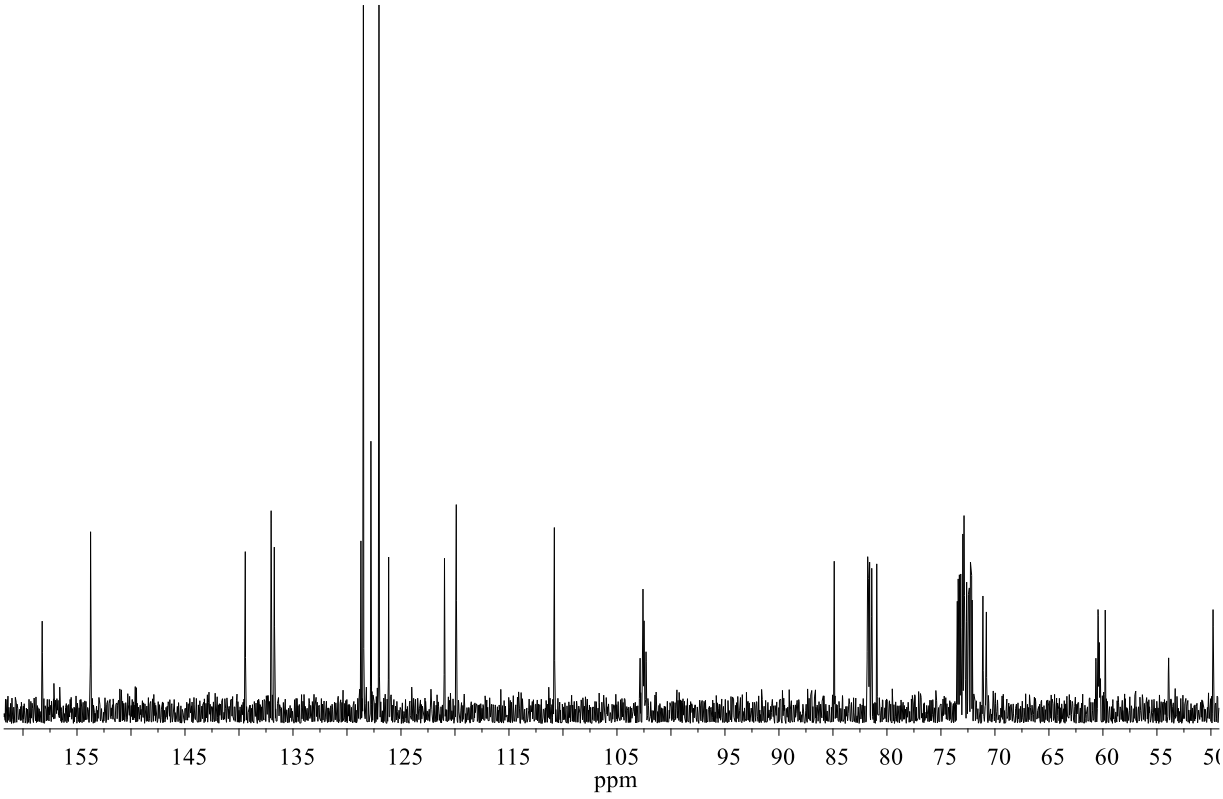

Figure 78. ^{13}C NMR spectrum of CD6RHQBn in CD_3OD at 125 MHz.

^{13}C NMR spectrum shows that Cs-1 resonate at about 102 ppm. All carbons can be easily assigned by HSQCAD (Figure 79). In particular, C-4A appears at 85 ppm, considerably shifted downfield compared to the other Cs-4, as typically observed for CyD derivatives. Benzylic carbons resonate at 70.7 ppm and 53.8 ppm. Finally, quinoline carbons are in the aromatic region δ = 158.2-110.8 ppm together with benzylic protons.

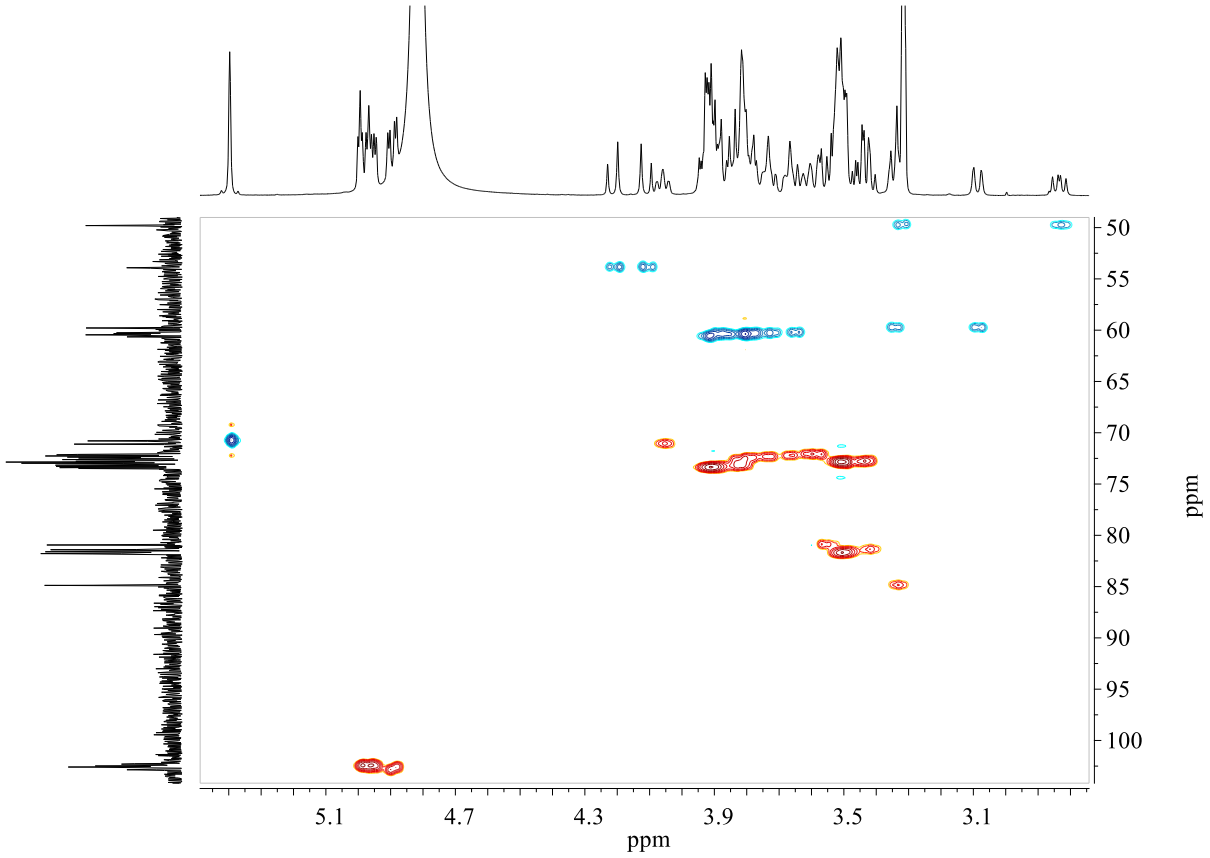

Figure 79. HSQCAD spectrum of CD6RHQBn in CD_3OD at 500 MHz.

Difuctionalized β-CyDs via an amide bond

ABCD6HQ (Figure 80) was synthesized starting from 6^A,6^B-diamino-6^A,6^B-dideoxy-β-cyclodextrin obtained previously using the regioselective procedure described by Di Blasio *et al.*[164]

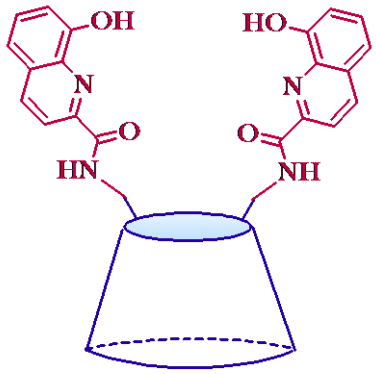

Figure 80. Schematic representation of ABCD6HQ.

The coupling of the former with 2.5 equivalents of 8-hydroxyquinoline-2-carboxylic acid *via* the DCC/HOBt method, allowed to afford the desired compound. Identification of CyD derivative was carried out by ESI-MS and NMR spectroscopy after purification through dialysis and ion-exchange chromatography. ESI-MS experiments provided evidence that the compound was difunctionalized. The spectrum displays peaks due to singly charged (at *m/z* 1475.2, 1497.2 and 1513.3 attributable to $[ABCD6HQ+H]^+$, $[ABCD6HQ+Na]^+$ and $[ABCD6HQ+K]^+$ ions) and doubly charged ions with M = different combinations of H, Na ions at *m/z* = 738.1, 749.1, 757.1, 768.1 $[ABCD6HQ+2M]^{2+}$ (Figure 81).

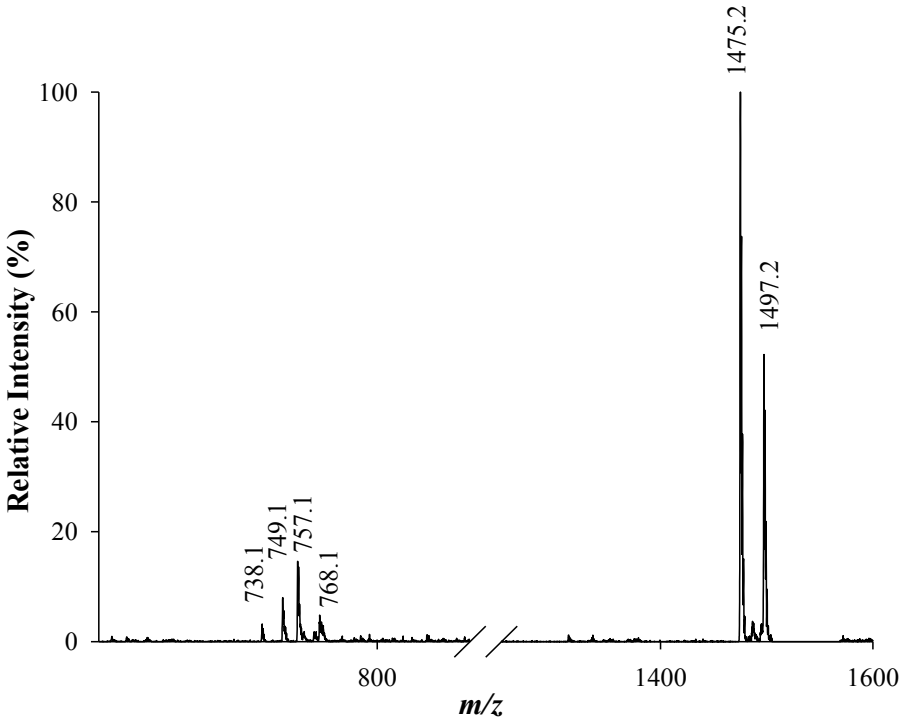

Figure 81. ESI-MS spectrum (positive ion mode) of ABCD6HQ in MeOH.

NMR experiments, recorded in CD_3OD, confirmed the identity of the AB regioisomer and full assignment was obtained using a combination of 2D experiments (COSY, TOCSY, ROESY, HSQC, HMBC). The NMR environments of the seven glucose units are not equivalent as disubstituted cyclodextrins lack the C7 symmetry of free or symmetrically substituted CyDs and this unsymmetrical CyD cavity shape leads to the well-resolved anomeric proton signals at 5.14-4.73 ppm (Figure 82).

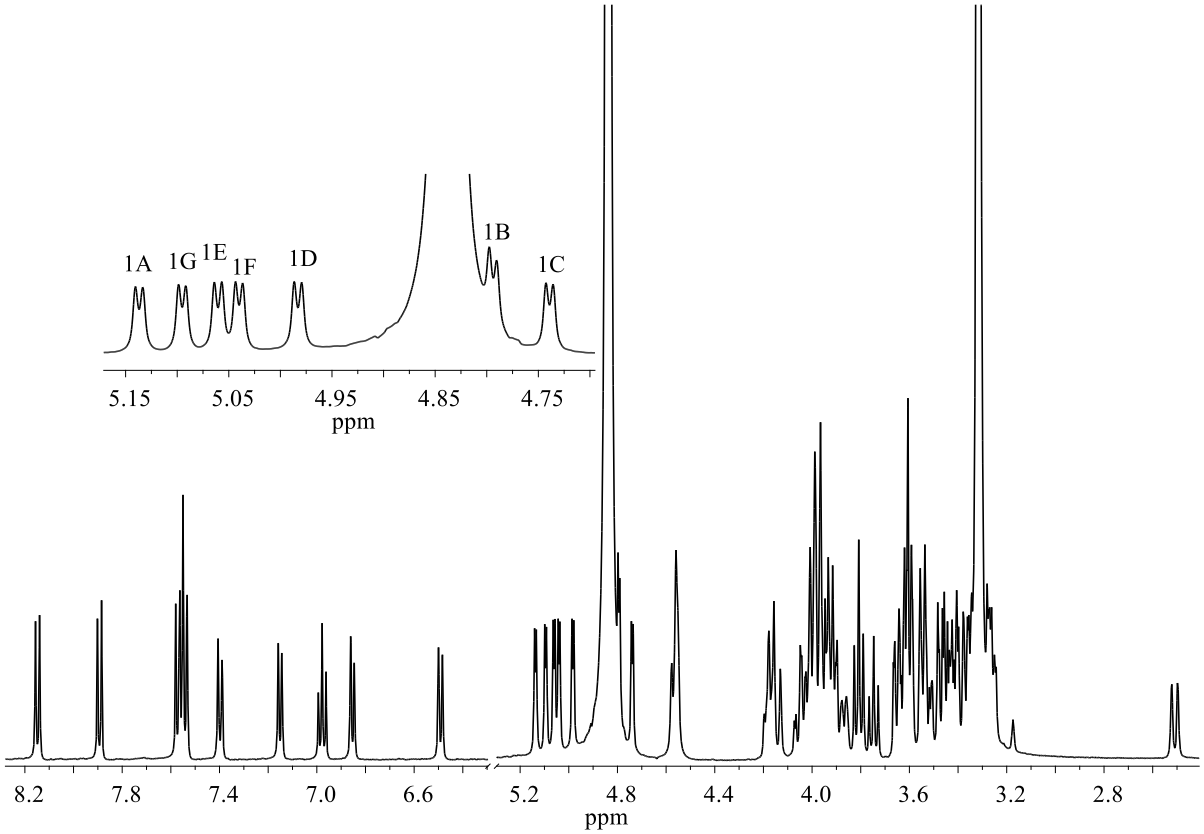

Figure 82. ^{1}H NMR spectrum of ABCD6HQ at 500 MHz in CD_3OD.

^{13}C-^{1}H correlation spectra can be used in order to assign the proton resonances, e.g. for the A and B glucose residues which bear the quinoline residue at C-6 position as a pendant. For this compound two cross-correlation peaks in HMBC between H-6A (4.56 ppm) and the carbonylic C=O (165.6), H-6'A (3.36 ppm) and the same carbon and finally H-6'B (3.33 ppm) and the carbonylic C=O (164.1) allowed to unequivocally identify the spin system belonging

to the B and A rings and thereof the unambiguous complete assignment of the glucopyranosidic resonances.

The sequence of the glucose residues was determined by a ROESY spectrum (Figure 83). The distance between the H-1 proton of a glucose residue and H-4 of the adjacent glucose residue is short enough to give a sizable NOE, which can be observed by ROESY.

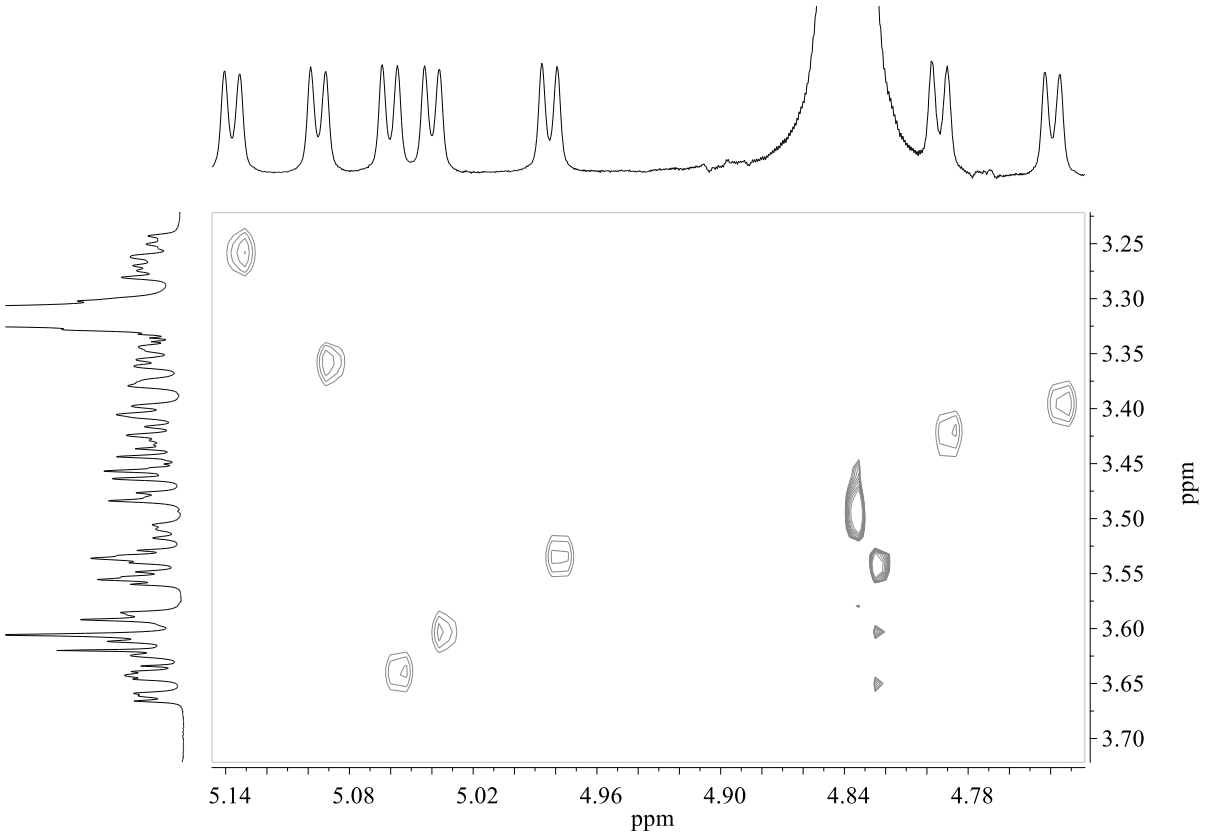

Figure 83. ROESY spectrum of ABCD6HQ at 500 MHz in CD_3OD.

Finally, the protons are completely assigned using COSY and TOCSY (Figure 84). NMR spectra show that some protons are susceptible to anisotropic shielding or deshielding by the aromatic moiety, and thus, upfield and downfield shifts occur. In particular H-6A is considerably shifted downfield at 4.56 ppm, on the contrary, H-6'C is strongly shifted at 2.51 ppm.

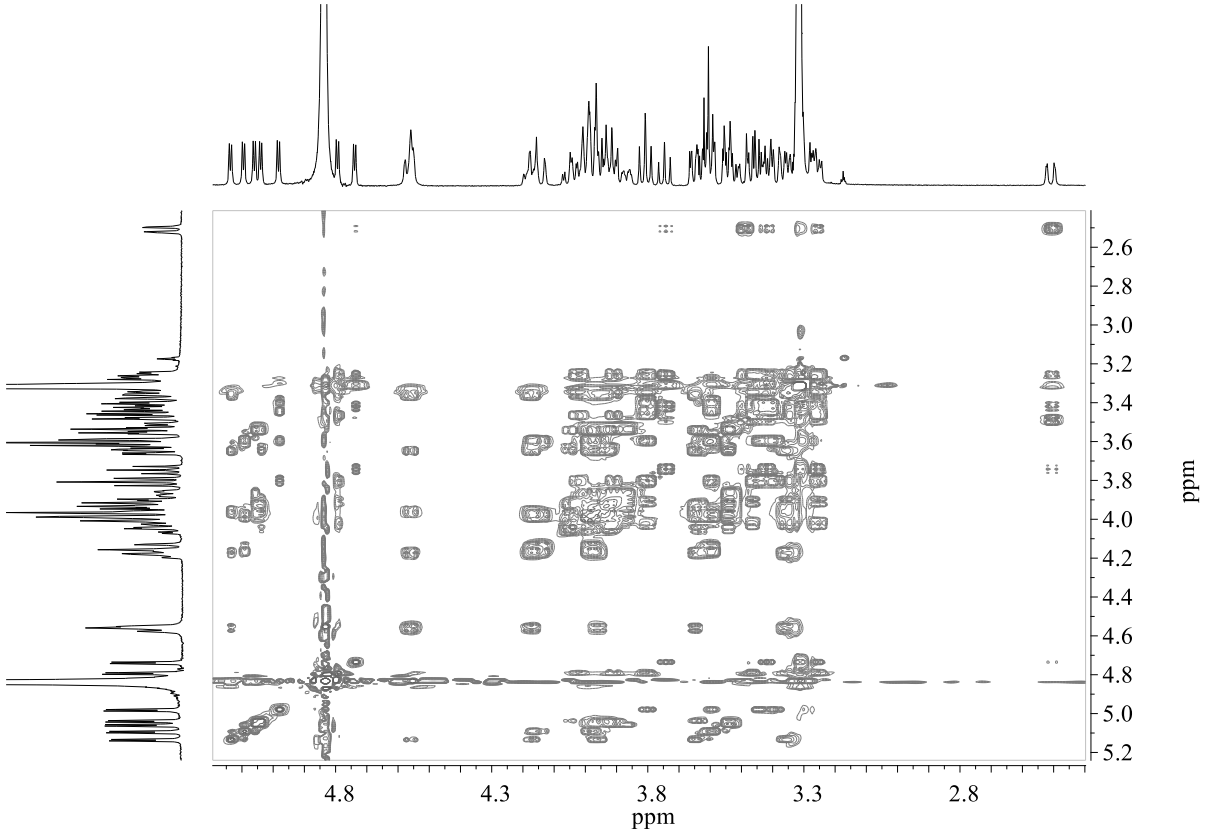

Figure 84. TOCSY spectrum (aliphatic region) of ABCD6HQ at 500 MHz in CD_3OD.

In addition to the signals of the cyclodextrin, the signals due to quinoline moieties are evident in the aromatic region δ = 6.40-8.20 ppm. The asymmetry of the compound also influences quinoline protons resulting in not equivalent protons and therefore H-4 and H-4' protons can be identified at 8.17 and 7.89 ppm. The other aromatic protons show a similar behavior, as well. TOCSY and HMBC allow to identify the aromatic protons belonging to the two different spin systems (Figure 85).

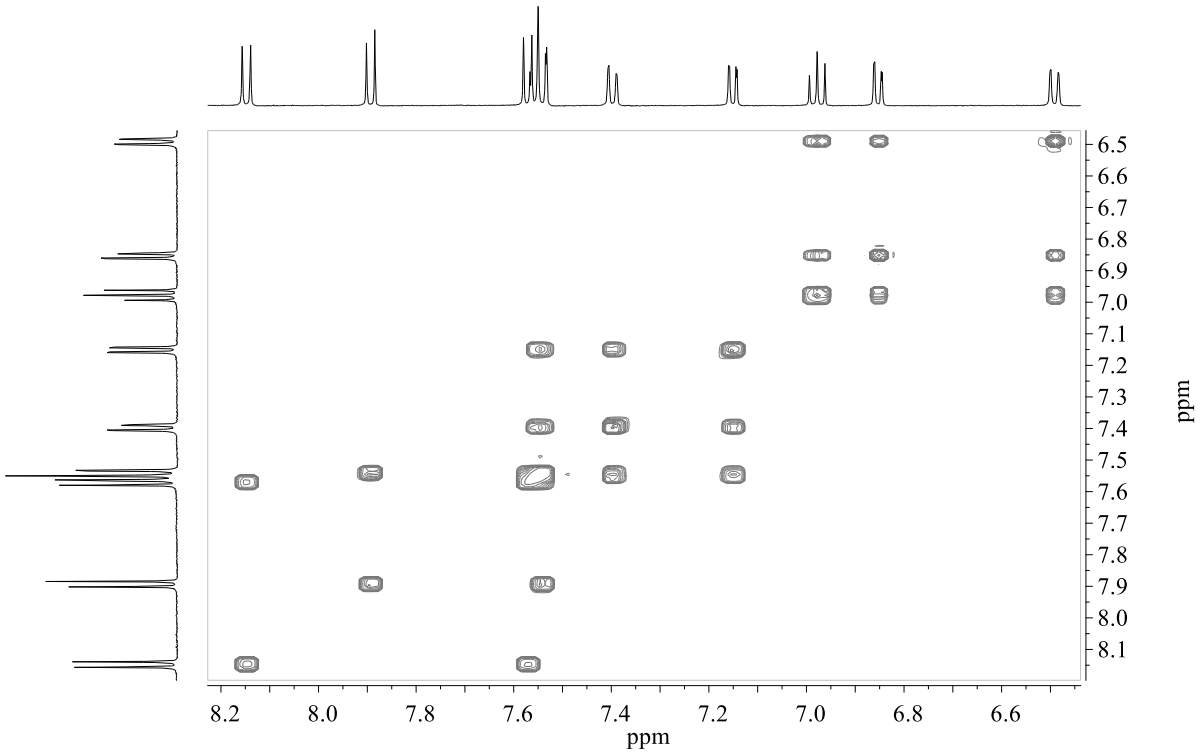

Figure 85. TOCSY spectrum (aromatic region) of ABCD6HQ at 500 MHz in CD_3OD.

^{13}C NMR spectrum was assigned using HSQCAD (Figure 86) and HMBC experiments. C-6 carbons were easily identified because of in the former experiment primary carbons were evidenced (blue cross peaks). As observed in the spectra, C-1B and C-1A show their resonances at 101.5 and 102.9 ppm. C-4B and C-4A appear shifted downfield at 85.7 and 85.1 suggesting that the 6-functionalization slightly influences the conformation of the functionalized glucose rings. C-6B and C-6A are strongly shifted at 40.4 and 41.2 ppm in comparison with the other Cs-6 (δ = 60.4-58.8 ppm).

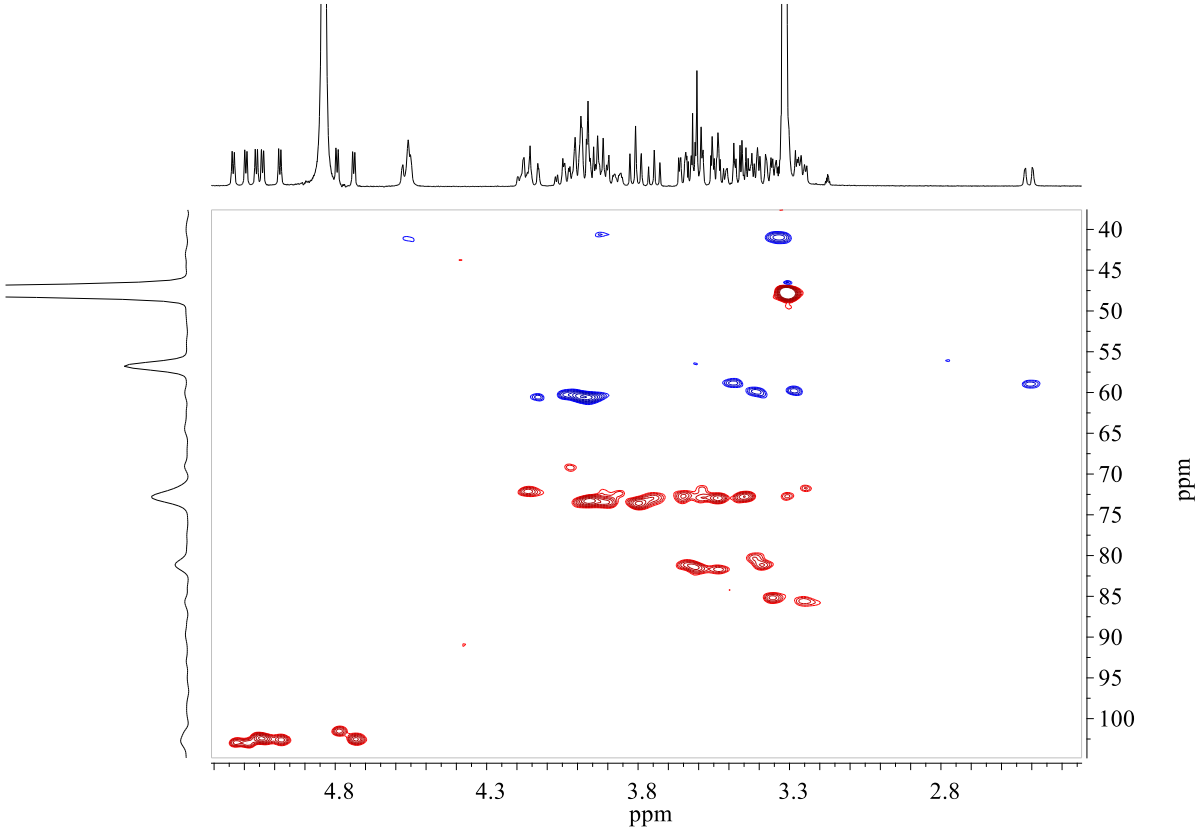

Figure 86. HSQCAD spectrum (aliphatic region) of ABCD6HQ in CD_3OD at 500 MHz.

ABCD6HQ show an interesting CD spectrum. CyD, which possesses a chiral cavity, provides a chiral microenvironment for the conjugated achiral chromophore (as it is closely attached to the CyD rim) and elicited an ICD signal in the corresponding transition band of quinoline moieties. According to the empirical rules that interpret the ICD observed for a chromophore inside or outside of the CyD cavity proposed by Kajtar, Harata and Kodaka,[192-194] it is possible to deduce that the aromatic rings are located near the CyD cavity. The CD spectrum shows a negative band centered at 209.5 with a shoulder band and a strong induced bisignate Cotton effects with a positive maximum at 254.5 nm and a negative maximum at 269.0 nm. This effect is due to the exciton coupling of the quinoline moieties in a chiral microenviroment. The intramolecular nature of this effect could be easily suggested by observation that the spectrum is not influenced by the concentration (Figure 87).

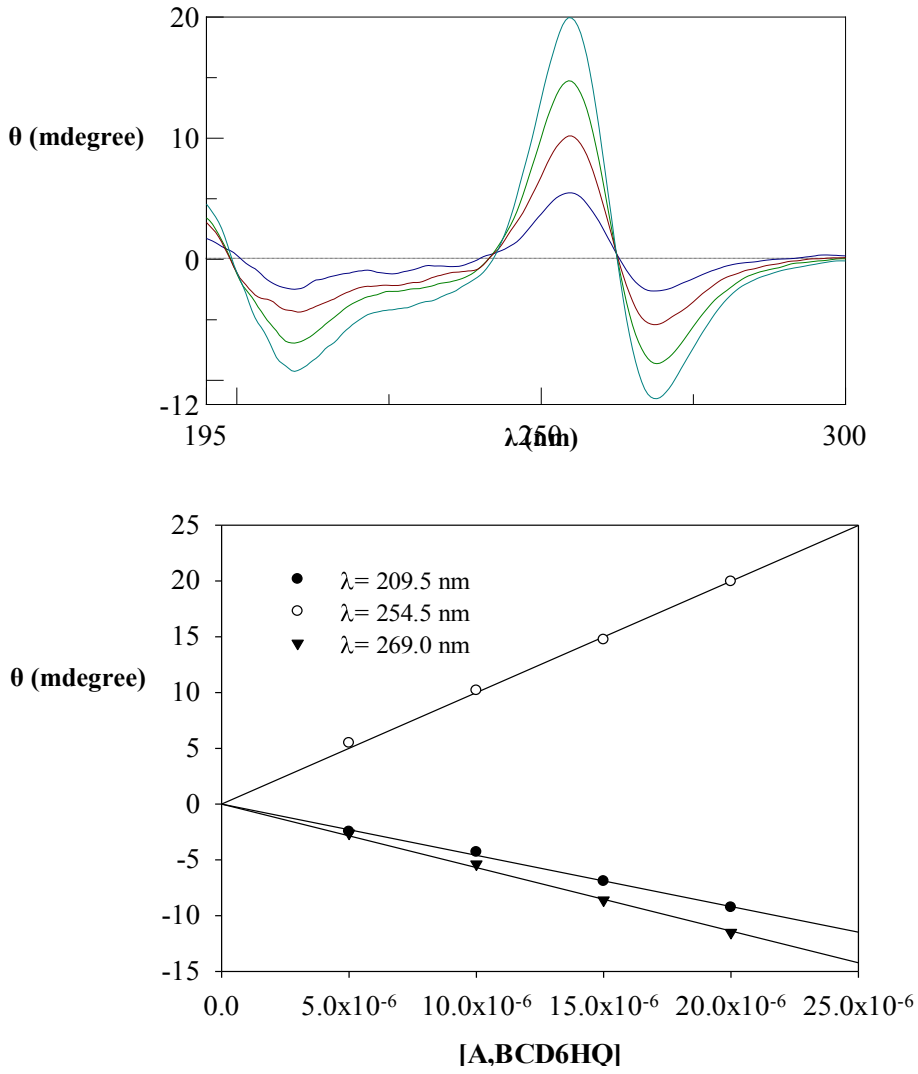

Figure 87. CD spectra of ABCD6HQ are not affected by its concentration in keeping with the intramolecular nature of this interaction.

The titration of ABCD6HQ with ADM led to a reduction of the Cotton effect (Figure 88). However, the Cotton effect remained suggesting only a slight modification of the orientation of quinoline moieties.

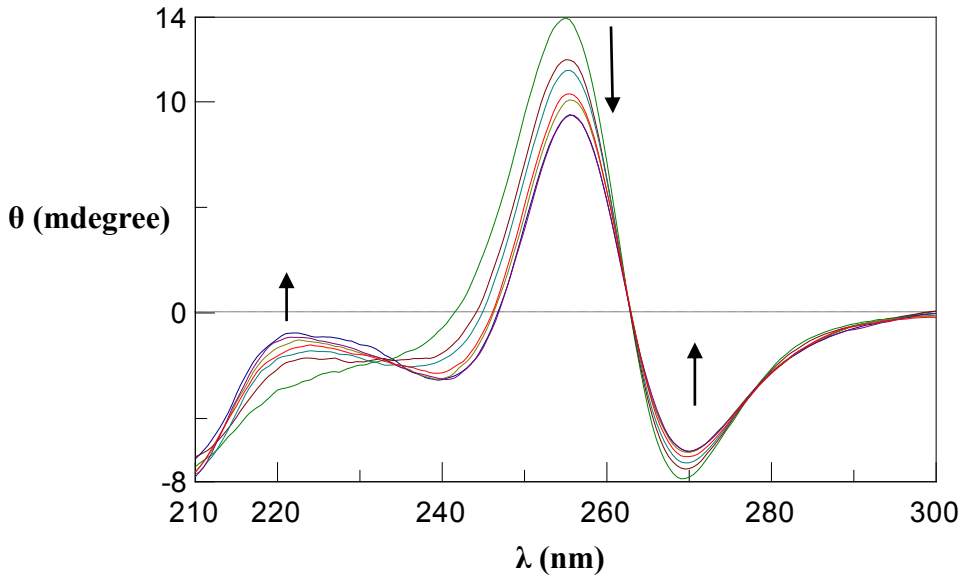

Figure 88. CD spectra of ABCD6HQ (1.5×10^{-5} M) in the presence of increasing concentrations of ADM (1.5×10^{-5} M to 7.5×10^{-4} M). Ratio ADM/ABCD6HQ 1, 2, 4, 10, 20, 50.

Finally, the CD spectrum of ABCD6HQ is influenced by pH as well as its UV spectrum owing to the deprotonation of phenolic groups of the quinoline moieties (Figure 89). The cotton effect decreases its intensity with increasing of pH and a shift of the bands at longer wavelengths is observed. At pH>12 an inversion of the cotton effect occurs. In particular, a band with a negative maximum at 264 nm and a band with a positive maximum at 277 nm appear.

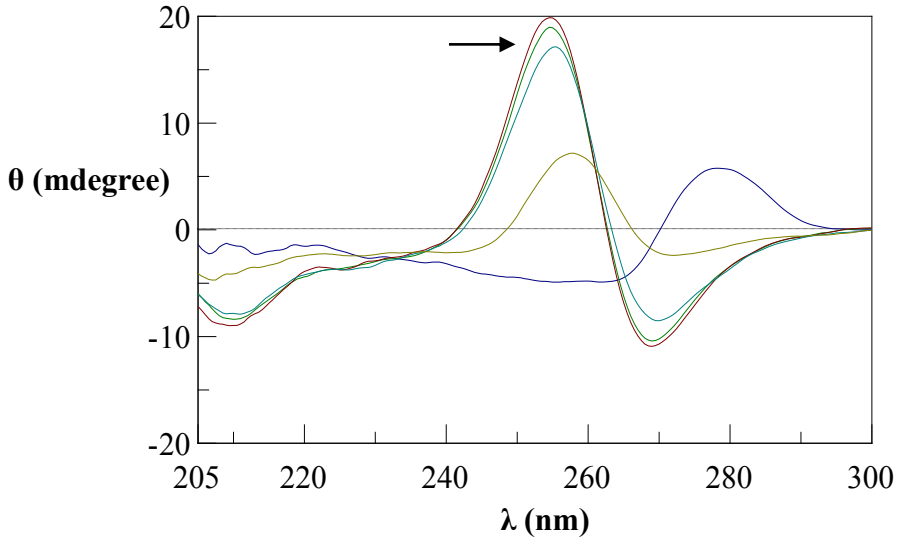

Figure 89. CD spectra of ABCD6HQ (2×10^{-5} M) at different pH (3.0, 7.0, 9.0, 10.0, 12.0).

4.4.2 Metal complexes

Cu^{2+} and Zn^{2+} complexes of CyD conjugates were characterized by several techniques such as ESI-MS spectrometry, UV-vis, NMR and CD spectroscopy. For clarity, the metal complexes of CyD derivatives are divided in three parts on the basis of type and number of donor atoms in order to better explain and compare their binding capacity.

Monofunctionalized CyDs via an amide bond

Conditional stability constants (Table 12) of Cu^{2+} and Zn^{2+} complexes of CD6HQ and CDNHQ were determined in buffered aqueous solution (3-N-morpholinopropanesulfonic acid, MOPS, pH 7.4). MOPS does not bind copper or zinc and then is typically used for metal complex studies.[195] For comparison, conditional stability constants (pH 7.4) of OHQ, 2-aminomethyl-8-hydroxyquinoline (AMQ) and HQ were also calculated using the stability constants reported elsewhere and are given in Table 12.

Table 12. Conditional stability constants (log β) of ligands CD6HQ, CDNHQ and other reference compounds (pH 7.4) at 25 °C.

Ligand	Metal	$\log \beta_1$	$\log \beta_2$
CD6HQ	Cu^{2+}	11.4(1)	16.1(1)
	Zn^{2+}	8.10(7)	13.8(3)
CDNHQ	Cu^{2+}	13.55(2)	17.97(4)
	Zn^{2+}	8.88(7)	14.2(1)
OHQ[a]	Cu^{2+}	9.75	18.4
	Zn^{2+}	6.27	11.3
AMQ[b]	Cu^{2+}	10.45	15.01
HQ[c]	Cu^{2+}	10.62	-
	Zn^{2+}	6.52	-

[a] Reference 200; [b] Reference 207; [c] Reference 202

As recommended by IUPAC, when the complex is too stable ($K > 10^6$) the stability constant value cannot be determined through a direct spectrophotometric titration[196] and competition experiments, which make use of a suitable competing ligand, have to be carried out. Furthermore, this method has been recently utilized to estimate the affinity of OHQ based ligands for Cu^{2+} and Zn^{2+}.[197,198] Conditional formation constants were determined by adding

increasing amounts of EDTA (ethylendiaminetetraacetic acid) to a metal/ligand 1:1 solution at pH 7.4 (MOPS) in order to mimic the medium used during biological experiments including TEAC and SOD-like activity (Figure 90). The stoichiometries of the complex species were initially figured out by the mole ratio method. Plots of the absorbance *vs.* the equivalents of titrant added show two inflections when about half and one equivalent of EDTA is added to the metal-ligand 1:1 solution suggesting the presence of more than one complex species in solution (likely ML and ML_2). A multiwavelength analysis of the spectral data (230-320 nm) was performed with a software (Hyperquad)[168] which refines data from different titrations and allows for the accurate determination of the species and their stability constants. Many species and combinations thereof were given to the program but the data analysis invariably converged to the species and values reported in Table 12.

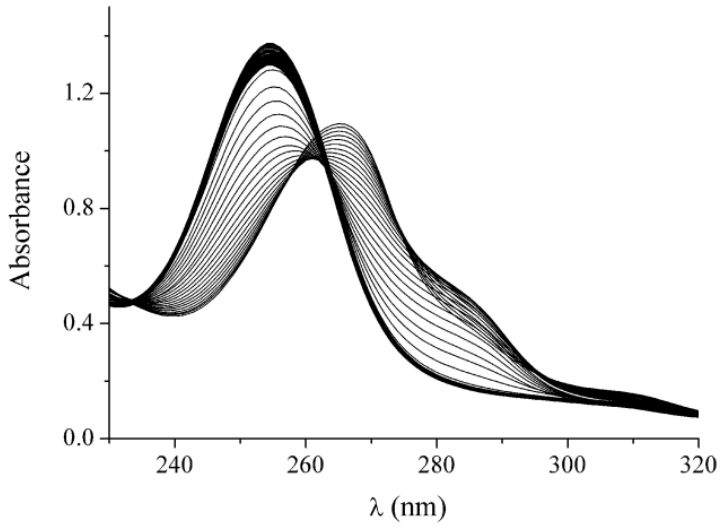

Figure 90. UV-vis competition titration of EDTA (7.9×10^{-4} M) into a Cu^{2+}-CD6HQ 1:1 solution (4.1×10^{-5} M).

OHQ binds Cu^{2+} in a square, planar arrangement[199] with moderate affinity.[200] Similar coordination features have been found in the case of other metal ions. The Cu^{2+} and Zn^{2+} complexes of HQ have been also characterized and the coordination of metal ion by N, phenolate O and COO groups has been reported.[201,202]

From data reported in Table 12, it is interesting to verify that CyD does not decrease the affinity of OHQ moiety for the metal ion. In these ligands in addition to donor atoms of quinoline moiety other potential donor atoms can be identified. Only the coordination ability

of the donor atoms bound to the cavity is generally influenced from the steric hindrance of the CyD.[203,182]

The conditional stability constant of CD6HQ in the CuL species is higher than that of OHQ. This datum can be explained considering the contribution of the amide group in the coordination of the metal ion as observed for analogous systems.[204] In fact, amide derivatives of HQ have been characterized and the coordination of the deprotonated amide nitrogen has been reported.[205,206] The amide N-H deprotonation occurs at relatively low pH promoted by Cu^{2+} ion complexation.[204] In the case of tertiary amides of HQ the coordination of the carboxylic oxygen has been reported.[205]

The Cu^{2+} stability constant of CDNHQ is significantly higher than that of CD6HQ, as expected. In this case the amino group of the ethylendiamine chain can coordinate the metal ion stabilizing the complex CuL in comparison to CD6HQ. Both the ligands form a CuL_2 complex but their conditional stability constants are significantly lower than those calculated for OHQ. A similar behavior has been found in the case of amino derivative of OHQ, where the presence of the exocyclic nitrogen destabilized the ML_2 species.[207,208]

Conditional stability constant of Zn^{2+} complexes of CD6HQ and CDNHQ were determined as well. As expected, the stability constant of Zn^{2+} complexes are lower than that of Cu^{2+}. The conditional constants of ZnL species are higher than that of the OHQ, especially in the case of CDNHQ. Also in this case, the presence of other donor atoms can explain this trend. A similar behavior has been reported in the case of Zn^{2+} complexes of 2-methylamine-OHQ.[208]

A picture of the metal complexes formed in solution has been also obtained by the mass spectrometric data. The ESI-MS experiments were carried out at different pH, from 4.0 to 10.0. In Table 13 the pseudo-molecular ions of the observed Cu^{2+} complex species are reported.

Table 13. ESI-MS characterization of the Cu^{2+} complexes of CD6HQ, CD3HQ, CDOHQ and CDNHQ ($[Cu^{2+}] = 9.0 \times 10^{-5}$ M, $[L] = 3.0 \times 10^{-5}$ M). L is a hydroxyquinolinate derivative.

Ligand	Assignment	Calcd (*m/z*)	Found (*m/z*)
CD6HQ	$[LH+H]^+$	1305.4	1305.3
	$[LH+Na]^+$	1327.4	1327.4
	$[CuL]^+$, $[CuLH_{-1}+H]^+$	1366.3	1366.2
	$[CuLH_{-1}+Na]^+$	1388.3	1388.3
	$[CuL+H]^{2+}$, $[CuLH_{-1}+2H]^{2+}$	683.6	683.6
	$[CuL+Na]^{2+}$, $[CuLH_{-1}+H+Na]^{2+}$	694.7	694.7
CDOHQ	$[LH+H]^+$	1349.4	1349.3
	$[LH+Na]^+$	1371.4	1371.4
	$[CuL]^+$	1410.4	1410.3
	$[CuL+H]^{2+}$	705.7	705.6
CDNHQ	$[LH+H]^+$	1348.5	1348.4
	$[LH+Na]^+$	1370.4	1370.4
	$[CuL]^+$, $[CuLH_{-1}+H]^+$	1409.4	1409.3
	$[CuLH_{-1}+Na]^+$	1431.4	1431.4
	$[Cu_2LH_{-1}-H]^+$	1470.3	1470.1
	$[CuL+Na]^{2+}$	716.2	716.1
	$[CuLH_{-1}+2Na]^{2+}$	727.2	727.1
	$[Cu_2LH_{-1}]^{2+}$	735.6	735.5
CD3HQ	$[LH+H]^+$	1305.4	1305.3
	$[LH+Na]^+$	1327.4	1327.4
	$[CuL]^+$, $[CuLH_{-1}+H]^+$	1366.3	1366.3
	$[CuLH_{-1}+Na]^+$	1388.3	1388.3
	$[CuL+H]^{2+}$, $[CuLH_{-1}+2H]^{2+}$	683.6	683.6
	$[CuL+Na]^{2+}$, $[CuLH_{-1}+H+Na]^{2+}$	694.7	694.7

The formation of complex species was observed at pH > 5. In addition to the peak of the ligand new peaks due to singly charged species $[CuL]^+$ or/and $[CuLH_{-1}+H]^+$, $[CuLH_{-1}+Na]^+$ and doubly charged species (see Table 13) appear for all derivatives. In the ESI-MS spectra, it is not possible to differentiate the CuL^+ from $CuLH_{-1}$ species because they have the same *m/z* value. In the case of CD6HQ and CDNHQ the peak assigned to the species $[CuLH_{-1}+Na]^+$ can be identified. This species is not observed in the case of CDOHQ and this behavior could be due to the presence of the tertiary amide group. For this reason the formation of $CuLH_{-1}$ species cannot be proposed.

A similar behavior was found in the case of Zn^{2+} complexes (see Table 14).

Table 14. ESI-MS characterization of the Zn^{2+} complexes of CD6HQ, CDOHQ and CDNHQ ([L] = 7.0 × 10^{-5} M). L is a hydroxyquinolinate derivative.

Ligand	Assignment	Calcd (*m/z*)	Found (*m/z*)
CD6HQ	$[LH+H]^+$	1305.4	1305.3
	$[LH+Na]^+$	1327.4	1327.5
	$[ZnL]^+$, $[ZnLH_{-1}+H]^+$	1367.3	1367.3
	$[ZnL+H]^{2+}$, $[ZnLH_{-1}+2H]^{2+}$	684.2	684.1
	$[ZnL+Na]^{2+}$, $[ZnLH_{-1}+H+Na]^{2+}$	695.2	695.1
CDOHQ	$[LH+H]^+$	1349.4	1349.3
	$[LH+Na]^+$	1371.4	1371.4
	$[ZnL]^+$	1411.4	1411.3
	$[ZnL+H]^{2+}$	706.2	706.1
CDNHQ	$[LH+H]^+$	1348.5	1348.4
	$[LH+Na]^+$	1370.4	1370.4
	$[ZnL]^+$, $[ZnLH_{-1}+H]^+$	1410.4	1410.2
	$[ZnLH_{-1}+Na]^+$	1432.4	1432.3
	$[Zn_2LH_{-1}-H]^+$	1472.3	1472.2
	$[ZnL+Na]^{2+}$	716.7	716.6
	$[ZnLH_{-1}+2Na]^{2+}$	727.7	727.6
	$[Zn_2LH_{-1}]^{2+}$	736.6	736.5

Copper complexes of CyD conjugates were also investigated by UV-Vis spectroscopy. The absorption spectra of ligands CD6HQ, CDOHQ, CD3HQ, CDNHQ are mainly due to the presence in their structure of OHQ moieties. The absorption bands of CyD derivatives dramatically change upon addition of Cu^{2+} ions. In the case of CDNHQ, the UV band near 255 nm is shifted to lower energy (267 nm), with concomitant appearance of absorption bands at 310 nm and in the visible region at 430 nm, due to a MLCT transition.[209] These findings are characteristic of the OHQ derivatives when the complexation is accompanied by the deprotonation of the hydroxyl group.[210] For comparison with similar systems[201,205] and in keeping with the stability constant values a main species where the metal ion is bound to N of py ring, phenolate, amino group and deprotonated amide nitrogen can be hypothesized.

In the case of CD6HQ, UV-vis spectra similar to that of CDNHQ can be observed in the presence of Cu^{2+} ions and a complex species where the copper is bonded to N of py ring, phenolate, amino group and deprotonated amide nitrogen can be hypothesized in keeping with the stability constant values.

As for CD3HQ, titration of $Cu(NO_3)_2$ into a solution of CD3HQ elicited the hypochromic and batochromic shift of the band at 255 nm and the appearance of the band at 265 nm. A coordination environment similar to that of CD6HQ can be hypothesized in keeping with the similar spectral changes.

Finally, the band at 250 nm decreases in intensity and is red-shifted to 253 nm upon the addition of copper ions into a CDOHQ solution and other two bands near 264 nm and 433 nm appear in the spectrum. In this case the amide is a tertiary amide and a complex species where the Cu^{2+} is complexed by N of py ring, phenolate and O of amide group can be hypothesized as reported for similar compounds.[211]

The UV-vis spectra of these CyD derivatives were carried out at different pH. The spectra were changed in keeping with the formation of the complex species. At pH higher than 8.0, the formation of a precipitate was observed.

Finally, the formation of copper complexes with CyD conjugates was investigated by CD spectroscopy. The titration of CD6HQ with copper sulfate at pH 7.4 dramatically affected its CD spectrum. Up to metal/ligand molar ratios of 1:1, two negative bands near 258 and 280 nm are evident in the spectrum. For higher metal/ligand ratios, the band at 258 nm disappears and the spectrum shows only one broad negative band at 269 nm. Upon addition of increasing amounts of $CuSO_4$, the CD spectrum of CDOHQ changed, giving rise to a decrease in intensity of the bands in a similar way to that caused by ADM (Figure 91). In particular the band at 273 nm becomes negative. These changes suggest that quinoline moiety moves out from the upper rim in order to complex copper.

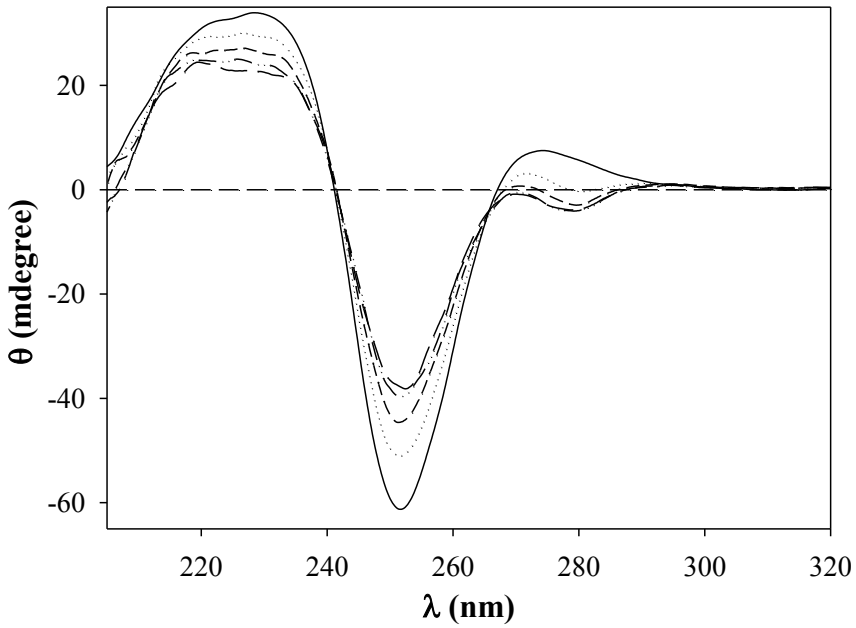

Figure 91. CD spectra of CDOHQ (6.4×10^{-5} M) in the presence of increasing concentrations of Cu^{2+}(3.2×10^{-5} M to 2.6×10^{-4} M).

The addition of ADM to the Cu–CDOHQ system did not modify the CD spectrum. This further suggests that a deep inclusion of the aromatic ring in the cavity cannot occur in the Cu^{2+} complex.

The titration of CD3HQ with $CuSO_4$ at pH 7.0 dramatically affected its CD spectrum. For metal/ligand 0.5 : 1 ratio, the band at 252.5 nm disappears and a broad negative band shows up at 265 nm. Upon increasing addition of amounts of Cu^{2+} sulfate (higher than metal/ligand ratio 1:1), the CD spectrum do not display significantly changes.

This behavior suggests that quinoline moiety changes its orientation in order to complex copper. The addition of ADM to the Cu–CD3HQ system did not modify the CD spectrum.

Difuctionalized β-CyD via an amide bond

A picture of the metal complexes formed in solution has been obtained through the mass spectrometric data. The ESI-MS experiments were carried out at different pH (from 5.0 to 8.0) at both 1:1 and 2:1 metal ion-to-ligand ratios. In Table 15 the pseudo-molecular ions of the observed Cu^{2+} complex species are reported. The formation of copper species was observed at pH > 5. The ESI-MS spectra of Cu^{2+}-systems clearly show the existence of the neutral complex species CuL and this is the main Cu^{2+} species over the explored pH range (pH 5.0-

8.0). ML species appears as singly charged species $[CuL+H]^+$, $[CuL+Na]^+$, $[CuL+K]^+$ and doubly charged species with different ion adducts $[CuL+2H]^{2+}$, $[CuL+H+Na]^{2+}$, $[CuL+H+K]^{2+}$ (see Table 15).

Table 15. ESI-MS characterization of the Cu^{2+} complexes of ABCD6HQ ([L] = $[Cu]^{2+}$ = 6.0×10^{-5} M) at pH 7.0. L is a hydroxyquinolinate derivative (both phenolic group are deprotonated).

Assignment	Calcd (*m/z*)	Found (*m/z*)
$[LH_2+H]^+$	1475.5	1475.4
$[LH_2+Na]^+$	1497.5	1497.5
$[LH_2+K]^+$	1513.4	1513.3
$[CuL+H]^+$	1536.4	1536.4
$[CuL+Na]^+$	1558.4	1558.4
$[CuL+K]^+$	1574.4	1574.4
$[Cu_2L-H]^+$	1597.3	1597.2
$[LH_2+H+Na]^{2+}$	749.2	749.1
$[LH_2+H+K]^{2+}$	757.2	757.2
$[CuL+2H]^{2+}$	768.7	768.5
$[CuL+H+Na]^{2+}$	779.7	779.6
$[CuL+H+K]^{2+}$	787.7	787.6
$[CuL+2Na]^{2+}$	790.7	790.6
$[Cu_2L]^{2+}$	799.1	799.1
$[Cu_2L-H+Na]^{2+}$	810.1	810.1
$[Cu_2L-H+K]^{2+}$	818.1	818.1

The typical isotopic pattern of naturally occurring copper isotopes confirms the attribution of these signals to species of the Cu^{2+}-ABCD6HQ system. MS spectra clearly show the decrease of the proton adduct (*m/z* 1536.4) as well as the increment of the sodium adducts (*m/z 1558.4*) as the pH increases upon the NaOH addition. For comparison with similar systems and taking account of the mass spectrometry data, a main species with the metal ion bound to both N of py ring and phenolate group could be hypothesized (Figure 92, right). This bis-hydroxyquinoline ligand is able to chelate copper in a tetradentate manner exploiting the proximity of the 8-hydroxyquinolines moieties as they are bound to adjacent rings. However, dinuclear copper species were also detected in ESI-MS experiments (Figure 92, left) . $[Cu_2L-H]^+$, $[Cu_2L]^{2+}$, $[Cu_2L-H+Na]^{2+}$, $[Cu_2L-H+K]^{2+}$ display typical isotopic patterns due to the presence of two copper ions. The relative intensity of the these peaks are higher (40 %) at 2:1

metal ion-to-ligand ratio in comparison to the experiments carried out at 1:1 metal ion-to-ligand ratio (<15%) as expected. Furthermore, another important aspect concerns the pH dependence of the dinuclear species formation probably owing to the deprotonation of the amide. It is clearly evident that the deprotonation of amidic NH already occurs in the dinuclear species at pH 7.0 as suggested by $[Cu_2L\text{-}H]^+$, $[Cu_2L\text{-}H+Na]^{2+}$, $[Cu_2L\text{-}H+K]^{2+}$ species.

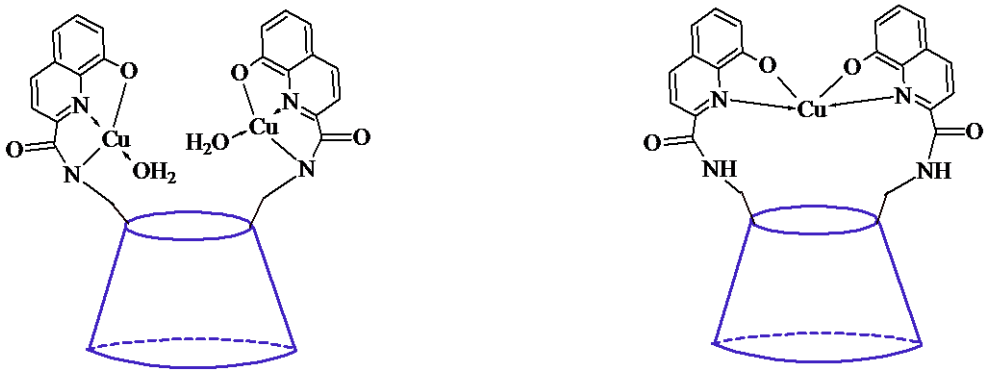

Figure 92. Hypothesized copper complex species of ABCD6HQ.

Zinc complexes of ABCD6HQ were also investigated by mass spectrometry considering the crucial role of zinc in many life-related processes. The ESI-MS experiments were carried out at different pH (from 5.0 to 8.0) at both 1:1 and 2:1 metal ion-to-ligand ratios. The pseudo-molecular ions of the observed Zn^{2+} complex species are shown in Table 16. The formation of zinc complex species was observed at pH > 5. The ZnL species is observed as singly charged proton adduct ion (*m/z* 1537.2), sodium adduct ion (*m/z* 1559.3) and double charged adduct ions (*m/z* 769.1). MS zoom scan spectra allow for the exact assignment of these peaks showing typical isotopic patterns attributable to zinc compared to the simulated isotopic patterns. At 1:1 zinc-to-ligand ratio, peaks due to a possible dinuclear zinc species was not observed whereas it was detected in the presence of an excess amount of metal though the relative intensity of these peaks was low (<5 %). Probably in this case, the deprotonation of NH amide does not significantly occur at pH 7.0 hence this dinuclear species is not favourite. This is also suggested by the absence of $[Zn_2L\text{-}H+Na]^{2+}$, $[Zn_2L\text{-}H+K]^{2+}$ species that, on the contrary, were detected in the case of Cu^{2+}.

Table 16. ESI-MS characterization of the Zn^{2+} complexes of ABCD6HQ ([L] = $[Zn]^{2+}$ = 6.0×10^{-5} M) at pH 7.0. L is a hydroxyquinolinate derivative (both phenolic groups are deprotonated).

Assignment	Calcd (*m/z*)	Found (*m/z*)
$[LH_2+H]^+$	1475.5	1475.4
$[LH_2+Na]^+$	1497.5	1497.5
$[LH_2+K]^+$	1513.4	1513.3
$[ZnL+H]^+$	1537.4	1537.2
$[ZnL+Na]^+$	1559.4	1559.3
$[Zn_2L-H]^+$ (A)	1599.3	1599.2
$[LH_2+H+Na]^{2+}$	749.2	749.1
$[LH_2+H+K]^{2+}$	757.2	757.1
$[ZnL+2H]^{2+}$	769.2	769.1
$[Zn_2L]^{2+}$ (A)	800.1	799.9

(A) These species were detected at 2:1 metal ion-to-ligand ratio.

The UV-vis spectrum of a solution of ABCD6HQ in MOPS pH 7.4 was characterized by absorption maxima at approximately 253, 307 and 350 nm due to ligand-centered (LC) charge-transfer bands arising from π–π* and n–π* transitions, respectively. Titration of $Cu(NO_3)_2$ into the solution of ABCD6HQ elicited the hypochromic shift of the LC charge transfer bands and hyperchromic shift of ligand-to-metal charge transfer (LMCT) transitions at 265 nm and 422 nm, with corresponding isosbestic points near 260 nm, 345 and 372 nm up to molar ratio of approximatively 0.9:1 Cu^{2+}/L. The isosbestic points are not well defined when the molar ratio were higher than 1:1, suggesting the presence of more complex species (ML and M_2L) in keeping with ESI-MS data. The electronic spectra in Figure 93 were very similar to those reported for other OHQs such as oxine and CQ. However, compared with these OHQs, which preferentially bind 0.5 equiv Cu^{2+} in a bis complex, the intensity of the absorption bands at 265 and 422 nm saturated at 2.0 equiv Cu^{2+}, indicating L could coordinate up to two copper ions. The sharp end point of the titration indicated the Cu^{2+} binding was tight (Kd $\ll$ μM) at the concentrations used and hence that UV-vis spectrophotometry was unsuitable for the determination of Cu^{2+} binding constants.

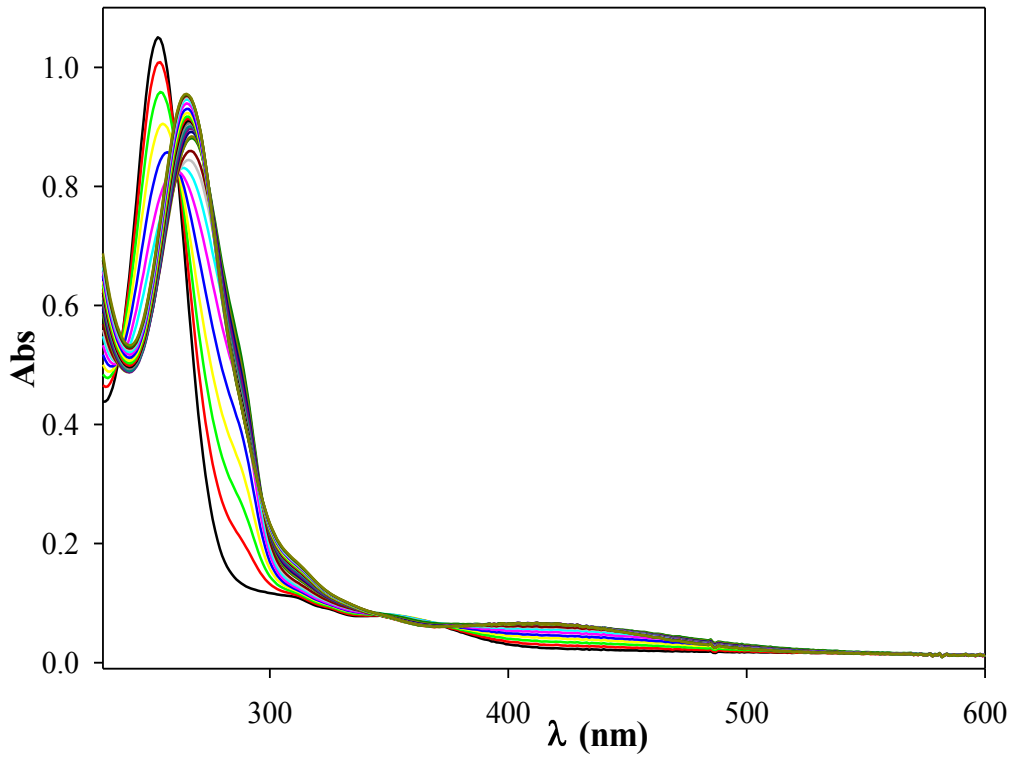

Figure 93. UV-vis absorption spectra of ABCD6HQ, following the titration of 0−2.5 equivalents of Cu^{2+}.

Copper complexes of the conjugate were also investigated by CD (Figure 94). CD spectra showed a similar behavior to that of UV-spectra, further confirming the existence of ML and M_2L species. Upon addition of increasing amounts of $CuSO_4$, the CD spectrum of ABCD6HQ changed, giving rise to a decrease in intensity of the bands at 254.5 and 269 nm. The band at 209.5 cannot be followed because of the absorption of sulphate anion. A new positive larger band centered near 264 nm appears, whereas a negative band at *ca* 282 nm was evident at low M/L ratio. However, the disappearance of the cotton effect suggests a change of the reciprocal quinoline orientation in order to complex copper.

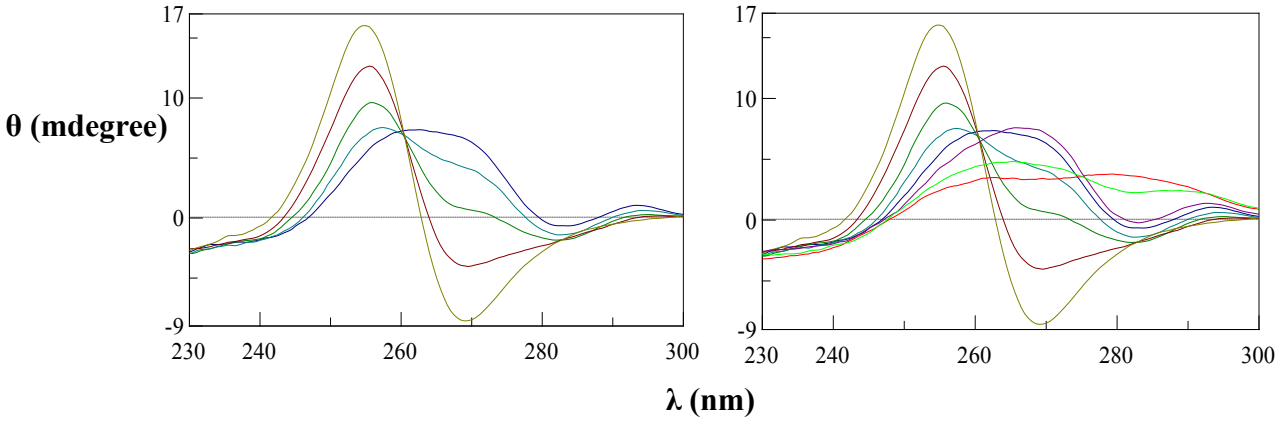

Figure 94. (A) CD spectra of ABCD6HQ (2×10^{-5} M) at pH 7.0 with increasing concentration of $CuSO_4$ (Cu^{2+}/L = 0.25, 0.5, 0.75, 1) (B) CD spectra of ABCD6HQ (2×10^{-5} M) at pH 7.0 with increasing concentration of $CuSO_4$ (Cu^{2+}/L = 0.25, 0.5, 0.75, 1, 1.25, 1.5, 2, 3). The last spectrum show clearly an increased base line maybe due to a partial precipitation.

The binding ability of ABCD6HQ for Zn^{2+} was investigated by UV-vis titration at 25 °C in a buffered solution (pH 7.0, MOPS). Figure 95 illustrates the typical UV-vis curves of ABCD6HQ with the gradual addition of Zn^{2+} (0.1 equivalents). As can be observed, two new absorption peaks appeared at 280 and 440 nm, and their intensity gradually increased with the stepwise addition of Zn^{2+}. On the contrary, the band centered at 253 nm gradually decreased and also showed a bathochromic shift. An absorption decrease was also observed for the bands at 307 and 350 nm. The presence of three well-defined isosbestic points could indicate that the ligand is able to form only one complex species. The molar ratio method suggests a ML species because a break in the slope of the curve occurs at a 1:1 metal ligand ratio corresponding to the combining ratio of the complex. Although further changes in UV-vis spectra are evident with the increase of Zn concentration and thereof it is possible that also the dinuclear species is formed at higher Zn^{2+}/L but this species is less favoured in comparison with that of copper. These data are in agreement with ESI-MS experiments that showed that the only a small amount of dinuclear species (5 %) was detected at 2:1 Zn^{2+}/L molar ratio.

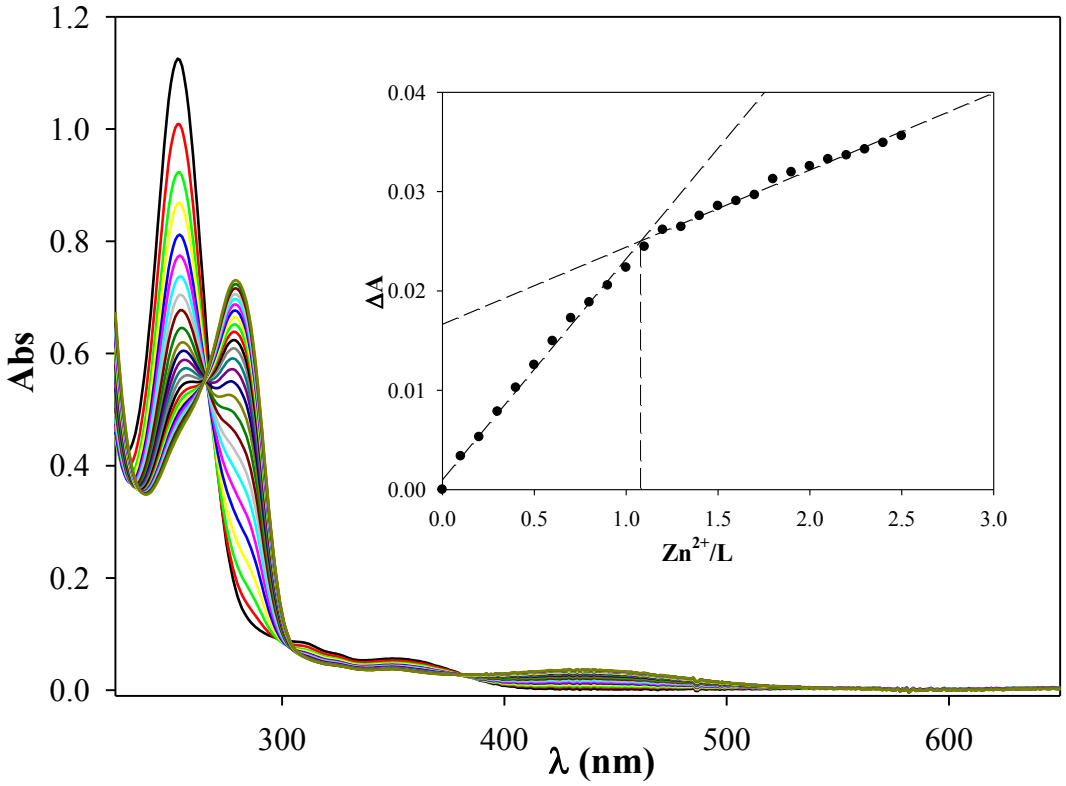

Figure 95. ABCD6HQ (2×10^{-5}M) was titrated with $Zn(NO_3)_2$ (final concentration 5×10^{-5}M). The inset show the changes in absorption *vs* the molar ratio Zn^{2+}/L.

Monofunctionalized CyDs via an amine bond

In Table 17 the ESI-MS characterization of the copper complexes with CD6RHQ is reported. The ESI-MS experiments were carried out at different pH, from 5.0 to 9.0. The formation of complex species was observed at pH > 5. In addition to the peak of the ligand new peaks due to singly charged species $[CuL]^+$ and $[CuL\text{-}H+Na]^+$ and doubly charged species appear in the presence of copper. The ESI-MS spectra of Cu^{2+}-systems clearly show the existence of the complex species CuL^+ and this is the main Cu^{2+} species over the explored pH range (pH 5.0-9.0). MS spectra display the decrease of the proton adduct (*m/z* 1352.3) as well as the increment of the sodium adducts (*m/z* 1374.3) as the pH increases upon the NaOH addition. The typical isotopic pattern of natural copper confirms the attribution of these signals to species of the Cu^{2+}-CD6RHQ system. In comparison with similar systems and taking account of the mass spectrometry data a main species with the metal ion bound to N of py

ring, phenolate, amino group could be hypothesized. The presence of a coordinating water molecule can be considered as suggested by the double charge species at 695.7 *m/z*. The elevated *m/z* ratio and the neutral nature of the possible ML_2 species could explain the absence of peaks attributable to a double charged ML_2 species in ESI-MS experiment condition.

Table 17. ESI-MS characterization of an equimolar mixture of CD6RHQ and Cu^{2+}. L is hydroxyquinolate.

Assignment	Calcd (*m/z*)	Found (*m/z*)	Relative intensity %			
			pH 6.0	pH 7.0	pH 8.0	pH 9.0
$[CuL+H]^{2+}$	676.7	676.7	2%	-	-	
$[CuL+Na]^{2+}$	687.7	687.7	18%	28%	34%	30%
$[CuL+K]^{2+}$, $[CuL+H_2O+Na]^{2+}$	695.7	695.7	2%	5%	10%	-
$[CuL-H+2Na]^{2+}$	698.6	698.6	4%	5%	4%	-
$[LH+H]^{+}$	1291.4	1291.3	28%	20%	19%	6%
$[LH+Na]^{+}$	1313.4	1313.4	3%	8%	10%	22%
$[CuL]^{+}$	1352.4	1352.3	100%	100%	100%	96%
$[CuL-H+Na]^{+}$	1374.3	1374.3	30%	60%	78%	100%

ESI-MS spectra were also detected in the presence of equimolar concentration of Zn^{2+} at different pH. Peaks due to singly charged species $[ZnL]^{+}$ and $[ZnL-H+Na]^{+}$ and doubly charged species (see Table 18) are observed. MS spectra clearly show the decrease of the proton adduct (*m/z* 1353.3) as well as the increment of the sodium adducts (*m/z 1375.3*) upon the NaOH addition in order to increase pH. The typical isotopic pattern of naturally occurring zinc isotopes confirms the identity of these Zn^{2+} complexes. However, the relative intensity of the peaks due to the zinc complexes is much lower than that of copper complexes, suggesting a minor affinity of the ligand for this metal ion as expected in keeping with Irving-Williams series and analogous systems. A coordination environment that involved N of py ring, phenolate, amino group could be also hypothesized, similarly to that of copper.

Table 18. ESI-MS characterization of an equimolar mixture of CD6RHQ and Zn^{2+}. L is hydroxyquinolate.

Assignment	Calcd (*m/z*)	Found (*m/z*)	Relative intensity %		
			pH 6.0	pH 7.0	pH 8.0
$[LH+H+Na]^{2+}$	657.2	657.1	10%	7%	10%
$[ZnL+2H]^{2+}$	677.2	677.0	12%	20%	15%
$[ZnL+K]^{2+}$, $[ZnL+H_2O+Na]^{2+}$	696.2	696.1	-	3%	14%
$[Zn_2L-H]^{2+}$	708.1	708.1	4%	15%	15%
$[LH+H]^{+}$	1291.4	1291.3	100%	100%	100%
$[LH+Na]^{+}$	1313.4	1313.4	-	20%	70%
$[ZnL]^{+}$	1353.4	1353.2	13%	30%	30%
$[ZnL-H+Na]^{+}$	1375.3	1375.1	-	10%	18%

ESI-MS characterization of the CD3RHQ-Cu^{2+} complexes was carried out and *m/z* values of the detectable peaks and their relative intensity are reported in Table 19.

Table 19. ESI-MS characterization of an equimolar mixture of CD3RHQ-Cu^{2+}. L is hydroxyquinolate.

Assignment	Calcd (*m/z*)	Found (*m/z*)	Relative intensity %			
			pH 6.0	pH 7.0	pH 8.0	pH 9.0
$[CuLH_{-1}+H+Na]^{2+}$, $[CuL+Na]^{2+}$	687.7	687.6	46%	80%	82%	80%
$[CuL+K]^{2+}$, $[CuL+H_2O+Na]^{2+}$	695.7	695.6	20%	44%	29%	20%
$[CuLH_{-1}+2Na]^{2+}$	698.6	698.7	10%	28%	58%	55%
$[CuLH_{-1}+Na+K]^{2+}$	706.7	706.7	4%	14%	27%	32%
$[CuLH_{-1}+2K]^{2+}$	714.6	714.6	-	2%	2%	-
$[CuL]^{+}$, $[CuLH_{-1}+H]^{+}$	1352.4	1352.3	100%	100%	100%	45%
$[Cu_2L_2H_{-1}+Na]^{2+}$	1363.3	1363.2	24%	30%	40%	44%
$[Cu_2L_2H_{-1}+K]^{2+}$	1371.3	1371.2	2%	15%	16%	8%
$[CuLH_{-1}+Na]^{+}$	1374.3	1374.3	30%	50%	80%	100%

The ESI-MS spectra were also recorded at different pH, from 6.0 to 9.0. Firstly, peaks due to singly charged species $[CuL]^{+}$ and $[CuL-H+Na]^{+}$ can be identified. It should be noted that their expected *m/z* values (1352.4 and 1374.3, respectively) are equal to those of $[CuLH_{-1}+H]^{+}$, $[CuLH_{-1}+Na]^{+}$ species. This complex species results neutral upon the loss of two protons (phenolic OH, an OH group of the CyD lower rim) and thereof they have to form ion adducts in order to be detected in ESI-MS experiments. Furthermore, ESI-MS spectra show doubly charged species (see Table 19) as evidenced by the relative isotopic clusters that differ

by 0.5. These species are attributable to $CuLH_{-1}$ with different combinations of H, Na and/or K ions. The typical isotopic pattern of naturally occurring copper isotopes confirms the attribution of these signals to species of the Cu^{2+}-CD3RHQ system. Doubly charged species provide a further proof of the different coordination environment of CD3RHQ respect to CD6RHQ as these species were not found in ESI-MS spectra of CD6RHQ.

MS spectra clearly show the decrease of the proton adduct (*m/z* 1352.3) as well as the increment of the sodium adducts (*m/z 1374.3*) that becomes the base peak at pH = 9 as the pH increases upon the NaOH addition. However, $CuLH_{-1}$ could be reasonably considered the main Cu^{2+} species over the explored pH range (pH 7-9) whereas CuL^{+} could be a minor component of the observed peak at acid pH. Nevertheless, the peak at 1352.3 *m/z* has another minority component (20 %) due to the dimeric species $[Cu_2L_2H_{-1}+H]^{2+}$ that could be assigned by the relative isotopic peaks that differ by 0.5 units. $[Cu_2L_2H_{-1}+H]^{2+}$ influences the isotopic cluster of the most abundant species because of the partial overlapping. Ion adducts of this dimeric species were also detected with other metallic cation (Na, K) at 1363.2 and 1371.2 *m/z*. It is worth noting that the percentage of the dimeric complex increases with pH, presumably because the deprotonation of the 2-hydroxyl group (to form the complex species) is favorite.

Finally, negative-ion ESI-MS spectrum of an equimolar mixture of CD3RHQ and $CuSO_4$ was also acquired (Figure 96). The spectrum displays only one peak attributable to $[CuLH_{-1}-H]^{-}$ with the typical isotopic pattern of copper confirming the existence of the neutral $CuLH_{-1}$ species.

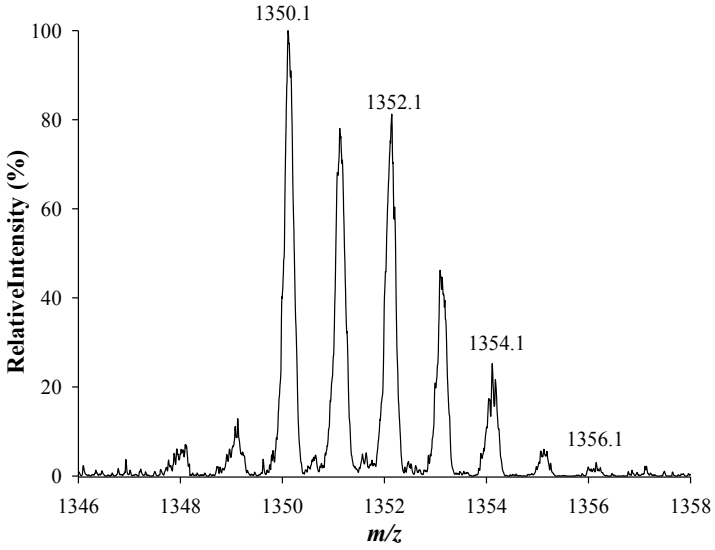

Figure 96. Zoom scan spectrum (negative-ion mode) of CD3RHQ in the presence of equimolar concentrantion of Cu^{2+}.

For comparison with similar systems and considering the mass spectrometry data, a main species with the metal ion bound to N of py ring, phenolate, amino group and O could be hypothesized. To sum up, the involvement of the hydroxyl group of the β-CyD rim is also suggested by literature data for CyD derivatives functionalized at the position 6 and 3.[159,212] The CD3RHQ ligand is able to bind the Cu^{2+} ion tightly, forming fused five-membered chelate rings (highly stable) with the involvement of the ionized OH group at 2 position of CyD (Figure 97).

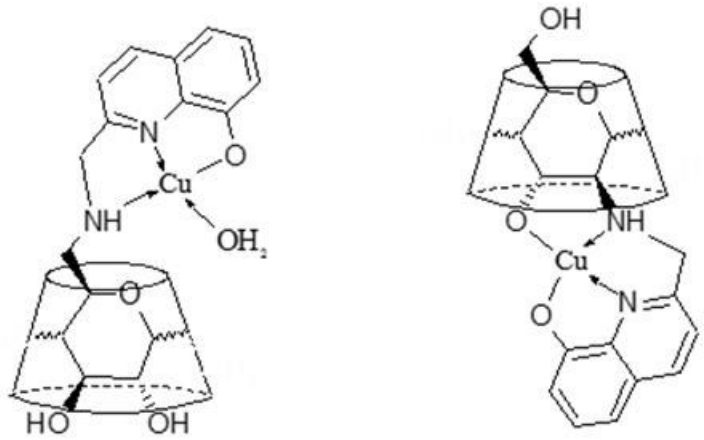

Figure 97. Hypothesized structures of main copper complex species of CD6RHQ and CD3RHQ (the charges are omitted for clarity).

Zn^{2+} complexes of CD3RHQ were also studied by ESI-MS spectrometry but in this case a highly signal/noise ratio was observed at pH>6, presumably indicating a partial precipitation of zinc complex species. Zn^{2+} complex species similar to those of Cu^{2+} was found suggesting that zinc has a similar behavior (Table 20).

Table 20. ESI-MS characterization of an equimolar mixture of CD3RHQ and Zn^{2+}. L is hydroxyquinolate.

Assignment	Calcd (*m/z*)	Found (*m/z*)
$[LH+H+Na]^{2+}$	657.2	657.1
$[ZnL+2H]^{2+}$	677.2	677.0
$[ZnLH_{-1}+H+Na]^{2+}$, $[ZnL+Na]^{2+}$	688.2	688.0
$[ZnL+K]^{2+}$, $[ZnLH_{-1}+H+K]^{2+}$	696.2	696.1
$[ZnLH_{-1}+2Na]^{2+}$	699.2	699.1
$[ZnLH_{-1}+Zn]^{2+}$, $[Zn_2LH_{-1}]^{2+}$	708.1	708.0
$[ZnL]^{+}$, $[ZnLH_{-1}+H]^{+}$, $[Zn_2L_2]^{2+}$, $[Zn_2L_2H_{-1}+H]^{2+}$	1353.4	1353.3
$[LH+H]^{+}$	1291.4	1291.3
$[LH+Na]^{+}$	1313.4	1313.4
$[Zn_2L_2H_{-1}+Na]^{2+}$	1364.3	1364.2
$[Zn_2L_2H_{-1}+K]^{2+}$	1372.3	1372.1
$[ZnLH_{-1}+Na]^{+}$	1375.3	1375.2

Copper complexes of CD6RHQ were also investigated by UV-Vis spectroscopy (Figure 98). The absorption spectra of CD6RHQ in water show three band centered at 208, 244 and 308 nm. The spectrum is not significantly modified by the presence of MOPS in the region between 220-600 nm. The environment of coordination of CD6RHQ with Cu^{2+} was investigated by spectrophotometric titration at 25 °C in aqueous buffer solution. As can be seen in Figure 94, the absorption bands of the CyD derivative dramatically change upon addition of Cu^{2+} ions. The UV band at 244 nm gradually decreased with concomitant appearance and thereof increase of absorption bands at 259 and 373 nm. These findings are characteristic of the OHQ derivatives when the complexation is accompanied by the deprotonation of the phenolic group.

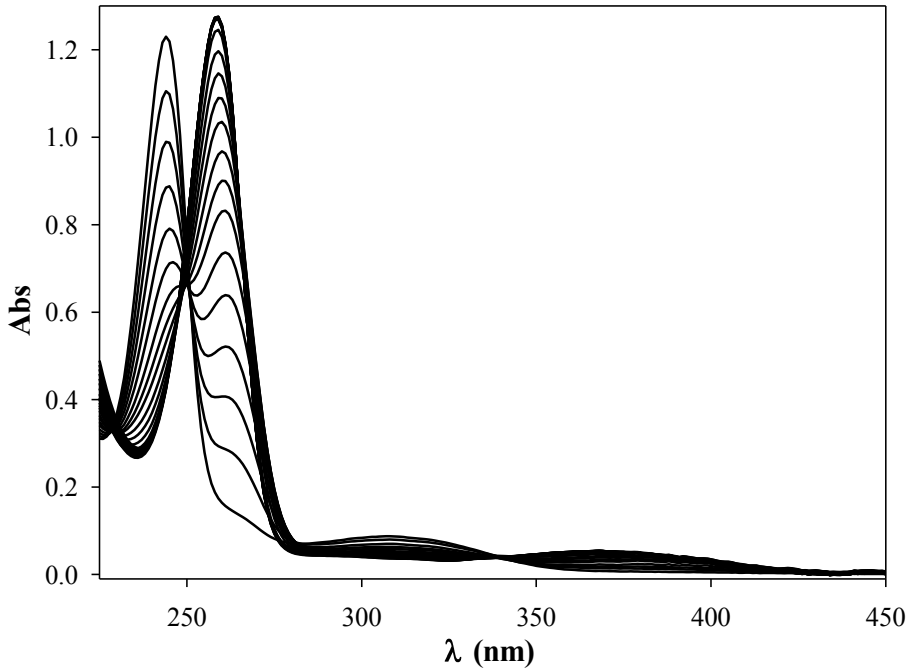

Figure 98. Titration of CD6RHQ (4.0×10^{-4} M) with $Cu(NO_3)_2$ (8.2×10^{-4} M).

The spectra obtained during the stepwise addition of Cu^{2+} showed, at the first, the appearance of three isobestic points at *ca* 250, 281 and 339 nm, indicating that initially only two species are present in solution (presumably the free ligand and a ML_2 species). Then, the absence of clear isosbestic points suggests the concomitant presence of more complex species.

Moreover, the coordination stoichiometry between CD6RHQ and Cu^{2+} was analyzed by the molar ratio method using UV-vis spectroscopy. As seen in Figure 99, the curve of ΔA *vs* Cu^{2+}/1 molar ratio at 373 nm shows an inflexion point at a molar ratio of 0.5, which corresponded to a 2:1 coordination stoichiometry between CD6RHQ and Cu^{2+}. Although, the curve of molar ratio analyzed at different wavelength displays the absence of a clear inflection suggesting the presence of more complex species including ML and ML_2 in keeping with ESI-MS data.

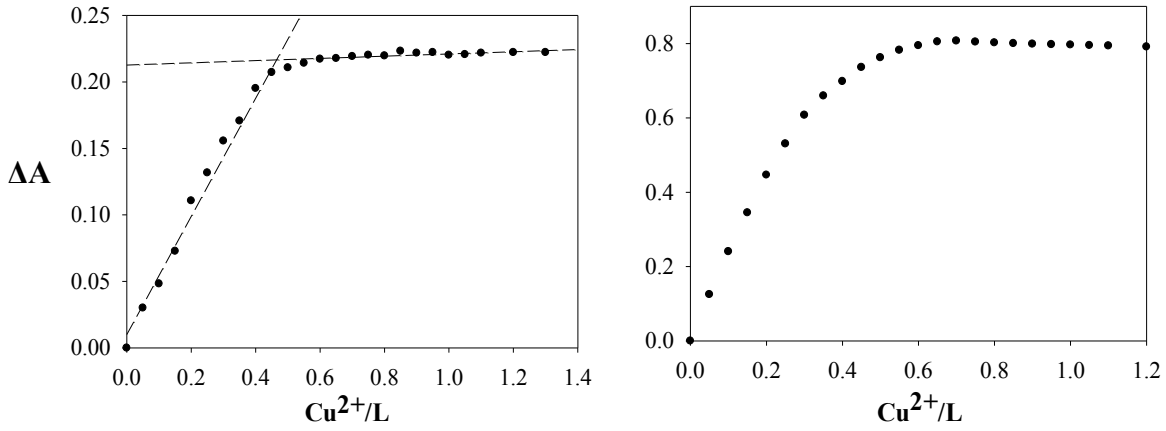

Figure 99. Absorption changes of CD6RHQ at 373 (left) and 244 (right) nm upon the addition of Cu^{2+}.

To conclude, CD6RHQ is able to complex copper with high stability constants.

The Uv-vis spectra were also recorded during the stepwise addition of Zn^{2+} (Figure 100). The bands at 244 and 308 nm gradually decreased in intensity with the concomitant appearance of the new bands at 262 and 375 nm in keeping with the complexation of the zinc.

It is also noteworthy the presence of three isobestic points at *ca* 251, 280 and 335 nm. Zinc complexes have a similar behavior to those of copper and thereof, the presence of more complex species including ML and ML_2 can be suggested in keeping with ESI-MS data and UV-vis spectroscopy.

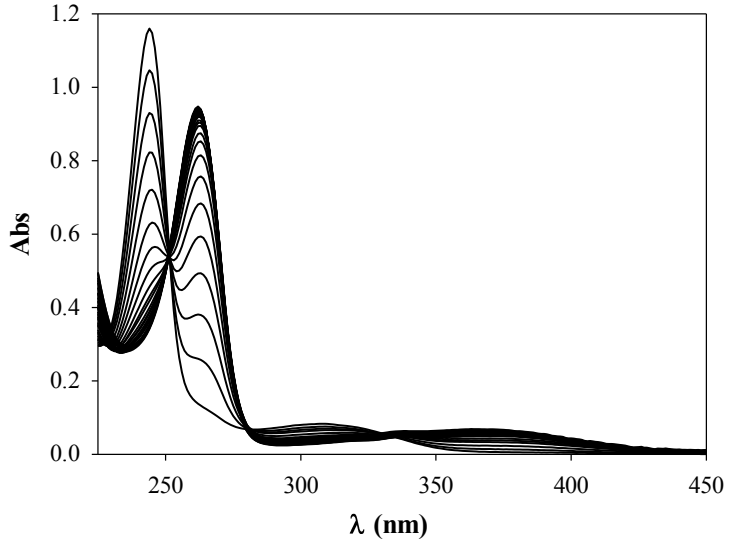

Figure 100. Titration of CD6RHQ (4.0×10^{-4} M) with $Zn(NO_3)_2$ (8.2×10^{-4} M).

Furthermore, Zn^{2+} complexes of CD6RHQ were preliminarily studied by ^{1}H NMR (Figure 101). A slow ligand exchange process was found with respect to the NMR timescale as the signals of the zinc complex and the free ligand can be individually observed.

NMR spectra were carried out at pH 7.0 in D_2O. The stepwise addition of a $ZnSO_4$ solution (in D_2O) displayed the appearance of a new set of small signals that enhanced their intensity with Zn^{2+} increase. As for the complex species, the H-4 signal of the aromatic moiety shows a downfield shift while the other protons are upfield shifted, especially H-5 and H-7. A similar behavior is reported for Zn^{2+} complexes of 8-hydroxyquinoline-5-sulfonate.[213] These signals become predominant and any free ligand signals disappears at a 1:2 M/L ratio. Furthermore, in the aliphatic region new signals due to complex formation are present.

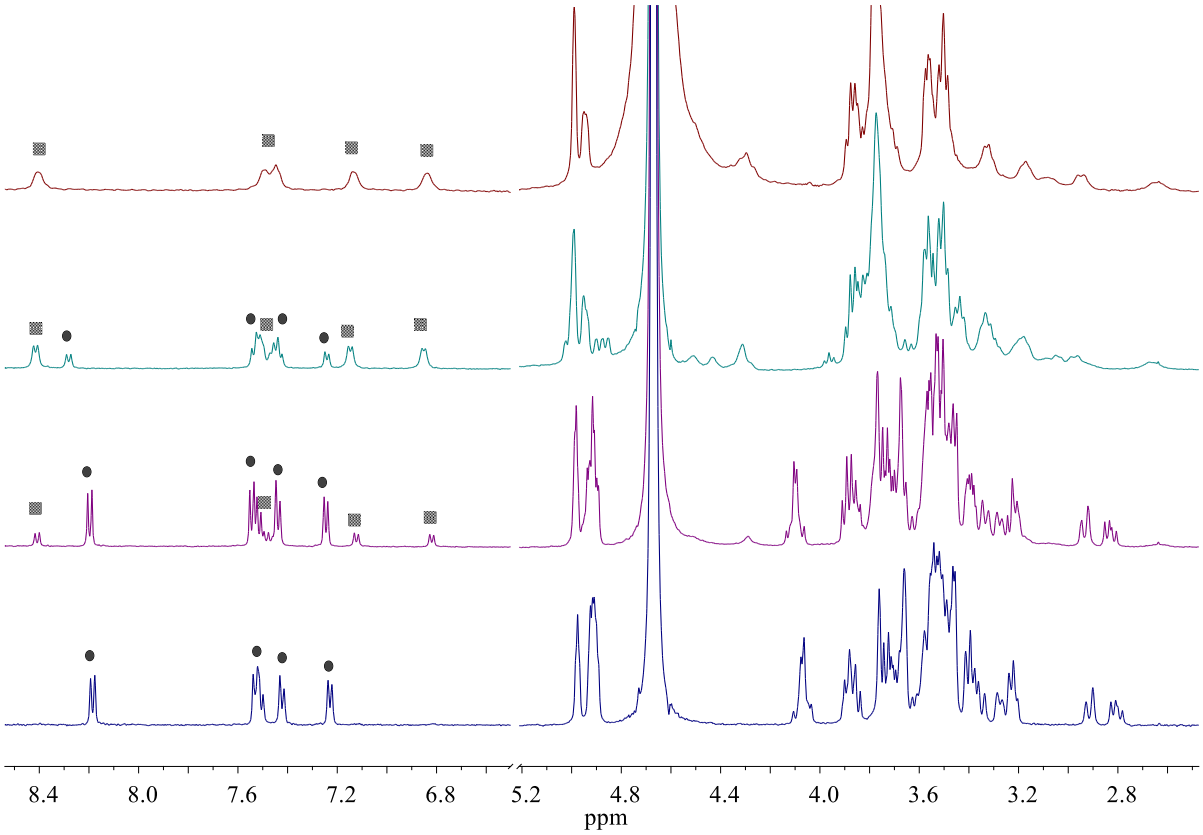

Figure 101. NMR spectra of Zn^{2+}-CD6RHQ at different M/L ratios (0:1 blue, 0.2:1 purple, 0.4:1 green, 0.5:1 red). The labeling of the signals refers to complex species (▩) and ligand (●).

The formation of a species ML_2 can be proposed as well as the involvement of the amino group in the complexation of Zn^{2+} since the proton resonances mainly influenced by complexation are those of the benzylic CH_2 and Hs-6A. Similar species have been reported for

some OHQ derivatives.[202] When zinc is added at 1:1 metal ligand ratio, new signals due to a new complex species appear in addition to the ML_2 species. A mixture of species seem to be present in this condition (Figure 102).

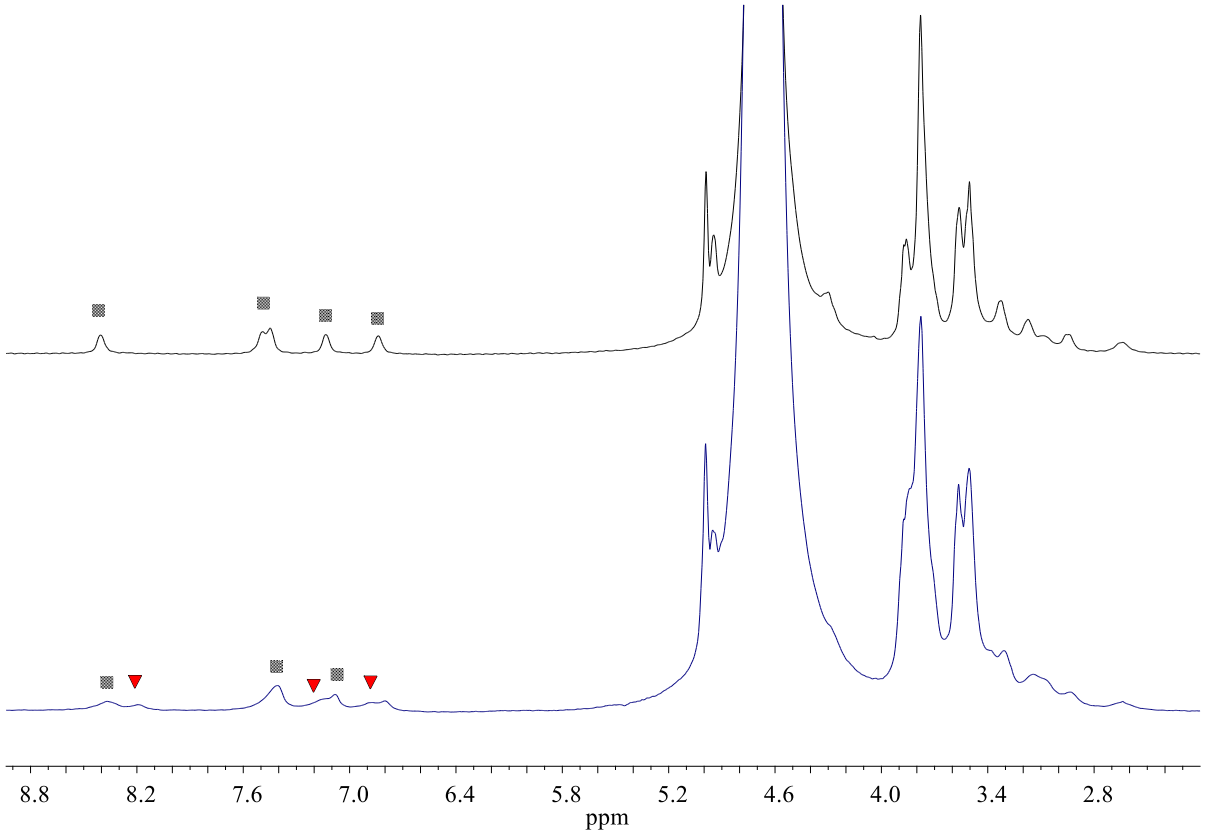

Figure 102. NMR spectra of Zn^{2+}-CD6RHQ at different M/L ratios (0.5:1 black, 1:1 blue). The labeling of the signals refers to different complex species.

4.4.3 Antiproliferative activity

OHQs, their glucoconjugates and their Cu^{2+} complexes have been found to show cytotoxic activity against human cancer cells.[214] In this scenario, the antiproliferative activity of some CyD conjugates (CD6HQ, CDNHQ, CDOHQ) was tested in the presence or absence of Cu^{2+} on different cell lines. Pancreatic cell lines, which are distinguished by significant expression of genes encoding digestive enzymes (amongst them α-amylase),[215] were also tested. The behavior shown by CyD derivatives is very different from that of the simple hydroxyquinolines or their glucoconjugates.

In all cell lines CyDs showed IC_{50}s always greater than 100 μM, even in the presence of copper ions. These results clearly show that the new cyclodextrin derivatives are not toxic in these cell lines at the concentration studied. Their behavior is different than that of OHQ, which has IC_{50} values of approximately 5 μM as previously determined.[216,217] The antiproliferative activity was also tested in the presence in the culture medium of copper ions and α-amylase, that is able to facilitate the hydrolysis of cyclooligosaccharides. The presence of α-amylase did not significant affect the IC_{50} of the CyD derivatives. These data suggest that CyD derivatives are not easy hydrolyzed into smaller sugar derivatives by amylase and are unable to cross the cell membranes. This hypothesis is also supported by preliminary ESI-MS studies after incubation of CyD conjugates with amylase. The compounds were only partially degraded by the enzyme over long periods of time. Taken all together, these results bode well for administering relatively high concentrations of these derivatives, for use as antioxidants, if necessary, without damage to tissues.

4.4.4 Antioxidant activity

Reactive oxygen species (ROS) may play a dual function in the human organism. On the one hand, they participate in cell signal transduction cascades, leading to the activation of some transcription factors responsible for regulating of the expression of genes relevant for cell growth and differentiation. On the other hand, overproduction of radical species can eventually lead to many diseases such as atherosclerosis, cancer, diabetics, rheumatoid arthritis, post-ischemic perfusion injury, myocardial infarction, cardiovascular diseases, chronic inflammation and aging AD,[218] HD and NPC.[9,219] In these diseases the generated ROS, such as the extremely reactive hydroxyl radical, $HO^{\bullet}$, can abstract hydrogen atoms thereby causing oxidative damage to lipids, proteins, DNA, etc. It has been reported in epidemiological studies that many of antioxidant compounds possess, antiatherosclerotic, antitumor, antimutagenic, anticarcinogenic, antibacterial and antiviral activities to greater or lesser extent.[220] In some cases, it has been observed that cyclodextrin increases antioxidant activity of functionalizing moiety. The proximity of the cavity to the catalytic center is crucial to improve the antioxidant activity as well as the rigidity and the structure of the system. Iron complexes of two deferiprone-cyclodextrin conjugates can clarify this statement.

CD6DFP shows a higher SOD-like activity, the I_{50} of its Fe^{3+} complex (6.8 ± 0.5 μM) is about twice better than those shown by CD3DFP (15.8 ± 0.8 μM) and DFP (16.7 ± 0.9 μM) complexes.[203] In the case of CD3DFP the DFP moiety is more rigid and catalytic center is too distant to take advantage of the cavity. In regard to this issue the antioxidant activity of these new ligands was evaluated performing two different assays: ABTS radical assay (to determine free radical scavenging capacity) and NBT assay (to determine SOD-like activity).

Free radical scavenging activity

Trolox equivalent antioxidant capacity (TEAC) examines the quenching of 2,2′-azinobis(3-ethylbenzothiazoline-6-sulfonic acid) radical cation ($ABTS^{\bullet+}$) in the presence of antioxidant compounds by means of UV-vis spectroscopy. TEAC values for quinoline derivatives are plotted in Figure 103. Free radical scavenging capacity is primarily attributed to the high reactivities of hydroxyl substituents on aromatic rings. The nature of substituent effects (electron-withdrawing, electron donator, inductive effects) have an influence on the H-donating ability of hydroxyl group. The results, expressed as the TEAC, indicated the high ability of these derivatives to scavenge free radical $ABTS^{\bullet+}$ after 1, 3, and 6 min. The compound activity is higher than those of known antioxidants like Trolox, a more hydrophilic analog of vitamin E. This behavior is generally associated with a good protective function against oxidative stress. The compounds are much more active than CQ, whose TEAC values were determined for comparison. The TEAC values for all compounds except ABCD6HQ are not significantly different, demonstrating that variation in the structure between the compounds has no effect on antioxidant capacity. ABCD6HQ presents the highest capacity to scavenge free radicals. At the end point (after 6 min), the bis derivative showed a TEAC value of 2.54, which is superior to the values of 1.76 and 2.00 reported for polyphenol antioxidants such as caffeic acid and chlorogenic acid and very close to the reported value of 2.60 for gallic acid that possesses three phenolic groups.[221] These data suggest that ABCD6HQ could be a powerful antioxidant with activity comparable to that of several polyphenols.

The presence of Cu^{2+} affects the ability to quench the radical $ABTS^{\bullet+}$ for the tested compounds. When Cu^{2+} is present, the TEAC value is reduced by about 10-15% compared to that of free ligand for the CyDs functionalized *via* an amide bond. However, copper alone does not interfere with radical $ABTS^{\bullet+}$ in the range of investigated concentrations. Conditional

stability constants of Cu^{2+} complexes of CD6HQ, CDNHQ and HQ strongly suggest that 100% of complex species ML is formed in the experimental conditions of this assay and hence the activity can be ascribed to the complex species. In case of Cu^{2+} complexes the hydroxyl group is less available to react with the radical cation because is involved in the binding of the metal ion. Taken together these data indicate that copper complexes of these derivatives retained a good antioxidant activity. Copper complexes of CD3RHQ, CD6RHQ showed a different behavior. Firstly, they displayed a different kinetic profile with slower reaction rates. These compounds did not reach the end point in 6 min, but in longer times. Furthermore, they showed lower TEAC values than that of the other CyD derivatives. Reaction mechanisms of these complexes with $ABTS^{\bullet+}$ clearly differ from those of ligands probably owing to either the strong ligand field of CD6RHQ and CD3RHQ or different redox potentials of their complexes.

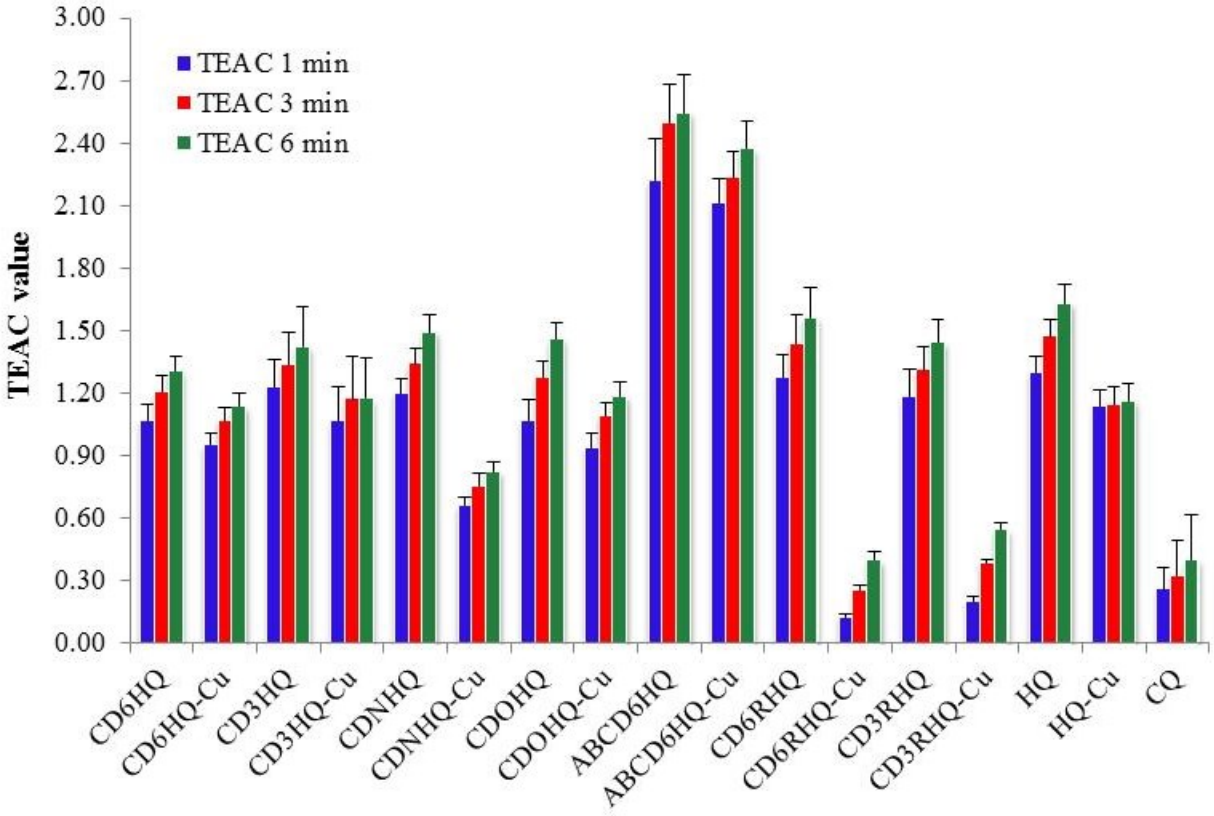

Figure 103. TEAC values at 1, 3, and 6 min for CyD derivatives and their parent compound in the presence or absence of Cu^{2+}. Means are the average of three independent trials, and error bars show standard deviations.

SOD-like activity

The SOD activity of ligands and Cu^{2+} complexes of CyD conjugates was determined by competition kinetics using NBT target as reported elsewhere.[222,223] The activity of HQ was also determined for comparison. The I_{50} values are reported in Table 21. The SOD activity of the free ligands was found to be very low with the I_{50} value of 10^{-4} M. The SOD activity of copper complexes is several orders of magnitude higher than that of their ligands. The most important result is that all complexes efficiently catalyze superoxide dismutation below the micromolar concentration range (0.19–0.39 μM). Although the complexes were not as effective as bovine erythrocyte SOD, their activities were on the same order of magnitude as the best SOD analogues described in the literature.[224,225] Conditional stability constants of Cu^{2+} complexes of CD6HQ, CDNHQ and HQ strongly suggest that 100% of complex species ML is formed in the experimental conditions of this assay and hence the activity can be ascribed to the complex species. In the case of CDOHQ and ABCD6HQ, stability constants similar (or higher) to (than) those of OHQ and of CD6HQ may be reasonably hypothesized for the Cu^{2+} complexes. Therefore, also in this case the SOD-like activity can be attributable to the Cu^{2+} complex of CDOHQ and ABCD6HQ. The lowest ability of CDNHQ complex to scavenge the superoxide anion could be due to the stronger ligand field of the coordination environment.

Table 21. NBT assay: I_{50} values of CD6HQ, CDOHQ, CDNHQ, ABCD6HQ and HQ in the presence of equimolar amount of Cu^{2+}.

System	I_{50} (M)
CD6HQ-Cu^{2+}	$2.6(2) \times 10^{-7}$
CDOHQ-Cu^{2+}	$2.3(1) \times 10^{-7}$
CDNHQ-Cu^{2+}	$3.9(3) \times 10^{-7}$
ABCD6HQ-Cu^{2+}	$1.9(3) \times 10^{-7}$
HQ-Cu^{2+}	$1.6(2) \times 10^{-7}$
Cu^{2+}	$5.1(6) \times 10^{-7}$

4.4.5 Antiaggregant activity

Protein aggregation process induced by metal ions has been the topic of many studies. Several diseases are closely related to the protein aggregation and metals play an important role in this process; for example, in the Alzheimer's disease (AD), Aβ precipitation and toxicity are caused by abnormal interactions with neocortical metal ions, especially Zn, Cu and Fe.[226] Aggregation assays of the protein β-lactoglobulin (BLG) were carried out in order to verify if CyD conjugates could inhibit metal induced protein aggregation. BLG was selected because of the its heat-induced aggregation is used as a general model for fibril formation.[227,228] BLG is a small globular protein of 162 amino acids (18.4 kDa) contained in the whey of ruminant milk. At neutral pH, it assumes a dimeric native conformation. Its secondary structure is composed of 15% of α-helices, 50% of β-strands and ~20% of reverse turn (Figure 104).

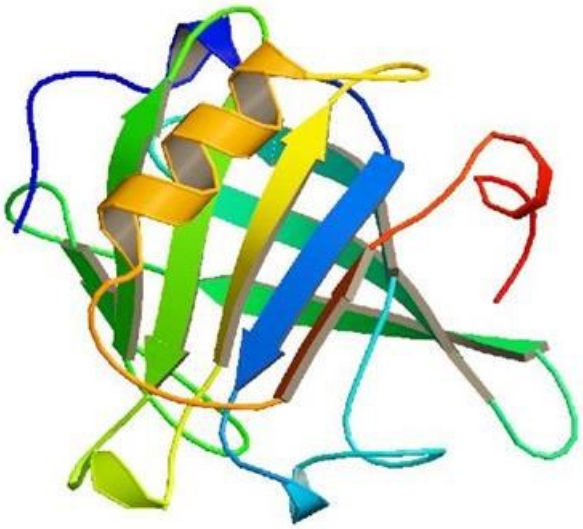

Figure 104. Structure of a β-lactoglobulin (monomer).

It has a core structural pattern formed by an α-helix and eight strands of antiparallel β-sheets and its tertiary structure is stabilized from two disulfide bonds; moreover, there is also one free, highly reactive –SH group, corresponding to Cys-121, buried in the hydrophobic core of the protein aggregation process appears strictly dependent on temperature and it starts only after rearrangement of the protein structure. When heated, monomerization and partial unfolding of the protein are induced with consequent exposure of SH group and formation of an intermolecular bond with a free cysteine of a close molecule.

BLG denaturation and aggregation is strongly influenced by different parameters such as ionic strength, pH, buffer, as well as by transition metal ions, i.e. copper and zinc. In this context, a study on the effects of Cu^{2+} and Zn^{2+} on the heat-induced aggregation of BLG, at pH 7.0 (MOPS,10 mM) was carried out and the ability of CyD conjugates to modulate the metal-mediated aggregation of the BLG was tested.

Figure 105 shows the dependence of the scattered light intensity as function of temperature for BLG in the absence or presence of metal ions (BLG, Cu-BLG and Zn-BLG). As observed, only in the presence of equimolar amount of Zn^{2+}, a rapid increase of the count rate is evident, indicating an aggregation process that starts at about 45 °C. In the presence of 0.2 equivalents of Cu^{2+}, a slight increase of the intensity is also observed at about 72 °C.

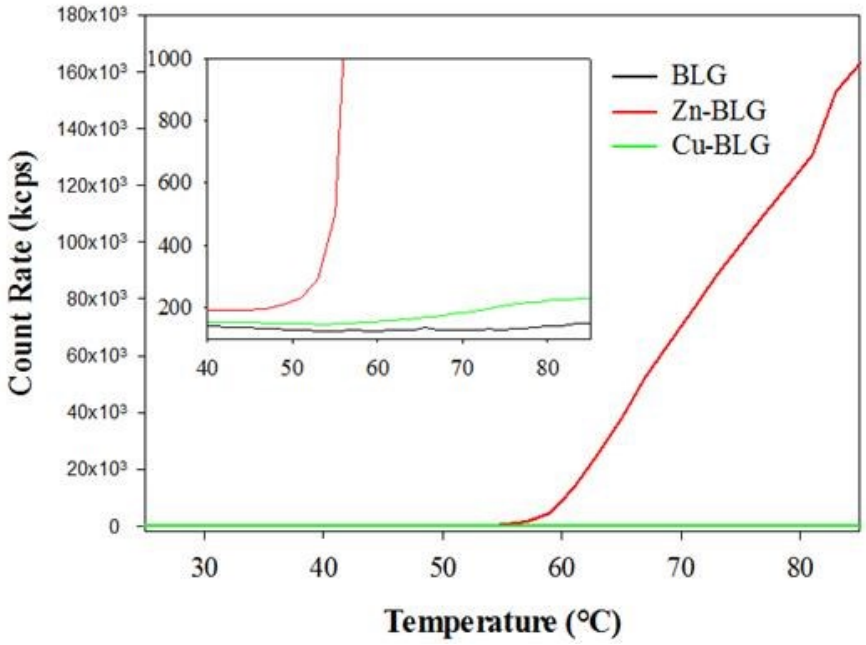

Figure 105. Scattered intensity as a function of temperature for BLG (black), Cu-BLG (green) and Zn-BLG (red). The inset shows a zoom to better appreciate the differences between BLG and Cu-BLG.

In order to verify if the Zn-induced BLG aggregation can be consider a model of beta-amyloid, a fluorescence kinetic in the presence of benzothiazole dye, thioflavin T (ThT) was carried out. Extrinsic fluorescence of ThT is widely used for the identification and quantification of amyloid fibrils *in vitro*. When ThT is added to samples containing β-sheet-rich deposits, such as amyloid fibrils, it fluoresces strongly with excitation and emission maxima at approximately 440 and 490 nm, respectively. An *in situ* real-time ThT assay was

performed, whereby fibril formation is carried out in the presence of ThT, providing a means to monitor fibrillation kinetics in real-time. The ThT fluorescence of Zn-BLG system incubated at 60 °C increased rapidly after the equilibration period and reached a plateau after 100–150 min (Figure 106), which is indicative of amyloid fibril formation.

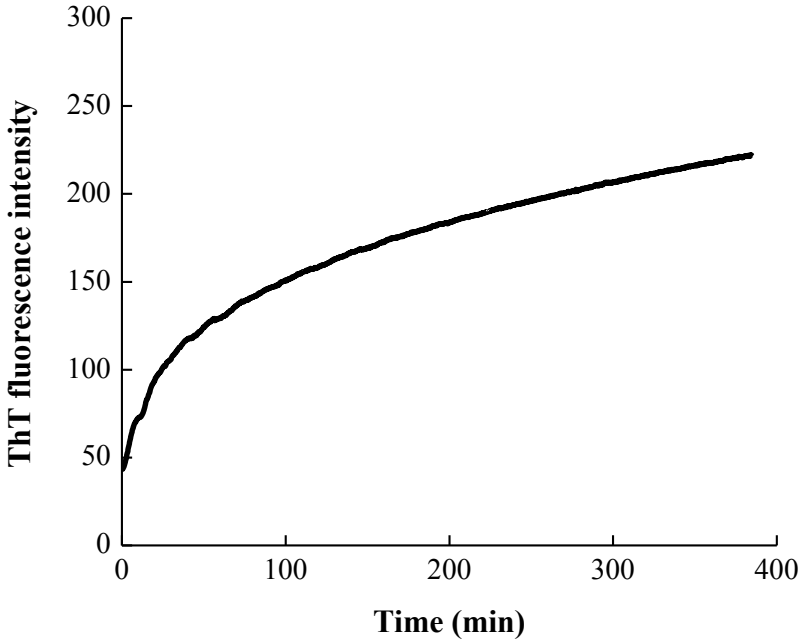

Figure 106. Graph of ThT fluorescence (60 °C) as a function of the incubation time for Zn-BLG.

The temperature trends were also carried out in the presence of CD6HQ, CD6RHQ and CD6RHQBn. Interestingly, the presence of these derivatives influences the metal ion induced thermal aggregation in the presence of metal ions whereas β-CyD does not affect the aggregation process. In particular, CD6HQ and CD6RHQ strongly inhibit the Zn^{2+}-induced thermal aggregation, probably avoiding the binding of the metal ion to the protein upon its own complexation (Figure 107). Furthermore, CD6RHQ results more effective in inhibiting the metal-induced aggregation, reasonably because of its higher affinity for Zn^{2+} compared to CD6HQ. Finally, it is noteworthy that CD6RHQBn, which is characterized by a protected phenolic group, is not able to significantly reduce the aggregate formation. In this case, the system can weakly complex the metal only through the pyridine ring. As a consequence, Zn^{2+} can induce BLG aggregation in the presence of CD6RHQBn.

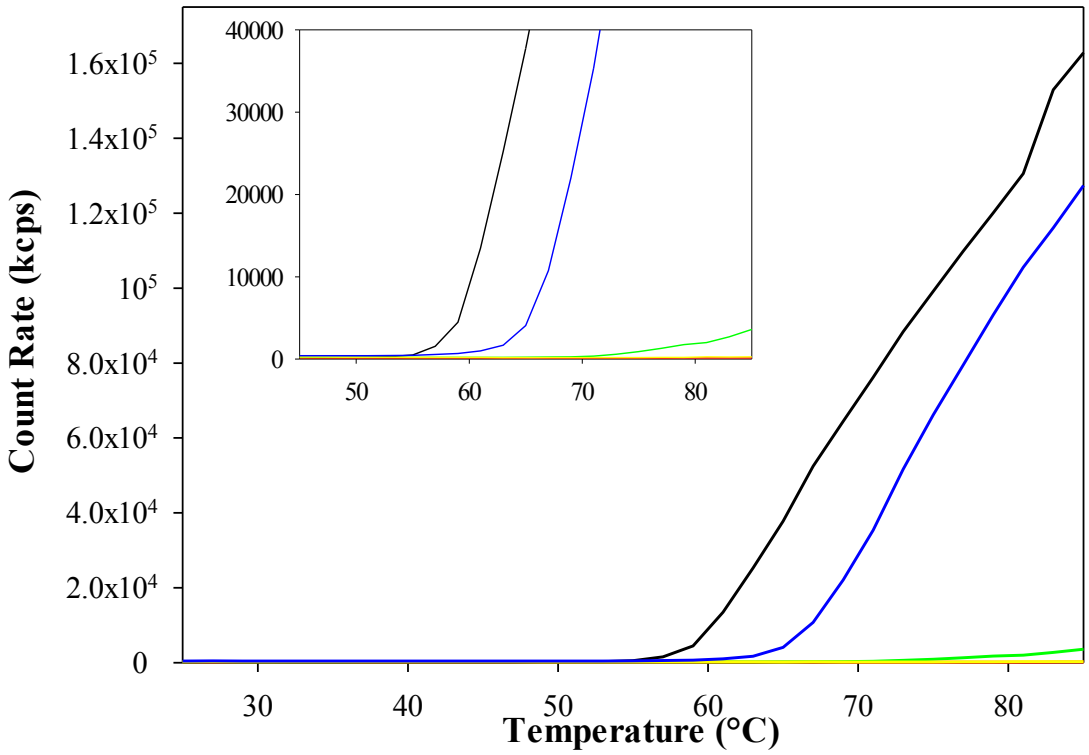

Figure 107. Scattered intensity as a function of temperature for BLG (red), Zn-CD6RHQ-BLG (yellow), Zn-CD6HQ-BLG (green), Zn-CD6RHQBn-BLG and Zn-BLG (black).

In order to monitor the extent of the aggregation, scattering measurements were also performed as a function of time.

In particular, Figure 108 reports the time evolution of the total scattered intensity for Zn-BLG, Zn-BLG-CD6HQ and Zn-BLG-CD6RHQ systems at 60 °C. As for Zn-BLG, the total scattered intensity exponentially increases due to aggregation, and after 85 min reaches a plateau. A slight increase of the total scattered intensity is observed in presence of CD6HQ, *versus* the time, suggesting that this compound prevents BLG from metal-induced aggregation. Finally, CD6RHQ more efficiently inhibits the metal-induced aggregation since the total scattered intensity remains essentially unchanged.

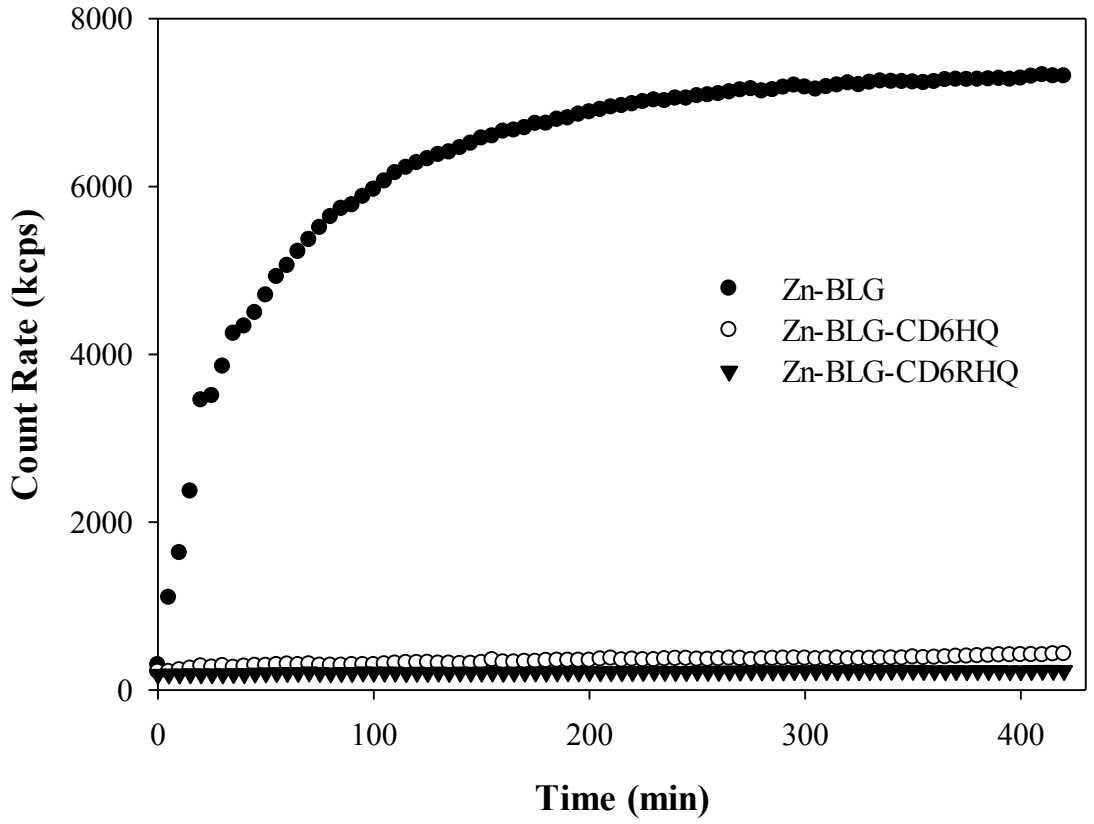

Figure 108. Time evolution of the normalized scattered intensity of the systems Zn-BLG and Zn-BLG-CD6HQ.

The aggregation kinetics of Cu-BLG and Cu-BLG-CD6HQ were carried out at 75 °C in order to observe a greater extent of aggregation (Figure 109). In this case, the kinetics are very similar, nevertheless a light increase of the total scattered intensity for Cu-BLG is observed in comparison with Cu-BLG-CD6HQ, probably due to different conformational changes induced by the metal presence as reported elsewhere.[229]

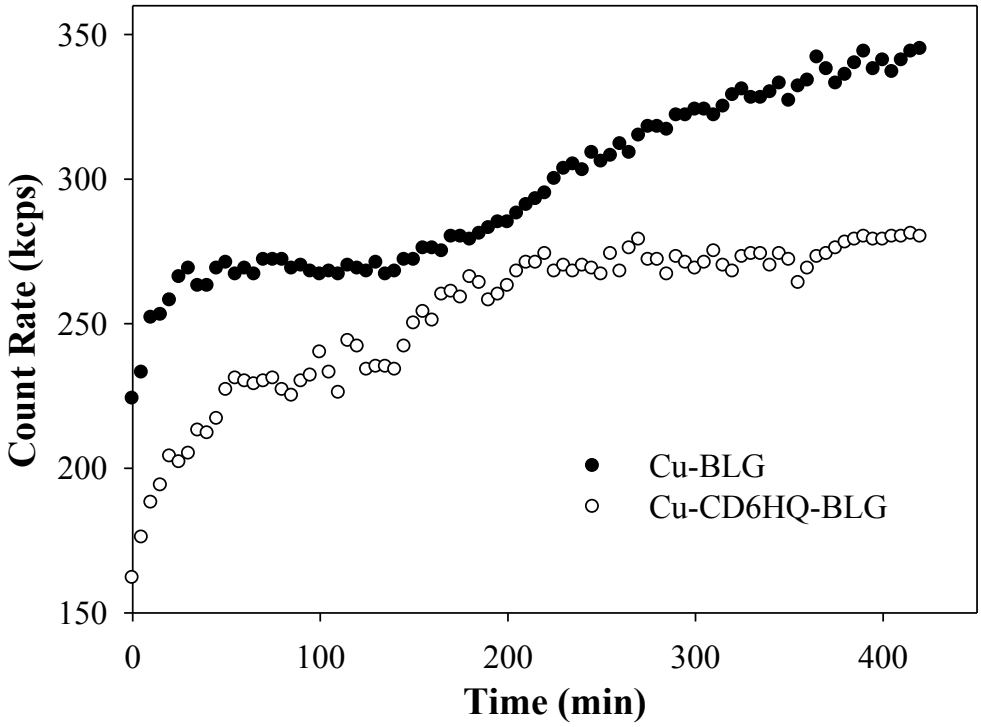

Figure 109. Time evolution of the normalized scattered intensity of the systems Cu-BLG and Cu-BLG-CD6HQ.

In order to evaluate the dimension of the aggregates during the kinetics, the distribution of the diameters values with respect to particle volume into solution and with respect to scattered intensity, were recorded at different times (Figure 110). As for Zn-BLG, the volume distribution at zero time shows one peak with dimension of 3.6 nm whereas peaks at about 37.8 and 48.8 nm are evident at the other considered times (25 and 85 min). In the presence of CD6HQ, the aggregate formation (at about 50 nm) does not occur, the slight changes in the volume distribution indicate that a small percentage of protein molecules increases its dimension up to 10 nm. As for Zn-BLG-CD6RHQ, the volume distribution remains essentially unchanged in the time range. Taken together, these results indicate that Zn-BLG produces a large amount of aggregates in a short time, whereas in Zn-BLG-CD6HQ and Zn-BLG-CD6RHQ (especially in this latter case) the protein has not yet had a significant aggregation after 420 min.

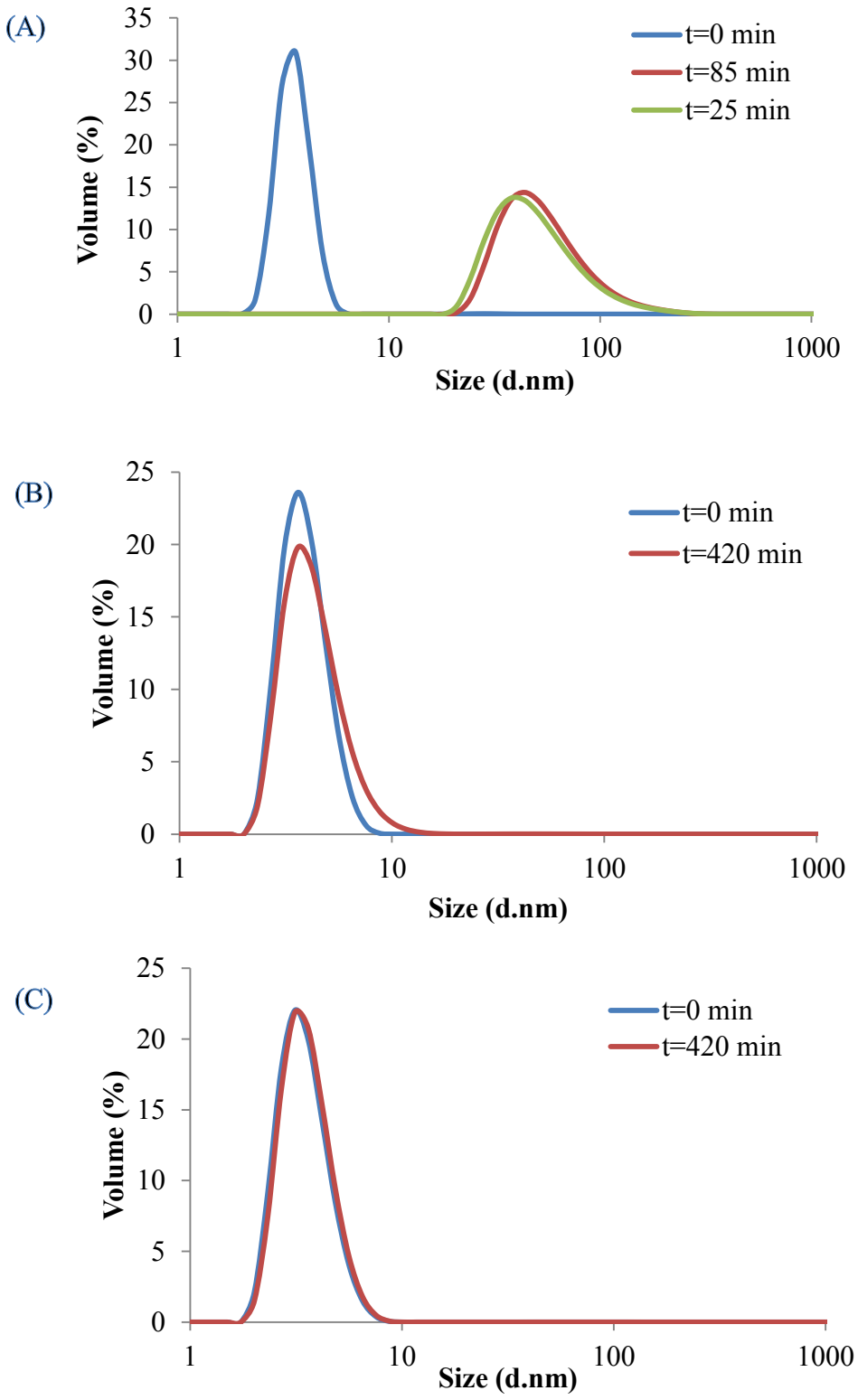

Figure 110. Size distribution of aggregate dimension (particle volume) present into (A) a Zn-BLG solution at initial (t = 0) and times (t = 25 and 85 min) of the scattering kinetics (T = 60 °C) (B) a Zn-CD6HQ-BLG soultion at initial (t = 0) and final time (t = 420 min) of the scattering kinetics (T = 60 °C) (C) a Zn-CD6RHQ-BLG soultion at initial (t = 0) and final time (t = 420 min) of the scattering kinetics (T = 60 °C).

It is noteworthy that, for Cu-BLG and Cu-BLG-CD6HQ, the species are differently distributed with a main size around to 4-5 nm (data not shown). This behavior could explain the different increase of the total scattered intensity shown by Cu-BLG (Figure 102) compared with Cu-BLG-CD6HQ.

5. CONCLUSIONS

The synthetized glycoconjugates are very promising and versatile compounds.

New glucoconjugates and galactoconjugates of OHQs were designed in order to exploit unique and frequent features of cancer cells such as the high expression of certain proteins (e.g. β-glucosidases and GLUT) and the high levels of Cu^{2+}. These features can be synergistically combined to obtain new compounds highly specific for neoplastic cells, minimizing chemotherapeutic side effects. The rationale behind the development of oxine glucoconjugates resides on glucose avidity of cancer cells (PMT approach) whereas galactoconjugates could exploit ADEPT strategy.

Apart from improving aqueous solubility, the main advantages of these glycosylated compounds are targeting and prevention of side effects due to systemic chelation. The chelating function of these compounds is masked and they must be subject to hydrolysis through specific β-glucosidases or β-galactosidases to liberate the active aglycone in targeted cells.

The studies on the glucoconjugates support this hypothesis. In particular, the data in the presence of a β-glucosidase inhibitor (DMDP) unequivocally confirm the crucial role of β-glucosidase activity to allow the release of the active quinoline moiety in order to develop the antiproliferative activity (Figure 111).

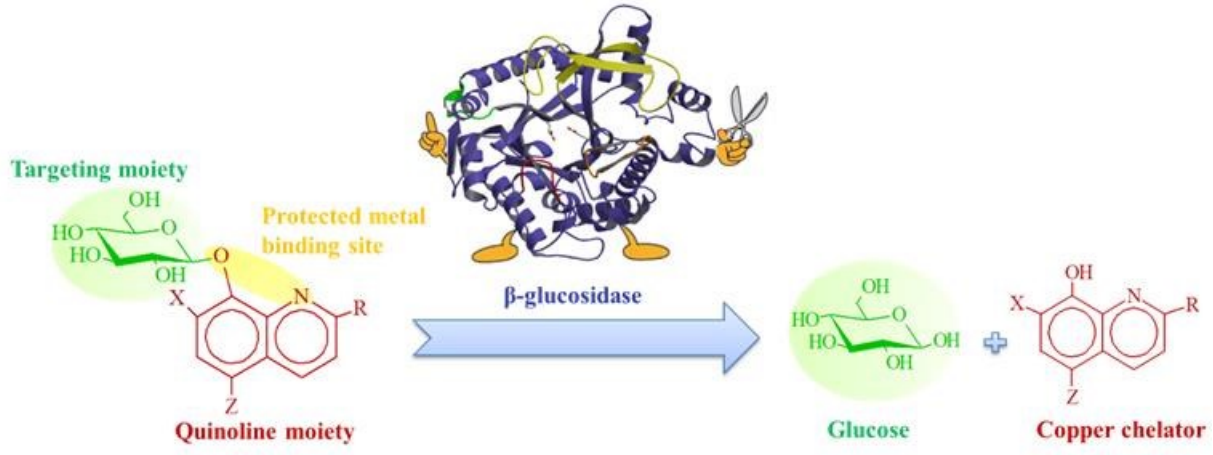

Figure 111. β-glucosidase is crucial in determining the effectiveness of glucoconjugates as the antiproliferative activity reflects their different hydrolysis.

Furthermore, the *in vitro* cleavage studies suggest that the glucoconjugates are differently hydrolyzed by β-glucosidase. These data are consistent with the antiproliferative activity assay and docking studies. In some cases (GluMeHQ, GluCQ and GluOHQ), the antiproliferative activity of the prodrugs was reduced compared to their parent compounds, this finding indicates the incomplete cleavage of the glycosidic bond for these compounds. In particular GluMeHQ, which results inactive, is the compound cleaved in longer times in comparison with the other glucosides. These experimental results are supported by docking studies as GluMeHQ, GluCQ and GluOHQ show a different binding pose compared to chlorinated compounds. More precisely, GluMeHQ has the best binding affinity for the active site of glucosidase. These results suggest that prodrugs with high half-life values are tighter bound to the active site than those with low half-life values. It can be deduced as a logical consequence that the glucoconjugates tightly bound to the enzyme are slowly hydrolyzed.

To sum up, the proposed mechanism of action for glucose-appended OHQ prodrugs can be graphically represented in Figure 112. The glucoconjugates could be actively transported into the cells (e.g. by GLUT). The cytosolic β-glucosidase would hydrolyzed the compounds that would complex Cu^{2+} ions (present in large amount in cancer tissues) and exert their own action. Free OHQs could have multiple targets causing cancer cells to self-destruct.

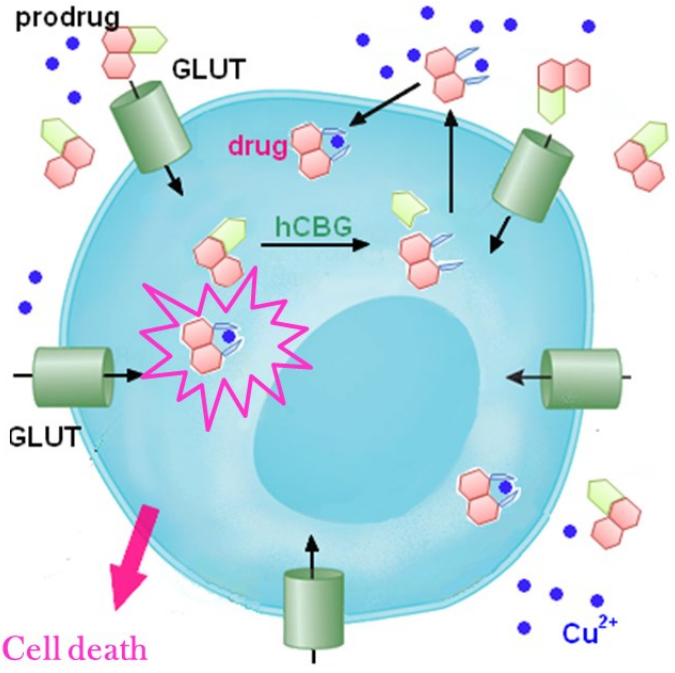

Figure 112. Proposed mechanism of action for OHQ glucoconjugates.

Chemical conjugation of OHQs with galactose leads to new prodrugs with a cytotoxic differential of approximately 100-fold compared to their parent compounds. This degree of prodrug activation is a necessary requirement in developing an ADEPT system. The results reported here strongly suggest that attachment of the galactose residue to OHQ leads to almost complete drug inactivation, and that the glycosidic bond is highly stable under the conditions used in the *in vitro* assay. Interestingly, GalAHQ and GalNHQ show pharmacological relevant activity in the presence of Cu^{2+}. Their activity depends on cancer cell line and they could be good candidates for targeted delivery to human ovarian carcinoma, exploiting PMT approach. Unlike glucoconjugates, galactosides do not easily reach the lysosomal enzyme within the cells and then they are not rapidly cleaved except GalNHQ and GalAHQ that are partially hydrolyzed in 72 h in cell lines where there is an overexpression of galactosidase.

However, the presence of exogenous β-galactosidase increases the antiproliferative activity of the galactoconjugates confirming that the compounds are hydrolyzed by the enzyme and the latter is able to exert its optimal activity at a pH close to that of the tumor extracellular fluid. To conclude, these prodrugs have interesting properties that render them suitable for ADEPT approach (Figure 113).

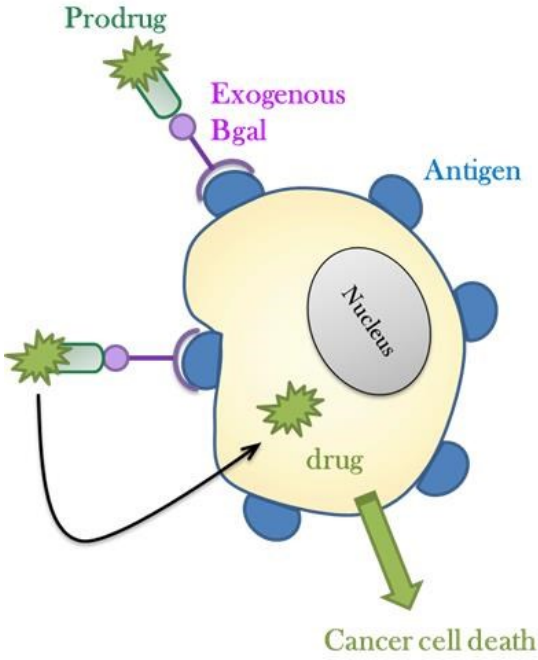

Figure 113. ADEPT approach for the galactoconjugates.

Chelating 8-hydroxyquinoline conjugates with monosaccharides and disaccharides have been synthetized in order to compare their properties to those of the glycosylated prodrugs. Unlike these latter compounds, they are able to complex Cu^{2+} and Zn^{2+} ions, essentially leading to the formation of ML species. Glucose and trehalose have been chosen for their similarity and their properties (Figure 114). In particular, antioxidant and antiproliferative activity assays are under way to verify if their activies depend on the sugar type. However, these systems are promising compounds for the treatment of diseases related to metal dyshomeostasis.

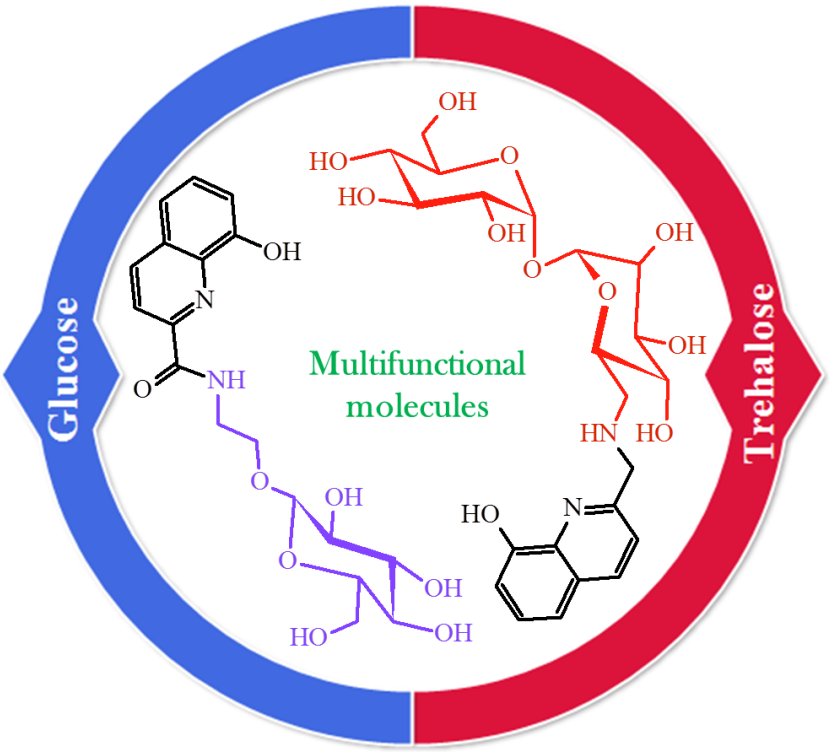

Figure 114. New versatile chelating compounds based on sugars and OHQ.

The new CyD-OHQ conjugates center on the belief that "one molecule-multiple targets" is an approach with remarkable advantages compared to "one molecule-one target" strategy.

CyD-OHQ conjugates have significant antioxidant capacity on the basis of *in vitro* antioxidant assays, superior to that of a well-known antioxidant, Trolox. In particular, ABCD6HQ presents the highest capacity to scavenge free radicals suggesting that it could be a powerful antioxidant with activity comparable to that of several polyphenols.

The compounds can complex Cu^{2+} and Zn^{2+} ions with conditional stability constants in aqueous solution similar or higher to/than those of OHQ. Their Cu^{2+} complexes exhibit high

SOD-like activity. Moreover, these derivatives are also able to strongly inhibit metal-induced protein aggregation and the formation of amyloid fibrils. Obviously, these features are highly desirable considering the critical involvement of metal ions in protein misfolding and aggregation, hallmarks of several neurodegenerative disorders.

Antiproliferative studies of the compounds in the absence or presence of Cu^{2+} on five different cell lines demonstrated relatively high IC_{50} values. These results bode well for administering relatively high concentrations of these derivatives, for use as antioxidant and antiaggregant drugs, if necessary, without damage to healthy tissues. It is clear that CyD moiety renders the systems less toxic compared to the respective OHQ derivatives.

These compounds could have great potential as therapeutic agents in the treatment of neurodegenerative diseases related to oxidative stress and metal dyshomeostasis, such as AD and especially NPC. Apart from improving the aqueous solubility due to the presence of the CyD saccharidic residue, the hybrid systems might have interesting characteristics including the possibility to form inclusion complexes with coformulating drugs and/or to include endogenous compounds (e.g. cholesterol) in order to remove them. Moreover, the presence of the bulky β-CyD moiety might provide a platform for improved pharmacokinetics of the drug conjugates avoiding, for example, glucuronidation or sulfation of OHQs.

Overall, these CyD conjugates are promising multifunctional molecules that combine antioxidant, SOD-like activity, chelating, antiaggregant and inclusion ability into one compound (Figure 115) designed for metal-associated neurodegenerative diseases.

Figure 115. CyD derivatives are multifunctional molecules.

6. ACKNOWLEDGEMENTS

I would like to express my special appreciation and thanks to all those who have contributed to this research proposal.

I want, above everybody else, to express my special appreciation and thanks to my supervisor Prof. Graziella Vecchio, without who nothing would have been possible.

I would like to thank Dr. Maurizio Viale and his colleagues of Department of Integrated Oncological Therapies, IRCCS AOU S. Martino-IST for the biological evaluation of the compounds.

I would like to thank Dr. John Spencer for giving me the opportunity of having an incredible work abroad experience and for his enthusiastic advice in the synthesis of the first cyclodextrin conjugates that has been carried out at Sussex University.

A special thanks goes to Dr. Antonino Puglisi and the other members of Sussex University for their advice and assistance during the period spent at Brighton.

I also wish to thank Dr. Giuseppa Ida Grasso for supplying 6-amino-6-deoxy-α,α'-trehalose.

Thanks also to Prof. Giulia Caron for the docking studies of the glucoconjugates.

A thanks goes to Dr. Carmelo Sgarlata for the determination of conditional stability constants.

Moreover, I am also thankful to my colleagues who have all brought something to help me in my progresses.

Last but not least, I would also like to thank the people who are not related to the chemistry world but whose presence has contributed to where I am today.

7. REFERENCES

1 R. Kitzberger, C. Madl, P. Ferenci, *Metab. Brain Dis.* **2005**, 20, 295.
2 L. M. Miller, Q. Wang, T. P. Telivala, R. J. Smith, A. Lanzirotti, J. J. Miklossy, *Struct. Biol.* **2006**, 155, 30.
3 M. A. Lovell, J. D. Robertson, W. J. Teesdale, J. L. Campbell, W. R. Markesbery, *J. Neurol. Sci.* **1998**, 158, 47.
4 N. B. Cole, D. D. Murphy, J. Lebowitz, L. Di Noto, R. L. Levine, R. L. Nussbaum, *J. Biol. Chem.* **2005**, 280, 9678.
5 M. C. Vazquez, P. Martınez, A. R. Alvarez, M. Gonzalez, S. Zanlungo, *Biometals* **2012**, 25, 777.
6 D. Waldvogel, P. Van Gelderen, M. Hallett, *Ann. Neurol.* **1999**, *46*, 123.
7 T. B. Chaston, D. R. Richardson, *Am. J. Hematol.* **2003**, 73, 200.
8 K. G. Daniel, R. Hope Harbach, W.C. Guida, Q. P. Dou, *Front. Biosci.* **2004**, 9, 2652.
9 M. C. Vazquez, E. Balboa, A. R. Alvarez, S. Zanlungo, *Oxid. Med. Cell. Longevity* **2012**, ID 205713.
10 G. Crisponi, V. M. Nurchia, D. Fanni, C. Gerosa, S. Nemolato, Gavino Faa*, Coord. Chem. Rev.* **2010**, 254, 876.
11 M. C. Linder, M. Hazegh-Azam, *Am. J. Clin. Nutr.* **1996**, 63, 7975.
12 H. Xie, Y. J. Kang, *Curr. Med. Chem.* **2009**, 16, 1304.
13 H. Antony, I. G. Macreadie, *Handbook of Behavior, Food and Nutrition*, V. R. Preedy, R. R. Watson,C. R. Martin, (Eds.), Springer **2011**.
14 T. D. Rae, P. J. Schmidt, R. A. Pufahl, V. C. Culotta, T. V. O'Halloran, *Science* **1999**, 284, 805.
15 A. C. Rosenzweig, *Chem. Biol.* **2002**, 9, 673.
16 P. Delangle, E. Mintz, *Dalton Trans.* **2012**, 41, 6359.
17 G. Mitteregger, S. Korte, M. Shakarami, J. Herms, H.A. Kretzschmar, *Brain Res*. **2009**, 1292, 155.
18 J. D. F. Wadsworth, A. F. Hill, S. Joiner, G. S. Jackson, A. R. Clarke, J. Collinge, *Nat. Cell Biol.* **1999**, 1, 55.
19 R. C. Nadal, S. R. Abdelraheim, M. W. Brazier, S. E. Rigby, D. R. Brown, J. H. Viles, *Free Radic. Biol. Med.* **2007**, 42, 79.
20 T. Canello, R. Engelstein, O. Moshel, K. Xanthopoulos, M. E. Juanes, J. Langeveld, T. Sklaviadis, M. Gasset, R. Gabizon, *Biochemistry*, **2008**, 47, 8866.
21 E. M. Sigurdsson, D. R. Brown, M. A. Alim, H. Scholtzova, R. Carp, H. C. Meeker, F. Prelli, B. Frangione, T. Wisniewski, *J. Biol. Chem.* **2003**, 278, 46199.
22 J. H. Fox, J. A. Kama, G. Lieberman, R. Chopra, K. Dorsey, V. Chopra, I. Volitakis, R. A. Cherny, A. I. Bush, S. Hersch, *PLoS One* **2007**, *2*, e334.
23 A. I. Bush, R. E. Tanzi, *Neurotherapeutics* **2008**, 5, 421.
24 A. Gupte, R. J. Mumpe, *Cancer Treat. Rev.* **2009**, 35, 32.
25 G. D. Kaiafa, Z. Saouli, M. D. Diamantidis, Z. Kontoninas, V. Voulgaridou, M. Raptaki, S. Arampatzi, M. Chatzidimitriou, V. Perifanis, *Eur. J. Intern. Med.* **2012**, 23, 738.

26 L. Finney, S. Mandava, L. Ursos,. W. Zhang, D. Rodi, S. Vogt, D. Legnini, J. Maser, F. Ikpatt, O. I. Olopade, D. Glesne, *Proc. Natl. Acad. Sci. U. S. A.* **2007**, 104, 2247.
27 K. S. Raju, G. Alessandri, M. Ziche, P. M. Gullino, *J. Natl. Cancer Inst.* **1982**, 69, 1183.
28 G. Alessandri, K. Raju, P. M. Gullino, *Microcirc. Endoth. Lym.* **1984**, 1, 329.
29 V. L. Goodman, G. J. Brewer, S. D. Merajver. *Endocr. Relat. Cancer.* **2004**, 11, 255.
30 C. Yanagimoto, M. Harada, H. Kumemura, M. Abe, H. Koga, M. Sakata, T. Kawaguchi, K. Terada, S. Hanada, E. Taniguchi, H. Ninomiya, T. Ueno, T. Sugiyama, M. Sata, *Hepatol. Res.* **2011**, 41, 484.
31 M. C. Vázquez, T. del Pozo, F. A. Robledo, G. Carrasco, L. Pavez, F. Olivares, M. Gonzalez, S. Zanlungo, *PLoS ONE* **2011**, 6, e28777.
32 C. E. Outten, T. V. O'Halloran, *Science* **2001**, 292, 2488.
33 M. R. Bleackley, R. T. A. MacGillivray, *Biometals* **2011**, 24, 785.
34 M. Valko, H. Morris, M. T. D. Cronin, *Curr. Med. Chem.* **2005**, 12, 1161.
35 E. John, T. C. Laskow, W. J. Buchser, B. R. Pitt, P. H. Basse, L. H. Butterfield, P. Kalinski, M. T. Lotze, *J. Transl. Med.* **2010**, 8, 118.
36 A. I. Bush, *Trends Neurosci.* **2003**, 26, 207.
37 S. L. Sensi, P. Paoletti, A. I. Bush, I. Sekler, *Nat. Rev. Neurosci.* **2009**, 10, 780.
38 G. J. Anderson, C. D. Vulpe, *Cell. Mol. Life Sci.* **2009**, 66, 3241.
39 A. Lawen, D. J. R. Lane, *Antioxid. redox sign.* **2013**, 18, 2473.
40 D. Ben-Shachar, G. Eshel, J. P. M. Finberg, M. B. H. Youdim, *J. Neurochem*. **1991**, 56, 1441.
41 D. Kaur, F. Yantiri, S. Rajagopalan, J. Kumar, J. Q. Mo, R. Boonplueang, V. Viswanath, R. Jacobs, L. Yang, M. F. Beal, D. DiMonte, I. Volitaskis, L. Ellerby, R. A. Cherny, A. I. Bush, J. K. Andersen, *Neuron* **2003**, 37, 899.
42 N. Olivieri, G. Koren, C. Hermann, Y. Bentur, D. Chung, J. Klein, S. T. P. Louis, M. H. Freedman, R. A. Mcclelland, D. M. Templeton, *Lancet* **1990**, 336**,** 1275.
43 A. Kolnagou, C. Economides, E. Eracleous, G. J. Kontoghiorghes, *Hemoglobin* **2008**, 32, 41.
44 F. Molina-Holgado, A. Gaeta, P. T. Francis, R. J. Williams, R. C. Hider, *J. Neurochem.* **2008**, 105, 2466.
45 D. R. Richardson, D. S. Kalinowski, S. Lau, P. J. Jansson, D. B. Lovejoy, *BBA-Gen. Subjects* **2009**, 1790, 702.
46 S. S. Brem, D. Zagzag, A. M. Tsanaclis, S. Gately, M. P. Elkouby, S. E. Brien, *Am. J. Pathol.* **1990**, 137, 1121.
47 Q. Pan, C. G. Kleer, K. L. van Golen, J. Irani, K. M. Bottema, C. Bias, M. De Carvalho, E. A. Mesri, D. M. Robins, R. D. Dick, G. J. Brewer, S. D. Merajver, *Cancer Res.* **2002**, 62, 4854.
48 M. Hayashi, H. Nishiya, T. Chiba, D. Endoh, Y. Kon, T. Ohui, *Lab. Animal. Sci*. **2007**, 69, 137.
49 J. Yoshii, H. Yoshiji, S. Kuriyama, Y. Ikenaka, R. Noguchi, H. Okuda, H. Tsujinoue, T. Nakatani, H. Kishida, D. Nakae, D. E. Gomez, M. S. De Lorenzo, A. M. Tejera, H. Fukui, *Int. J. Cancer* **2001**, 94, 768.
50 G. J. Brewer, R. D. Dick, D. K. Grover, V. LeClaire, M. Tseng, M. Wicha, K. Pienta, B.G. Redman, T. Jahan, V. K. Sondak, M. Strawderman, G. LeCarpentier, S. D. Merajver, *Clin Cancer Res.* **2000**, 6, 1.

51 B. G. Redman, P. Esper, Q. Pan, R. L. Dunn, H. K. Hussain, T. Chenevert, G. J. Brewer, S. D. Merajver, *Clin. Cancer Res*. **2003**, 9, 1666.
52 A. D. Schimmer, *Curr. Cancer Drug Targets* **2011**, 11, 325.
53 L. W. Hung, K. Barnham, *Future Med. Chem.* **2012**, 4, 955.
54 S. Gal, H. Zheng, M. Fridkin, M. B. H. Youdim, *Neurotox. Res.* **2010**, 17, 15.
55 X. Mao, A. D. Schimmer, *Toxicol. Lett.* **2008**, 182, 1.
56 C. Grossi, S. Francese, A. Casini, M. C. Rosi, I. Luccarini, A. Fiorentini, C. Gabbiani, L. Messori, G. Moneti, F. Casamenti, *J. Alzheimer's Dis.* **2009**, 17, 423.
57 R. A. Cherny, J. T. Legg, C. A. McLean, D. P. Fairlie, X. Huang, C. S. Atwood, K. Beyreuther, R. E. Tanzi, C. L. Masters, A. I. Bush, *J. Biol. Chem.* **1999**, 274, 23223.
58 C. W. Ritchie, A. I. Bush, A. Mackinnon, S. Macfarlane, M. Mastwyk, L. MacGregor, L. Kiers, R. Cherny, Q.-X. Li, A. Tammer, D. Carrington, C. Mavros, I. Volitakis, M. Xilinas, D. Ames, S. Davis, K. Beyreuther, R. E. Tanzi, C. L. Masters, *Arch. Neurol.* **2003**, 60, 1685.
59 L. Cahoon, *Nat. Med.* **2009**, 15, 356.
60 http://clinicaltrials.gov.
61 R. A. Cherny, S. Ayton, D. I. Finkelstein, A. I. Bush, G. McColl, S. M. Massa, *J. Huntington Dis.* **2012**, 1, 211.
62 S. R. Bareggi, U. Cornelli, *CNS Neurosci. Ther.* **2012**, 18, 41.
63 http://clinicaltrials.gov/ct2/show/study/NCT00963495
64 S. Zhai, L. Yang, Q. C. Cui, Y. Sun, Q. P. Dou, B. Yan, *J. Biol. Inorg. Chem.* **2010**, 15, 259.
65 A. D. Schimmer, *Curr. Cancer Drug Targets* **2011**, 11, 325.
66 V. Milacic, P. Jiao, B. Zhang, B. Yan, Q. P. Dou, *Int. J. Oncol.* **2009**, 35, 1481.
67 W. Q. Ding, B. Liu, J. L. Vaught, H. Yamauchi, S. E. Lind, C*ancer Res.* **2005**, 65, 3389.
68 M. A. Cater, Y. Haupt, *Biochem. J*. **2011**, 436, 481.
69 M. Katsuyama, K. Iwata, M. Ibi, K. Matsuno, M. Matsumoto, C. Yale-Nishimura, *Toxicology* **2012**, 299, 55.
70 J. Kopecek, P. Kopeckova, T. Minko, Z. R. Lu, C. Peterson, *J. Control. Release* **2001**, 74, 147.
71 S. S. Dharap, B. Qiu, G. Williams, P. Sinko, S. Stein, T. Minko, *J. Control. Release* **2003**, 91, 61.
72 N. Bodor, P. Buchwald, *Drug Discov. Today* **2002**, 7, 766.
73 B. Testa, *Curr. Opin. Chem. Biol.* **2009**, 13, 338
74 S. Wang, D. Liu, X. Zhang, S. Li, Y. Sun, J. Li, Y. Zhou, L. Zhang, *Carbohydr. Res.* **2007**, 342, 1254.
75 L. F. Tietze, H. J. Schuster, B. Krewer, I. Schuberth, *J. Med. Chem.* **2009**, 52, 537.
76 I. Niculescu-Duvaz, C. J. Springer, *Adv. Drug Deliver. Rev.* **1997**, 26, 151.
77 K. D. Bagshawe, *Curr. Drug Targets* **2009**, 10, 152.
78 H. Devalapallya, R. S. Navath, V. Yenamandra, R. R. Akkinepally1, R. K. Devarakonda, *Arch. Pharm. Res.* **2007,** 30, 723.
79 M. de Graaf, E. Boven, H. W. Scheeren, H. J. Haisma, H. M. Pinedo, *Curr. Pharm. Des.* **2002**, 8, 1391.
80 E. Bakina, Z. Wu, M. Rosenblum, D. Farquhar, *J. Med. Chem.* **1997**, 40, 4013.

81 B. Sperker, U. Werner, T. E. Mürdter, C. Tekkaya, P. Fritz, R. Wacke, U. Adam, M. Gerken, B. Drewelow, H. K. Kroemer, *Arch. Pharmacol.* **2000**, 362, 110.
82 D. J. Burkhart, B. L. Barthel, G. C. Post, B. T. Kalet, J. W. Nafie, R. K. Shoemaker, T. H. Koch, *J. Med. Chem.* **2006**, 49, 7002.
83 G. Xu, W. Zhang, M. K. Ma, H. L. McLeod, *Clin. Cancer Res.* **2002**, 8, 2605.
84 M. Kovar, J. Strohalm, T. Etrych, K. Ulbrich, B. Rihova, *Bioconjugate Chem.* **2002**, 13, 206.
85 N. Agarwal, D. H. Rich, *Anal. Biochem.* **1983**, 130, 158.
86 R. Denmeade, J. T. Isaacs, *Nat. Rev. Cancer* **2002**, 2, 389.
87 T. Kline, M. Y. Torgov, B. A. Mendelsohn, C. G. Cerveny, P. D. Senter, *Mol. Pharm.* **2004**, 1, 9.
88 F . Kratz, J. Drevs, G. Bing, C. Stockmar, K. Scheuermann, P. Lazar, C. Unger, *Bioorg. Med. Chem. Lett.* **2001**, 11, 2001.
89 F. Kratz, I. A. Muller, C. Ryppa, A. Warnecke, *Chem. Med. Chem.* **2008**, 3, 20.
90 D. Schrama, R. A. Reisfeld, J. C. Becker, *Nature Rev.* **2006**, 5, 147.
91 G. Xu, H. L. McLeod, *Clin. Cancer Res.* **2001**, 7, 3314.
92 H. Lahm, S. Andre, A. Hoeflich, J. R. Fisher, *J. Cancer Res. Clin. Oncol.* **2001**, 127, 375.
93 E. J. Bilsky, R. D. Egleton, S. A. Mitchell, M. M. Palian, P. Davis, J. D. Huber, H. Jones, H. I. Yamamura, J. Janders, T. P. Davis, F. Porreca, V. J. Hruby, R. Polt, *J. Med. Chem.* **2000**, 43, 2586.
94 C. Fernandez, O. Nieto, E. Rivas, G. Montenegro, J. A. Fontenla, A. Fernandez-Mayoralas, *Carbohydr. Res.* **2000**, 327, 35.
95 M. Zhang, Z. H. Zhang, D. Blessington, H. Li, T. M. Busch, V. Madrak, J. Miles, B. Chance, J. D. Glickson, G. Zheng, *Bioconjugate Chem*. **2003**, 14, 709.
96 L. E. Scott, B. D. G. Page, B. O. Patrick, C. Orvig**,** *Dalton Trans.* **2008**, 6364.
97 L. E. Scott, M. Telpoukhovskaia, C. Rodrıguez, M. Merkel, M. L. Bowen, B. D. G. Page, D. E. Green, T. Storr, F. Thomas, D. D. Allen, P. R. Lockman, B. O. Patrick, M. J. Adam, C. Orvig, *Chem. Sci.* **2011**, 2, 642.
98 C. D. Young, S. M. Anderson, *Breast Cancer Res.* **2008**, 10, 202.
99 Y.-S. Lin, R. Tungpradit, S. Sinchaikul, F.-M. An, D.-Z. Liu, S. Phutrakul, S.-T. Chen, *J. Med. Chem.* **2008**, 51, 7428.
100 K. C. Carvalho, I. W. Cunha, R. M. Rocha, F. R. Ayala, M. M. Cajaíba, M. D. Begnami, R. S. Vilela, G. R. Paiva, R. G. Andrade, F. A. Soares, *Clinics* (Sao Paulo) **2011**, 66, 965.
101 T. Nishioka, Y. Oda, Y. Seino, T. Yamamoto, N. Inagaki, H. Yano, H. Imura, R. Shigemoto, H. Kikuchi, *Cancer Res.* **1992**, 52, 3972.
102 H. M. M. Arafa, *Eur. J. Pharmacol.* **2009**, 616, 58.
103 K. N. Syrigos, G. Rowlinson-Busza, A. A. Epenetos, *Int. J. Cancer* **1998**, 78, 712.
104 M. De Graaf, H. M. Pinedo, R. Quadir, H. J. Haisma, E. Boven, *Biochem. Pharmacol.* **2003**, 65, 1875.
105 M. Nomoto, K. Yamada, M. Haga, M. Hayashi, *J. Pharm. Sci.* **1998**, 87, 326.
106 W. Li, Z.-W. Zhang, S.-X. Wang, S.-M. Ren, T. Jiang, *Chem. Biol. Drug Des.* **2009**, 74, 80.
107 H. M. Arafa, *Invest. New Drugs* **2010**, 28, 306.

108 H. Schugar, D. E. Green, M. L. Bowen, L. E. Scott, T. Storr, K. Bohmerle, F. Thomas, D. D. Allen, P.R. Lockman, M. Merkel, K. H. Thompson, C. Orvig, *Angew. Chem. Int. Ed. Engl.* **2007**, 46, 1716.
109 T. Storr, L. E. Scott, M. L Bowen, D. E. Green, K. H. Thompson, H. J. Schugar, C. Orvig, *Dalton Tans.* **2009**, 3034.
110 T. Storr, M. Merkel, G. X. Song-Zhao, L. E. Scott, D. E. Green, M. L. Bowen, K. H. Thompson, B. O. Patrick, H. J. Schugar, C. Orvig, *J. Am. Chem. Soc.* **2007**, 23, 7459.
111 D. E. Green, M. L. Bowen, L. E. Scott, T. Storr, M. Merkel, K. Bohmerle, K. H. Thompson, B. O. Patrick, H. J. Schugar, C. Orvig, *Dalton Trans.* **2010**, 39, 1604.
112 M. S. Wadhwa, K. G. Rice, *J. Drug Target.* **1995**, 3, 111.
113 C. Bies, C. M. Lehr, J. F. Woodley, *Adv. Drug Deliv. Rev.* **2004**, 56, 425.
114 J. Almkvist, A. Karlsson, *Glycoconjugate J.* **2004**, 19, 575.
115 M. Hirashima, Y. Kashio, N. Nishi, A. Yamauchi, T. A. Imaizumi, T. Kageshita, N. Saita, T. Nakamura, *Glycoconjugate J.* **2004**, 19, 593.
116 M. Huflejt, H. Leffler, *Glycoconjugate J.* **2004**, 20, 247.
117 Y. Takenaka, T. Fukumori, A. Raz, *Glycoconjugate J.* **2004**, 19, 543.
118 B. A. Salameh, A. Sundin, H. Leffler, U. J. Nilsson, *Bioorg. Med.Chem,* **2006**, 14, 1215.
119 P. J. Davidson, M. J. Davis, R. J. Patterson, M. A. Ripoche, *Glycobiology* **2002**, 12, 329.
120 R.Y. Yang, D. K. Hsu, F. T. Liu, *Proc. Natl. Acad. Sci. USA,* **1996**, 93, 6737.
121 W. Zhu, H. Sano, R. Nagai, K. Fukuhara, A. Miyazaki, S. Horiuchi, *Biochem. Biophys. Res. Commun.* **2001**, 280, 1183.
122 V. Furtak, F. Hatcher, J. Ochieng, *Biochem. Biophys. Res. Commun.* **2001**, 289, 845.
123 H. Lahmm, S. Andre, A. Hoeflich, *J. Cancer Res. Clin. Oncol.* **2001**, 127, 375.
124 R. Grutzmann, C. Pilarsky, O. Ammerpohl, J. Luttges, A. Bohme, B. Sipos, M. Foerder, I. Alldinger, B. Jahnke, H. K. Schackert, H. Kalthoff, B. Kremer, G. Kloppel, H. D. Saeger, *Neoplasia* **2004**, 6, 611.
125 J. Shen, M. D. Person, J. Zhu, J. L. Abbruzzese, D. Li, *Cancer Res.* **2004**, 64, 9018.
126 G. Choufani, N. Nagy, S. Saussez, H. Marchant, P. Bisschop, M. Burchert, A. Danguy, S. Louryan, I. Salmon, H. J. Gabius, R. Kiss, S. Hassid, *Cancer* **1999**, 86, 2353.
127 V. Balan, P. Nangia-Makker, A. Raz, *Cancers* **2010**, 2, 592.
128 A. M. Pujol, M. Cuillel, O. Renaudet, C. Lebrun, P. Charbonnier, D. Cassio, C. Gateau, P. Dumy, E. Mintz, P. Delangle, *J. Am. Chem. Soc.* **2010**, 133, 286.
129 A. M. Pujol, M. Cuillel, A.-S. Jullien, C. Lebrun, D. Cassio, E. Mintz, C. Gateau P. Delangle, *Angew. Chem.* **2012**, 124, 7563.
130 E. N. Olsufyeva, A. N. Tevyashova, I. D. Trestchalin, M. N. Preobrazhenskaya, D. Platt, A. Klyosov, *Carbohydr. Res.* **2003**, 338, 1359.
131 H. Cheng, X. Cao, M. Xian, L. Fang, T. Bill Cai, J. J. Ji, J. B. Tunac, D. Sun, P. G. Wang, *J. Med. Chem.* **2005**, 48*,* 645.
132 M. de Graaf, H. M. Pinedo, R. Quadir, H. J. Haisma, E. Boven, *Biochem. Pharmacol.* **2003**, 65, 1875.
133 A. I. Rosenbaum, G. Zhang, J. D. Warren, F. R. Maxfield, *Proc. Natl. Acad. Sci. USA* **2010**, 107, 5477.
134 F. Hirayama, K. Uekama, *Adv. Drug Delivery Rev*. **1999,** 36, 125.
135 M. Komiyama, M. L. Bender, *The Chemistry of Enzyme Action*, M. I. Page (Ed.), Elsevier, **1984**.

136 I. Tabushi, Y. Kuroda, T. Mizutani, *Tetrahedron* **1984**, 40, 545.
137 V. T. Souza, M. L. Bender, *Acc. Chem. Res.* **1987**, 20, 146.
138 R. Breslow, *Adv. Enzymol. Relat. Areas. Mol. Biol.* **1986**, 58, 1.
139 R. Breslow, *Pure and Appl. Chem*. **1994**, 66, 1573.
140 W. Tagaki, H. Yamamoto, *Tetrahedron Lett.* **1991,** 32, 1207.
141 S. Tamagaki, J. Narikawa, A. Katayama, *Bull. Chem. Soc. Jpn.* **1996***,* 69, 2265.
142 I. Tabushi, Y. Kuroda, T. Mizutani, *J. Am. Chem. Soc.* **1986**, 108, 4514.
143 G. Galaverna, R. Corradini, A. Dossena, R. Marchelli, G. Vecchio, *Electrophoresis* **1997**, 18, 905.
144 K. Kano, *J. Phys. Org. Chem.* **1997**, 10, 286.
145 C. J. Easton, S. F. Lincoln*, Chem. Soc. Rev.* **1996***,* 163.
146 S. E. Brown, J. H. Coates, P. A. Duckworth, S. F. Licoln, C. J. Easton, B. May, *J. Chem. Soc. Faraday Trans. 2* **1993**, 1035.
147 Y. Liu, B-H. Han, B. Li, Y.-M. Zhang, P. Zhang, P. Zhao, Y.-T. Chen, T. Wada, Y. Inoe, *J. Org. Chem*. **1998**, 63, 1444.
148 P. K. Owens, A. F. Fell, M. W. Coleman, J. C. Berridge, *J .Chromatogr. A*, **1998**, 797, 149.
149 A. M. Amorini, F. Bellia, V. Di Pietro, B. Giardina, D. La Mendola, G. Lazzarino, S. Sortino, B. Tavazzi, E. Rizzarelli, G. Vecchio, *Eur. J. Med. Chem.* **2007**, 42, 910.
150 T. Liu, B. Li, B.-H. Han, Y.-M. Li, R.-T. Chen, *J. Chem. Soc. Perkin Trans 2* **1997**, 1275.
151 Y. Liu, Y-M. Zhang, A-D. Qi, R-T. Chen, K. Yamamoto, T. Wada, Y. Inoe, *J. Org. Chem*. **1997**, 62, 1826.
152 H. Ikeda, M. Nakamura, N. Ise, N. Oguma, A. Nakamura, T. Ikeda, F. Toda, A. Ueno, *J. Am. Chem. Soc.* **1996**, 118, 10980.
153 I. Tabushi, N. Shimizu, T. Sugimoto, M. Shiozuka, K. Yamamura, *J. Am. Chem. Soc.* **1977**, 99, 7100.
154 R. Corradini, A. Dossena, G. Galaverna, R. Marchelli, A. Panagia, G. Sartor, *J. Org. Chem.* **1997**, 62, 6283.
155 R. Breslow, L.E. Overman*, J. Am. Chem. Soc.* **1970**, 92, 1075.
156 M. Rezac, R. Breslow, *Tetrahedron Lett.* **1997**, 38, 5763.
157 R. P. Bonomo, V. Cucinotta, F. D' Alessandro, G. Impellizzeri, G. Maccarrone, G. Vecchio, E. Rizzarelli, *Inorg. Chem*. **1991**, 30, 2708.
158 D. La Mendola, S. Sortino, G. Vecchio, E. Rizzarelli, *Helv. Chim. Acta* **2002**, 85, 1633.
159 R. P. Bonomo, V. Bruno, E. Conte, G. De Guidi, D. La Mendola, G. Maccarrone, F. Nicoletti, E. Rizzarelli, S. Sortino, G. Vecchio, *Dalton Trans*. **2003**, 4406.
160 M. Voicescu, G. Ionita, M. Vasilescu, A. Meghea, *J. Inc. Phenom. Macrocycl. Chem.* **2006**, 54, 217.
161 S. Svenson , M. Wolfgang, J. Hwang, J. Ryan, S. Eliasof, *J. Control. Release* **2011**, 153, 49.
162 J. Kralova, Z. Kejık, T. Brıza, P. Pouckova, A. Kral, P. Martasek, V. Kral, *J. Med. Chem.* **2010**, 53, 128.
163 A. Puglisi, J. Spencer, J. Clarke, J. Milton, *J. Inclusion Phenom. Macrocyclic Chem.* **2012**, 73, 475.
164 B. Di Blasio, S. Galdiero, M. Saviano, C. Pedone, E. Benedetti, E. Rizzarelli, S. Pedotti, G. Vecchio, W. A. Gibbons, *Carbohydr. Res*. **1996**, 282, 41.

165 V. Cucinotta, A. Giuffrida, D. La Mendola, G. Maccarrone, A. Puglisi, E. Rizzarelli, G. Vecchio, *J. Chromatogr. B*, **2004**, 800, 127.
166 H. A. Flaschka, *EDTA Titrations*, Pergamon, **1959**.
167 R. M. Smith, A. E. Martell, *Critical Stability Constants*, Plenum, **1976**.
168 P. Gans, A. Sabatini, A. Vacca, *Talanta* **1996**, 43, 1739.
169 M. Viale, C. Cordazzo, D. de Totero, R. Budriesi, C. Rosano, A. Leoni, P. Ioan, C. Aiello, M. Croce, A. Andreani, M. Rambaldi, P. Russo, A. Chiarini, D. Spinelli, *Invest. New Drugs* **2011**, 29, 98.
170 http://www.molecular-networks.com/node/1
171 O. Trott, A. J. Olson, *J. Comput. Chem.* **2010**, 31, 455.
172 S. Cross, M. Baroni, E. Carosati, P. Benedetti, S. Clementi, *J. Chem. Inf. Model.* **2010**, 50, 1442.
173 S. Tribolo, J.-G. Berrin, P. A. Kroon, M. Czjzek, N. Juge, *J Mol. Biol.* **2007**, 370, 964.
174 Y. Mimaki, K. Watanabe, Y. Ando, C. Sakuma, Y. Sashida, S. Furuya, H. Sakagami, *J. Nat. Prod.* **2001**, 64, 17.
175 A. Budimir, N. Humbert, M. Elhabiri, I. Osinska, M. Birus, A-M. Albrecht-Gary, *J. Inorg. Biochem.* **2011**, 105, 490.
176 C. Bruyère, S. Madonna, G. Van Goietsenoven, V. Mathieu, J. Dessolin, J.-L. Kraus, F. Lefranc, R. Kiss, *Transl. Oncol.* **2011**, 4, 126.
177 Y. Mimaki, K. Watanabe, Y. Ando, C. Sakuma, Y. Sashida, S. Furuya, H. Sakagami, *J. Nat. Prod.* **2001**, 64, 17.
178 A. Rodger, B. Norden, *Circular Dichroism and Linear Dichroism*, Oxford University Press, **1997**.
179 A. Kamal, V. Tekumalla, A. Krishnan, M. Pal-Bhadra, U. Bhadra, *Chem. Med. Chem.* **2008**, 3, 794.
180 E. Gil-Martín, S. Gil-Seijo, C. Nieto-Novoa, A. Fernández-Briera, *Int. J. Biochem. Cell. Biol.* **1996**, 28, 651.
181 C. Donzè, E. Rizzarelli, G. Vecchio, *J. Inclusion Phenom. Mol. Recognit. Chem*. **1998**, 31, 27.
182 F. Bellia, D. La Mendola, C. Pedone, E. Rizzarelli, M. Saviano, G. Vecchio, *Chem. Soc. Rev.* **2009**, 38, 2756 and references therein.
183 M. Kodaka, *J. Phys. Chem.* **1991**, 95, 2110.
184 B. Balan, D. L. Sivadas, K. R. Gopidas, *Org. Lett.* **2007**, 9, 2709.
185 R. Corradini, A. Dossena, R. Marchelli, A. Panagia, G. Sartor, M. Saviano, A. Lombardi, V. Pavone, *Chem. Eur. J.* **1996**, 2, 373.
186 N. Kobayashi, *J. Chem. Soc. Chem. Commun.* **1988**, 918.
187 X.-M. Gao, L.-H. Tong, Y.-L. Zhang, A.-Y. Hao, Y. Inoue, *Tetrahedron Lett.* **1999**, 40, 969.
188 M. Karplus, *J. Am. Chem. Soc.* **1963**, 85, 2870.
189 R. P. Bonomo, V. Bruno, E. Conte, G. De Guidi, D. La Mendola, G. Maccarrone, F. Nicoletti, E. Rizzarelli, S. Sortino, G. Vecchio, *Dalton Trans.* **2003**, 4406.
190 L. Xue, H.-H. Wang, X.-J. Wang, H. Jiang, *Inorg. Chem.* **2008**, 47, 4310.
191 E. Terazzi, L. Guènée, B. Bocquet, J.-F. Lemonnier, N. Dalla Favera, C. Piguet, *Chem. Eur. J.* **2009**, 15, 12719.

192 M. Kajtar, C. Horvath-Toro, E. Kuthi, J. Szejtli, *Acta Chim. Acad. Sci. Hung*. **1982**, 110, 327.
193 K. Harata, H. Uedaira, *Bull. Chem. Soc. Jpn.* **1975**, 48, 375.
194 M. Kodaka, *J. Am. Chem. Soc.* **1993**, 115, 3702.
195 H. E. Mash, Y.-P. Chin, L. Sigg, R. Hari, H. Xue, *Anal. Chem.* **2003**, 75, 671.
196 G. H. Nancollas, M. B. Tomson, *Pure Appl. Chem.* **1982**, 54, 2675.
197 C. Deraeve, A. Maraval, L. Vendier, V. Faugeroux, M. Pitiè, B. Meunier, *Eur. J. Inorg. Chem.* **2008**, 5622.
198 C. Deraeve, C. Boldron, A. Maraval, H. Mazarguil, H. Gornitzka, L. Vendier, M. Pitiè, B. Meunier, *Chem. Eur. J.* **2008**, 14, 682.
199 M. Di Vaira, C. Bazzicalupi, P. Orioli, L. Messori, B. Bruni, P. Zatta, *Inorg. Chem.* **2004**, 43, 3795.
200 A. Budimir, N. Humbert, M. Elhabiri, I. Osinska, M. Birus, A.-M. Albrecht-Gary, *J. Inorg. Biochem.* **2011**, 105, 490.
201 M. Nakamura, C. Kitamura, H. Ueyama, K. Yamana, A. Yoneda, *Anal. Sci. X-ray Struct. Anal. Online* **2005**, 21, 403.
202 F. C. McDonald, R. C. Applefield, C. J. Halkides, J. H. Reibenspies, R. D. Hancock, *Inorg. Chim. Acta* **2008**, 361, 1937.
203 A. Puglisi, J. Spencer, V. Oliveri, G. Vecchio, X. Kong, J. Clarke, J. Milton, *Dalton Trans.* **2012**, 41, 2877.
204 H. Sigel, R. B. Martin, *Chem. Rev.* **1982**, 82, 385.
205 K. V. Reddy, S.-J. Jin, P. K. Arora, D. S. Sfeir, S. C. F. Maloney, F. L. Urbach, L. M. Sayre, *J. Am. Chem. Soc.* **1990**, 112, 2332.
206 J. Sanmartin-Matalobos, C. Portela-Garcia, L. Martinez-Rodriguez, C. Gonzalez-Bello, E. Lence, A. M. Garcia- Deibe, M. Fondo, *Dalton Trans.* **2012**, 41, 6998.
207 V. B. Kenche, I. Zawisza, C. L. Masters, W. Bal, K. J. Barnham, S. C. Drew, *Inorg. Chem.* **2013**, 52, 4303.
208 R. L. Stevenson, H. Freiser, *Anal. Chem.* **1967**, 39, 1354.
209 A. R. Amundsen, J. Whelan, B. Bosnich, *J. Am. Chem. Soc.* **1977**, 99, 6730.
210 M. Mameli, M. C. Aragoni, M. Arca, C. Caltagirone, F. Demartin, G. Farruggia, G. De Filippo, F. A. Devillanova, A. Garau, F. Isaia, V. Lippolis, S. Murgia, L. Prodi, A. Pintus, A. Zaccheroni, *Chem. Eur. J.* **2010**, 16, 919.
211 J. L. Hickey, P. J. Crouch, S. Mey, A. Caragounis, J. M. White, A. R. White, P. S. Donnelly, *Dalton Trans.* **2011**, 40, 1338.
212 F. Bellia, D. La Mendola, G. Maccarrone, P. Mineo, D. Vitalini, E. Scamporrino, S. Sortino, G. Vecchio, E. Rizzarelli, *Inorg. Chim. Acta* **2007**, 360, 945.
213 M. L. Ramos, L. L. G. Justino, A. Branco, C. M. G. Duarte, P. E. Abreu, S. M. Fonseca, H. D. Burrowsa, *Dalton Trans.* **2011**, 40, 11732.
214 H. Jiang, J. E. Taggart, X. Zhang, D. M. Benbrook, S. E. Lind, W-.Q. Ding, *Cancer Lett.* **2011**, 312, 11.
215 T. Terada, Y. Kitamura, K. Ashida, Y. Matsunaga, M. Kato, K. Harada, T. Morita, T. Ohta, Y. Nakanuma, *Virchows Arch.* **1997**, 431, 195.
216 V. Oliveri, M. L. Giuffrida, G. Vecchio, C. Aiello, M. Viale, *Dalton Trans.* **2012**, 41, 4530.

217 V. Oliveri, M. Viale, G. Caron, C. Aiello, R. Gangemi, G. Vecchio, *Dalton Trans.* **2013**, 42, 2023.
218 G. Perry, A. D. Cash, M. A. Smith, *J. Biomed. Biotechnol.* **2002**, 2120.
219 R. Fu, N. M. Yanjanin, S. Bianconi, W. J. Pavan, F. D. Porter, *Mol. Genet. Metab.* **2010**, 101, 214.
220 B. Uttara, A. V. Singh, P. Zamboni, R. T. Mahajan, *Curr. Neuropharmacol.* **2009**, 7, 65.
221 R. B. Walker, J. D. Everette, *J. Agric. Food Chem.*, **2009**, 57, 1156.
222 V. Oliveri, G. Vecchio, *Eur. J. Med. Chem.* **2011**, *46*, 961.
223 I. Spasojevic, I. Batinic-Haberle, D. R. Stevens, P. Hambright, N. A. Thorpe, J. Grodkowski, P. Neta, I. Fridovich, *Inorg. Chem.* **2001**, 40, 726.
224 S. Durot, C. Policar, F. Cisnetti, F. Lambert, J. P. Renault, G. Pelosi, G. Blain, H. Korri-Youssoufi, J. P. Mahy, *Eur. J. Inorg. Chem.* **2005**, 17, 3513.
225 B. Verdejo, S. Blasco, E. Garcıa-Espana, F. Lloret, P. Gavina, C. Soriano, S. Tatay, H. R. Jimenez, A. Doménech, J. Latorre, *Dalton Trans.* **2007**, 41, 4726.
226 A. I. Bush, *Trends Neurosci.* **2003**, 26, 207.
227 M. R. H. Krebs, G. L. Devlin, A. M. Donald, *Biophys. J.* **2009**, 96, 5013.
228 D. Hamada, C. M. Dobson, *Protein Sci.* **2002**, 11, 2417.
229 G. Navarra, M. Leone, V. Militello, *Biophys. Chem.* **2007**, 131, 52.

A1. Appendix: Publications

1. V. Oliveri, M. Viale, C. Aiello, G. Vecchio, submitted.
2. V. Oliveri, F. Attanasio, A. Puglisi, J. Spencer, G. Vecchio, submitted.
3. M. Anzaldi, M. Viale; C. Macciò, C. Aiello, P. Castagnola, V. Oliveri, A. Balbi, submitted.
4. V. Oliveri, A. Puglisi, M. Viale, C. Aiello, C. Sgarlata, G. Vecchio, J. Clarke, J. Milton, J. Spencer, New cyclodextrin-bearing 8-hydroxyquinoline ligands as multifunctional molecules. *Chemistry, A European Journal* **2013**, 19, 13946.
5. F. Bellia, V. Oliveri, E. Rizzarelli, G. Vecchio, New derivative of carnosine for nanoparticle assembly. *European Journal of Medicinal Chemistry* **2013**, 70, 225.
6. V. Oliveri, R. D'Agata, V. Giglio, G. Spoto, G. Vecchio, Cyclodextrin-functionalised gold nanoparticles via streptavidin: A supramolecular approach. *Supramolecular Chemistry* **2013**, 25, 465.
7. V. Oliveri, M. Viale, G. Caron, C. Aiello, R. Gangemi, G. Vecchio, Glycosylated copper(II) ionophores as prodrugs for β-glucosidase activation in targeted cancer therapy. *Dalton Transactions* **2013**, 42, 2023-2034.
8. C. Tudisco, V. Oliveri, M. Cantarella, G. Vecchio, G. Condorelli, Functionalization of magnetic nanoparticles with phosphonic linkers for cyclodextrin immobilization. *European Journal of Inorganic Chemistry* **2012**, 5323.
9. V. Oliveri, M.L. Giuffrida, G. Vecchio, C. Aiello, M. Viale. Gluconjugates of 8-hydroxyquinolines as potential anti-cancer prodrugs. *Dalton Transactions* **2012**, 41, 4530.
10. A. Puglisi, J. Spencer, V. Oliveri, X. Kong, J. Clarke, J. Milton. Synthesis, Physicochemical properties and antioxidant activity of deferiprone-cyclodextrin conjugates and their iron(III) complexes. *Dalton Transactions* **2012**, 41, 2877.
11. V. Oliveri, A. Puglisi, G. Vecchio. New conjugates of β-cyclodextrin with manganese(III) salophen and porphyrin complexes as antioxidant systems. *Dalton Transactions* **2011**, 40, 2913.

12. V. Oliveri, G. Vecchio. A novel artificial superoxide dismutase: non covalent conjugation of albumin with a Mn(III) salophen-type complex. *European Journal of Medicinal Chemistry* **2011**, 46, 961.

A2. Proceedings

1. V. Oliveri, M. Viale, C. Aiello, G. Vecchio, β-galactosidase-responsive prodrugs of copper(II) chelating agents. *Biomet 13*, Catania 25-26 October **2013**.
2. V. Giglio, V. Oliveri, G. Natile, F. Intini, M. Viale, C. Aiello, G. Vecchio, Folic acid-β-cyclodextrin conjugates for drug targeting. *Biomet 13*, Catania 25-26 October **2013**.
3. V. Giglio, V. Oliveri, G. Natile, F. Intini, M. Viale, C. Aiello, G. Vecchio, Folate-β-cyclodextrin conjugates as drug targeting systems. *3rd European Conference on Cyclodextrins*, Antalya, 2-4 October **2013**.
4. V. Oliveri, A. Puglisi, M. Viale, C. Aiello, C. Sgarlata, G. Vecchio, J. Spencer, New multifunctional 8-hydroxyquinoline-appended cyclodextrins: exploring their antioxidant and metal binding abilities. *XLI Congresso Nazionale della Divisione di Chimica Inorganica della Società Chimica Italiana*, Parma, 3-6 September **2013**.
5. V. Oliveri, M. Viale, C. Aiello, G. Vecchio, Glycosylated conjugates of copper(II) chelating agents as beta-galactosidase-activated prodrugs. *XLI Congresso Nazionale della Divisione di Chimica Inorganica della Società Chimica Italiana*, Parma, 3-6 September **2013**.
6. G. Vecchio, V. Oliveri, A. Puglisi, M. Viale, C. Aiello, J. Spencer, New cyclodextrin-bearing 8-hydroxyquinoline ligands as multifunctional molecules. *ICBIC 16*, Grenoble, 22-26 July **2013**.
7. V. Oliveri, M. Viale, G. Caron, C. Aiello, G. Vecchio, Glycosylated conjugates of copper(II) chelating agents as β-galactosidase-activated prodrugs. *ICBIC 16*, Grenoble, 22-26 July **2013**.
8. C. Tudisco, V. Oliveri, E. Fantechi, G. Vecchio, C. Sangregorio, G. G. Condorelli Synthesis and characterization of bifunctional magnetic iron nanoparticles. *Samic 2012*, Bressanone , 2-6 December **2012**.
9. V. Oliveri, M. Viale, G. Caron, C. Aiello, R. Gangemi, G. Vecchio, New prodrugs of copper(II) chelators for enzyme-specific activation in targeted cancer therapy. *Biomet 12*, Padova, 26-28 October **2012**.

10. V. Oliveri, M. Viale, G. Caron, C. Aiello, G. Vecchio, Glycosylated prodrugs of oxines for enzyme-specific activation in targeted cancer therapy, *Congresso nazionale della divisione di chimica dei sistemi biologici*, Napoli, 24-25 September **2012**.
11. V. Oliveri, R. D'agata, V. Giglio, G. Spoto, G. Vecchio, β-cyclodextrin-functionalized gold nanoparticles via streptavidin. *Congresso nazionale della divisione di chimica dei sistemi biologici*, Napoli, 24-25 September **2012**.
12. V. Oliveri, M.Viale, G. Caron, C. Aiello, G. Vecchio, Novel anticancer prodrugs: oxine glucoconjugates, *EUROBIC11*, Granada, 12-16 September **2012**.
13. C. Tudisco, V. Oliveri, M. Cantarella, G. Vecchio, G. Condorelli, Functionalization of magnetic nanoparticles with phosphonic linkers for cyclodextrin immobilization. *E-MRS & Nature Materials Workshop*, 14-18 May **2012**.
14. V. Oliveri, M.Viale, C. Aiello, G. Vecchio, Glucoconjugates of oxines as a new class of anticancer prodrugs. *13th RSC-SCI Joint Meeting on Heterocyclic Chemistry*, Catania, 10-12 May **2012**.
15. C. Tudisco, M. Cantarella, V. Oliveri, G. Vecchio, G. Condorelli., Functionalization of magnetic nanoparticles with phosphonic linkers for cyclodextrin immobilization, *Samic 2011*, Bressanone , 4-8 December **2011**.
16. A. Puglisi, J. Spencer, V. Oliveri, X. Kong, J. Clarke, J. Milton, Synthesis, physicochemical properties and antioxidant activity of deferiprone-cyclodextrin conjugates and their iron(III) complexes. *II European Conference on Cyclodextrins*, Asti, 2-4 October **2011**.
17. V. Oliveri, F. Tomasello, A. Puglisi, G. Vecchio , Internalization of metal complexes of porphyrin-β-cyclodextrin conjugate into cancer cells. *II European Conference on Cyclodextrins*, Asti, 2-4 October **2011**.
18. V. Oliveri, M.L. Giuffrida, G. Vecchio, Clioquinol Glycoconjugates as Potential Anti-Cancer Prodrugs . *XXIV Congresso Nazionale della Società Chimica Italiana*, Lecce, 11-16 September **2011**.
19. V. Oliveri, M.L. Giuffrida, G. Vecchio, Clioquinol glycoconjugates as potential agents for cancer. *Scuola Nazionale di Chimica Bioinorganica*, Certosa di Pontignano (SI), 3-6 July **2011**.

20. V. Oliveri, A. Puglisi, G. Vecchio, Manganese(III) complexes of β-cyclodextrin conjugates with antioxidant activity. *Congresso nazionale della divisione di chimica dei sistemi biologici*, San Vito di Cadore (BL), 9-11 September **2010**.
21. V. Oliveri, G. Vecchio, Coniugati con β-ciclodestrina di sistemi ad attività antiossidante. *V Convegno Congiunto delle Sezioni Sicilia e Calabria della Societa Chimica Italiana*, Aci Castello (CT), 1-2 December **2009**.

A3. Appendix: Symbols and Abbreviations

A-2780	Human ovarian carcinoma cells
A-549	Adenocarcinomic human alveolar basal epithelial cells
ABCD6HQ	6^{A},6^{B} -Dideoxy-6^{A},6^{B}-di[[(8-hydroxyquinolyl)-2-carboxyl]amino]-β-CyD
ABTS	Diammonium 2,2′-azino-bis(3-ethylbenzothiazoline-6-sulfonate)
Ac	Acetyl
AcOEt	Ethyl acetate
AD	Alzheimer's disease
ADEPT	Antibody-directed enzyme therapy
ADME	Absorption, distribution, metabolism and excretion
AHQ	2-Amino-8-hydroxyquinoline
ALS	Amyotrophic lateral sclerosis
ASGP-R	Asialoglycoprotein receptor
ATP7A	Menkes disease-associated protein
ATP7B	Wilson disease protein
Aβ	Amyloid-beta
BBB	Blood brain barrier
BE	Bystander effect
BLG	β-Lactoglobulin
Bn	Benzyl group
bs	Broad singlet
BSE	Bovine Spongiform Encephalopathy
Capan-1	Pancreatic carcinoma cell lines
CCS	Copper chaperone for superoxide dismutase
CD	Circular dichroism
CD3HQ	2^{A}(S),3^{A}(R)-3^{A}-[[(8-Hydroxyquinolyl)-2-carboxyl]amino]-3^{A}-deoxy-β-CyD
CD3RHQ	2^{A}(S),3^{A}(R)-3^{A}-[(8-Hydroxyquinolyl)-2-methylamino]-3^{A}-deoxy-β-CyD
CD6HQ	6^{A}-Deoxy-6^{A}-[[(8-hydroxyquinolyl)-2-carboxyl]amino]-β-CyD
CD6RHQ	6^{A}-Deoxy-6^{A}-[(8-hydroxyquinolyl)-2-methylamino]-β-CyD
CD6RHQBn	6^{A}-Deoxy-6^{A}-[(8-benzyloxyquinolyl)-2-methylamino]-β-CyD
CDNHQ	6^{A}-Deoxy-6^{A}-[[(8-hydroxyquinolyl)-2-carboxyl]aminoethylamino]-β-CyD
CDOHQ	6^{A}-Deoxy-6^{A}-[[(8-hydroxyquinolyl)-2-carboxyl]ethylamino]-β-CyD
CJD	Creutzfeldt–Jakob disease
Cl_2HQ	5,7-Dichloro-8-hydroxyquinoline
ClHQ	5-Chloro-8-hydroxyquinoline
CNS	Central nervous system
COSY	Correlation spectroscopy
COX17	Cytochrome c oxidase copper chaperone

CQ	Clioquinol
CTR1	Copper transport protein
CWD	Chronic wasting disease
CyD	β-Cyclodextrin
d	Doublet
DAPI	4'-6-Diamidino-2-phenylindole
DCC	N,N'-dicyclohexylcarbodiimide
dd	Double doublet
ddd	Double double doublet
DDS	Drug delivery System
DFO	Deferoxamine
DFP	Deferiprone
DMDP	2,5-Dideoxy-2,5-imino-D-mannitol
DMF	Dimethylformamide
DMSO	Dimethylsulfoxide
DNR	Daunorubicin
DOX	Doxorubicin
D-pen	D-penicillamine
DTPA	Diethylene triamine pentaacetic acid
EDTA	Ethylenediaminetetraacetic acid
en	Ethylenediamine
EPI	Epirubicin
ESI-MS	Electrospray ionization mass spectrometry
EtOH	Ethanol
FCS	Fetal calf serum
FDA	Food and drug administration
FDG	Fluorodeoxyglucose
GA	Geldanamycin
Gal	Galactose
GalAHQ	2-Amino-8-quinolinyl-β-D-galactopyranoside
$GalCl_2HQ$	5,7-Dichloro-8-quinolinyl-β-D-galactopyranoside
GalClHQ	5-Chloro-8-quinolinyl-β-D-galactopyranoside
GalCQ	5-Chloro-7-iodo-8-quinolinyl-β-D-galactopyranoside
GalMeHQ	2-Methyl-8-quinolinyl-β-D-galactopyranoside
GalNAc	N-Acetylgalactosamine
GalNHQ	5-Nitro-8-quinolinyl-β-D-galactopyranoside
GDEPT	Gene-directed enzyme prodrug therapy
gHMBCAD	Gradient heteronuclear multiple-bond correlation spectroscopy
gHSQCAD	Gradient heteronuclear single quantum coherence
Glc	Glucose
GlcHQ	2'-[(8-Hydroxyquinolyl)-2-carboxyl]aminoethyl]-β-D-glucopyranoside

$GluCl_2HQ$	5,7-Dichloro- 8-quinolinyl-β-D-glucopyranoside
GluClHQ	5-Chloro-8-quinolinyl-β-D-glucopyranoside
GluCQ	5-Chloro-7-iodo-8-quinolinyl-β-D-glucopyranoside
GluMeHQ	2-Methyl-8-quinolinyl-β-D-glucopyranoside
GluOHQ	8-Quinolinyl -β-D-glucopyranoside
GLUT	Glucose transporter
GSH	Glutathione
HAH1	Human ATPase copper chaperone
hAng	Human Angiogenin
hCBG	Human cytosolic β-glucosidase
HD	Huntington's disease
Hep-G2	Human liver carcinoma cell line
HLA-20	5-((4-(Prop-2-ynyl)piperazin-1-yl)methyl)quinolin-8-ol
HMBC	Heteronuclear multiple bond correlation
HOBt	1-Hydroxybenzotriazole
HRMS	High resolution mass spectrometry
HSQC	Heteronuclear single quantum coherence
I_{50}	Half maximal inhibitory concentration (SOD assay)
IC_{50}	Half maximal inhibitory concentration (MTT assay)
IDA	Idarubicin
IDE	Insulin-degrading enzyme
J	Coupling constant
JNK	Jun N-terminal kinases
LiDEPT	Ligand directed enzyme therapy
m	Multiplet
m/z	Mass/charge
M-30	5-((Methyl(prop-2-ynyl)amino)methyl)quinolin-8-ol
MAO	L-Monoamine oxidases
MDA-MB-231	Human breast adenocarcinoma cell line
Me	Methyl
MeHQ	2-Methyl-8-hydroxyquinoline
MeOH	Methanol
MMP	Matrix metalloproteinases
MOPS	3-Morpholinopropane-1-sulfonic acid
MTT	3-(4,5-Dimethythiazol-2-yl)-2,5-diphenyl tetrazolium bromide
NHQ	5-Nitro-8-hydroxyquinoline
NMDA	N-methyl-D-aspartate
NMR	Nuclear magnetic resonance
NPC	Niemann–Pick disease, type C
OHQ	8-Hydroxyquinoline
Panc-1	Human pancreatic carcinoma, epithelial-like cell line

PBS	Phosphate buffered saline
PBT2	A second-generation 8-hydroxyquinoline analog
PD	Parkinson's disease
PDB	Protein data bank
PET	Positron emission tomography
PMT	Prodrug monotherapy
Pr	Propyl
PrOH	1-Propanol
PrP	Prion protein
PrPSc	Scrapie form of Prion protein
r.t.	Room temperature
ROESY	Rotating-frame Overhauser effect correlation spectroscopy
ROS	Reactive oxygen species
s	Singlet
SMON	Subacute myelo-optic neuropathy
S_N2	Bimolecular nucleophilic substitution
SOD	Superoxide dismutase
t	Triplet
TEAC	Trolox equivalent antioxidant capacity
TETA	Triethylenetetramine
THRHQ	6-Deoxy-6-(8-hydroxyquinolyl)-2-methylamino]-α,α'-trehalose
ThT	Thioflavin T
TLC	Thin-layer chromatography
TM	Tetrathiomolybdate
TOCSY	Total correlation spectroscopy
UPS	Ubiquitin-proteasome system
UV-vis	Ultraviolet–visible spectroscopy
VDEPT	Virus-directed enzyme prodrug therapy
VEGF	Vascular endothelial growth factor
VK-28	5-((4-(2-Hydroxyethyl)piperazin-1-yl)methyl)quinolin-8-ol
WD	Wilson's disease
ZIP	Zinc transport protein
ZnT	Zinc transporter
δ	Chemical shift
Δε	Molar circular dichroism
ε	Molar absorptivity
λ	Wavelength
λ_{max}	Wavelength of maximum absorption